UNIVERSIDAD DE OVIEDO

Departamento de Química Orgánica e Inorgánica

Programa de Doctorado: Síntesis y Reactividad Química

OXIDOREDUCTASES AND HALOGENATED SUBSTRATES: BIOCATALYTIC AND CRYSTALLOGRAPHIC STUDIES

Tesis Doctoral

KINGA WERONIKA KĘDZIORA

2014

UNIVERSIDAD DE OVIEDO

Departamento de Química Orgánica e Inorgánica

Programa de Doctorado: Síntesis y Reactividad Química

OXIDOREDUCTASES AND HALOGENATED SUBSTRATES: BIOCATALYTIC AND CRYSTALLOGRAPHIC STUDIES

Memoria presentada por Kinga Weronika Kędziora para optar al grado de Doctor en Química por la Universidad de Oviedo

RESUMEN DEL CONTENIDO DE TESIS DOCTORAL

1.- Título de la Tesis	
Español/Otro Idioma: Oxidorreductasas y sustratos halogenados: Estudios biocatalíticos y cristalográficos	Inglés: Oxidoreductases and halogenated substrates: Biocatalytic and crystallographic studies

2.- Autor	
Nombre: Kinga Weronika Kędziora	
Programa de Doctorado: Síntesis y Reactividad Química	
Órgano responsable: Química Orgánica e Inorgánica	

RESUMEN (en español)

En 2007 se implementó una regulación dentro de la Unión Europea conocida como "REACH" (Registro, Evaluación, Autorización y Restricción de Sustancias Químicas), cuyo objetivo es proveer una protección máxima a la salud humana y al medioambiente frente a los riesgos asociados con el manejo de los productos químicos. Estas normativas requieren que la industria aborde el problema del impacto ambiental causado en los procesos de producción y que se desarrollen metodologías más ecológicas. La Biocatálisis cumple perfectamente dichas normativas debido al uso de enzimas biodegradables que no solo actúan con alta eficacia en condiciones muy suaves de reacción, sino que además permiten acceder a una amplia gama de compuestos químicos. Por este motivo, la investigación en este campo ha aumentado de manera exponencial en las últimas décadas, aprovechando además los avances en las áreas de ingeniería molecular, biología estructural y bioinformática, con el fin de desarrollar una nueva generación de biocatalizadores más eficientes.

Esta Tesis Doctoral está estructurada en tres capítulos precedidos por una introducción general que incluye algunos conceptos básicos sobre la Biocatálisis. En esta introducción se abordarán brevemente aspectos generales que han servido como base para el posterior desarrollo de los tres capítulos. Así, se ha realizado un breve resumen de la aplicación industrial de las oxidorreductasas, tales como alcohol deshidrogenasas (ADHs) y lacasas.

El **Capítulo 1** está dedicado a la reducción asimétrica de cetonas aromáticas α,α-dihalogenadas catalizada por alcohol deshidrogenasas, dirigida hacia la preparación de los correspondientes alcoholes secundarios enantiopuros. A pesar de que el alto potencial redox de la reducción de estos compuestos favorece dichos procesos, el gran tamaño de los sustituyentes en las proximidades del grupo carbonilo hace que la transformación requiera de ADHs muy específicas que puedan alojar en su centro activo sustratos muy voluminosos. De este modo, se ha conseguido desarrollar y optimizar los procesos de biorreducción de una amplia familia de cetonas proquirales de manera satisfactoria, aislando los correspondientes alcoholes con excelentes rendimientos y purezas ópticas, siendo posible la preparación de los citados alcoholes con configuraciones tanto (*R*) como (*S*). Por otro lado, ha sido posible extender esta metodología a dos cetonas racémicas de interés, desarrollando procesos eficientes de resolución cinética dinámica para obtener los correspondientes alcoholes con distintos niveles de estereo- y diastereoselección y con buenos rendimientos globales. Los resultados de esta investigación están recogidos en el artículo de investigación: "Expanding the Scope of Alcohol Dehydrogenases towards Bulkier Substrates: Stereo- and Enantiopreference for α,α-Dihalogenated Ketones", Kinga Kędziora, Fabricio R. Bisogno, Iván Lavandera, Vicente Gotor-Fernández, José Montejo-Bernardo, Santiago García-Granda, Wolfgang Kroutil, y Vicente Gotor, *ChemCatChem* **2014**, *6*, 1066-1072.

En el **Capítulo 2** se describe el trabajo realizado durante una estancia en el York Structural Biology Laboratory de la Universidad de York. El objetivo principal de este capítulo es el aislamiento, purificación y cristalización de la alcohol deshidrogenasa de *Sphingobium yanoikuae* DSM 6900 unida al cofactor de nicotinamida NADPH. La determinación de la estructura junto con estudios de modelización molecular usando como sustrato la fenil *n*-pentil cetona, ha permitido demostrar la especificidad de este enzima por el NADPH, así como su estereoselectividad de tipo Prelog con sustratos voluminosos. Los resultados más destacados de este capítulo se encuentran recogidos en la publicación: "Structures of Alcohol Dehydrogenases from *Ralstonia* and *Sphingobium spp*. Reveal the Molecular Basis for Their Recognition of 'Bulky–Bulky' Ketones", Henry Man, Kinga Kędziora, Justyna Kulig, Annika Frank, Iván Lavandera, Vicente Gotor-Fernández, Dörte Rother, Sam Hart, Johan P. Turkenburg, y Gideon Grogan, *Top. Catal.* **2014**, *54*, 356-365.

Finalmente, en el **Capítulo 3** se ha abordado la oxidación de sustratos termodinámicamente desfavorecidos como son los derivados de 2,2-dihalo-1-feniletanol. Para ello se ha puesto a punto una metodología sintética empleando un sistema redox formado por una lacasa y el mediador TEMPO. Debido al mecanismo de oxidación de tipo iónico mediado por TEMPO, y una vez superados los problemas de solubilidad de los sustratos mediante el uso de un sistema bifásico, se obtuvieron las correspondientes cetonas a través de procesos muy limpios y eficientes con rendimientos excelentes. Además, en combinación con una ADH, se llevó a cabo la desracemización del 2,2-dicloro-1-feniletanol en *one-pot*. Los resultados más representativos de esta investigación han sido publicados en: "Laccase/TEMPO-Mediated System for the Thermodynamically Disfavored Oxidation of 2,2-Dihalo-1-phenylethanol Derivatives", Kinga Kędziora, Alba Díaz-Rodríguez, Iván Lavandera, Vicente Gotor-Fernández, y Vicente Gotor, *Green Chem*. **2014**, 16, 2248-2253.

RESUMEN (en Inglés)

In 2007 came into force the European Union Regulation known under the abbreviation "REACH" (Registration, Evaluation, Authorization and Restriction of Chemicals), which aims to provide high level of protection to human health and the environment from the risks posed by chemicals. These regulations made obligatory for industry to address the environmental impact of their manufacturing processes in order to develop greener methodologies. Biocatalysis meets perfectly the objectives of these directives, as uses biodegradable enzymes combining their high efficiency while working under mild conditions to produce a broad range of fine chemicals. These characteristics tagged Industrial Biocatalysis as White Biotechnology. Therefore, investigation in this field shows exponential growth and is fueled by the advances in the fields of protein engineering, structural biology and bioinformatics, allowing the development of an improved generation of biocatalysts.

This Doctoral Thesis has been structured into three chapters preceded by a general introduction that covers basic concepts on Biocatalysis with special focus on industrial application of oxidoreductases such as alcohol dehydrogenases and laccases. All these thematic issues give background to the following three Chapters, where the experimental results have been discussed in depth.

Chapter 1 is dedicated to the alcohol dehydrogenase-catalyzed asymmetric reduction of α,α-dihalogenated aryl ketones into the corresponding enantiopure secondary alcohols which are valuable intermediates in organic chemistry. High redox potential of the reduction of these ketones favored these processes, however due to the increased size of the substituents at the vicinity to the carbonyl group, the transformation required ADHs that could accommodate the so-called "bulky-bulky" substrates. Screening identified not only stereocomplementary enzymes for these sterically challenging ketones, but also enantiopreference with racemic α,α-disubstituted ketones. Thus, on the one hand the production of target alcohols has been possible in excellent yields and optical purities with both (*R*) and (*S*)-configurations. On the other hand, this methodology has been applied to the dynamic kinetic resolution of two racemic ketones, yielding the corresponding alcohols with different levels of stereo- and

diastereoselection and good overall conversions. These results have been published in the article: "Expanding the Scope of Alcohol Dehydrogenases towards Bulkier Substrates: Stereo- and Enantiopreference for α,α-Dihalogenated Ketones", Kinga Kędziora, Fabricio R. Bisogno, Iván Lavandera, Vicente Gotor-Fernández, Jose Montejo-Bernardo, Santiago García-Granda, Wolfgang Kroutil, and Vicente Gotor, *ChemCatChem* **2014**, *6*, 1066-1072.

Chapter 2 describes the work performed at York Structural Biology Laboratory, University of York, during a short-term placement. The aim was to obtain suitable crystals of alcohol dehydrogenase from *Sphingobium yanoikuae* DSM 6900 in a complex with its nicotinamide cofactor NADPH. The resolved structure together with a molecular modelling study using *n*-pentyl phenyl ketone as substrate, allowed gaining insight into the NADPH cofactor specificity and Prelog stereoselectivity of this enzyme towards "bulky-bulky" substrates. The results obtained have been published in: "Structures of Alcohol Dehydrogenases from *Ralstonia* and *Sphingobium spp*. Reveal the Molecular Basis for Their Recognition of 'Bulky–Bulky' Ketones", Henry Man, Kinga Kędziora, Justyna Kulig, Annika Frank, Iván Lavandera, Vicente Gotor-Fernández, Dörte Rother, Sam Hart, Johan P. Turkenburg, and Gideon Grogan, *Top. Catal.* **2014**, *54*, 356-365.

Chapter 3 deals with the thermodynamically disfavored oxidation of 2,2-dihalo-1-phenylethanol derivatives using the laccase/TEMPO redox pair as method of choice using oxygen as final electron acceptor, due to the lack of suitable (bio)catalytic methodologies. Taking advantage of the ionic mechanism of TEMPO-mediated oxidation of alcohols, and once overcome the substrate solubility issue by using a biphasic system, it was possible to yield the corresponding ketones in excellent yields as the only products through clean and efficient processes. Additionally, in combination with an ADH in a *one-pot* reaction, an alcohol deracemization process was achieved. These results have been summarized in the article: "Laccase/TEMPO-Mediated System for the Thermodynamically Disfavored Oxidation of 2,2-Dihalo-1-phenylethanol Derivatives", Kinga Kędziora, Alba Díaz-Rodríguez, Iván Lavandera, Vicente Gotor-Fernández, and Vicente Gotor, *Green Chem*. **2014**, *16*, 2248-2253.

SR. DIRECTOR DE DEPARTAMENTO DE QUÍMICA ORGÁNICA E INORGÁNICA/
SR. PRESIDENTE DE LA COMISIÓN ACADÉMICA DEL PROGRAMA DE DOCTORADO EN SÍNTESIS Y REACTIVIDAD QUÍMICA

Así, en el primer capítulo se aborda la síntesis de una amplia familia de cetonas halogenadas para llevar a cabo procesos de biorreducción empleando ADHs. Se ha abordado tanto la desimetrización de cetonas proquirales, como la resolución cinética dinámica de otras en forma racémica. Los resultados obtenidos han sido publicados en el artículo: "Expanding the Scope of Alcohol Dehydrogenases towards Bulkier Substrates: Stereo- and Enantiopreference for α,α-Dihalogenated Ketones", K. Kędziora, F. R. Bisogno, I. Lavandera, V. Gotor-Fernández, J. Montejo-Bernardo, S. García-Granda, W. Kroutil, V. Gotor, *ChemCatChem* **2014**, *6*, 1066-1072.

La revista *ChemCatChem* en el año 2012 se encuentra encuadrada dentro de la categoría "Química Física", con un índice de impacto de 5.181, ocupando la posición 26 de 135, y por lo tanto en el primer cuartil.

En el segundo capítulo se muestra el trabajo realizado durante una estancia en la Universidad de York, donde se llevó a cabo el aislamiento, purificación y cristalización de la alcohol deshidrogenasa de *Sphingobium yanoikuae* unida al cofactor de nicotinamida NADPH. La determinación de la estructura junto con estudios de modelización molecular ha permitido demostrar la especificidad de este enzima por el NADPH, así como su estereoselectividad de tipo Prelog con sustratos voluminosos. Los resultados obtenidos han sido publicados en el artículo: "Structures of Alcohol Dehydrogenases from *Ralstonia* and *Sphingobium spp*. Reveal the Molecular Basis for Their Recognition of 'Bulky–Bulky' Ketones", H. Man, K. Kędziora, J. Kulig, A. Frank, I. Lavandera, V. Gotor-Fernández, D. Rother, S. Hart, J. P. Turkenburg, G. Grogan, *Top. Catal.* **2014**, *54*, 356-365.

La revista *Topics in Catalysis* en el año 2012 está encuadrada dentro de dos categorías:

- "Química Aplicada" ocupando la posición 16 de 71 (primer cuartil)
- "Química Física" ocupando la posición 53 de 135 (segundo cuartil)

Su índice de impacto es 2.608.

En el tercer capítulo se ha abordado la oxidación termodinámicamente desfavorecida de derivados 2,2-dihalo-1-feniletanol, empleando un sistema redox formado por una lacasa y el mediador químico TEMPO. Así, empleando sistemas bifásicos se obtuvieron las correspondientes cetonas a través de procesos muy limpios y eficientes con rendimientos excelentes. Asimismo se ha desarrollado un procesos de desracemización del 2,2-dicloro-1-feniletanol en *one-pot* empleando este sistema junto con una alcohol deshidrogenasa. Los resultados más representativos de esta investigación han sido publicados en: "Laccase/TEMPO-Mediated System for the Thermodynamically Disfavored Oxidation of 2,2-Dihalo-1-phenylethanol Derivatives", K. Kędziora, A. Díaz-Rodríguez, I. Lavandera, V. Gotor-Fernández, V. Gotor, *Green Chem.* **2014**, 16, 2248-2253.

La revista *Green Chemistry* en el año 2012 se encuentra encuadrada dentro de la categoría "Química Multidisciplinar", con un índice de impacto de 6.828, ocupando la posición 18 de 152, y por tanto está en el primer cuartil.

Esta Tesis Doctoral en su conjunto muestra un gran interés en distintos campos de la Química y la Biología Molecular, destacando además que la estudiante Doña Kinga Weronika Kędziora, es primera autora de dos de las publicaciones (capítulos 1 y 3), y segunda de otra de ellas (capítulo 2), todas emanadas de este trabajo de investigación, por lo que se considera una Tesis Doctoral idónea tanto por su contenido como por su presentación en la presente forma.

Oviedo, 24 de julio de 2014

Directores de la Tesis Doctoral

Fdo.: Iván Lavandera Garcia

Fdo.: Vicente Gotor Fernández

Gracias a la vida que me ha dado tanto
Me dio dos luceros que cuando los abro
Perfecto distingo lo negro del blanco
Y en el alto cielo su fondo estrellado
Y en las multitudes el hombre que yo amo.

Gracias a la vida que me ha dado tanto
Me ha dado la marcha de mis pies cansados
Con ellos anduve ciudades y charcos,
Playas y desiertos montañas y llanos…

Gracias a la vida que me ha dado tanto
Me dio el corazón que agita su marco
Cuando miro el fruto del cerebro humano,
Cuando miro al bueno tan lejos del malo…

Gracias a la vida que me ha dado tanto
Me ha dado la risa y me ha dado el llanto,
Así yo distingo dicha de quebranto
Los dos materiales que forman mi canto…
(Violeta Parra)

ACKNOWLEDGMENTS

I would like to express my gratitude to a number of persons thanks to whom my experience in Asturias has gone beyond this Doctoral thesis and it is very hard for me to leave this beautiful county and its generous people.

At professional level, I am grateful to Prof. Gotor for hosting me in the Bioorganic Group, where my doctoral thesis could be accomplished. My special *thank you* is reserved for Dr. Iván Lavandera and Dr. Vicente Gotor Fernández for putting up with me during the past four years as my supervisors. I am especially grateful for the support shown to me at the toughest moments. Your understanding and paternal care will not be forgotten.

I also would like to acknowledge Dr. Fabricio Bisogno for his guidance during my first months in the bioorganic lab. I appreciate helpful hand of the technicians: Lara Fernandez and Rodolfo Iglesias, as well as Dr. Isabel González Albuerne for the assistance with NMR experiments.

I would like to thank Dr. Gideon Grogan form YSBL, York, for the opportunity of completing the placement at his research group, and Dr. Franck Escalletes from Ingenza, Roslin, Scotland, for the valuable experience gained in the R&D molecular biology laboratory during the industrial placement. Here, I would like to acknowledge the ITN Marie Skłodowska-Curie BIOTRAINS network for financial funding and the opportunity of professional development.

Finally, my words of appreciation go to my excellent fellow colleagues from Bioorganic lab for warm welcome, friendly environment and time spent together both in and out of the Faculty. Two persons

deserve a special note: Angela for passing as Alba, and Nico for Juan, I do apologize for unintended moral damage caused. ¡Que Dios os lo pague con muchos hijos!

At personal level my heartfelt *thank you* goes to Anina and Ana Belén (and their respective families), Ana R, Ibo, Fabri, Egu, Cris, Alba Díaz and Wioleta for shown friendship, acceptance and time spent together. Each of you occupies special place in my heart.

At personally personal level I would like to say *gracias* to María simply for everything and for giving me the feeling of home, especially.

The last line is invariably reserved for the VIP, without you S. this thesis could have taken forever to be written.

Mojej rodzinie i przyjaciołom serdecznie dziękuję za wiare we mnie i wsparcie.

ABBREVIATIONS AND ACRONYMS

[EA], [EB]	Enzyme-substrate complex
$[EA]^{\neq}$, $[EB]^{\neq}$	Transition state of the enzyme-substrate complex
3β/17β-HSD	3β/17β-Hydroxysteroid dehydrogenase
Å	Angstrom
A	Alanine
ABTS	2,2-Azinobis-(3-ethylbenzothiazoline)-6-sulfonic acid
AC	Affinity chromatography
ACS GCIPR	The American Chemical Society Green Chemistry Institute® Pharmaceutical Roundtable
ADH-A	Alcohol dehydrogenase from *Rhodococcus ruber*
ADHD	Attention deficit hyperactivity disorder
ADHs	Alcohol dehydrogenases
ADP(R)	Adenosine diphosphate (ribose)
AE	Atom economy
APIs	Active pharmaceutical intermediates
APS	Ammonium persulfate
ARPP	Adenine ribose pyrophosphate moiety of NADH
Asn	Asparagine
Asp	Aspartic acid
atm	atmosphere
ATP	Adenosine triphosphate
BDE	Bond dissociation energy
Boc	*tert*-Butoxycarbonyl
BSA	Bovine serum albumin
Bu	Butyl
^{i}Bu	Isobutyl
ºC	Degrees Celcius
c	Conversion
CAD	Cinnamyl alcohol dehydrogenase
cal	Calorie
Cbz	Benzyloxycarbonyl
CE	Carbon efficiency
CF	Chromatofocusing
CSSI	Clear Strategy Screen I

Cys	Cysteine
de	Diastereomeric excess
DH	Dehydrogenase
DKR	Dynamic kinetic resolution
DMF	*N*,*N*-Dimethylformamide
DMSO	Dimethylsulfoxide
DNA	Deoxyribonucleic acid
DTT	Dithiothreitol
D_x	Domain x
dTTPs	Deoxythymidine triphosphates
E	Enzyme
E_a	Activation energy
EATOS	Environmental assessment tool for organic syntheses
EC	Enzyme Commission
ECHA	European Chemical Agency
EDTA	Ethylenediaminetetraacetic acid
ee	Enantiomeric excess
EPR	Electron Paramagnetic Resonance
equiv.	Equivalent
ET	Electron transfer
Et	Ethyl
Et_2O	Diethyl ether
Et_3N	Triethylamine
EtOAc	Ethyl acetate
EU	European Union
EWG	Electron-withdrawing group
F	Phenylalanine
FAD	Flavin adenine dinucleotide
FAS	Fatty acid synthase
FDH	Formate dehydrogenase
FMN	Flavin mononucleotide
g	Gram
GC	Gas chromatography
GDH	Glucose dehydrogenase

GF	Gel filtration
Glu	Glutamic acid
GST	Glutathione-S-transferase
GXLs	Gas-expanded liquids
h	Hour
HAT	Hydrogen atom transfer
HBT	1-Hydroxybenzotriazole
HEPES	2-[4-(2-Hydroxyethyl)piperazin-1-yl]ethanesulfonic acid
Hhe	Halohydrin dehalogenase
HIC	Hydrophobic interaction chromatography
His	Histidine
His-tag	Hexahistidine tag
HIV	Human immunodeficiency virus
HPLC	High performance liquid chromatography
I	Isoleucine
I.U.	International Units
IEX	Ion exchange chromatography
ILs	Ionic liquids
IMAC	Immobilized metal affinity chromatography
IPA	Isopropanol (2-propanol)
IPTG	Isopropyl β-D-1-thiogalactopyranoside
IUPAC	The International Union of Pure and Applied Chemistry
K	Kelvin
k_{cat}	Catalytic constant of an enzyme
kDa	Kilodalton
L	Leucine
LBADH	Alcohol dehydrogenase from *Lactobacillus brevis*
LDR	Long chain dehydrogenases/reductases
Leu	Leucine
LIC	Ligation independent cloning
LKADH	Alcohol dehydrogenase from *Lactobacillus kefir*
LMS	Laccase-mediator systems
Lys	Lysine
M	Methionine

M	Molar concentration
M	Molecular weight
MAD/SAD	Multi/single-wavelength anomalous dispersion
MBP	Maltose binding protein
MDR	Medium chain dehydrogenases/reductases
Me	Methyl
MeCN	Acetonitrile
MES	2-(*N*-morpholino)ethanesulfonic acid
Met	Methionine
MI	Mass intensity
min	Minute
mRNA	Messenger ribonucleic acid
MTBE	Methyl *tert*-butyl ether
NAD(P)H	Nicotinamide adenine dinucleotide (phosphate)
NBS	*N*-Bromosuccinimide
NCS	*N*-Chlorosuccinimide
NHA	*N*-Hydroxyacetanilide
NHPI	*N*-Hydroxyphthalimide
NMR	Nuclear magnetic resonance
OATS	Organic-aqueous tunable solvents
PAHs	Polycyclic aromatic hydrocarbons
PCL	Lipase from *Pseudomonas cepacia*
PCR	Polymerase chain reaction
PDB	Protein Data Bank
PDH	Pyruvate dehydrogenase
PEGs	Polyethylene glycols
PG	Protecting group
$PhCF_3$	Benzotrifluoride
Phe	Phenylalanine
$PhO^{\bullet}$	Phenoxyl radical
PINO	Phthalimide-*N*-oxyl radical
PQQ	Pyrroloquinoline quinone
PSL	*Pseudomonas cepacia* lipase
PTGR	Prostaglandin reductases

***p*-TsOH**	*para*-Toluenesulfonic acid
QOR	Quinone oxidoreductase
r.t.	Room temperature
RasADH	Alcohol dehydrogenase from *Ralstonia* sp**.**
REACH	Registration, Evaluation, Authorisation and Restriction of Chemicals
RPC	Reversed phase chromatography
s	Second
S	Serine
SCFs	Supercritical fluids
SDR	Short chain dehydrogenases/reductases
SDS PAGE	Sodium dodecyl sulfate polyacrylamide gel electrophoresis
SEC	Size exclusion chromatography
Ser	Serine
SVHC	Substances of very high concern
SyADH	Alcohol dehydrogenase from *Sphingobium yanoikuyae*
T	Temperature
TDH	Threonine dehydrogenase
TEMED	*N,N,N',N'*-Tetramethylethylenediamine
TEMPO	2,2,6,6-Tetramethylpiperidine-*N*-oxyl radical
THF	Tetrahydrofuran
T_m	Melting temperature
TNC	Trinuclear cluster
TOF	Turnover frequency
TON	Turnover number
Tris	Tris(hydroxymethyl)aminomethane
Trp	Tryptophan
Ts	Tosyl
Tyr	Tyrosine
U	Unit
V	Valine
V	Volt
v/v	Volume to volume ratio
Val	Valine
VLA	Violuric acid

WET	Water at elevated temperatures
w/v	weight to volume ratio
Y	Tyrosine
$\Delta\Delta G^{\neq}$	Difference in the activation energy at the transition state
$\Delta\Delta H^{\neq}$	Difference in entropy at the transition state
$\Delta\Delta S^{\neq}$	Difference in enthalpy at the transition state

TABLE OF CONTENTS

INTRODUCTION **1**

I.1. Efficiency in organic chemistry **3**

I.2. Reaction media in a sustainable chemical process **5**

I.2.1. Water as solvent in organic chemistry **6**

I.2.2. Neoteric solvent systems in organic chemistry **9**

I.3. EU legislation towards sustainable chemical processes **9**

I.4. Biocatalysis **10**

I.4.1. Advantages and disadvantages of Biocatalysis **12**

I.5. Thermodynamic aspects of enzyme catalysis **14**

I.6. Enzyme classification and catalytic efficiency metrics **17**

I.7. Oxidoreductases **18**

I.7.1. Cofactor regeneration **19**

I.8. Alcohol dehydrogenases **23**

I.8.1. Medium chain dehydrogenases (MDR) **24**

I.8.1.1. Role of zinc in MDRs **26**

I.8.1.2. Alcohol dehydrogenase from* Rhodococcus ruber *(ADH-A) **29**

I.8.2. Short chain dehydrogenases (SDR) **31**

I.8.2.1. Mechanism of SDR catalysis **32**

I.8.2.2. Alcohol dehydrogenase from* Lactobacillus brevis *(LBADH) **33**

I.8.2.3. Alcohol dehydrogenase from* Ralstonia *sp. (RasADH) **35**

I.9. Copper-dependent oxidases **38**

I.9.1. Laccase from *Trametes versicolor* **39**

I.10. Nitroxyl radicals **43**

I.11. Laccase-TEMPO oxidation systems **44**

I.12. Non-enzymatic-TEMPO oxidation systems **50**

I.13. Industrial applications of oxidoreductases **51**

CHAPTER I: Bioreductions of *α,α*-dihalogenated ketones catalyzed by alcohol dehydrogenases **55**

1.1. Introduction **57**

1.1.1. Bioreduction of α-halo ketones 59

1.1.2 Biocatalyzed synthesis of β,β-dihalogenated alcohols 64

1.2. Objectives 67

1.3. Results and discussion 71

1.4. Conclusions 79

1.5. Conclusiones 83

1.6. Experimental part 87

1.6.1. General information 89

1.6.2. General synthetic procedures 90

1.6.2.1. Synthesis of α,α-dichlorosubstituted acetophenones 2a-h 90

1.6.2.2. Synthesis of 2,2-dichloro-1-(3,4-dichlorophenyl) ethanone (2i) 90

1.6.2.3. Synthesis of 2,2-dibromo-1-phenylethanone (2j) 90

1.6.2.4. Synthesis of racemic 2-bromo-2-chloro-1-phenylethanone (2k) 90

1.6.2.5. Synthesis of racemic 2-chloro-2-fluoro-1-phenylethanone (2l) 91

1.6.2.6. General procedure for synthesis of racemic alcohols 3a-l 91

1.6.2.7. Derivatization of enantiopure alcohol 3k with 4-nitrobenzoyl chloride 91

1.6.3. General enzymatic procedures 92

1.6.3.1. Reduction of 2a-l with ADH from *Rhodococcus ruber* overexpressed in *E. coli* 92

1.6.3.2. Reduction of 2a-l with ADH from *Sphingobium yanoikuyae* overexpressed in *E. coli* 92

1.6.3.3. Reduction of 2a-l with ADH from *Ralstonia* sp. overexpressed in *E. coli* 92

1.6.3.4. Reduction of 2a-l with ADH from *Lactobacillus brevis* (LBADH) 93

1.6.3.5. Reduction of 2a-j with ADH from *Lactobacillus kefir* (LKADH) 93

1.6.3.6. Reduction of 2a-j with PR2ADH 93

1.6.3.7. Effect of the base on the racemization rate of ketone 2k 94

1.6.3.8. Effect of non-conventional media on the racemization rate of ketone 2k 94

Publication 95

CHAPTER II: Crystal structure of alcohol dehydrogenase from *Sphingobium yanoikuyae* 105

2.1. Introduction 107

2.1.1. X-ray crystallography of macromolecules 109

2.1.1.1. Gene cloning 109

2.1.1.2. Protein expression and purification 111

***2.1.1.2.1. Immobilized metal affinity chromatography (IMAC)* 113**

***2.1.1.2.2. Size exclusion chromatography (SEC)* 114**

2.1.2. X-ray crystallography of proteins 115

2.1.3. Crystal formation phenomena 117

2.1.4. Selected crystallization techniques 118

2.1.4.1. High throughput screenings 118

2.1.4.2. Hanging drop vapor diffusion technique 119

2.1.5. Alcohol dehydrogenase from *Sphingobium yanoikuyae* (SyADH) 120

2.2. Objectives 123

2.3. Results and discussion 127

2.4. Conclusions 135

2.5. Conclusiones 139

2.6. Experimental part 143

2.6.1. General procedures 145

2.6.1.1. Primers preparation for subcloning 145

2.6.1.2. Gradient PCR protocol 145

2.6.1.3. Agarose gel electrophoresis protocol 146

2.6.1.4. SyADH-LIC ends gene purification from gel 146

2.6.1.5. Insert LIC T4 polymerase reaction-protocol 147

2.6.1.6. LIC Annealing protocol 147
2.6.1.7. Transformation of competent *E. coli* 147
2.6.1.8. Protein expression 148
2.6.1.9. Protein purification and His-tag cleavage 148
2.6.1.10. Sodium dodecyl sulfate polyacrylamide gel electrophoresis (SDS PAGE) 149
2.6.1.11. Crystallization of SyADH 150
2.6.1.12. Data collection and processing 151

Publication 153

CHAPTER III: Laccase/TEMPO-mediated system for oxidation of 2,2-dihalo-1-phenylethanol derivatives 165
3.1. Introduction 167
3.1.1. Laccase/TEMPO system for the oxidation of secondary alcohols 169
3.1.2. Effect of organic cosolvents in laccase-TEMPO systems 172
3.1.3. Biocatalytic oxidation of halohydrins 173
3.1.4. Deracemization processes applied to the synthesis of halohydrins 175
3.2. Objectives 179
3.3. Results and discussion 183
3.4. Conclusions 191
3.5. Conclusiones 195
3.6. Experimental part 199
3.6.1. Enzymatic protocols 201
3.6.1.1. Optimization of the conditions for the laccase/TEMPO-mediated oxidation of 1a in the monophasic aqueous/organic solvent system 201
***3.6.1.1.1. Effect of oxygen supply (open air)* 201**
***3.6.1.1.2. Effect of the temperature* 201**
***3.6.1.1.3. Effect of the TEMPO equivalents* 201**
***3.6.1.1.4. Effect of the NaOAc buffer pH* 202**
***3.6.1.1.5. Effect of the buffer type* 202**

3.6.1.1.6. Effect of the organic solvent (Figure 3.5) **203**

3.6.1.1.7. Effect of the organic solvent concentration (Figure 3.2) **204**

3.6.1.2. Oxidation of 1a in a biphasic aqueous/MTBE system **205**

3.6.1.2.1. Use of a lower amount of TEMPO equivalents **205**

3.6.1.2.2. Time course study of the laccase/TEMPO-mediated oxidation of 1a in a biphasic aqueous/MTBE system or in plain buffer (Figure 3.3) **205**

3.6.1.2.3. Effect of the substrate concentration **206**

3.6.1.3. General method for the oxidation of alcohols 1a-j using laccase and TEMPO in a biphasic aqueous/organic solvent system **207**

3.6.1.4. Scale-up of the laccase/TEMPO-mediated synthesis of dihalogenated ketones 2a,c,d in a biphasic system **208**

3.6.1.5. Selectivity in the laccase/TEMPO system to oxidize simultaneously two *sec*-alcohols **208**

3.6.1.6. One-pot two-step sequential reaction with the laccase/TEMPO system and *E. coli*/ADH-A for the deracemization of racemic alcohol 1a (Scheme 3.8) **209**

3.6.2. Other chemical systems used to oxidize alcohol 1a (Figure 3.4) **210**

3.6.2.1. Laccase from *Trametes versicolor*/4-OH-TEMPO **210**

3.6.2.2. NaOCl/TEMPO system **211**

3.6.2.3. NaOCl/KBr/TEMPO system **211**

3.6.2.4. $NaOCl_2$/NaOCl/TEMPO system **211**

3.6.2.5. CuCl/TEMPO system **212**

3.6.2.6. $CuBr_2$/TEMPO system **212**

3.6.2.7. I_2/TEMPO system **212**

3.6.2.8. NaOCl **213**

3.6.2.9. NaOCl/KBr system **213**

3.6.2.10. $NaOCl_2$ **213**

3.6.2.11. Dess-Martin periodinane in aqueous media **213**

3.6.2.12. Dess-Martin periodinane in CH_2Cl_2 **214**

3.6.3. *Ab initio* calculations 214

3.6.4. Environmental assessment using EATOS 216

Publication 217

REFERENCES 225

INTRODUCTION

I.1. Efficiency in organic chemistry

In the recent history of organic chemistry the concept of reaction efficiency has undergone substantial changes. For long time the success of the chemical process was entirely relied upon the afforded yield of the desired product. Aspects such as waste generation and toxic properties of the chemicals used were neglected. For example, till 1980 the manufacture of 1 kg of a chemical such as phloroglucinol (1,3,5-benzenetriol), an antispasmodic agent with multiple applications as precursor of pharmaceuticals and explosives, could generate up to 40 kg of solid wastes in an approved industrial process.[1] Another example is the common usage of benzene as solvent, hand-cleaner and even as an aftershave, until its adverse carcinogenic properties were proved.[2]

Changes in perception of process efficacy began in 90's when Trost redefined the reaction efficiency in terms of atom economy, as the percentage of molecular mass from the reactants that are incorporated in the final product.[3] In this context, processes based on transition-metal catalysis outdo traditional stoichiometric procedures as they present the highest degree of atom economy resulting from catalyst selectivity and their economical availability. Examples of the measurement of reaction efficiency calculated with this approach are shown in Scheme I.1.[4]

[1] R. A. Sheldon, *Green Chem*. **2007**, *9*, 1273-1283.
[2] K. Alfonsi, J. Colberg, P. J. Dunn, T. Fevig, S. Jennings, T. A. Johnson, H. P. Kleine, C. Knight, M. A. Nagy, D. A. Perry, M. Stefaniak, *Green Chem*. **2008**, *10*, 31-36.
[3] B. M. Trost, *Science* **1991**, *254*, 1471-1477.
[4] (a) R. A. Sheldon, *Chem. Commun*. **2008**, 3352-3365; (b) R. A. Sheldon, *Chem. Soc. Rev*. **2012**, *41*, 1437-1451.

$$AE\ (\%) = \frac{M_{product} \times 100}{\sum M_{reactants}}$$

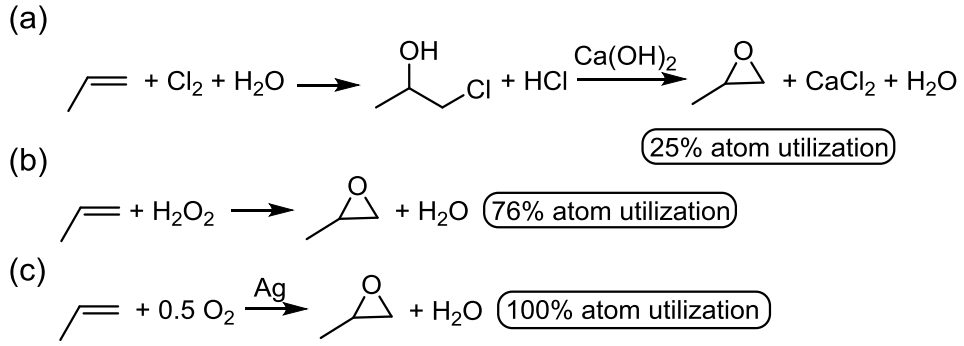

Scheme I.1. Comparison of the atom economy for three different processes to afford propylene oxide.

Additionally, increasing environmental concerns of society gave foundation to the publication of Anastas and Warner from 1998 on principles of environmentally-focused chemical processes.[5] Two main topics were mentioned: (i) the efficient utilization of raw materials with minimization of waste production through implementation of catalytic processes; and (ii) safety matters associated with the manufacture, use and disposal of chemical products with emphasis on the search for alternative reaction media to replace the most health hazardous conditions. In this way, the concept of green chemistry was coined and its principles have become relevant in chemical processes designs.

As a result, an efficient chemical process started to be understood as a procedure where minimal amount of waste was produced. In this way, more focus has been placed on prevention of environmental pollution rather than development of expensive systems for waste treatment. In this context, more global metrics such as the E-factor became commonly applied to assess the environmental impact of the chemical process.[6] By definition E-factor is the weight of waste generated in producing one kg of product, including all auxiliary reagents such as salts, catalyst(s), waste solvents and others.[7] Noteworthy, water is not usually considered as waste in this approximation. Other

[5] P. T. Anastas, J. C. Warner, *Green Chemistry: Theory and Practice*, Oxford University Press, Oxford, 1998.
[6] R. A. Sheldon, CHEMTECH **1994**, *24*, 38-47.
[7] J. Clark, R. Sheldon, C. Raston, M. Poliakoff, W. Leitner, *Green Chem*. **2014**, *16*, 18-23.

definitions of efficiency have also been developed, such as mass intensity (MI) or carbon efficiency (CE), among others,[4b] especially used by the pharma and fine chemical industries (Figure I.1).[8]

$$\mathbf{E} = \frac{\text{Total mass of waste}}{\text{Mass of final product}} \qquad \mathbf{MI} = \frac{\text{Total mass in process}}{\text{Mass of final product}} \qquad \mathbf{CE(\%)} = \frac{\text{Carbon in product x 100}}{\text{Total carbon in reactants}}$$

Figure I.1. Most commonly used metrics for process efficiency assessment.

However, atom economy and E-factor have become milestones in perception of how efficient is a given process, as they give complementary information in terms of resources usage and wastes generated.

Furthermore, rising calls for responsible management of natural resources through development of sustainable processes, has spurred the search for renewable resources such as biomass (cellulose lignin leftovers) to replace reliance on fossils, and produce biofuels, commodity chemicals and biomass-based materials like bioplastics.[2] Therefore, sustainability allows "meeting the needs of the present generation without compromising the ability of the future generations to meet their own". In terms of new chemical processes, continuous flow and cascade reactions are replacing in some extent the traditional batch production.[7]

I.2. Reaction media in a sustainable chemical process

Particular attention has been paid to the reaction medium in organic synthesis, since solvent accounts for the major source of the wasted mass (around 50%) of a given process or a synthetic pathway.[9] Moreover, organic solvents possess certain toxicity and thus are hazardous to the public health, contribute to the environmental pollution and require the development of waste treatment procedures. On the other hand usage of solvent is essential for mass and heat transfer during the reaction and affects the reaction rate and selectivity.

[8] W. J. W. Watson, *Green Chem*. **2012**, *14*, 251-259.
[9] http://www.acs.org/content/acs/en/greenchemistry/industry-business/pharmaceutical.html, ACS GCI Pharmaceutical Roundtable Solvent Selection Guide 2011.

Therefore, by taking into account two major concerns associated with the usage of organic media such as: (i) carcinogenicity of halogenated solvents, and (ii) flammability of highly volatile ones, a solvent guide was proposed by The American Chemical Society Green Chemistry Institute® Pharmaceutical Roundtable (ACS GCIPR), to replace the most health threatening with alternative solutions in order to implement the green chemistry advances worldwide (Figure I.2).[2,9]

Preferred	**Usable**	**Undiserable**
Water	Cyclohexane	Pentane
Acetone	Heptane	Hexane(s)
Ethanol	Toluene	Diisopropyl ether
2-Propanol	Methyl *t*-butyl ether	Dichloromethane
1-Propanol	Methylcyclohexane	Dichloroethane
Ethyl Acetate	Isooctane	Chloroform
Methanol	2-Methyl-THF	Dimethylformamide
Methyl ethyl ketone	Tetrahydrofuran	*N*-Methylpyrrolidine
1-Butanol	Xylenes	Pyridine
t-Butanol	Dimethylsulfoxide	Dimethyl acetate
	Acetic acid	Dioxane
	Ethylene glycol	Dimethoxyethane
		Benzene
		Carbon tetrachloride

Figure I.2. Guide to organic solvents regarding safety principles.

I.2.1. Water as solvent in organic chemistry

In this context, water has been regarded as naturally green solvent for conducting reaction processes. It presents many advantages from both economic and environmental points of view, because it is a cheap, readily available, non-toxic and non-flammable solvent.[10] Although water at ambient temperatures is considered a poor media for most organic reactants, it has been significant the increasing number of studies where its employment has contributed to: (i) improve reactivities and selectivities; (ii) simplify the work-up procedure; and (iii) recycle the catalyst.

The most prominent examples involve the considerable rate enhancement of Diels-Alder reactions conducted in so-called ‘‘on water’’ conditions, referred to the reaction carried out in water as solvent and with reactants hardly soluble in water at

[10] M. O. Simon, C. J. Li, *Chem. Soc. Rev*. **2012**, *41*, 1415-1427.

room temperature. For example, the cycloaddition of quadricyclane and dimethyl azodicarboxylate was performed in sole water affording excellent product yields in very short time, as shown in Scheme I.2a, outdoing a number of organic solvents.[11] A similar phenomenon was observed in the case of the Passerini condensation reaction of 3-methylbut-2-enoic acid, 3-methylbutanal and 2-isocyano-2-methylpropane, where the use of water furnished the expected product quantitatively within 3.5 h, as shown in Scheme I.2b.[12]

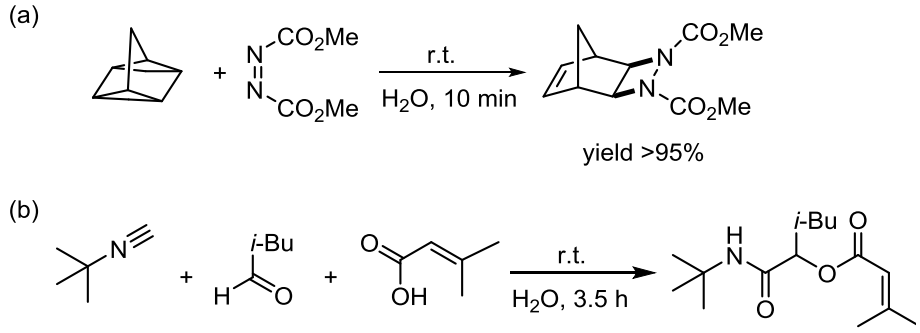

Scheme I.2. Water as solvent of choice for: (a) the Diels-Alder cycloaddition reaction; (b) for the multicomponent Passerini condensation reaction.[10] In both cases, the reactions are characterized by the negative activation volume.[13]

The observed acceleration of the reaction rate is the result of the repulsive interactions between the hydrophobic reactant molecules and water. Hydrophobic aggregates are formed to reduce the surface contact between water and the organic substrates. In turn, water molecules wrap themselves around these aggregates in attempt to maintain the network of hydrogen bonds. In this way, water acts as an internal pressure which accelerates reactions with negative activation volumes,[13] such as Diels-Alder reactions or multicomponent Passerini condensation reactions.

[11] S. Narayan, J. Muldoon, M. G. Finn, V. V. Fokin, H. C. Kolb, K. B. Sharpless, *Angew. Chem. Int. Ed*. **2005**, *44*, 3275-3279.
[12] M. C. Pirrung, K. D. Sarma, *J. Am. Chem. Soc*. **2003**, *126*, 444-445.
[13] Activation volume $\Delta V^{\neq}$ is defined as the difference between the volume occupied in the reaction transition state V_{TS} and the occupied by the reactants V_R; $\Delta V^{\neq} = V_{TS} - V_R$. The negative sign of the activation volume indicates that the reaction rate can be increased with the rising pressure in the system.

Other advantage that may possess water when used as media for organic reactions is the suppression or reduction of side reactions. For instance, this approach was employed at industrial level by Novartis for the synthesis of 1-substituted-4-cyano-1,2,3-triazoles from 2-chloroacrylonitrile and organic azides, as shown in Scheme I.3a.[10] In this transformation, the 1,3-dipolar cycloaddition is followed by an aromatization, which generates hydrogen chloride as by-product. It acts as acidic catalyst triggering polymerization of 2-chloroacrylonitrile in organic solvents which results in a decreased yield of the desired product. In this context, employment of water enabled the reaction to take place in the organic phase while the generated hydrogen chloride was solubilized in the aqueous phase, thus allowing minimization of the polymerization of the alkene.

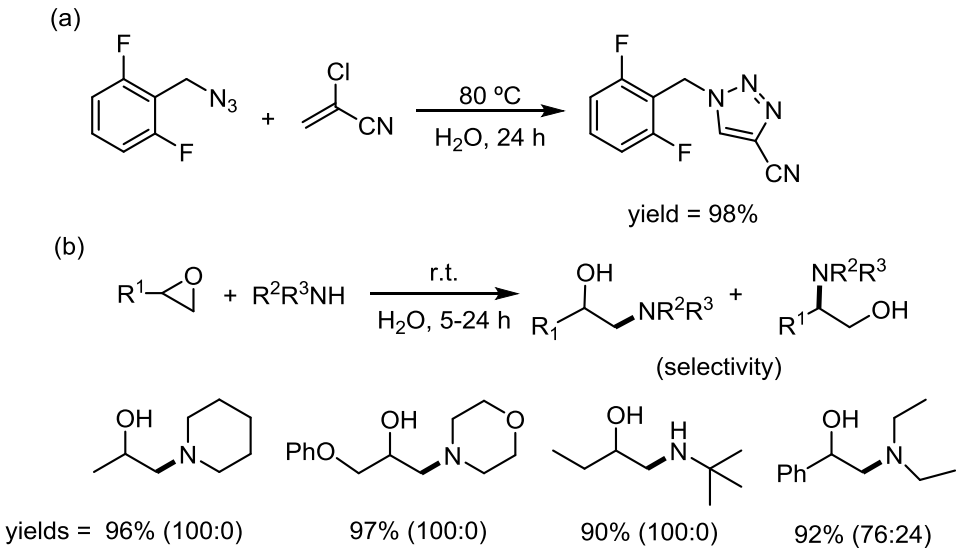

Scheme I.3. Employment of water as reaction media of organic reactions to: (a) minimize side products formation; and (b) enhance the chemo- and regioselectivity in comparison to organic solvents.

In another example, water has been successfully used as reaction media for the selective nucleophilic opening of racemic epoxides. For instance, the efficient synthesis of β-amino alcohols was achieved in high yields from the reaction of epoxides and amines in water at room temperature, as shown in Scheme I.3b. Noteworthy, a total regio- and stereocontrol was obtained in most cases.[14]

[14] N. Azizi, M. R. Saidi, *Org. Lett*. **2005**, *7*, 3649-3651.

I.2.2. Neoteric solvent systems in organic chemistry

Many new solvent systems have been developed as alternative reaction media to comply with the principles of green chemistry. An ideal sustainable and green solvent should address environmental issues and at the same time improve process in terms of: (i) reaction yields and selectivities; (ii) product separation; and (iii) recycling strategies of, *e.g.* the catalyst.[15] Transport properties (expressed as diffusion coefficient) and solvation (expressed as polarizability) are two parameters that characterize any solvent, which can be gas, liquid, or solid, capable to dissolve a solute either partially or completely. Among the different neoteric solvent systems that have been designed to simultaneously address reaction, separation and recycling challenges,[15] supercritical fluids (SCFs), gas-expanded liquids (GXLs), organic-aqueous tunable solvents (OATS), and (reversible) ionic liquids (ILs) can be mentioned. Also, water at elevated temperatures (WET) has substantially different physicochemical properties and can be employed for conducting a wide range of synthetic transformations and subsequent separations.[16]

I.3. EU legislation towards sustainable chemical processes

Tighter legislations within the European Union such as "REACH" Regulation have placed chemical industry under the control of the European Chemical Agency (ECHA). "REACH" stands for Registration, Evaluation, Authorisation and Restriction of Chemicals and it was introduced in June 2007 with the implementation phase spanned till 2018. This new law aims to ensure the highest possible protection of public health and environment from the risks that can be posed by chemicals, as well as promotion of alternative test methods, free circulation of substances on the internal market and enhancement of competitiveness and innovation.[17] REACH shifts responsibility for safety assessments from governments to industry and encourages the substitution of hazardous chemicals with safer ones for various chemical applications. The document defines hazardous substances as those that: (i) cause cancer, mutations or interfere with the body's reproductive function; (ii) take a long time to break down,

[15] P. Pollet, E. A. Davey, E. E. Ureña-Benavides, C. A. Eckert, C. L. Liotta, *Green Chem*. **2014**, *16*, 1034-1055.
[16] W. Medina-Ramos, M. A. Mojica, E. D. Cope, R. J. Hart, P. Pollet, C. A. Eckert, C. L. Liotta, *Green Chem.* **2014**, *16*, 2147-2155.
[17] ECHA, "REACH Regulation", http://echa.europa.eu/regulations/reach/understanding-reach.

accumulate in the body and are toxic; (iii) take a very long time to break down and accumulate in the body; or (iv) have serious and irreversible effects on humans and the environment, for example substances that disturb the body's hormone system. Finally, and labeled as "substances of very high concern"[18] (SVHC), can be used by companies only if they obtain authorization from ECHA and demonstrate that the risks can be adequately controlled.

By tough policy of prohibited or limited usage of certain substances, companies have been forced to seek safer alternatives. This in turn has promoted research and development of new products and technologies. Under previous regulations companies were obliged to test chemicals that entered in the European market after 1981 and those used before that year were exempt. It means that the development of new products and technologies was seen as uneconomical and therefore hampered.

Under REACH regulation, any chemical produced or imported in quantities above 1 ton per year has to be tested unless sufficient safety information already exists. The impact of REACH spans beyond the chemical industry and also implies other industries such as electronics, toys, textiles and tires to comply with new directives. For example, manufacturers and importers of toys shall ensure that the concentrations of REACH restricted substances and SVHC in their products do not exceed certain threshold limits.[19]

I.4. Biocatalysis

In the context of recently implemented legislative regulations within EU, application of Biocatalysis, as cornerstone of biotechnology, in pharmaceutical and chemical industry has gained considerable attention as a technology that meets the requirements of environmentally benign processes, showing high selectivity and

[18] ECHA, "Authorisation List," http://echa.europa.eu/web/guest/addressing-chemicals-of-concern/authorisation/recommendation-for-inclusion-in-the-authorisation-list/authorisation-list. The chemicals listed in here are: trichloroethylene, chromium trioxide, acids generated from chromium trioxide and their oligomers, sodium dichromate, potassium dichromate, ammonium dichromate, potassium chromate, sodium chromate, hexabromocyclododecane, tris(2-chloroethyl)phosphate, 2,4-dinitrotoluene, lead chromate, diarsenic pentaoxide, diarsenic trioxide, lead sulfochromate yellow, lead chromate molybdate sulphate red, bis(2-ethylhexyl) phthalate, benzyl butyl phthalate, diisobutyl phthalate, dibutyl phthalate, 5-*tert*-butyl-2,4,6-trinitro-*m*-xylene, and 4,4'-diaminodiphenylmethane.
[19] http://www.cirs-reach.com/REACH/.

conversion values.[20] The employment of enzymes in different sectors of industry either in the form of whole cell systems or isolated proteins has been known for a long time.[21] In this sense, biotechnology has delivered different enzymes and services to the food industry. Production of glucose from starch (hydrolytic enzymes), synthesis of high fructose syrup (glucose isomerase) and vitamin C (oxidoreductase), conversion of lactose to galactose and glucose (hydrolase), or cheese production (protease) are examples of these large-scale applications.[22]

Nevertheless, wider implication of Biotechnology in the pharmaceutical area has been constrained by the insufficient access to biocatalysts that could meet the industry needs. The following enzymes have been indicated as of primary interest in biotransformations for small-molecule pharmaceuticals, pharma intermediates and fine chemicals: (i) oxidoreductases such as P450 or Bayer-Villiger monooxygenases, dehydrogenases, peroxidases and enoate reductases; (ii) lyases such as aldolases (asymmetric C-C bond formation), ammonia lyases (C-N bond formation) and hydratases (C-O bond formation); (iii) transferases, such as transaminases, glucoronyl transferases and sulfotransferases.[22] Simple comparison of number of enzyme structures deposited at the Protein Data Bank (PDB) within the enzyme class in the last decade serves as indicator of the research focus, as showed in Figure I.3. However, it can be clearly seen that investigation of oxidoreductases and lyases still lies far behind hydrolases and in lesser extend to transferases.

[20] (a) S. Sánchez, A. L. Demain. *Org. Process Res. Dev.* **2011**, *15*, 224-230; (b) B. M. Nestl, B. A. Nebel, B. Hauer, *Curr. Opin. Chem. Biol.* **2011**, *15*, 187-193.
[21] U. T. Bornscheuer, G. W. Huisman, R. J. Kazlauskas, S. Lutz, J. C. Moore, K. Robins, *Nature* **2012**, *485*, 185-194.
[22] (a) R. Wohlgemuth, *Curr. Opin. Biotechnol.* **2010**, *21*, 713-724; (b) H.-P. Meyer, *Org. Process Res. Dev.* **2011**, *15*, 180-188.

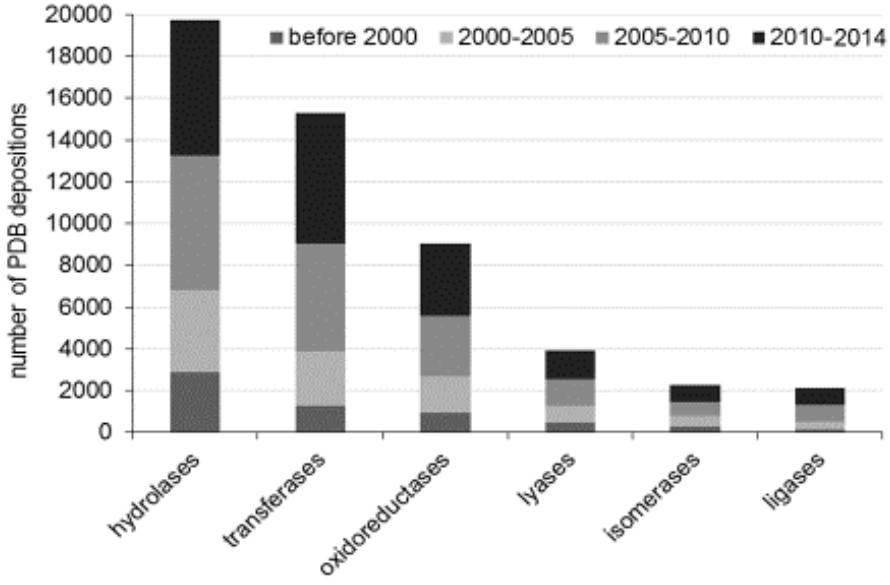

Figure I.3. Overview of enzyme structures deposited at PDB till March 2014 (based on the release data archive at http://www.rcsb.org/pdb/home/home.do).

I.4.1. Advantages and disadvantages of Biocatalysis

Biocatalysis combines many appealing characteristics that could outweigh their certain limitations. Definitely the most important advantage presented by enzymes is the high activity and selectivity resulting from the intrinsic properties of the chiral proteins. Triple-level of substrate recognition by a biocatalyst consists of chemo-, regio- and stereodiscrimination which in practice leads to shorter times of synthesis due to elimination of protection-deprotection steps, as well as cleaner work-up due to prevailed formation of only one product. In detail, chemoselectivity refers to the discrimination between different functional groups but with similar reactivity in the substrate molecule. Regioselectivity implies discrimination between two identical functional groups on the substrate molecule located at different positions. Finally, stereoselectivity allows the discrimination between two enantiotopic groups or faces of a prochiral substrate or the differentiation between two enantiomers or several diastereomers.[23]

Furthermore, most of the enzymes work at mild reaction conditions: in water around physiological pH and temperatures between 20-40 ºC, though enzymes from thermophile microorganisms exhibit a temperature tolerance up to 125 ºC. Biocatalysts are biodegradable substances obtained from renewable materials. Moreover, it is

[23] K. Faber, *Biotransformations in Organic Chemistry. A textbook*, 5th Ed., Springer, Heidelberg, **2004**.

possible to carry out sequential reactions using (multi)enzyme systems due to compatibility of enzymatic processes in the same reaction conditions.[24] In this manner, isolation of unstable intermediates can be avoided and unfavorable equilibrium can be shifted by linking several enzymatic steps together. Clear advantage of sequential reactions is the simplification of the process and reduced waste generation. Additionally, the compatibility of enzymes with other chemical catalysts has been extensively demonstrated through a myriad of chemoenzymatic *one-pot* processes.[25]

Furthermore, in many cases enzymes are able to accept a broad range of substrates apart from their natural ones, and possess considerable tolerance to organic solvents. However, for those enzymes sensitive to this medium, biphasic systems can be the method of choice to circumvent substrate solubility problems. Finally, enzymatic reaction can usually proceed in both directions since enzymes do not modify the thermodynamic equilibrium of the reaction, but act on the activation energy.

On the other hand, the same advantageous traits of enzymes also constitute their limitations. Due to the narrow operational window, changes of pH and temperature as well as salt concentrations seriously affect the enzyme activity, thus limiting options for reaction optimization. A similar drawback presents the aqueous environment, medium preferred by most of the enzymes while the majority of organic compounds are hardly soluble in water. The addition of cosolvents, either miscible or immiscible, affects to certain extent the catalytic activity of the enzyme, but still enzymatic reactions can be feasible. In terms of substrate specificity, though many non-natural substrates have been readily accepted by enzymes, no such flexibility has been shown towards cofactors, in case they are necessary. Enzyme binds mostly exclusively to their natural co-substrates such as nicotinamide NAD(P)H and ATP, which role is to carry redox equivalents or chemical energy, respectively, although some efforts have been demonstrated in order to broaden the scope to non-natural cofactors.[26] In addition, low stability of these molecules significantly contributes to the overall costs when working with cell-free extracts or isolated enzymes.

Another obstacle arises from enzyme enantiospecificity which means that in nature can be found just one form of a given enzyme made from L-amino acids, while

[24] P. A. Santacoloma, G. Sin, K. V. Gernaey, J. M. Woodley, *Org. Process Res. Dev.* **2011**, *15*, 203-212.
[25] (a) C. A. Denard, J. F. Hartwig, H. Zhao, *ACS Catal.* **2013**, *3*, 2856-2864; (b) H. Pellissier, *Tetrahedron* **2013**, *69*, 7171-7210.
[26] C. E. Paul, I. W. C. E. Arends, F. Hollmann, *ACS Catal.* **2014**, *4*, 788-797.

its natural enantiocomplementary counterpart does not exist. However, it is very common to find in nature enzymes that show stereocomplementarity as they possess "mirror-image" active sites.[27] Therefore, a desired stereospecific enzyme has to be found in tedious screenings or, since recently, by means of molecular engineering techniques.[28] They allow altering the enzyme structure to produce the opposite enantiomer, though such manipulation usually results in lower activity in comparison to the original enzyme. Another drawback associated with enzymatic processes is the inhibition caused by elevated concentrations of substrate or product in the reaction mixture, which considerably limits the efficiency of the process measured at industrial scale as space-time yield. Finally, the final goal when employing a catalyst implies its recycling to cut down the costs of the process. However, in the case of enzymes, soluble in aqueous media, their recovery is impeded unless they are immobilized.

Taken together, wide industrial application of some of the enzymes, such as cofactor-dependent oxidoreductases, faces certain hindrances. However, strategies such as *in situ* cofactor regeneration systems, usage of non-conventional media for improving substrate solubility or enzyme engineering and/or immobilization have enabled large-scale production of high added value compounds by means of biocatalysts, as shown later in this Introduction.

I.5. Thermodynamic aspects of enzyme catalysis

By analogy to other catalytic processes, enzymes act on the activation energy of the reaction by lowering the energy barrier between substrate and product. Assuming that the enzyme binds more strongly to the transition state than to the ground state of the substrate, the reaction rate is accelerated thanks to the stabilization of this transition-state by the enzyme. Stereoselectivity of the biocatalyst originates from the energy difference in the multiple enzyme-substrate complexes. Enantiotopic faces of a prochiral substrate compete for correct accommodation in the active site of the enzyme which forms a chiral environment. When diastereomeric enzyme-substrate complexes with two enantiomers [EA] and [EB] are formed, they differ in Gibbs free energy values

[27] P. F. Mugford, U. G. Wagner, Y. Jiang, K. Faber, R. J. Kazlauskas, *Angew. Chem. Int. Ed.* **2008**, *47*, 8782-8793.
[28] (a) G. A. Behrens, A. Hummel, S. K. Padhi, S. Schätzle, U. T. Bornscheuer, *Adv. Synth. Catal.* **2011**, *353*, 2191-2215; (b) M. T. Reetz, *Tetrahedron* **2012**, *68*, 7530-7548.

of their respective transition states $[EA]^{\neq}$ and $[EB]^{\neq}$. This fact results in a difference in the activation energy ($\Delta\Delta G^{\neq}$) for both orientations, which implies a faster transformation of one of them, as shown in Figure I.4.[23]

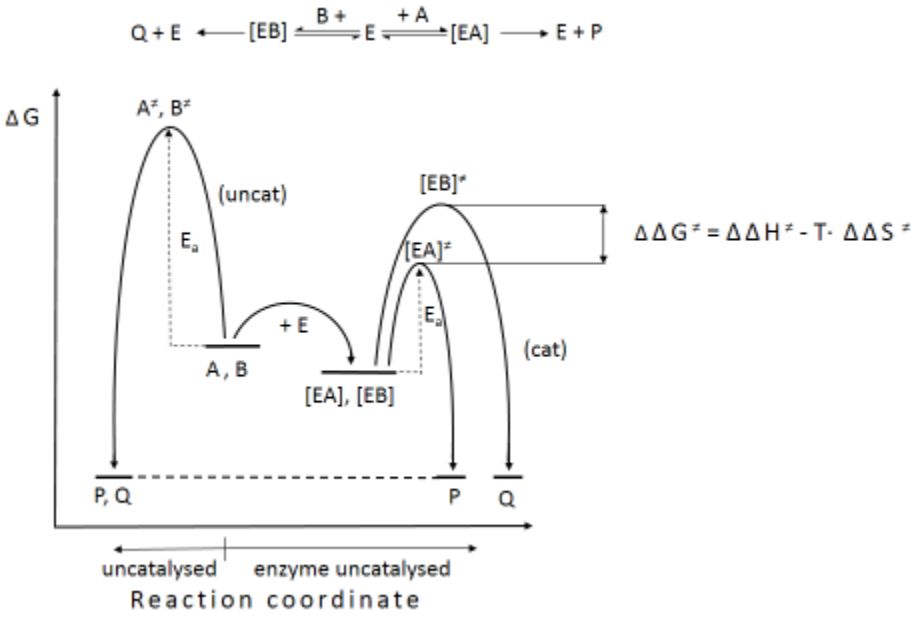

Figure I.4. Energy diagram of an enzyme-catalyzed stereoselective reaction. Enzyme (E); Activation energy (E_a); Enantiotopic faces of a prochiral substrate or enantiomers (A, B); Enzyme-substrate complex ([EA], [EB]); Transition state ($\neq$); Enantiomeric products (P, Q); Free energy, enthalpy and entropy difference between both transition states ($\Delta\Delta G^{\neq}$, $\Delta\Delta S^{\neq}$, $\Delta\Delta H^{\neq}$); Temperature (T). Adapted from reference 23.

Therefore, $\Delta\Delta G^{\neq}$ is a direct measurement of the reaction selectivity giving rise to, *e.g.* an optically pure product. Free energy difference is an indicator of the spontaneity of a reaction and is made up of two components: (i) enthalpy ($\Delta H^{\neq}$) that can be linked to the cleavage and formation of bonds during the product formation; and (ii) entropy ($\Delta S^{\neq}$) that expresses the disorder of the system through reactants reorientation and conformational changes of the enzyme. The condition for any reaction to occur spontaneously is that the difference in free energies $\Delta G^{\neq} \leq 0$, meaning that a process is favored if entropy of the system has positive sign (*i.e.* disorder of the system has increased). Nevertheless, even a thermodynamically disfavored process, which is described by $\Delta G^{\neq} > 0$, can be driven forward under certain conditions by the input of free energy. This can be achieved by a temperature change (as explained in Figure I.5a

and b) or by coupling a highly favored reaction (Figure I.5c).[29] Due to the additive character of free energy differences $\Delta G^{\neq}$, a thermodynamically disfavored (endergonic) reaction can be driven forward through a common intermediate shared by a coupled exergonic reaction (which $\Delta G^{\neq} < 0$). Provided that $\Delta G_1 + \Delta G_2 < 0$, during the progress of reaction 2 the common intermediate is removed, thus forcing reaction 1 to operate in the forward direction to replenish the equilibrium concentration of the intermediate, as shown in Figure I.5c. As will be shown later, this is the principle used to obtain high conversions in a redox process by coupling it with a second reaction thermodynamically highly favored.

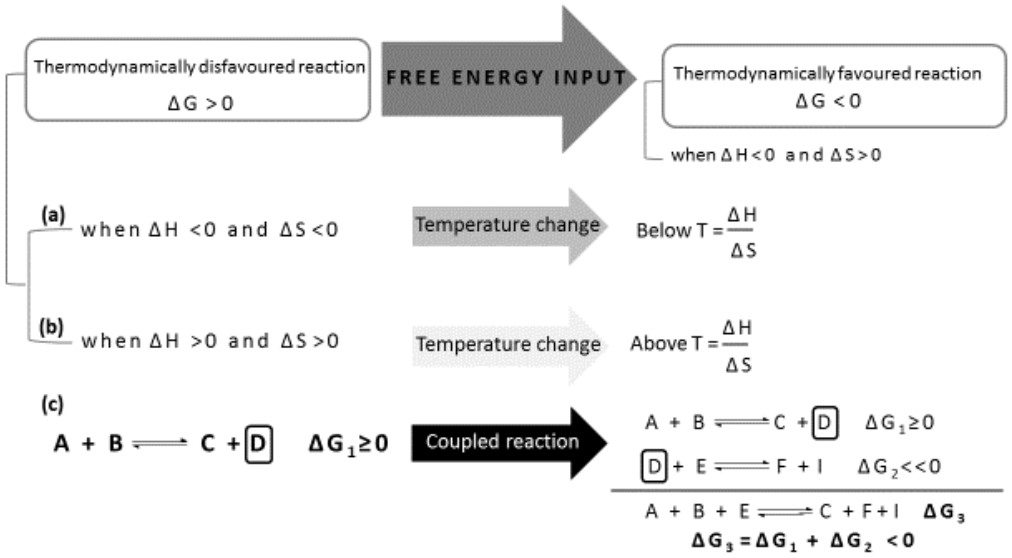

Figure I.5. Strategies to overcome the unfavorable thermodynamics of a reaction.

In case of processes at equilibrium, forward and backward reactions are exactly balanced and $\Delta G^{\neq} = 0$. Such equilibrium can be shifted by changing the reactants concentrations which also affects entropy of the system. The direction of many biological enzymatic reactions is controlled by the availability of their substrates, best examples being metabolic pathways, where by the so-called feedback inhibition, the final product controls the activity of an enzyme close to the beginning of that metabolic pathway.

[29] P. Atkins, J. de Paula, *Physical Chemistry*, 8th Ed., Chapter 3, Oxford University Press, New York, **2006**, pp. 95-109.

I.6. Enzyme classification and catalytic efficiency metrics

The widely accepted international classification of enzymes was introduced by the Enzyme Commission and consists of a four-digit number in a general form of EC A.B.C.D. that encodes the following information: (A) type of reaction catalyzed, as shown in Table I.1; (B) substrate class or type of transferred molecule; (C) co-substrate class; and (D) individual enzyme number.

Table I.1. Enzyme classification.

EC number	Enzyme class	Reaction type
1	Oxidoreductases	Oxidation of alcohols, double bonds, carbonyl groups; reduction of ketones, double bonds
2	Transferases	Transfer of amino, acyl, carbonyl, phosphoryl, glycosyl, methyl groups
3	Hydrolases	Hydrolysis-formation of esters, amides, lactones, lactams, epoxides, nitriles, anhydrides, glycosides
4	Lyases	Addition-elimination of small molecules to multiple bounds like C=C, C=N and C=O
5	Isomerases	Racemization, epimerization, rearrangement
6	Ligases	Formation-cleavage of C-O, C-S, C-N and C-C bonds with concomitant triphosphate cleavage

Information on catalytic activity is expressed as International Units (I.U.), one I.U. being equal to 1 μmol of a specific substrate transformed per minute. This has been more commonly used than the one proposed by IUPAC, *katal*, being 1 *kat* equal to 1 mol of a specific substrate transformed per second. Another value used for the description of the enzyme performance is the turnover frequency (TOF) or the catalytic constant of an enzyme (k_{cat}), which stands for the number of catalytic cycles performed by an enzyme active site per a given interval of time.[30] In other words, it indicates the number of substrate molecules converted by a single catalyst molecule during a certain time. In case of enzymatic reactions, TOF values span between 10 and 1000 s^{-1}.

[30] P. Atkins, J. De Paula, *Physical Chemistry*, 8th Ed., Chapter 23, Oxford University Press, New York, **2006**, p. 842.

Although in theory a catalyst is not used up during the process, in practice the enzyme durability is limited and therefore can be characterized by the turnover number (TON). It denotes the number of molecules of a substrate converted by a single enzyme molecule during its lifetime.

I.7. Oxidoreductases

This class of enzymes, responsible for redox transformations in living organisms, is made up of three families: (i) dehydrogenases; (ii) oxygenases; and (iii) oxidases (Figure I.6).[31] Additionally, some authors refer peroxidases as a separate family. Common feature shared by the members of oxidoreductases it their dependence on a specific cofactor molecule whose presence in the active site ensures the enzyme performance. This molecule can be transition metal ion(s) or low molecular weight organic compound(s), and some authors also call it prosthetic group when it is covalently bound to the enzyme active site. In case not, it can also be denoted as coenzyme.

However, there are known examples of cofactor-free oxygenases and oxidases such as luciferase monooxygenase from *Renilla* sp. It is believed that the mechanism of action of this enzyme involves initial substrate activation *via* base-catalyzed reaction and proceeds through "substrate-assisted catalysis", although exact details are yet to be established.[32]

[31] D. Gamenara, G. A. Seoane, P. Saenz-Méndez, P. Domínguez de María, *Redox Biocatalysis: Fundamentals and Applications*, Wiley & Sons, New Jersey, **2013**, pp. 12-18.
[32] (a) R. C. Hart, K. E. Stempel, P. D. Boyer, M. J. Cormier, *Biochem. Biophys. Res. Commun.* **1978**, *81*, 980-986; (b) S. Fetzner, R. A. Steiner, *Appl. Microbiol. Biotechnol.* **2010**, *86*, 791-804.

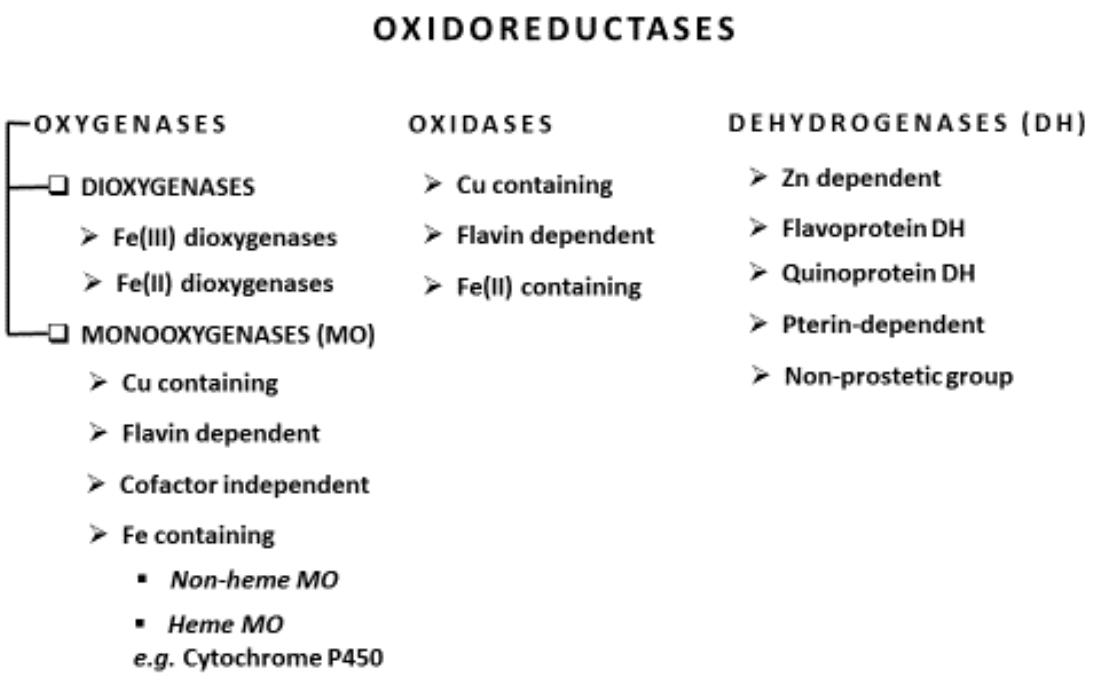

Figure I.6. Classification of oxidoreductases according to the function: (i) oxygenases catalyze the hydroxylation of non-activated C-H bonds, epoxidation or dihydroxylation of C=C double bonds; (ii) oxidases catalyze electron transfer processes; and (iii) dehydrogenases catalyze the oxidation of alcohols to ketones and formation of double bonds, as well as the reverse reductive reactions. Adapted from reference 31.

I.7.1. Cofactor regeneration

Cofactor-dependence of most of the oxidoreductases is based on the central role played by molecules like nicotinamide NAD(P), flavin FMN or FAD derivatives or pyrroloquinoline quinone (PQQ), by providing the necessary redox equivalents for a given reaction, acting as electron donor or acceptor (Figure I.7).

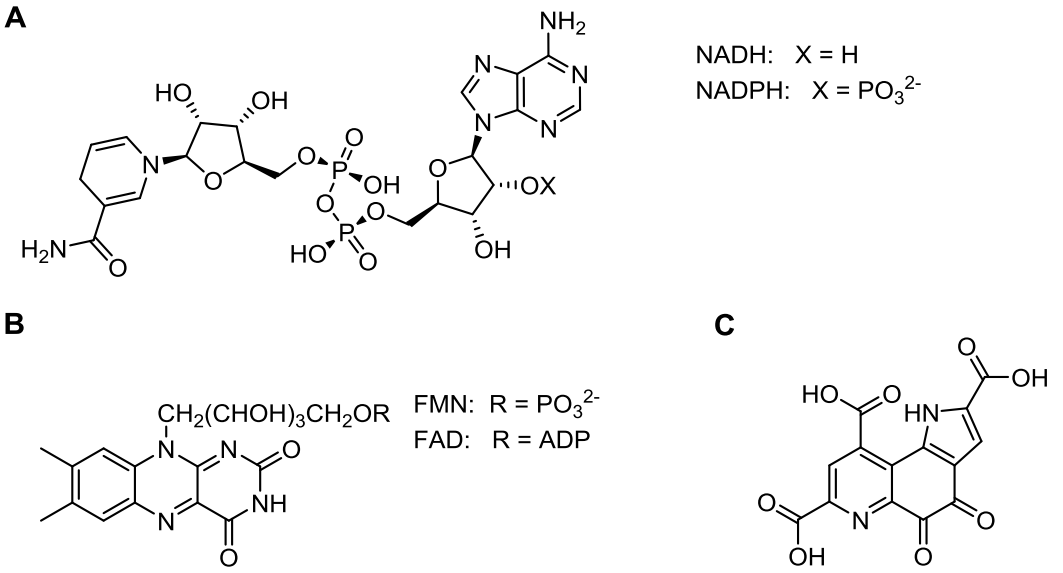

Figure I.7. Chemical structure of oxidoreductase cofactors: (A) nicotinamide; (B) flavin; and (C) pyrroloquinoline quinone.

Due to the high costs of the cofactors, industrial applications of oxidoreductases have been somehow impeded till this problem has been overcome by the development of *in situ* recycling techniques allowing the application of catalytic amounts of these compounds, as shown in Scheme I.4.

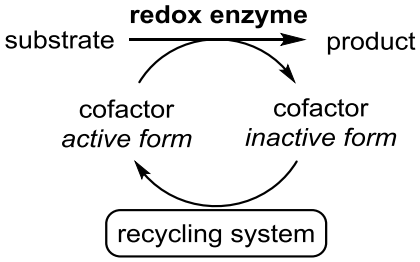

Scheme I.4. Redox process with the integrated regeneration system of the cofactor.

Among the most commonly used regeneration systems of redox cofactors, the following approaches have been described:[33]

- *electrochemical regeneration* which usually employs organic compounds or metals to perform the electron transfer between an electrode and the reduced/oxidized form of the cofactor;
- *chemical regeneration* which usually utilizes transition metal complexes of rhodium, ruthenium and platinum as electron mediator;
- *photochemical regeneration* which takes advantage of photosensitizers in homogenous phase derived from, *e.g.* zinc complexes, dies like methylene blue and coloids such as derivatives from cadmium sulfide or titanium dioxide;
- *enzymatic regeneration* which is based on the utilization of another enzyme (in the process called coupled-enzyme), for example glucose dehydrogenase (GDH) with glucose or formate dehydrogenase (FDH) with a formate salt, or employing an auxiliary co-substrate (in the process called coupled-substrate), such as 2-propanol or acetone, which is achieved by the same enzyme in ADH-catalyzed reactions, as shown in Scheme I.5.

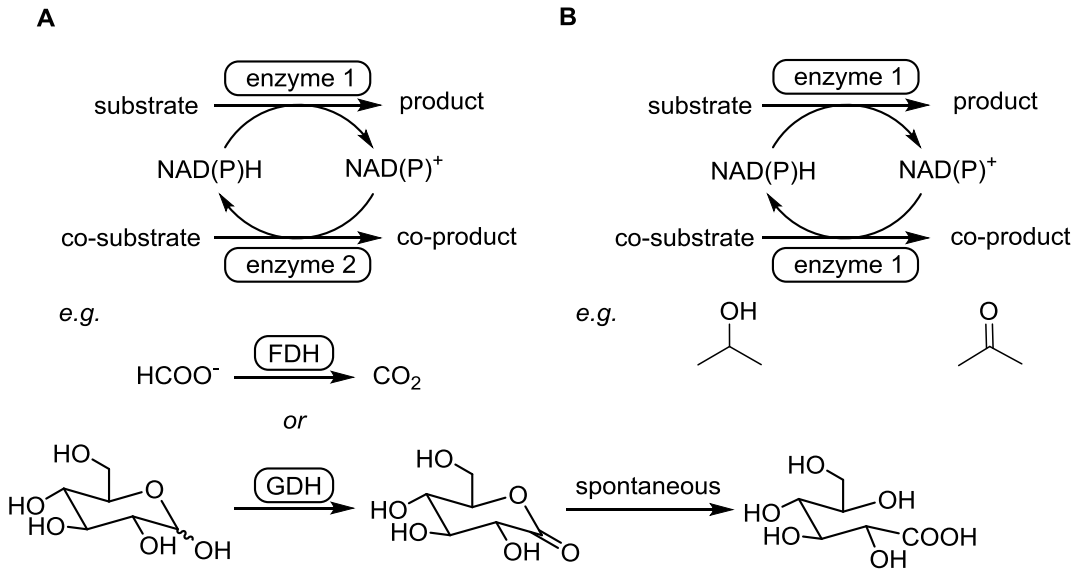

Scheme I.5. Enzymatic regeneration of the cofactor: (A) "coupled-enzyme" system; (B) "coupled-substrate" system.

[33] (a) F. Hollmann, I. W. C. E. Arends, K. Buehler, *ChemCatChem* **2010**, *2*, 762-782; (b) C. Rodríguez, I. Lavandera, V. Gotor, *Curr. Org. Chem.* **2012**, *16*, 2525-2541; (c) H. Wu, C. Tian, X. Song, C. Liu, D. Yang, Z. Jiang, *Green Chem.* **2013**, *15*, 1773-1789; (d) S. Kara, J. H. Schrittwieser, F. Hollmann, M. B. Ansorge-Schumacher, *Appl. Microbiol. Biotechnol.* **2014**, *98*, 1517-1529.

The "coupled-enzyme" system for cofactor regeneration consists of two parallel reactions that are catalyzed by different enzymes. The primary reaction involves the conversion of the substrate into the desired product, while the secondary one allows the regeneration of the cofactor at the expense of the co-substrate. This system requires that employed biocatalysts differ in substrate specificity, but present high affinity for the same cofactor, so that the potential competence reactions would not take place. Moreover, these coupled reactions are thermodynamically favored shifting the equilibrium towards the formation of the desired product, even if this process is thermodynamically disfavored.

On the other hand, in the regeneration systems based on the "coupled-substrate" process, it is the proper enzyme that constantly regenerates the cofactor due to the addition of an auxiliary co-substrate. This auxiliary substrate allows that biocatalyst performs a secondary reaction to recover the cofactor in the desired form. In this case the coupled reaction tends to be less thermodynamically favored than in the previous regeneration system, therefore it is a common practice to use a huge molar excess of the co-substrate to force the equilibrium of the primary transformation towards the desired direction.[34] In this sense, the co-substrate is usually a cheap compound and facile to eliminate once the reaction is completed.

Interestingly, laccase-mediator systems (LMS) have been reported in the recycling of the oxidized forms of nicotinamide cofactors $NAD(P)^+$ to achieve the ADH-catalyzed oxidations of glucose to gluconic acid and 1,4-butanediol to γ-butyrolactone.[35] As mediator was employed the natural phenolic compound acetosyringone together with laccase from *Myceliophthora thermophila*, which optimum activity at neutral pH was compatible with the ADH preference for pHs around 7-8. Substituted phenols at *ortho*-positions with electron donating groups such as methoxy in acetosyringone, were readily oxidized by the laccase to a stable

[34] Although some recent approaches have been used to overcome these thermodynamic limitations employing a small excess of the co-substrate. See, for instance: (a) I. Lavandera, A. Kern, V. Resch, B. Ferreira-Silva, A. Glieder, W. M. F. Fabian, S. de Wildeman, W. Kroutil, *Org. Lett.* **2008**, *10*, 2155-2158; (b) S. Kara, D. Spickermann, J. H. Schrittwieser, C. Leggewie, W. J. H. van Berkel, I. W. C. E. Arends, F. Hollmann, *Green Chem.* **2013**, *15*, 330-335.

[35] P. Könst, S. Kara, S. Kochius, D. Holtmann, I. W. C. E. Arends, R. Ludwig, F. Hollmann, *ChemCatChem* **2013**, *5*, 3027-3032.

dimethoxy phenoxyl radical ($PhO^{\bullet}$), that mediates the oxidation of the nicotinamide cofactor *via* hydrogen atom transfer (HAT).[36]

I.8. Alcohol dehydrogenases

Alcohol dehydrogenases (ADHs), also called ketoreductases or carbonyl reductases, are capable of reducing carbonyl groups into alcohols, as well as the reversible process of oxidation of primary and secondary alcohols into aldehydes and ketones, respectively. This redox reaction can be only carried out by the enzyme in the presence of the nicotinamide cofactor NAD(P)H or $NAD(P)^+$ which provides the hydride atom to the carbonyl substrate or abstract the hydride from the alcohol. In more detail, this hydride atom can be transferred in 4 different stereochemical ways to the substrate as shown in Figure I.8.

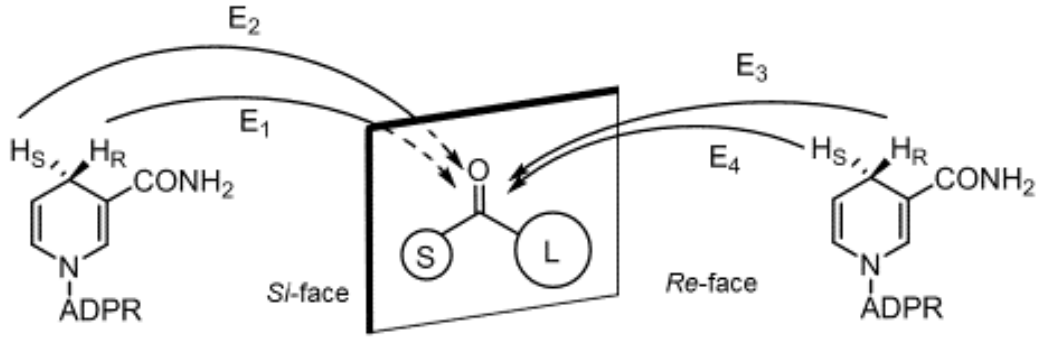

E_1: *pro*-R/*si*-face, *Pseudomonas sp.* PED, *Lactobacillus kefir* (LKADH)
E_2: *pro*-S/*si*-face, *Mucor javanicus* ADH
E_3: *pro*-R/*re*-face, yeast (YADH), horse liver (HLADH), *Rhodococcus erythropolis, Thermoanaerobacter ethanolicus, Thermoanaerobium brockii*
E_4: *pro*-S/*re*-face, plausible *Ralstonia* sp., *Sphingobium yanoikuyae* ADHs

Figure I.8. Stereospecificity of alcohol dehydrogenases is determined by the mutual position of the nicotinamide cofactor and the carbonylic substrate in the active site. Adenosine diphosphate ribose (ADPR); small substituent (S); large substituent (L) with higher priority in Cahn-Ingold-Prelog rule. Adapted from reference 31 and 37.

[36] A. I. Cañas, S. Camarero, *Biotechnol. Adv.* **2010**, *28*, 694-705.
[37] C. W. Bradshaw, H. Fu, G. J. Shen, C. H. Wong, *J. Org. Chem.* **1992**, *57*, 1526-1532.

It can attack either *Si* or *Re* face of the carbonyl group depending on the orientation of the bound substrate in the active site which results in the production of (*R*)- or (*S*)-alcohol, respectively. On the other hand, enzyme facilitates the transfer either of pro-(*R*) or pro-(*S*) hydride of the coenzyme depending on the alcohol dehydrogenase. Examples of ADHs representing different mechanisms E1-E4 are included in Figure I.8.

Importantly, stereospecificity of ADH-catalyzed reactions is classified by Prelog's rule which is based on the size of the substituents at both sides of the carbonyl group.[38] When the hydride is transferred to the *Re* face of the carbonyl group affording the (*S*)-enantiomer, the enzyme follows the Prelog's rule. In case the (*R*)-enantiomer is produced, the ADH is described as an anti-Prelog enzyme. Until now, the number of Prelog enzymes greatly exceeds in number to those that do not follow this rule.

Moreover, increasing the genetic and structural information deposited in the protein databases has allowed a more detailed classification of dehydrogenases/reductases. Based on the observed sequence motifs, chain length, mechanistic features and structure comparison, dehydrogenases have been divided into three superfamilies: (i) short chain dehydrogenases/reductases (SDR); (ii) medium chain dehydrogenases/reductases (MDR); and (iii) long chain dehydrogenases/reductases (LDR).[39]

I.8.1. Medium chain dehydrogenases (MDR)

MDR superfamily has been recently classified into numerous families, among which the most prominent are:[40] (i) MDR001 alcohol dehydrogenases (ADHs); (ii) MDR002 prostaglandin reductases (PTGR); (iii) MDR003 multidomain fatty acid synthases (FAS); (iv) MDR010 cinnamyl alcohol dehydrogenases, mannitol and sinapyl alcohol dehydrogenases (CAD); (v) MDR011 quinone oxidoreductases (QOR); (vi) MDR004 putative quinone oxidoreductases; and (vii) MDR014 threonine dehydrogenases (TDH). Gene and structure analysis[41] has allowed some generalizations

[38] V. Prelog, *Pure Appl. Chem.* **1964**, *9*, 119-130.
[39] K. L. Kavanagh, H. Jörnvall, B. Persson, U. Oppermann, *Cell. Mol. Life Sci*. **2008**, *65*, 3895-3906.
[40] J. Hedlund, H. Jörnvall, B. Persson, *BMC Bioinformatics* **2010**, *11*, 534-550.
[41] H. Jörnvall, J. Hedlund, T. Bergman, U. Oppermann, B. Persson, *Biochem. Biophys. Res. Commun*. **2010**, *396*, 125-130.

when describing dehydrogenases/reductases superfamilies. The common features shared by all members are: (i) their presence in all life forms; (ii) their low gene homology with the highly retained structural motif of the co-substrate binding known as Rossmann fold; and (iii) their dependence on ribonucleotide cofactors. In Figure I.9 representative structures of the different dehydrogenase superfamilies have been gathered to illustrate the increasing level of complexity, while retaining some common structural motifs through all groups.

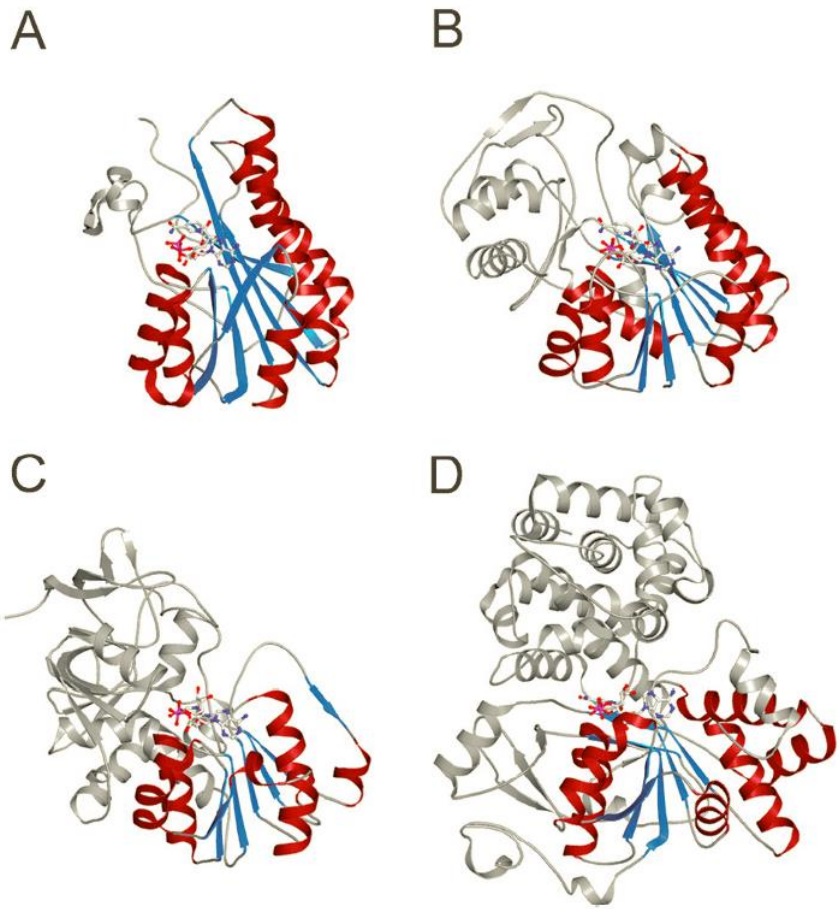

Figure I.9. Comparison of the quaternary structures from MDR superfamilies indicates the order of emergence from a universal cellular ancestor: (A) classical SDR: 3α/20β hydroxysteroid dehydrogenase; (B) extended SDR: galactose epimerase; (C) MDR: horse liver ADH; (D) LDR: mannitol dehydrogenase. Rossmann fold, which is a common structural motif among all these enzymes, has been depicted showing beta sheets in blue and alpha helices in red. Adapted from reference 39.

Typical quaternary structure for MDR proteins is a two-domain subunit, where the C-terminal domain binds the coenzyme within the Rossmann fold. This structural motif comprises of six stranded parallel β-sheets sandwiched between α-helices on each side. The N-terminal domain is the substrate binding zone with a core made of antiparallel β-strands and α-helices exposed on the outer surface. These domains are separated by a cleft containing a deep pocket which shapes the active site. MDR proteins generally form homodimers, but examples of monomers or tetramers have also been described. The metal dependence also varies between families as they can possess none, one or two Zn^{2+} ions per subunit. For example, while many MDR families bind one catalytic and one structural tetrahedral coordinated Zn^{2+} per subunit, some sorbitol dehydrogenases in the pyruvate dehydrogenase family (PDH) have only the catalytic Zn^{2+} and prostaglandin reductases in the PTGR family bind no Zn^{2+}. Additionally, structural analysis revealed correlation between Zn^{2+} content and coenzyme preference.[41] It was found that most of the MDR families with 2 zinc ions prefer NAD as cofactor and thereby they generally act as dehydrogenases. Similarly, utilization of NADP as cofactor was correlated to the absence of Zn^{2+} ions and this pattern was usually shown by reductases. Furthermore, zinc-free MDR families are typical for prokaryotic organisms while the zinc metalloenzyme MDR families have been mostly found among eukaryotes.

I.8.1.1. Role of zinc in MDRs

Zinc is a commonly found metal in metalloproteins and its distinctive physico-chemical properties define its reactivity and role for catalysis and structural stabilization. The zinc ion is stable towards reduction and oxidation due to its filled d orbitals (d_{10}), although participates in enzymatic redox reactions in combination with organic cofactors. It is a relatively strong Lewis acid (*i.e.* electron-pair acceptor) and its amphoteric character is shown by the coordination of water molecules as hydronium ions (H_3O^+) or hydroxide ions (OH^-) at physiological pH. As Lewis acid catalyst stabilizes negative charges that appear during the catalytic cycle. Coordination numbers allowed for Zn span from 2 to 8 and in proteins the most common zinc-based structures involve 4, 5 or 6 coordinated ligands. Additionally, catalytic potential of Zn^{2+} lies in

rapid ligand exchange which means fast dissociation of products and high turnover numbers.[42]

It has been distinguished four types of zinc binding sites in enzymes: (i) catalytic; (ii) co-catalytic; (iii) structural; and (iv) protein interface. Among amino acid residues commonly found as ligands to the Zn center, histidine (His), glutamic acid (Glu), aspartic acid (Asp) and cysteine (Cys) can be found. The first-shell ligands play a crucial role in the stabilization of the metal complex and in the selectivity of the binding site. In addition, they can alter the metal coordination symmetry and the substrate binding mode.

Catalytic Zn^{2+} coordinates 3 protein ligands and a water molecule, with a His residue as predominant ligand and typically two Cys. X-ray structures revealed the presence of spacing between the three ligands, which seems to have certain importance in the activation of a water molecule in the zinc active site. Water can be activated in three ways: by ionization, polarization or poised for displacement, depending on the ligands type. Mechanism involves facile four-to-five coordinate interconversion during the catalysis, where Zn acts as a Lewis acid and facilitates the zinc-bound water to ionize to a nucleophilic hydroxide in the enzyme active site, as shown in Scheme I.6.

[42] (a) M. K. Tiwari, R. K. Singh, R. Singh, M. Jeya, H. Zhao, J. K. Lee, *J. Biol. Chem*. **2012**, *287*, 19429-19439; (b) D. S. Auld, T. Bergman, *Cell. Mol. Life Sci*. **2008**, *65*, 3961-3970.

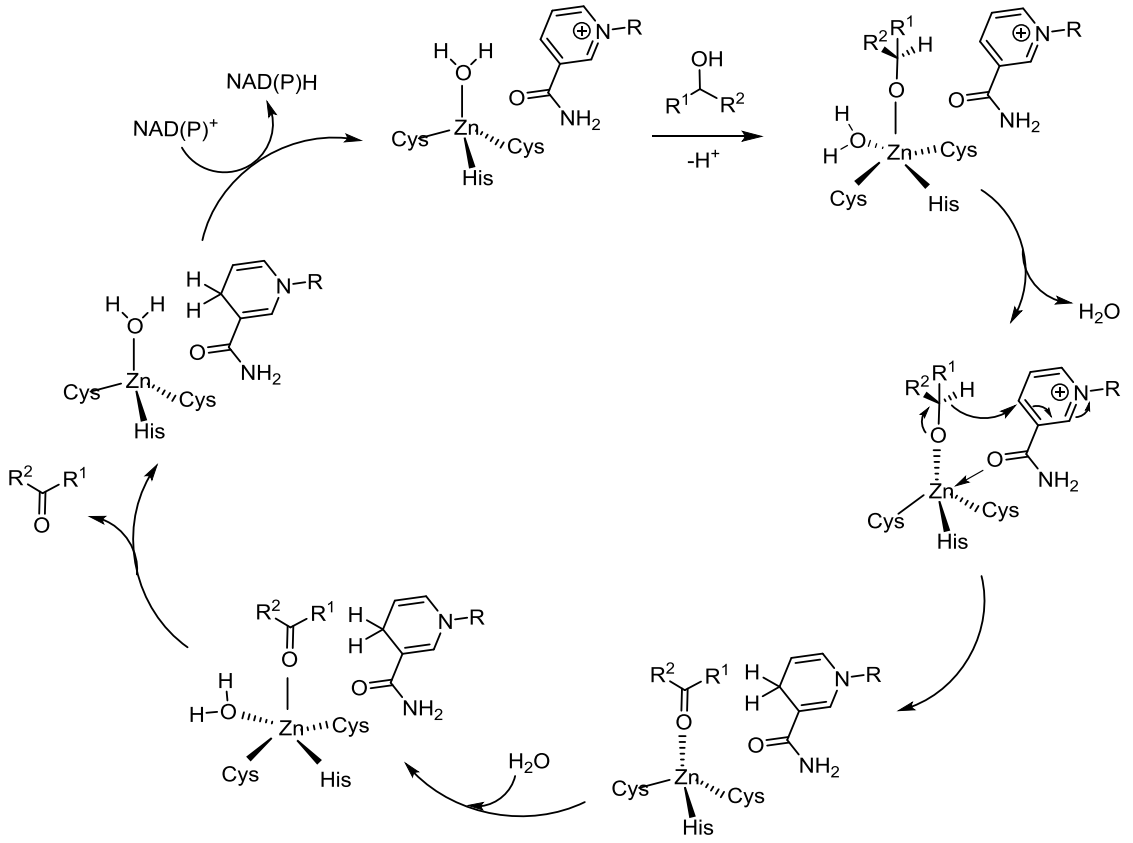

Scheme I.6. Proposed mechanism of a MDR alcohol dehydrogenase-catalyzed oxidation of a secondary alcohol. Adapted from reference 31.

In more detail, the tetrahedral coordinated zinc undergoes a geometry transition upon acceptance of the fifth ligand, the secondary alcohol prior to the water molecule release. Two hydrogen atoms from the alcohol substrate are removed in a coupled process of proton abstraction and hydride ion transfer to C4 of the nicotinamide cofactor that is accommodated in the close proximity to the zinc catalytic site. The intermediate releases the corresponding ketone product with concomitant cofactor reduction to NAD(P)H, which is replaced by another molecule of the oxidized cofactor starting a new cycle.[31]

Remarkably, the catalytic zinc, when present, possesses a double function. Apart from catalysis its occurrence contributes to the maintenance of the domains architecture for the coenzyme binding and for the conformational changes in the substrate binding site providing in this way an ordered reaction mechanism. Thus, the catalytic zinc appears to allow domain communications, compatible with the observation that catalytic zinc atoms frequently have one large, inter-ligand distance along the protein chain.

On the contrary to catalytic Zn, structural zinc sites are formed by the coordination of four amino acid residues to the metal ion and no water. The most common combination of protein ligands involves four Cys, but His, Glu and Asp have also been found in place of one Cys residue in this type of zinc-site. The presence of structural zinc-sites accounts for the proper quaternary structure maintenance in its immediate vicinity, which in turn effects the protein folding. This structure is highly conserved for all ADH families.

Co-catalytic zinc-sites are present in enzymes containing two or more metal ions in close proximity to each other and operating together with the catalytic metal site. Metal ions are bridged by sharing the side chain of a single residue such as Asp, His or through a water molecule. Importantly, these metal ions play a role not only in catalysis but also in protein stability.

Finally, zinc binding sites have also been found on the protein interface coordinating ligands in the surface between two interacting protein subunits or proteins. The significance of the protein interface zinc binding sites is based on their impact on the quaternary structure of the overall protein. The coordination properties are generally those of catalytic or structural zinc binding sites.

I.8.1.2. Alcohol dehydrogenase from **Rhodococcus ruber** *(ADH-A)*

ADH-A from *Rhodococcus ruber* (DSM 44541) exhibits a homotetrameric quaternary structure where each 38 kDa monomer hosts one structural Zn^{2+} ion coordinated by a four-cysteine cluster and one catalytic zinc at the active site closely associated to the NAD^{+} cofactor. The catalytic Zn^{2+} is coordinated by His62, Cys38, Ser40 and Asp153, as shown in Figure I.10.[43]

[43] M. Karabec, A. Łykowski, K. C. Tauber, G. Steinkellner, W. Kroutil, G. Grogan, K. Gruber, *Chem. Commun.* **2010**, *46*, 6314-6316.

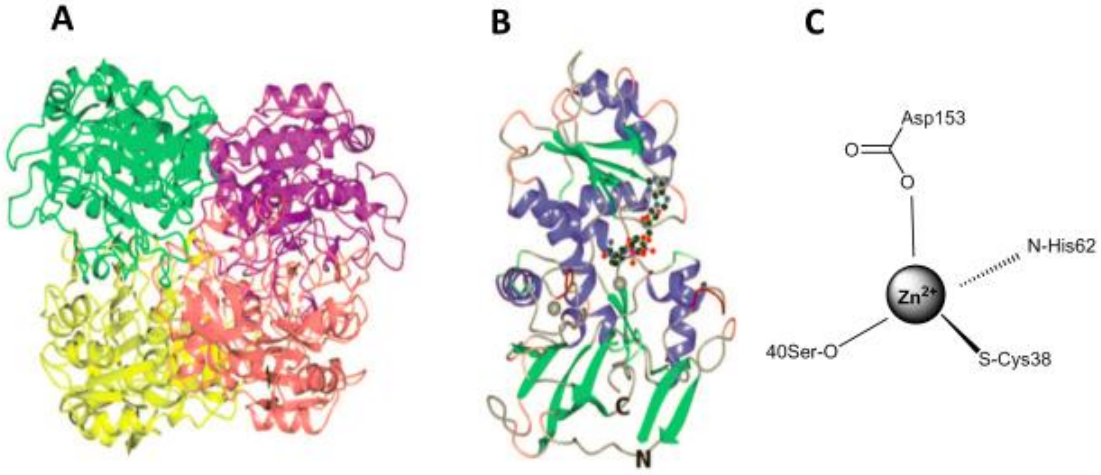

Figure I.10. Crystal structure of ADH-A: (**A**) homotetrameric structure; (**B**) monomer with NAD^+ in ball-and-stick representation; and (**C**) active site pocket with a schematic representation of the amino acids surrounding the catalytic Zn^{2+}. Adapted from reference 43.

ADH-A, discovered in 2002,[44] shows many advantageous characteristics especially valued by industrial research. It possesses NAD^+ specificity (cheaper in comparison with $NADP^+$), is thermostable, and tolerates high cosolvent concentrations such as acetone (up to 50% v/v), isopropanol (up to 80% v/v) and hexane (up to 99% v/v).[45] Moreover, this Prelog ADH accepts a broad range of substrates including aromatic and aliphatic ketones, fused bicyclic ketones, diketones, keto esters and α,β-unsaturated substrates affording the corresponding alcohols with excellent selectivities.[46] Crystallographic data reveals the structural homology to the enzymes found in thermophile organisms that inhabit harsh environments, and that could account for its extraordinary tolerance to stress caused by high organic media content. The exceptional stability of ADH-A could be ascribed to a compact structure and the presence of numerous salt bridges that connect major dimers. Hydrophobicity of the external surface seems to play a minor role based on the structural comparative studies

[44] W. Stampfer, B. Kosjek, C. Moitzi, W. Kroutil, K. Faber, *Angew. Chem. Int. Ed*. **2002**, *41*, 1014-1017.
[45] (a) B. Kosjek, W. Stampfer, M. Pogorevc, W. Goessler, K. Faber, W. Kroutil, *Biotechnol. Bioeng.* **2004**, *86*, 55-62; (b) G. de Gonzalo, I. Lavandera, K. Faber, W. Kroutil, *Org. Lett.* **2007**, *9*, 2163-2166.
[46] See, for instance: (a) W. Stampfer, B. Kosjek, K. Faber, W. Kroutil, *J. Org. Chem.* **2003**, *68*, 402-406; (b) M. Kurina-Sanz, F. R. Bisogno, I. Lavandera, A. A. Orden, V. Gotor, *Adv. Synth. Catal.* **2009**, *351*, 1842-1848; (c) J. Mangas-Sánchez, E. Busto, V. Gotor-Fernández, V. Gotor, *Catal. Sci. Technol.* **2012**, *2*, 1590-1595; (d) A. Díaz-Rodríguez, W. Borzęcka, I. Lavandera, V. Gotor, *ACS Catal.* **2014**, *4*, 386-393.

with another alcohol dehydrogenase from *Thermoanaerobium brockii* that also shows high organic solvent stabilities though lower than ADH-A.[43]

I.8.2. Short chain dehydrogenases (SDR)

Within SDR class, 5 different families exist, among which classical and extended SDRs have been further classified into subfamilies as shown in Figure I.11.[47]

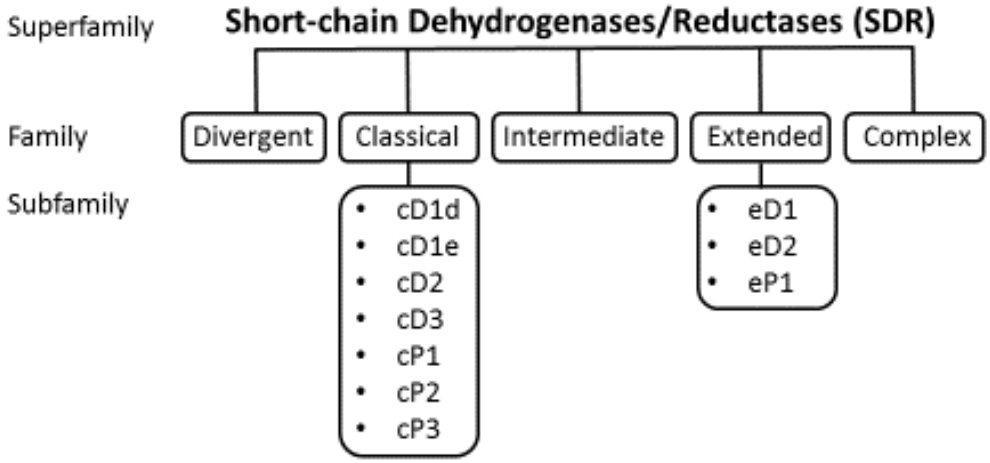

Figure I.11. SDR superfamily has been classified into 2 levels, where classical and extended SDR families have been divided into 7 and 3 subfamilies, respectively, based on the coenzyme binding residue pattern (Gly-X_3-Gly-X-Gly). Adapted from reference 47.

In contrast to MDR superfamily, SDR proteins have a simpler molecular architecture, with largely one-domain subunit without metal derived from the coenzyme-binding fold, with more or less extensions. Members of the short-chain dehydrogenase/reductase superfamily (SDR) are non-metalloenzymes with molecular masses between 25 and 35 kDa. Most of them are NAD(P)H-dependent oxidoreductases, but examples of SDR among lyases and isomerases are also known. Substrates for the short-chain oxidoreductases include steroids, prostaglandins, aliphatic alcohols and xenobiotics. Additional features of SDR enzymes are their low sequence identity among their members (maximum 30%), while retaining the structural pattern of

[47] Y. Kallberg, U. Oppermann, H. Jörnvall, B. Persson, *Eur. J. Biochem*. **2002**, *269*, 4409-4417.

previously described Rossmann fold. The highly conserved sequence regions correspond to the dinucleotide binding region and the active site catalytic triad of serine, tyrosine and lysine residues. An additionally conserved asparagine (Asn) also plays an important structural role by maintaining the active site configuration during the proton transfer.[48]

The dependence on non-phosphorylated or phosphorylated nicotinamide adenine dinucleotide cofactor has been related to the role that SDR plays. Thus, NAD^+ is exclusively employed in oxidative catabolic reactions affording ATP, while the usage of NADPH has been predominantly found in anabolic pathways of reductive biosynthesis. Additionally, the N-terminal nucleotide binding domain reveals common Rossmann fold and presents the variable sequence of Gly-X_3-Gly-X-Gly with three glycines highly conserved. NAD-specificity in oxidoreductases is dictated by the presence of a negatively charged aspartic acid residue at the C-terminus of the second β-strand. Asparagine side chain forms hydrogen bonds with both the 2'-hydroxyl and 3'-hydroxyl groups of the adenosine ribose in NAD^+. In contrast, $NADP^+$-specific enzymes lack this Asp residue in the cofactor binding domain and instead possess a positively charged arginine which favors the formation of an electrostatic interaction with the 2'-phosphate group.[49]

I.8.2.1. Mechanism of SDR catalysis

As mentioned above, the typical catalytic tetrad of the active side in a SDR is comprised of a Tyr, a Lys and a Ser, which form a proton relay system, and an Asn that plays a structural role by maintaining the Lys position in the proton relay and also by its stabilizing side chain interactions. Central to the acid/base catalysis in SDRs is the Tyr residue which abstracts or donates (in oxidation or reduction, respectively) the proton from/to the substrate, as shown in Scheme I.7. The acidity of the Tyr side chain is enhanced by the adjacent Lys residue and the positively charged nicotinamide cofactor in its oxidized state. In addition, the ε-amino group of Lys participates in binding the nicotinamide ribose group, while Ser residue stabilizes and polarizes the oxygen atom of the product resulting from the ADH reaction.[49] Finally, the carbonyl group of the main chain of Asn residue binds via hydrogen bond a conserved water molecule to the

[48] C. Filling, K. D. Berndt, J. Benach, S. Knapp, T. Prozorovski, E. Nordling, R. Ladenstein, H. Jörnvall, U. Oppermann, *J. Biol. Chem*. **2002**, *277*, 25677-25684.
[49] A. Lerchner, A. Jarasch, W. Meining, A. Schiefner, A. Skerra, *Biotechnol. Bioeng*. **2013**, *110*, 2803-2814.

Lys side chain.[48] In this way, an extended proton relay system is established connecting the bulk solvent to the Tyr residue from the active site.

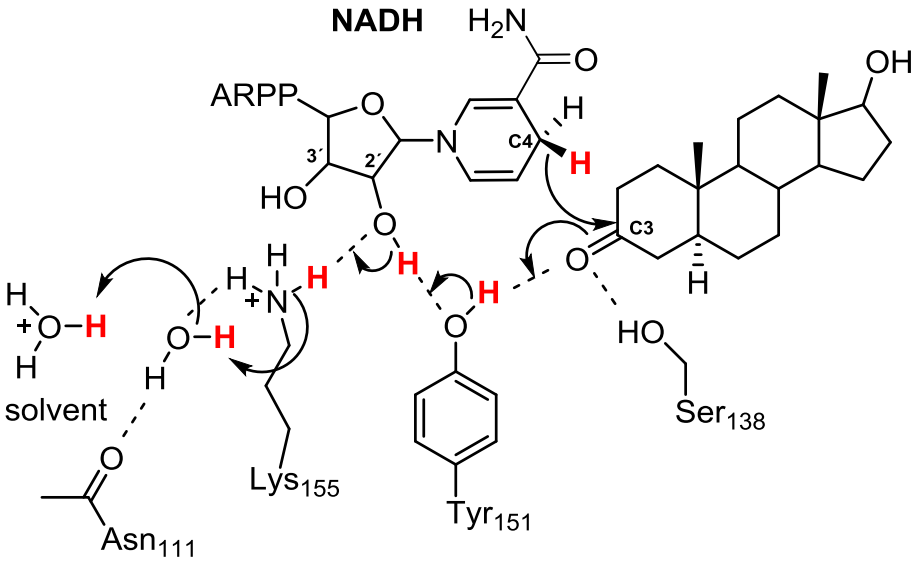

Scheme I.7. Postulated mechanism for SDR 3β/17β-hydroxysteroid dehydrogenase (3β/17β-HSD).[48] Tyr151 functions as the catalytic base, whereas Ser138 fixes the substrate, and Lys155 forms a hydrogen bond with the nicotinamide ribose moiety and lowers the pK_a of Tyr-OH to promote the proton transfer. In the 3β/17β-HSD apo structure, water molecules are bound to the Tyr and Lys side chains, mimicking substrate and ribose hydroxyl group positions. Catalytic reduction at the enzyme active site involves the following steps: (i) proton transfer from Tyr151 to the substrate carbonyl group; followed by (ii) hydride transfer from the C4 of the nicotinamide ring to C3 of the steroid; a proton relay is extended to (iii) 2'-OH of the ribose; (iv) Lys155 side chain; and (v) a water molecule bounded to the backbone carbonyl group of Asn111. ARPP means adenine ribose pyrophosphate moiety of NADH.

I.8.2.2. Alcohol dehydrogenase from Lactobacillus brevis *(LBADH)*

(*R*)-Specific alcohol dehydrogenase from *Lactobacillus brevis* is a NADPH-dependent SDR member made of 251 amino acids (family: classical; subfamily: cP2), whose function is strongly affected by Mg^{2+} ions. The crystal structure reveals the typical homotetrameric quaternary assembly and localization of two Mg^{2+} ions per each monomer of 26.6 kDa, as shown in Figure I.12.[50]

[50] K. Niefind, J. Müller, B. Riebel, W. Hummel, D. Schomburg, *J. Mol. Biol*. **2003**, *327*, 317-328.

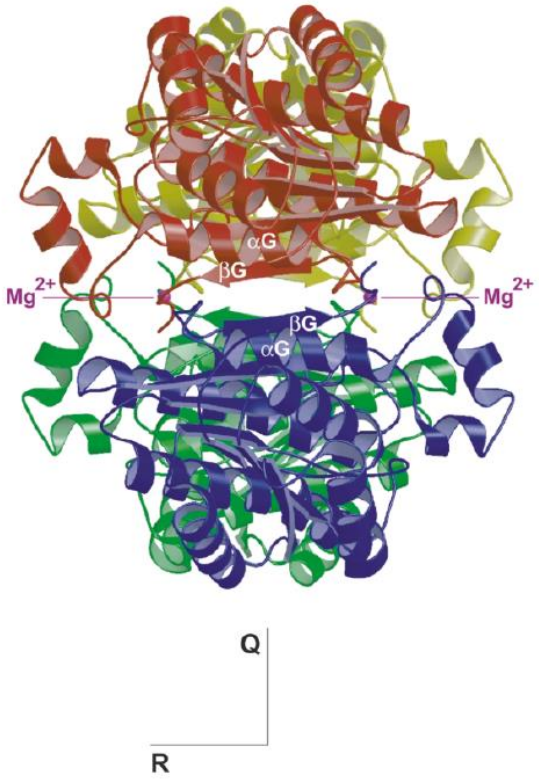

Figure I.12. Quaternary structure of LBADH showing four monomeric units comprising tetramer with two magnesium ions. Structure adapted from reference 50.

LBADH is known to accept a broad range of substrates affording the corresponding anti-Prelog alcohols with excellent selectivities, and also exhibits a remarkable thermostability.[51] ADH from *Lactobacillus brevis* is able to convert even bulky aromatic ketones with relatively high activity,[52] while shows preference towards aliphatic α-hydroxy ketones. The catalytic tetrad consists of Tyr155, Ser142, Lys159 and Asn113 residues, following the mechanism shared by other SDR enzymes. Interestingly, in LBADH structure it was established that though magnesium ion is located far away from the active site of the enzyme, through a hydrogen bonding network rising from the metal ion and expanded by water molecules in the cavities between the amino acid residues, it can provides the necessary structural stability for the activity performance.

[51] S. Leuchs, L. Greiner, *Chem. Biochem. Eng. Q.* **2011**, *25*, 267-281.
[52] C. Rodríguez, W. Borzęcka, J. H. Sattler, W. Kroutil, I. Lavandera, V. Gotor, *Org. Biomol. Chem.* **2014**, *12*, 673-681.

Lack of Mg^{+2} imposes destabilization in the direct neighborhood to the active site deactivating the enzyme. In detail, the LBADH monomer folds into a single large Rossmann fold domain with a central parallel β-sheet consisting of eight β-strands. Typical for SDR, the active site is located at the C-terminal end of the β-strands in a cleft shielded from the solvent by an extended substrate binding loop comprising helices αFG1 and αFG2. Two magnesium ions lie on the opposite sites of the R-axis (Figure I.12) and have an octahedral coordination shell of six oxygen ligands, four of which belong to water molecules in an equatorial plane. The only direct connection between Mg^{2+} and the monomer is formed by the coordination bond with one of the carboxylate oxygens from Gln251 at C-terminus end.

I.8.2.3. Alcohol dehydrogenase from Ralstonia *sp. (RasADH)*

Crystal structure of RasADH from *Ralstonia* sp. (DSM 6428) has been recently solved,[49,53] providing insight into its ability to accept "bulky-bulky" ketones[54] as substrates.[55] Previous detailed biochemical studies of the purified protein indicated on a broad optimum pH range for the reduction reaction (pH 6-9.5) and a sharp window of pH 10-11.5 for the oxidation reaction. In addition, stability studies at 25 ºC established a half-life of the enzyme at 80 h, which allows performing the typical 24 h experiments without loss of the biocatalyst activity. Since many enzymes exhibit enhanced stability upon the presence of certain ions, a thorough study found that Ca^{2+}-ions had such positive effect on this NADP(H)-dependent ADH.[56]

This enzyme shows high preference for aromatic and cyclic aliphatic compounds, such as cyclohexanone, acetophenone and 4-phenyl-2-butanone, whereas aliphatic ketones such as acetone or 2,5-hexanedione are hardly accepted (Figure I.13).[57] Reduction of aryl alkyl α-hydroxy ketones affords diols at high *ee* (>99%) and

[53] H. Man, K. Kędziora, J. Kulig, A. Frank, I. Lavandera, V. Gotor-Fernández, D. Rother, S. Hart, J. P. Turkenburg, G. Grogan, *Top. Catal*. **2014**, *57*, 356-365.
[54] By definition, the so-called "bulky-bulky" ketones possess both substituents larger than ethyl, azido-, cyano- or halomethyl groups.
[55] I. Lavandera, A. Kern, B. Ferreira-Silva, A. Glieder, S. de Wildeman, W. Kroutil, *J. Org. Chem.* **2008**, *73*, 6003-6005.
[56] J. Kulig, A. Frese, W. Kroutil, M. Pohl, D. Rother, *Biotechnol. Bioeng*. **2013**, *110*, 1838-1848.
[57] J. Kulig, R. C. Simon, C. A. Rose, S. M. Husain, M. Häckh, S. Lüdeke, K. Zeitler, W. Kroutil, M. Pohl, D. Rother, *Catal. Sci. Technol*. **2012**, *2*, 1580-1589.

de (>99%), while bulky α-substituted β-keto esters have also shown moderate to good selectivities in dynamic processes.[58]

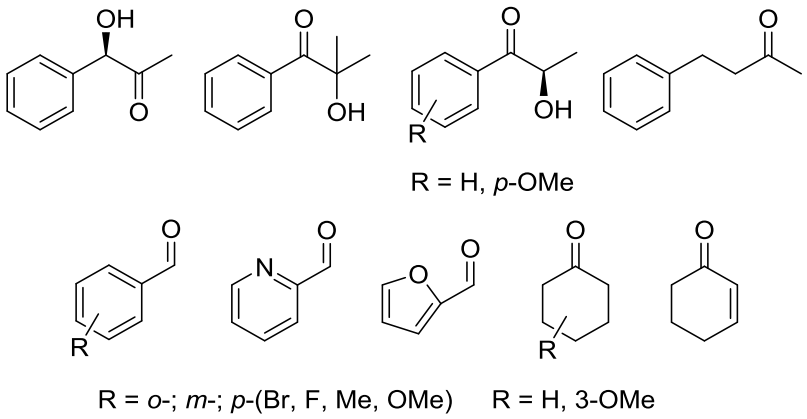

Figure I.13. Examples of substrates accepted by RasADH.[57]

Crystallographic analysis have revealed that RasADH displays an homotetrameric quaternary structure, and each monomer is made up following a classical Rossmann fold with a central β-sheet composed of seven β-strands flanked by three α-helices on each side (Figure I.14). The stability of the quaternary structure is provided by surface contact through hydrophobic side-chain interactions (stacking of α4 and α5 phenylalanines) and salt bridges between aspartate and arginine residues of neighboring monomers.

[58] A. Cuetos, A. Rioz-Martínez, F. R. Bisogno, B. Grischek, I. Lavandera, G. de Gonzalo, W. Kroutil, V. Gotor, *Adv. Synth. Catal.* **2012**, *354*, 1743-1749.

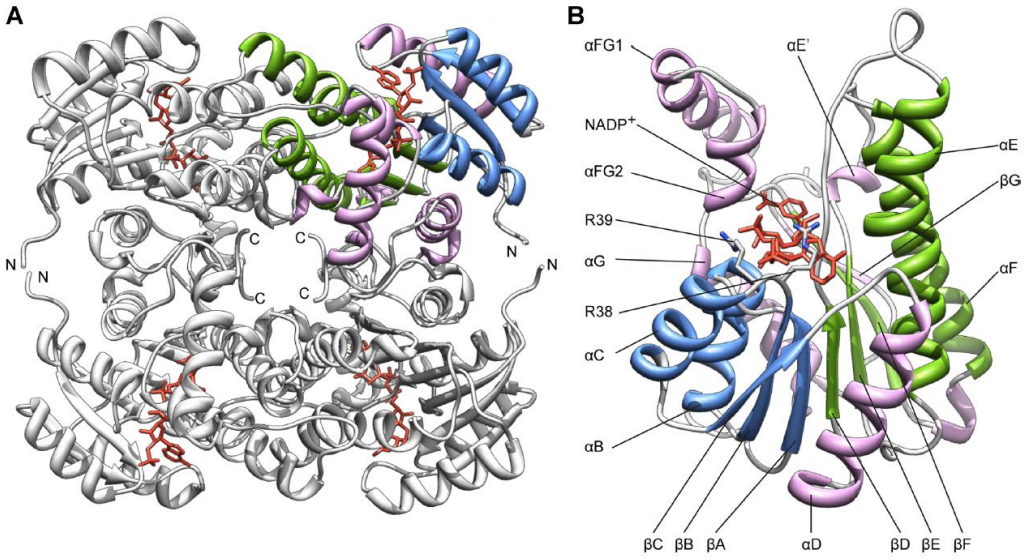

Figure I.14. Crystal structure of RasADH: (A) Tetrameric quaternary structure of RasADH with bound $NADP^+$ (red) and with one monomer colored; and (B) monomer with colored Rossmann motif elements: flanking helices (magenta) and dinucleotide binding zone (blue and green). Adapted from reference 49.

A comparative study of apo- and holoenzyme structures identified the presence of a loop over the active site that appears to act as a lid, closing over the cofactor in the holo-form of the enzyme.[49] The active site of RasADH resembles a hydrophobic tunnel that is formed at the top by the central β-sheet of the Rossmann fold. The nicotinamide ring of NADPH sits at the base of this tunnel, lined by residues forming the catalytic tetrad (asparagine, tyrosine, serine and lysine), as well as by large hydrophobic amino acids: one phenylalanine, three leucines, one valine, one isoleucine and additionally one histidine.

The strict specificity for the phosphorylated cofactor NADPH is governed by stabilizing interactions of adjacent positively charged arginine residues 38 and 39, negatively charged Asn15 and neutral Gly37. Both arginine side chains form a salt bridge with the 2'-phosphate group of $NADP^+$, while asparagine forms a hydrogen bond to the 3'-OH of the adenine nucleotide sugar of $NADP^+$ with the carbonyl oxygen of the backbone. Interestingly, it was also tried the change in its cofactor specificity replacing the glycine into asparagine, which is highly conserved in many NAD-dependent SDRs.

As a result, negatively charged Asp interacted with 2'- and 3'-hydroxyl groups of adenosine ribose of NAD^+, and electrostatically repulsed the 2'-phosphate group of $NADP^+$.

Moreover, other residues that accounted for the high affinity with the phosphate group like Arg and Asp were replaced with valine, serine and glycine. However, catalytic efficiencies achieved for new NAD-dependent RasADH variants were far inferior (by 500-fold) regarding the wild-type enzyme.

I.9. Copper-dependent oxidases

Copper and iron have been traditionally related to the field of biological oxygen chemistry and play an important role in homogeneous and heterogeneous catalysis. Proteins containing copper ions are involved in a wide range of biological oxidation-reduction processes. The scope of these reactions encompasses:

(i) reversible dioxygen binding (*e.g.*, hemocyanin);
(ii) two-electron reduction to peroxide coupled to the oxidation of a substrate (*e.g.*, amine, galactose, and catechol oxidases);
(iii) activation for hydroxylation (*e.g.*, dopamine β-hydroxylase, peptidylglycine α-hydroxylating monooxygenase, tyrosinase, and particulate methane monooxygenase);
(iv) the four-electron reduction of oxygen to water coupled to a substrate oxidation (*e.g.*, laccase, ascorbate oxidase, ceruloplasmin); or
(v) proton pumping (*e.g.*, cytochrome c oxidase, which also contains heme iron centers).[59]

In terms of structural organization of the active site, copper-dependent proteins have been divided into groups based on the number and properties of the copper ions, as presented in Scheme I.8.

[59] E. I. Solomon, P. Chen, M. Metz, S. K. Lee, A. E. Palmer, *Angew. Chem. Int. Ed*. **2001**, *40*, 4570-4590.

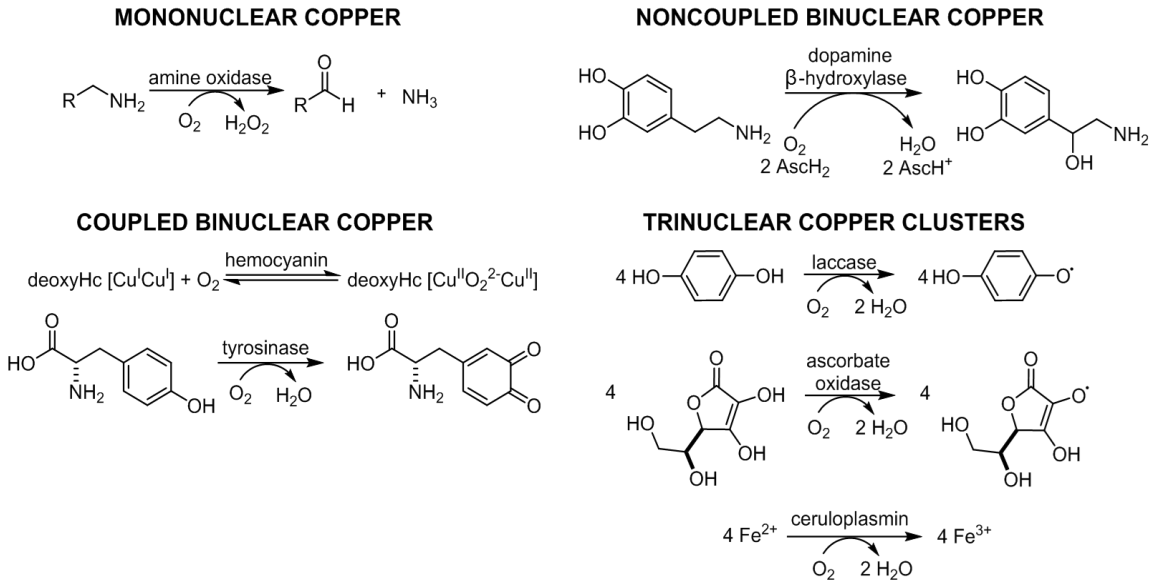

Scheme I.8. Examples of copper-dependent proteins involved in molecular oxygen binding, activation and reduction. "Coupling" here refers to the magnetic interaction between two nuclei observed in EPR spectra. Lack of such interaction indicates on a minimum 7 Å distance between both Cu^{2+} ions in the enzyme active center and lack of bridging ligation. Adapted from reference 59.

I.9.1. Laccase from *Trametes versicolor*

Laccases (*para*-diphenol:dioxygen oxidoreductases, benzenediol oxygen oxidoreductases, EC 1.10.3.2), are the simplest oxidases that belong to the family of blue multicopper oxidases, like ascorbate oxidase and human serum enzyme ceruloplasmin. These enzymes possess the capability of performing a four-electron reduction of molecular oxygen to water with simultaneous one-electron oxidation of four substrate molecules. Laccases exhibit low substrate specificity and thus can catalyze the oxidation of a broad range of phenolic substrates, such as *o*-, *p*-diphenols, polyphenols, arylamines, or methoxy-substituted phenols, affording reactive radical intermediates that easily undergo self-coupling reactions.[60] As a result, C-C and C-O dimers, oligomers and eventually polymers are formed. Laccases are produced by plants, bacteria and fungi, being involved in lignin biosynthesis (plants) and degradation

[60] (a) S. Riva, *Trends Biotechnol.* **2006**, *24*, 219-226; (b) S. Witayakran, A. J. Ragauskas, *Adv. Synth. Catal*. **2009**, *351*, 1187-1209; (c) T. Kudanga, G. S. Nyanhongo, G. M. Guebitz, S. Burton, *Enzyme Microb. Technol.* **2011**, *48*, 195-208; (d) D. Gamenara, G. A. Seoane, P. Saenz-Méndez, P. Domínguez de María, *Redox Biocatalysis: Fundamentals and Applications*, Wiley & Sons, New Jersey, **2013**, pp. 317-330; (e) M. Mogharabi, M. A. Faramarzi, *Adv. Synth. Catal.* **2014**, *356*, 897-927.

processes (bacteria and fungi). Special interest is paid to the fungal laccases as they can oxidize phenolic fragments of lignin in a direct reaction on substrates such as ferulic acid or adlerol (Figure I.15, structures **I.2** and **I.4**, respectively).

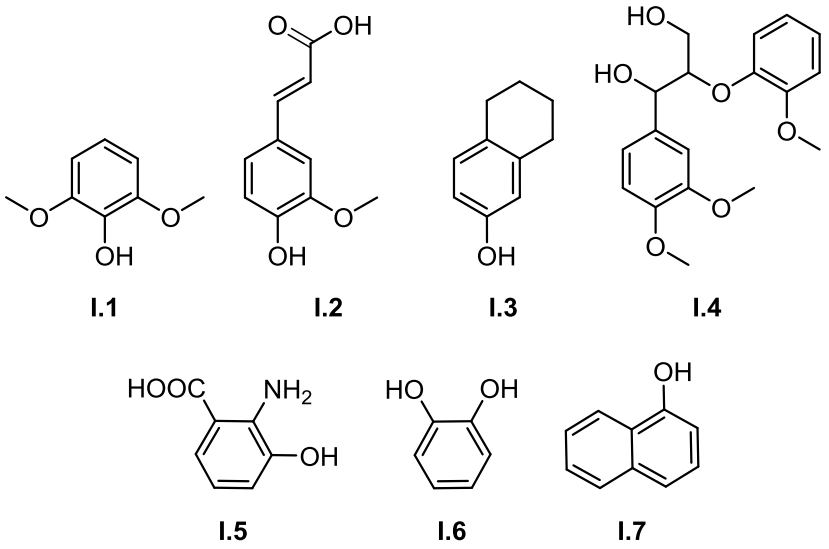

Figure I.15. Chemical structure of typical phenolic substrates for laccases: dimethoxyphenol (**I.1**); ferulic acid (**I.2**); 5,6,7,8-tetrahydronaphthalen-2-ol (**I.3**); adlerol (**I.4**); 3-hydroxyanthranilic acid (**I.5**); catechol (**I.6**); and 1-naphthol (**I.7**).

In addition, the application of laccases in oxidative processes has grown considerably since the discovery of laccase-mediator coupled systems (LMS), where a second molecule (mediator) is the primary oxidant while the laccase regenerates it by reduction of oxygen to water, as discussed in more detail in Section I.11.

The crystal structure of the native form of laccase from *Trametes versicolor* was resolved independently in 2002 by Piontek *et al.* and Bertrand *et al.*,[61] revealing a monomeric, globular glycoprotein with a molecular mass of about 70 kDa, divided into three distinguishable domains, as shown in Figure I.16. The resolved structure clearly showed four copper ions.

[61] (a) K. Piontek, M. Antorini, T. Choinowski, *J. Biol. Chem*. **2002**, *277*, 37663-37669; (b) T. Bertrand, C. Jolivalt, P. Briozzo, E. Caminade, N. Joly, C. Madzak, C. Mougin, *Biochemistry* **2002**, *41*, 7325-7333.

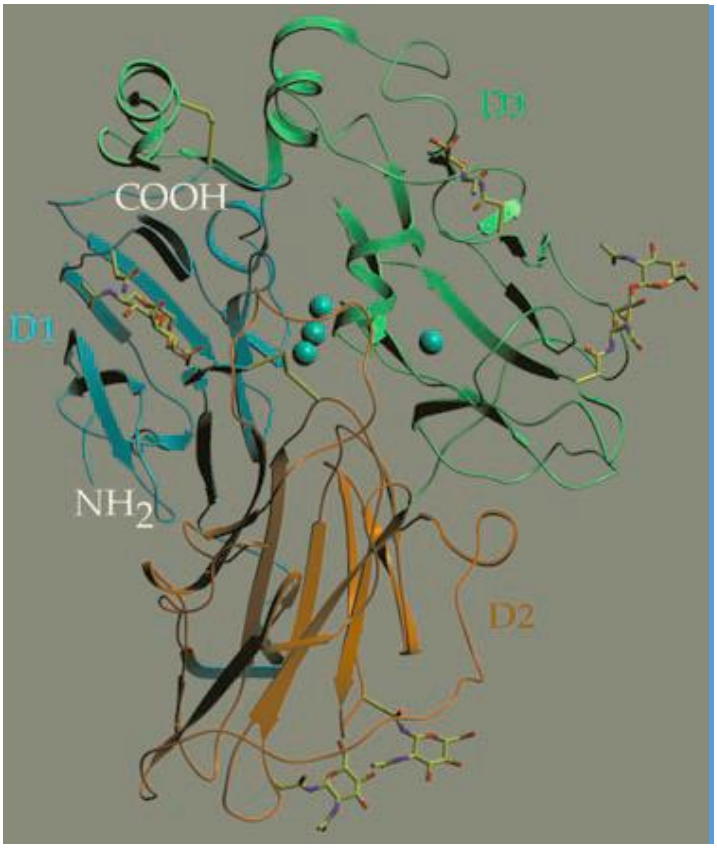

Figure I.16. Crystal structure of native laccase from *Trametes versicolor* reveals a monomeric protein comprised of 3 domains (colored in blue, green and gold), and 4 copper ions (blue balls) with visible glycosylation sites (stick representation) on the peripheries of the protein. Adapted from reference 61a.

These copper ions were divided into three groups based on their spectroscopic properties. Type 1 (T1) copper (Cu1) is tightly coordinated to a cysteine and produces an intense absorption band around 600 nm, that accounts for the enzyme characteristic color. Type 2 (T2) copper (Cu2) and type 3 (T3) coppers (Cu3a and Cu3b) form a perfect trigonal cluster, in which Cu2 is EPR-active, while the pair of hydroxide-bridged T3 coppers are EPR-silent in the presence of molecular oxygen (Figure I.17). Spatial separation of T1 Cu from the trinuclear cluster (TNC) site corresponds to the different role played by the copper ions. Cu1 participates in the substrate oxidation and is localized on domain 3 (D3), while Cu2, Cu3a and Cu3b are embedded between domains 1 (D1) and D3 acting as oxygen reduction site.

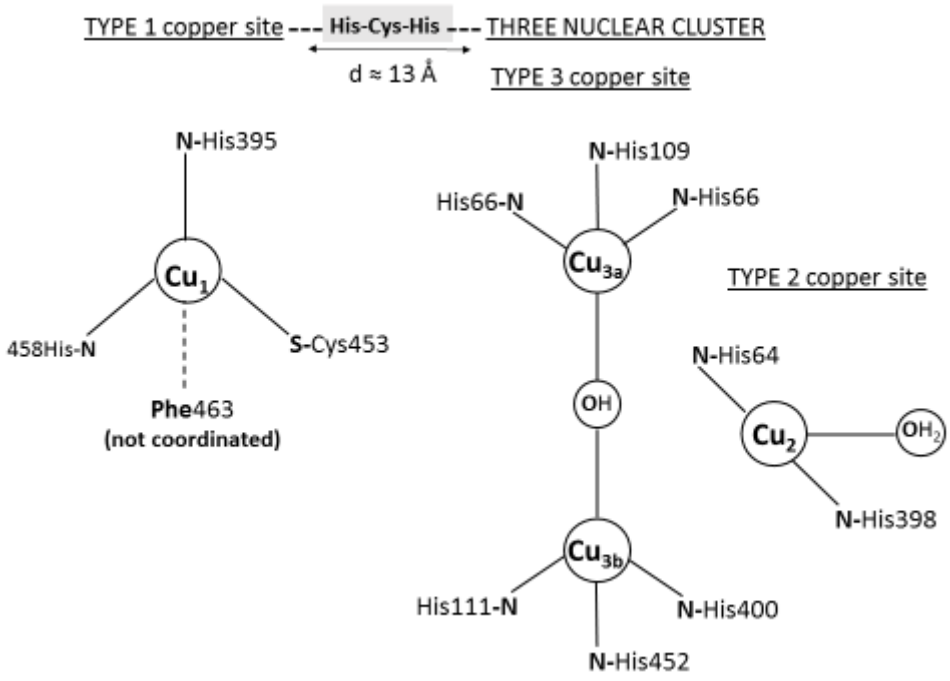

Figure I.17. Schematic representation of the active site in the laccase from *Trametes versicolor*. It is comprised of four Cu ions arranged in: (i) a T1 Cu site; and (ii) a trinuclear Cu-cluster composed of a T2 Cu and two T3 Cu bridged by a hydroxide anion. T1 Cu center is 13 Å away from the trinuclear cluster, but linked to it through an electron-transfer pathway (T1─His─Cys─His─T3). Adapted from reference 61b.

Closer analysis of Cu1 environment shows a trigonal planar coordination to two histidines (His395 and His458) and a cysteine (Cys453), while nearby exists the presence of a phenylalanine (Phe463) in the axial position. T1 Copper is connected to the trinuclear cluster by a His-Cys-His tripeptide, which is highly conserved among blue multicopper oxidases. In the case of Cu3a and Cu3b, both are coordinated to three histidine residues and bridged through an oxygen atom in a coordination sphere that can be best described as distorted tetrahedral. Finally, Cu2 is coordinated to only two histidines, and to a labile water molecule forming a trigonal coplanar configuration (Figure I.17). Additionally, extensive mechanistic studies of the laccase-catalyzed molecular oxygen reduction to water have allowed gaining insight into the reaction pathway.[62]

[62] (a) S.-K. Lee, S. DeBeer George, W. E. Antholine, B. Hedman, K. O. Hodgson, E. I. Solomon, *J. Am. Chem. Soc*. **2002**, *124*, 6180-6193; (b) J. Yoon, L. M. Mirica, T. D. P. Stack, E. I. Solomon, *J. Am. Chem.*

I.10. Nitroxyl radicals

Nitroxyl radicals or nitroxides can be defined as *N*,*N*-disubstituted NO radicals with an unpaired delocalized electron between the nitrogen and the oxygen atom,[63] stabilized by both thermodynamic and kinetic effects. The delocalization of the free electron is stabilized by resonance as shown in Figure I.18. Additionally, depending on the character of R^1 and R^2 groups, the unpaired electron can be further delocalized over these substituents. R^1 and R^2 can be primary, secondary or tertiary alkyl groups. Nitroxides bearing heteroatom substituents or aryl substituents are less stable than the alkyl-substituted nitroxides. In fact, delocalization of the radical into the aromatic ring weakens the nitrogen-oxygen bond in diaryl-substituted nitroxides. Historically, the first stable nitroxide radical was Fremy's salt (compound **I.8**, Figure I.18), synthesized in 1845.[64] In 1901, the first organic nitroxide, namely porphyrexide (compound **I.9**, Figure I.18), was prepared.[65] Later, the synthesis of 4-oxo-2,2,6,6-tetramethylpiperidine-*N*-oxyl radical (4-oxy-TEMPO) was accomplished in 1959 by Lebedev and Kazarnovsky,[66] an important contribution to the field of nitroxide chemistry (structure **I.11**, Figure I.18), as this compound can catalyze the oxidation of primary and secondary alcohols to the corresponding carbonylic compounds.

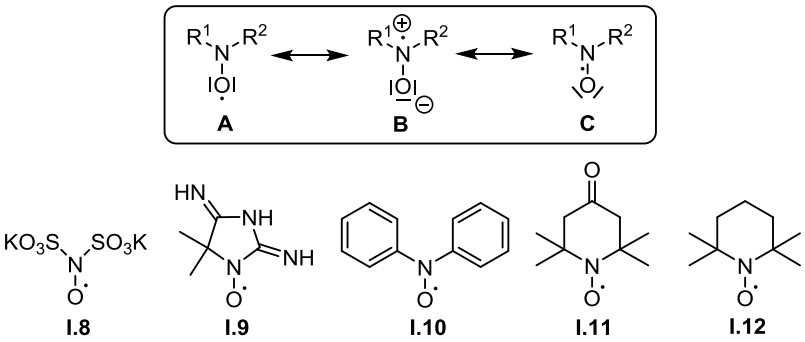

Figure I.18. A-**C** represent resonance structures of a nitroxyl radical. Below appear the chemical structures of stable nitroxides, *i.e.* persistent radicals: potassium nitrosodisulfanate (**I.8**); porphyrexide (**I.9**); diphenylnitroxide (**I.10**); 4-oxy-TEMPO (**I.11**); and 2,2,6,6-tetramethylpiperidine-*N*-oxyl radical (TEMPO, **I.12**).[67]

Soc. **2005**, *127*, 13680-13693; (c) D. E. Heppner, C. H. Kjaergaard, E. I. Solomon, *J. Am. Chem. Soc*. **2013**, *135*, 12212-12215; (d) D. Gamenara, G. A. Seoane, P. Saenz-Méndez, P. Domínguez de María, *Redox Biocatalysis: Fundamentals and Applications*, Wiley & Sons, New Jersey, **2013**, pp.54-56.

[63] T. Vogler, A. Studer, *Synthesis* **2008**, 1979-1993.

[64] E. Fremy, *Ann. Chim. Phys.* **1845**, *15*, 408.

[65] O. Piloty, B. G. Schwerin, *Ber. Dtsch. Chem. Ges.* **1901**, *34*, 1870.

[66] O. L. Lebedev, S. N. Kazarnovsky, *Tr. Khim. Khim. Tekhnol.* **1959**, *3*, 649.

The N-O bond in these radicals is described as a 3-electron-2-centre bond showing partial double bond character (1.23-1.29 Å versus 1.20 Å in double bond). As a result, dimerization is thermodynamically disfavored since the stabilization effect in the nitroxide cannot be compensated by the relatively low contribution of the O-O bond energy in the dimer. Steric effects can also stabilize nitroxides such in the case of TEMPO, due to the four α-methyl groups flanking the access to the nitroxide moiety, hampering a possible reaction between two radical molecules. Nitroxides are weak Brønsted bases and the oxygen atom is only partially protonated under strong acidic conditions. They act as Lewis bases since they function as ligands for metal ions. Electrochemical studies have revealed that many nitroxides undergo reversible oxidation to oxoammonium salts (E, Scheme I.9), while irreversible reduction to aminoalkoxide anions (D, Scheme I.9), heavily dependent on the pH of the reaction mixture.

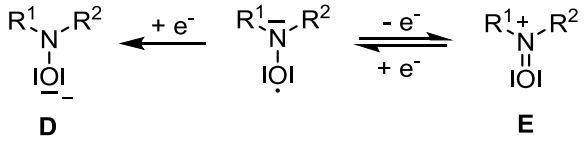

Scheme I.9. Electrochemical reduction (irreversible) of a nitroxide to an aminoalkoxide anion and oxidation (reversible) to an oxoammonium salt.

Nitroxyl radicals are readily prepared from the secondary amines through direct oxidation using metal-based catalysts (W, Mo, V) and stoichiometric amounts of H_2O_2 or other peroxides.[67] Nitroxides have found application in the oxidation of primary and secondary alcohols, although the radical form is a weak oxidant itself. In fact, it is the direct precursor of the oxoammonium salt which is the active oxidizing species.

I.11. Laccase-mediator oxidation systems

As already mentioned, laccases can be applied in synthetic chemistry: (i) as direct oxidant of phenolic substrates; (ii) as indirect oxidant of non-phenolic substrates acting through mediator molecules that are actually the oxidant species (Scheme I.10). An effective redox mediator should possess the following characteristics: (i) be a good

[67] L. Tebben, A. Studer, *Angew. Chem. Int. Ed*. **2011**, *50*, 5034-5068.

laccase substrate; (ii) its oxidized (radical) form should have sufficiently long half-life to permit its diffusion towards the substrate; (iii) possess a high oxidation potential to effectively oxidize the target substrate; and (iv) be cheap and commercially available.[68]

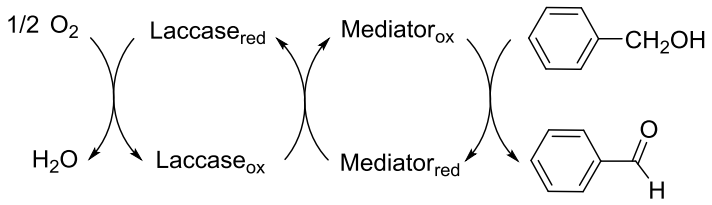

Scheme I.10. Role of a mediator coupled with a laccase.

As described previously, the laccase substrate, in this case the mediator, undergoes one electron oxidation at the T1 copper site, which has a redox potential of the Cu^{II}/Cu^{I} pair of ca. 0.8 V versus the normal hydrogen electrode for some fungal laccases (*e.g.*, *Trametes hirsuta* or *Trametes versicolor*). In comparison, the redox potential for the Cu^{II}/Cu^{I} pair in aqueous solution is ca. 0.15 V. Consequently the T1 copper(II) center in fungal laccases can oxidize such compounds like TEMPO to the corresponding oxoammonium cation which has a redox potential of 0.75 V.

In general these mediators can be divided into 3 groups depending on the mechanism of action.[36] 2,2-Azinobis-(3-ethylbenzothiazoline)-6-sulfonic acid (ABTS), was the first mediator[69] proved to mediate the laccase-catalyzed oxidation of 3,4-dimethoxybenzyl alcohol to the corresponding aldehyde *via* electron transfer (ET) mechanism (Scheme I.11).[70] ET route proceeds through the formation of the radical cation of the substrate and is truly a redox reaction, therefore the redox potential of the substrate should be preferably low.[68]

[68] P. Giardina, V. Faraco, C. Pezzella, A. Piscitelli, S. Vanhulle, G. Sannia, *Cell. Mol. Life Sci.* **2010**, *67*, 369-385.
[69] R. Bourbonnais, M. G. Paice, *FEBS Lett.* **1990**, *267*, 99-102.
[70] R. A. Sheldon, I. W. C. E. Arends, *J. Mol. Catal. A: Chem.* **2006**, *251*, 200-214.

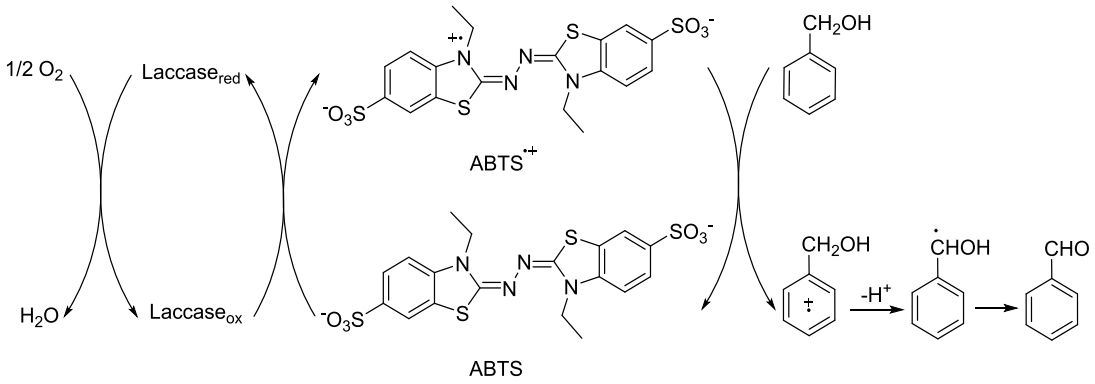

Scheme I.11. ET mechanism steps: (i) laccase oxidizes the mediator molecule ABTS to its radical cation; (ii) subsequently it reacts with the target substrate and abstracts an electron from it (in this case benzyl alcohol). In this way ABTS is regenerated and can enter in another cycle again, while (iii) the radical cation of the substrate molecule releases protons affording the final aldehyde.

A second group of mediators is formed by (di)acyl *N*-hydroxyl amines like *N*-hydroxyphthalamide (NHPI), violuric acid (VLA), 1-hydroxybenzotriazole (HBT) or *N*-hydroxyacetanilide (NHA), which are precursors of *N*-oxyl radicals generated *in situ* by laccases following a radical hydrogen atom transfer (HAT) mechanism. It is believed that one-electron laccase-catalyzed oxidation of the mediator molecule affords an intermediate radical cation that upon release of the proton gives rise to the nitroxyl radical, as shown in Scheme I.12.[70]

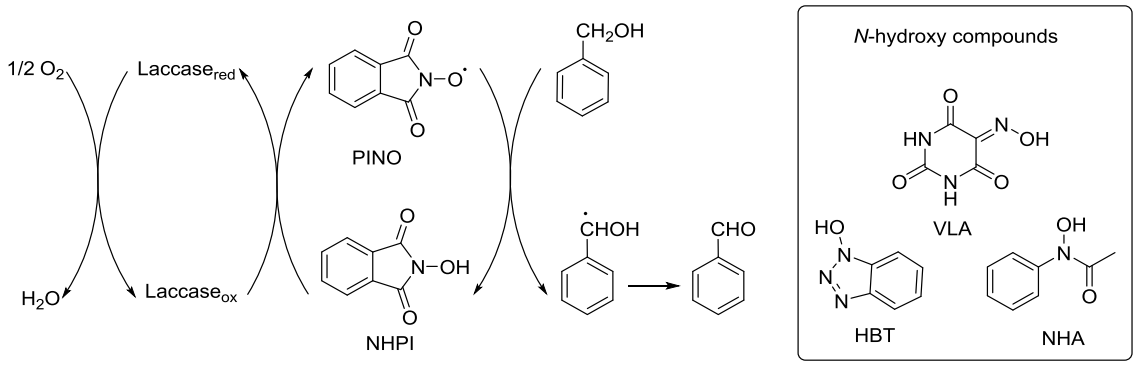

Scheme I.12. Radical hydrogen atom transfer mechanism involves the formation of transient *N*-oxyl radicals from *N*-hydroxy mediators such as NHPI, VLA, HBT or NHA. Since the driving force of the radical HAT is the enthalpic balance between the dissociated C-H bond in the target molecule and the forming NO-H bond in the mediator, the preferable substrates should possess relatively weak C-H bond.[36]

The relative instability of these radicals can be linked to their high redox potential which in turn reflects the bond dissociation energy (BDE) of the O-H bond. For example, NHPI has a redox potential of 1.01 V due to the high BDE of the O-H (86 kcal/mol, in comparison to *N*-hydroxy TEMPO, 70 kcal/mol), which in turn comes from the resonance stability of the N-OH species in NHPI through intramolecular hydrogen bond formation. This accounts for the high radical reactivity of PINO, being able to abstract a hydrogen atom from many organic compounds as the reaction is exothermic, though at the expense of a decreased stability of the radical intermediate (Scheme I.13).[71]

[71] S. Wertz, A. Studer, *Green Chem*. **2013**, *15*, 3116-3134.

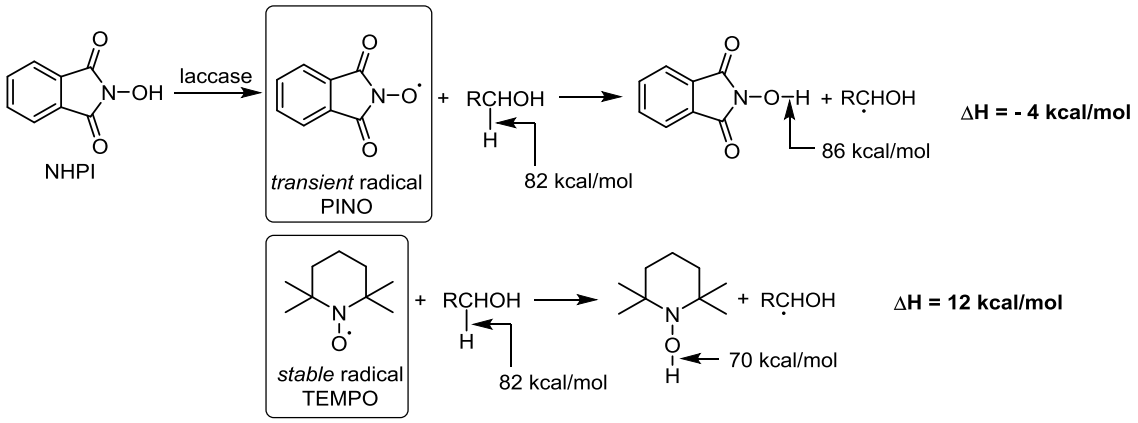

Scheme I.13. Thermodynamic explanation for the disfavored radical HAT mechanism in the case of stable nitroxyl radicals such as TEMPO in comparison to transient radicals such as PINO.

The third group of mediators is made up of dialkyl nitroxides that form stable nitroxyl ($NO^{\bullet}$) radicals, such as TEMPO (**I.12**, Figure I.18), as shown in Figure I.19.

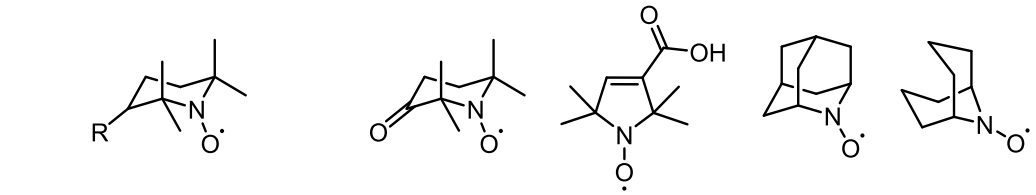

Figure I.19. Selected chemical structures of *N*-oxyl mediators derived from TEMPO.

The mechanism of action of TEMPO and its analogues is different from the previously shown for diacyl hydroxyl amines due to the much lower BDE values for their O-H bonds. As a result, the thermodynamic driving force for the direct hydrogen abstraction from the substrate by TEMPO is low. Radical HAT mechanism would be highly endothermic and therefore disfavored, as shown in Scheme I.13.[72] It was proved that laccase oxidizes dialkyl nitroxide radical into non-radical-ionic oxoammonium ion

[72] F. d'Acunzo, P. Baiocco, M. Fabbrini, C. Galli, P. Gentili, *Eur. J. Org. Chem*. **2002**, 4195-4201.

intermediate that acts over the substrate (Scheme I.14).[73] Thus, a nucleophilic attack of the hydroxyl group of the alcohol on the electrophilic nitrogen atom of the oxoammonium species forms an adduct. Next, it is deprotonated either in an intramolecular way by transient N-O$^-$ formed or in a intermolecular manner by a base from the reaction medium to afford the carbonylic product and hydroxylamine species TEMPOH. The final TEMPO radical is regenerated *via* comproportionation between the hydroxylamine and the oxoammonium ion.

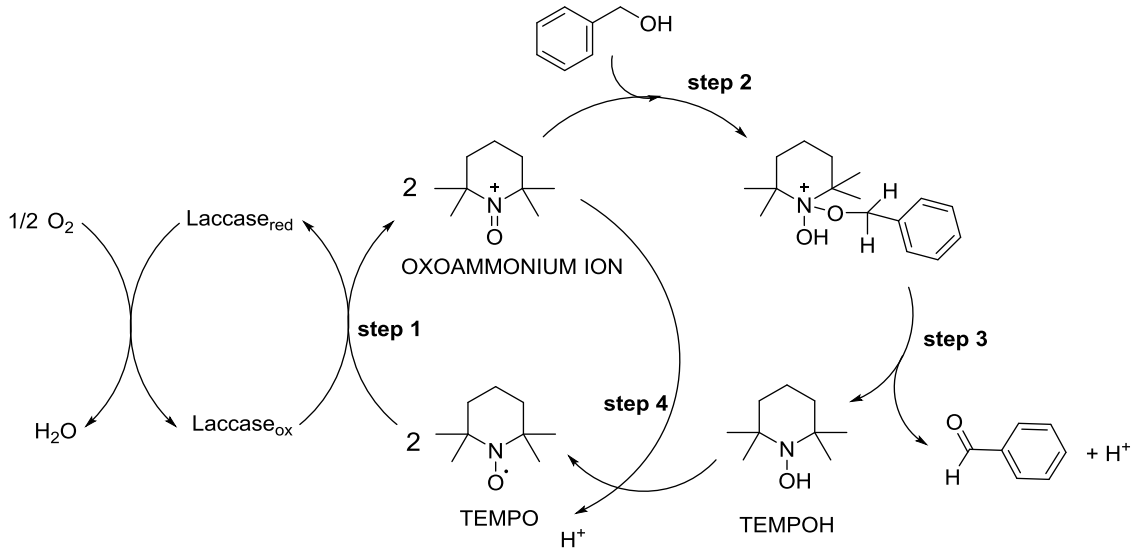

Scheme I.14. Laccase/TEMPO mediated oxidation of benzyl alcohol based on a 4-step process: (1) Oxidation of TEMPO radical to oxoammonium cation; (2) nucleophilic attack of the hydroxyl group of the substrate onto TEMPO-oxoammonium ion to form an adduct; (3) deprotonation of the adduct to afford the carbonylic product and TEMPOH; (4) spontaneous comproportionation of hydroxylamine and oxoammonium ion to form 2 molecules of TEMPO radical.

The important implications stemming from the ionic mechanism is that the redox potential of the alcohol does not play a role.[74] Rather steric hindrance presented by the

[73] S. A. Tromp, I. Matijošyte, R. A. Sheldon, I. W. C. E. Arends, G. Mul, M. T. Kreutzer, J. A. Moulijn, S. de Vries, *ChemCatChem* **2010**, *2*, 827-833.
[74] (a) M. Fabbrini, C. Galli, P. Gentili, *J. Mol. Catal. B: Enzym*. **2002**, *16*, 231-240; (b) I. W. C. E. Arends, Y. X. Li, R. Ausan, R. A. Sheldon, *Tetrahedron* **2006**, *62*, 6659-6665; (c) M. B. Lauber, S. S. Stahl, *ACS Catal.* **2013**, *3*, 2612-2616; (d) J. Gross, K. Tauber, M. Fuchs, N. G. Schmidt, A. Rajagopalan, K. Faber, W. M. F. Fabian, J. Pfeffer, T. Haas, W. Kroutil, *Green Chem*. **2014**, *16*, 2117-2121.

mediator and/or the substrate can influence the reaction outcome,[75] as well as the mediator stability.[74b] The preference for primary over secondary alcohols has been widely reported for laccase-TEMPO oxidation systems, as well as the preference for benzylic rather than aliphatic alcohols.[72,76] This can be ascribed, at least partially, to the minor steric hindrance during the formation of the adduct coming from the attack of the alcohol to the oxoammonium species.

I.12. Non-enzymatic-TEMPO oxidation systems

A large number of different inorganic and organic co-oxidants have been used for the two-electron oxidative regeneration of the oxoammonium ion from TEMPOH.[67,71,77] A catalytic amount of TEMPO in combination with a stoichiometric co-oxidant has been used in most cases. One of the original works that used TEMPO as catalytic oxidant (1-5% mol) of alcohols was performed by Anelli *et al.*,[78] who applied sodium hypochlorite as stoichiometric co-oxidant in the presence of bromide salts as co-catalyst in biphasic media (CH_2Cl_2), as shown in Scheme I.15.

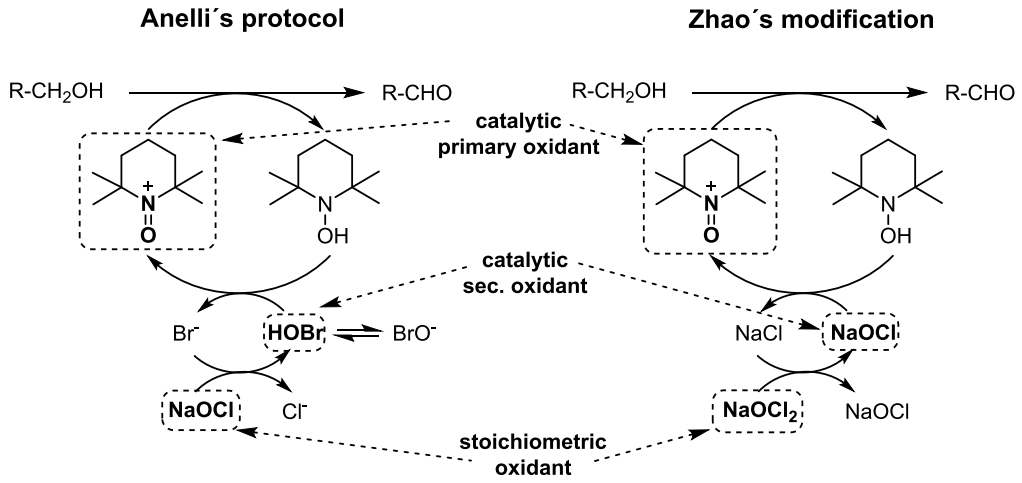

Scheme I.15. Examples of catalytic oxidations with TEMPO in non-enzymatic systems.

[75] C. Zhu, Z. Zhang, W. Ding, J. Xie, Y. Chen, J. Wu, X. Chen, H. Ying, *Green Chem*. **2014**, *16*, 1131-1138.
[76] A. Díaz-Rodríguez, I. Lavandera, S. Kanbak-Aksu, R. A. Sheldon, V. Gotor, V. Gotor-Fernández, *Adv. Synth. Catal.* **2012**, *354*, 3405-3408.
[77] (a) F. Minisci, F. Recupero, A. Cecchetto, C. Gambarotti, C. Punta, R. Faletti, R. Paganelli, G. F. Pedulli, *Eur. J. Org. Chem.* **2004**, 109-119; (b) C. Jin, L. Zhang, W. Su, *Synlett* **2011**, 1435-1438.
[78] (a) P. L. Anelli, C. Biffi, F. Montanari, S. Quici, *J. Org. Chem.* **1987**, *52*, 2559-2562; (b) P. L. Anelli, S. Banfi, F. Montanari, S. Quici, *J. Org. Chem.* **1989**, *54*, 2970-2972.

In this protocol the regeneration of the oxoammonium ion is performed by hypobromite produced from the oxidation of bromide by NaOCl. Although the system proves to be efficient for the oxidation of primary alcohols, the strong chlorination tendency of hypochlorite of more sensitive substrates comprises serious limitations of this protocol. Zhao's modification circumvents this undesired side effect by the employment of a catalytic amount of NaOCl, while using sodium chlorite ($NaOCl_2$) as stoichiometric oxidant, as shown in Scheme I.15.[79]

Another example of aerobic oxidation of benzylic and allylic alcohols using TEMPO was presented by Semmelhack, whose procedure involved the usage of cuprous chloride (CuCl) as catalyst to generate the oxoammonium ion in *N*,*N*-dimethylformamide (DMF).[80] In a first description, it was assumed that Cu(I) was oxidized by oxygen to Cu(II), which in turn oxidized TEMPO that performed the oxidation of the corresponding alcohol. However, a revised mechanism (Scheme I.16) postulates a copper-centered oxidative dehydrogenation of the alcohol rather than an oxoammonium cation-based oxidation.[70] The key step in the oxidation process is the intramolecular hydrogen abstraction within an alkoxycopper(II)-TEMPO complex. This produces a coordinated ketyl radical anion and TEMPOH followed by an internal electron transfer affording Cu(I) and the carbonylic product.

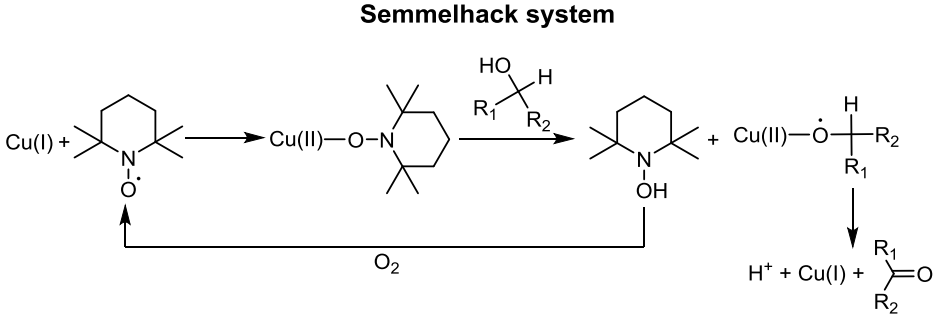

Scheme I.16. Mechanism of the Semmelhack's oxidation system.

I.13. Industrial applications of oxidoreductases

Creating complex product from simple starting materials with a minimum number of steps by avoiding protection-deprotection loops is an objective of any

[79] M. Zhao, J. Li, E. Mano, Z. Song, D. M. Tschaen, E. J. J. Grabowski, P. J. Reider, *J. Org. Chem*. **1999**, *64*, 2564-2566.
[80] M. F. Semmelhack, C. R. Schmid, D. A. Cortés, C. S. Chou, *J. Am. Chem. Soc.* **1984**, *106*, 3374-3376.

industrial process. Solutions delivered by biocatalytic protocols have been proved efficient and working under mild conditions. For those reasons, pharmaceutical industry shows special interest in the production of fine chemicals with defined stereogenic centers by employment of biocatalysts.[8,20] Oxidoreductases in combination with aminotransferases have been applied in industrial production of chiral alcohols, amino alcohols, amino acids and amines. Monooxygenases have been used to perform enantioselective and stereoselective hydroxylations, epoxidations and Baeyer-Villiger reactions. Diooxygenases have been utilized in the chemoenzymatic synthesis of chiral diols.[22a,81] Moreover, protein engineering has greatly contributed to the higher scope of enzymatic processes incorporated into the pharma sector, allowing the access to pharmaceutically active ingredients with high yields and optical purities. For example, ADH performance has been improved by direct evolution techniques in terms of activity, stability and coenzyme specificity, being employed in the production of intermediates such as **I.13** and **I.14** for large-scale production of atorvastatin (Lipitor) by Kaneka and Codexis (Figure I.20). This medicine is being used in cholesterol-lowering treatment as it acts as inhibitor of 3-hydroxy-3-methyl-glutaryl-CoA reductase (HMG-CoA), which plays a central role in cholesterol production in liver.

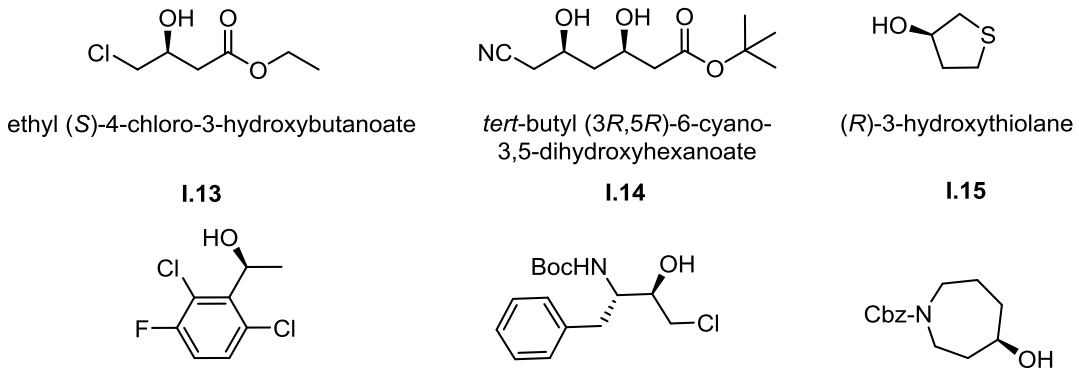

Figure I.20. Industrial application of ADHs in the production of active pharmaceutical intermediates (APIs).[21]

Other engineered ADHs have allowed accessing intermediates **I.15** and **I.16** which are intermediates of sulopenem-type antibiotics and crizotinib (drug prescribed

[81] R. N. Patel, *Coord. Chem. Rev*. **2008**, *252*, 659-701.

for non-small lung cell cancer), respectively. Intermediate **I.17** has been used for the production of atazanavir, an antiretroviral drug for HIV treatment by Bristol Myers Squibb and Codexis. Finally, intermediate **I.18** has been synthesized in a large scale process by Merck as a precursor of a novel β-lactamase inhibitor, drugs used in combination with β-lactam antibiotics (like penicillin) to prevent certain bacteria strains from breaking down the β-lactam ring and extend the activity of these antibiotics.

On the other hand, interest in broader applications of laccases and LMS as oxidation systems, stems from their potential to catalyze polymerization reactions. Examples of monomers used in these reactions include: catechol derivatives, 2,6-dimethylphenol, flavonoids such as rutin and catechin, coumarins, 1-naphtol, acrylamide, 2-hydroxydibenzofuran, bisphenol A, 8-hydroxyquinoline and aniline.[82] In addition to self-coupling reactions, cross-coupling between two different molecules and domino reactions are other types of radical pathways triggered by laccases. As a result reactive intermediates are trapped and do not give rise to the usual dimers or oligomers.

Potentially interesting applications of laccase biocatalysis in food industry can enhance the color appearance due to their oxidative potential towards carbohydrates, phenols, and thiol-containing compounds. For example, laccase-based processes include baking, juice processing and wine stabilization (cork stoppers with fungal laccases for wine bottles). Other fields of wider application of laccases are pulp bleaching, delignification and bioremediation of contaminating environmental pollutants, for example proceeding from textile industry. Furthermore, these enzymes can be found in the cosmetic industry as substitute of hydrogen peroxide as oxidizing agent in hair dye formulations. For instance, fungal laccases have been employed to obtain yellow to brown coloration *via* enzymatic oxidation of flavonoids such as morin, quercetin and rutin (polyphenol compounds) into quinones. Finally, laccase-based processes present a tremendous potential for the synthesis of fine chemicals and biologically active compounds such as amino acids, antibiotics and antioxidants at mild reaction conditions.[60e]

[82] D. Gamenara, G. A. Seoane, P. Saenz-Méndez, P. Domínguez de María, *Redox Biocatalysis: Fundamentals and Applications*, , Wiley & Sons, New Jersey, **2013**, pp. 327-346.

CHAPTER I

Bioreductions of α,α-dihalogenated ketones catalyzed by alcohol dehydrogenases

Introduction

Halogenated ketones are versatile building blocks in organic synthesis,[83] giving access to a wide family of compounds such as alcohols or keto esters. In this Chapter, the synthesis and bioreduction of a variety of α,α-dihalogenated ketones will be conducted. For that reason, a brief introduction regarding the state of the art for enzymatic reductions of the related substrates has been undertaken.

1.1.1. Bioreduction of α-halo ketones

Prochiral substituted α-halo ketones represent an attractive starting point to target more complex molecules of biological interest, in which one or more stereocenters can be defined depending on the reaction conditions. As described previously, application of oxidoreductases in synthetic processes at industrial and academic level has undergone significant changes due to key advances in cofactor design[26,84] and regeneration strategies,[33,85] the possibility of biocatalyst modification through enzyme engineering being also of great relevance to achieve the asymmetric synthesis of the aim enantiopure alcohols.[28b,86]

Recently, Moody and coworkers from Almac Sciences have applied a panel of commercially available recombinant enzymes to selectively reduce various *N*-protected derivatives of (*S*)-3-amino-1-chloro-4-phenylbutan-2-one.[87] The corresponding alcohols (Scheme 1.1) were obtained with high diastereomeric excess (*de*). For instance, the (2*S*,3*S*)-diastereoisomer is a precursor of different compounds of pharmacological interest such as amprenavir and fosamprenavir, while the (2*S*,3*R*)-diastereoisomer constitutes the basic skeleton of atazanavir. All mentioned compounds have demonstrated biological activity in the treatment of infections caused by human immunodeficiency virus (HIV).

[83] B. I. Roman, N. De Kimpe, C. V. Stevens, *Chem. Rev.* **2010**, *110*, 5914-5988.
[84] T. Quinto, V. Köhler, T. R. Ward, *Top. Catal.* **2014**, *57*, 321-331.
[85] M. Richter, *Nat. Prod. Rep.* **2013**, *30*, 1324-1345.
[86] S. Lutz, *Science* **2010**, *329*, 285-287.
[87] E. Alanvert, C. Doherty, T. S. Moody, N. Nesbit, A. S. Rowan, S. J. C. Taylor, F. Vaughan, T. Vaughan, J. Wiffen, I. Wilson, *Tetrahedron: Asymmetry* **2009**, *20*, 2462-2466.

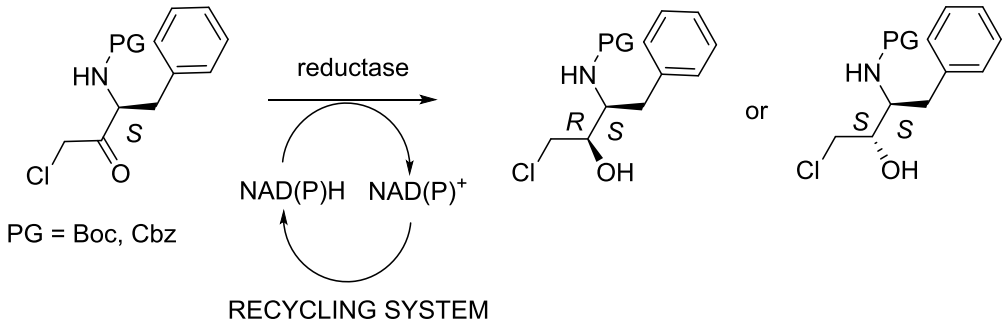

Scheme 1.1. Asymmetric reduction of *N*-protected (*S*)-3-amino-1-chloro-4-phenylbutan-2-one with carbonyl reductases, using glucose dehydrogenase or 2-propanol as cofactor recycling system.

Interestingly, slight changes in the chemical structure of the precursor molecule resulted in the alternation of the enzyme selectivity, giving access to the corresponding alcohol diastereoisomers. In particular, good results were obtained by using different amino protecting groups such as Boc or Cbz. Although some enzymes were highly enantioselective (>99% *de*), poor to moderate conversion rates were attained (18-58%), so further optimization of the reactions was carried out. Tuning parameters such as concentration of co-substrate and substrate, pH, time or use of co-solvents, quantitative conversions were successfully achieved with 50 g/L substrate concentration with 30% v/v IPA, used as hydrogen donor, at pH 7 after 21 hours.

ADHs have also been applied in our research group for the synthesis of biologically active derivatives using α-halo ketones as starting materials.[88] In the search for asymmetric approaches towards target antifungal agents, namely miconazole and econazole, a chemoenzymatic route was designed in which the key step to introduce the chirality involved the bioreduction of an α-bromo- or an α-chloro aryl ketone (Scheme 1.2). Once that the lipase-catalyzed resolution of the racemic halohydrins failed to obtain satisfactory conversions and stereoselectivities, the bioreduction of 2-bromo-1-(2,4-dichlorophenyl)ethanone and 2-chloro-1-(2,4-dichlorophenyl)ethanone were examined, finding excellent results using various commercial ADHs. For example, ADH-A from *Rhodococcus ruber* and ADH-T from *Thermoanaerobacter* sp. allowed the production of the desired enantiopure (*R*)-alcohols with high yields, being direct

[88] J. Mangas-Sánchez, E. Busto, V. Gotor-Fernández, F. Malpartida, V. Gotor, *J. Org. Chem.* **2011**, *76*, 2115-2121.

precursors of (*R*)-miconazole and (*R*)-econazole. For the synthesis of (*S*)-alcohols it was envisaged a chemical inversion of the stereocenter bearing the hydroxyl function through Mitsunobu reaction.

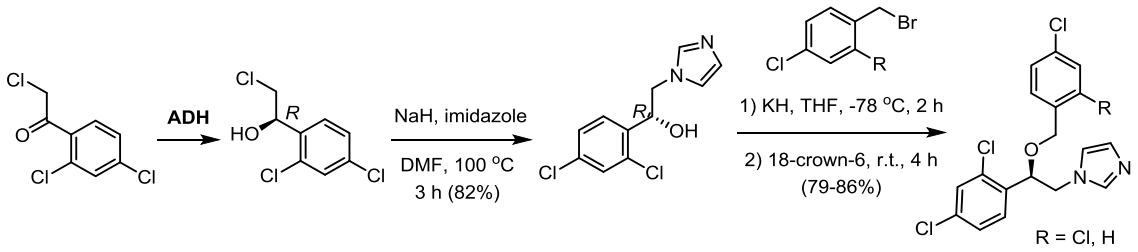

Scheme 1.2. Chemoenzymatic synthesis of (*R*)-miconazole (R = Cl) and (*R*)-econazole (R = H) through asymmetric reduction of a precursor α-halo ketone with an ADH.

Other examples of α-chlorohydrins as direct precursors of pharmacologically active compounds (Figure 1.1), obtained by ADH-catalyzed bioreductions include: (i) selective α_1-adrenergic receptor agonists that mediate smooth muscle contraction, phenylephrine;[89] (ii) β_2-adrenergic receptor agonists that mediate smooth muscle relaxation, such as prodrug bambuterol and its active form terbutaline;[90] (iii) denopamine[91] used in asthma treatment; and (iv) atomoxetine and fluoxetine,[92] which are selective norepinephrine reuptake inhibitors used in treatment of attention deficit hyperactivity disorder (ADHD) and depression.

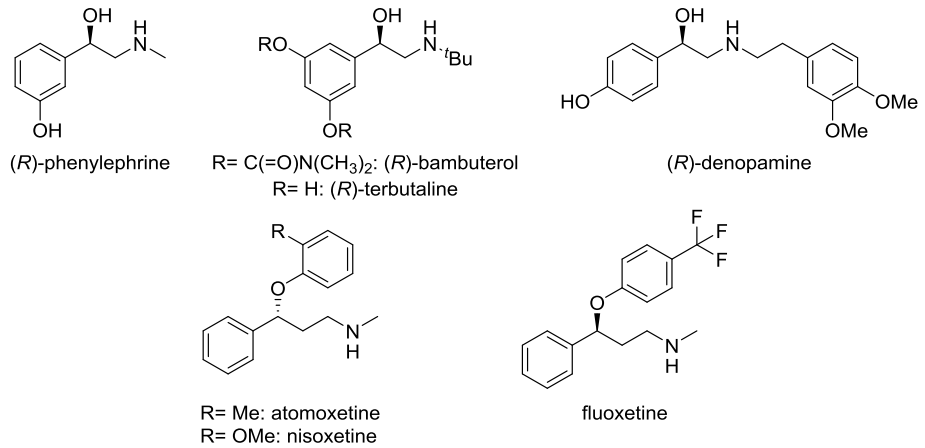

Figure 1.1. Chemical structures of selected compounds with pharmacological activity. Suitable precursors can be obtained through bioreduction processes.

[89] D. Tokoshima, K. Hanaya, M. Shoji, T. Sugai, *J. Mol. Catal. B: Enzym*. **2013**, *97*, 95-99.
[90] K. Asami, T. Machida, S. Jung, K. Hanaya, M. Shoji, T. Sugai, *J. Mol. Catal. B: Enzym*. **2013**, *97*, 106-109.
[91] D. M. Lee, J. C. Lee, N. Jeong, K. I. Lee, *Tetrahedron: Asymmetry* **2007**, *18*, 2662-2667.
[92] D. Zhu, C. Mukherjee, L. Hua, *Tetrahedron: Asymmetry* **2005**, *16*, 3275-3278.

Also, terminal α-halo ketones play a special role in cascade or tandem reactions due to the high reactivity of the corresponding chiral halohydrins obtained. Once that their bioreductions were successfully achieved, those intermediates have been used as direct precursors of enantioenriched epoxides, which exhibit broad applicability in organic synthesis as they can be easily modified with different nucleophiles (Scheme 1.3).[93]

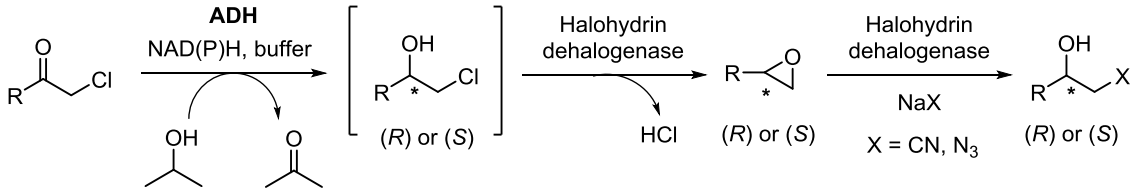

Scheme 1.3. Biocatalytic cascade sequence for the synthesis of enantiopure β-azidoalcohols and β-hydroxynitriles.

A study conducted in our research group employed α-bromo ketones that once reduced by an ADH led to enantiopure bromohydrins, which subsequently underwent spontaneous cyclization in a buffer solution at pH 9-10.[94] Addition of 5% hexane hampered the formation of byproducts and using stereocomplementary biocatalysts, both antipodes of the oxirane ring were accessible. It was also proved the chemoselectivity of the process by carrying out the bioreductions at different pHs: (i) *via* tandem process in which apart from the bioreduction at basic pH, an elevated temperature of 45 ºC was used to force the formation of the epoxides; (ii) through simple bioreduction at pH 7.5 and 30 ºC, synthesizing the bromohydrins in high yields. Finally, taking advantage of the chemodivergency of this process, and starting from 5-azido-1-bromopentan-2-one, it was possible to afford *N*-protected derivatives of (*R*)-prolinol and (*S*)-piperidin-3-ol employing LBADH in a three-reaction sequence (Scheme 1.4).

[93] (a) J. H. Schrittwieser, I. Lavandera, B. Seisser, B. Mautner, J. H. L. Spelberg, W. Kroutil, *Tetrahedron: Asymmetry* **2009**, *20*, 483-488; (b) J. H. Schrittwieser, I. Lavandera, B. Seisser, B. Mautner, W. Kroutil, *Eur. J. Org. Chem.* **2009**, 2293-2298.
[94] F. R. Bisogno, A. Cuetos, A. A. Orden, M. Kurina-Sanz, I. Lavandera, V. Gotor, *Adv. Synth. Catal.* **2010**, *352*, 1657-1661.

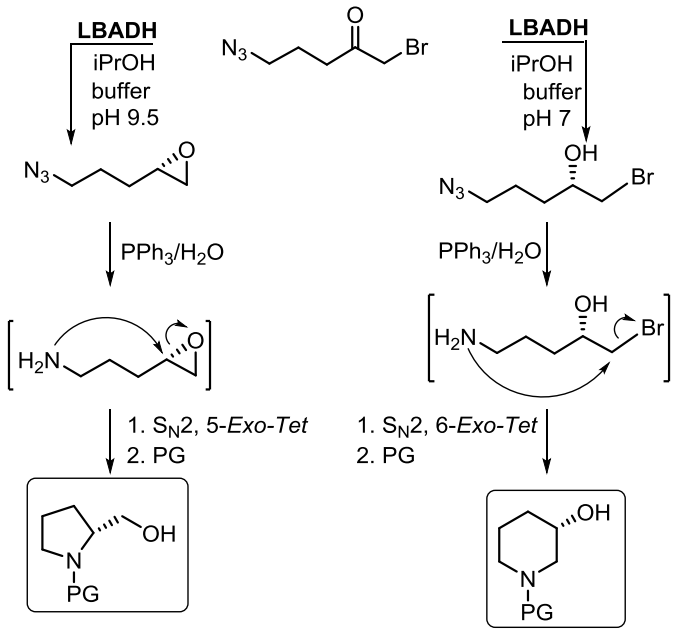

Scheme 1.4. Biocatalyzed chemodivergent synthesis of enantiopure *N*-protected (*R*)-prolinol and (*S*)-piperidin-3-ol.

An interesting feature presented by α-halo ketones is that they can be reduced through hydrogen transfer in a quasi-irreversible manner. As a result, while ketone smoothly undergoes reduction using enzymes or metals as catalysts, the opposite oxidation of the corresponding halohydrin is clearly disfavored. Although at the beginning it can be perceived as a limitation of this methodology, it has been favorably employed in the oxidation of secondary alcohols.[34a] In this way, ADH from *Sphingobium yanoikuyae* (SyADH) was employed to oxidize various secondary alcohols while α-chloroacetone served as hydrogen acceptor. In the reaction conditions, it was sufficient to use 1.5 equivalents of the chlorinated ketone to carry out the oxidation in a quantitative manner. In subsequent studies it was proved that this effect was mainly due to the thermodynamics that control the formation of the halohydrin in comparison to the α-halo ketone.[52,95]

[95] F. R. Bisogno, E. García-Urdiales, H. Valdés, I. Lavandera, W. Kroutil, D. Suárez, V. Gotor, *Chem. Eur. J.* **2010**, *16*, 11012-11019.

1.1.2. Biocatalyzed synthesis of β,β-dihalogenated alcohols

While the bioreduction of α-halo ketones has widely been studied due to their availability, just few examples about the bioreduction of α,α-dihalogenated ketones are found in the literature. For example, Nakamura and coworkers used whole cells of *Geotrichum candidum* to synthesize enantioenriched aromatic alcohols bearing mono-, di- or trihalogenated substituents (F and Cl) at β-position by bioreduction of the corresponding ketones.[96] It was observed that α-halo ketones could be reduced with high *ee* yielding the (*R*)-halohydrins, while the presence of additional halogen atoms affected significantly the selectivity of the process, even favoring the formation of the (*S*)-enantiomer. In other study, (*R*)-2,2-dibromo-1-(4'-benzyloxy-3'-hydroxymethylphenyl)ethanol was obtained in 82% yield and 92% *ee* by using *Rhodotorula rubra* whole cells in the presence of a surfactant.[97] A more recent report on the stereoselective bioreduction of α-chloro-α-fluoroacetophenone using baker's yeast, described conversions below 50% over 3 days producing the corresponding alcohol in moderate optical purity (62% *ee*) and due to the lack of a proper separation technique, *de* was not determined.[98] Finally, in other studies α,α-difluoroacetophenone was a substrate for a number of ADHs, among which ADH-A and LBADH allowed accessing the complementary enantiomers in excellent yields and *ee* at unusually high substrate concentrations (0.5 M).[99]

In case of other enzymatic protocols used to obtain optically pure β,β-dihalohydrins, the lipase-catalyzed resolution of 2,2-dichloro-1-phenylethanol was carried out using *Pseudomonas cepacia* lipase (PSL). However, 44% conversion of the final product was reached after 142 h.[100]

Since the potential interest of the pharma sector in the dihalogenated secondary alcohols is conditioned by the development of an efficient route to obtain these intermediates in the optically pure form, we have been encouraged to study a family of dihalogenated ketones as precursors to obtain the corresponding alcohols using alcohol dehydrogenases as biocatalysts. Additionally, activated ketones, such as α,α-

[96] T. Matsuda, T. Harada, N. Nakajima, T. Itoh, K. Nakamura, *J. Org. Chem*. **2000**, *65*, 157-163.
[97] A. Goswami, R. L. Bezbaruah, J. Goswami, N. Borthakur, D. Dey, A. K. Hazarika, *Tetrahedron: Asymmetry* **2000**, *11*, 3701-3709.
[98] B. Barkakty, Y. Takaguchi, S. Tsuboi, *Tetrahedron* **2007**, *63*, 970-976.
[99] (a) K. Nakamura, R. Yamanaka, *Tetrahedron: Asymmetry* **2002**, *13*, 2529-2533; (b) W. Borzęcka, I. Lavandera, V. Gotor, *J. Org. Chem*. **2013**, *78*, 7312-7317.
[100] K. Lundell, T. Raijola, L. T. Kanerva, *Enzyme Microb. Technol*. **1998**, *22*, 86-93.

dihalogenated aryl substrates, undergo quasi-irreversible bioreduction when reacting with alcohol dehydrogenases due to the high redox potential of the ketone/alcohol pair. Thus, it allows reducing substantially the amount of cosubstrate used in the cofactor recycling system to approximately 2 equiv. instead of larger amounts normally used.[95] Therefore, it seemed crucial to find adequate biocatalysts to yield enantiopure β,β-dihaloalcohols in high conversion with complementary stereoselectivity.

Until now, β,β-dibromohydrins have been reported as direct intermediates to gain access to alkenes[101] or terminal alkynes[102] as shown in Scheme 1.5. Additionally, these substrates were used to synthesize epoxides[103] or α-methoxy aryl acetic acid derivatives,[104] compounds of high interest if synthesized in enantiopure form.

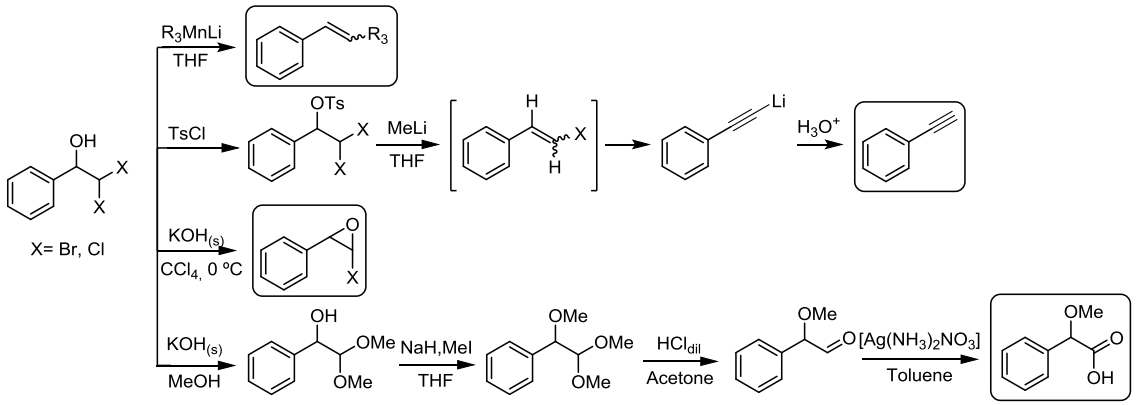

Scheme 1.5. Examples of applications of aryl β,β-dihalohydrins in organic synthesis.

[101] H. Kakiya, H. Shinokubo, K. Oshima, *Tetrahedron* **2001**, *57*, 10063-10069.
[102] Z. Wang, J. Yin, S. Campagna, J. A. Pesti, J. M. Fortunak, *J. Org. Chem*. **1999**, *64*, 6918-6920.
[103] R. N. McDonald, R. C. Cousins, *J. Org. Chem*. **1980**, *45*, 2976-2984.
[104] B. Singh, P. Gupta, A. Chaubey, R. Parshad, S. Sharma, S. C. Taneja, *Tetrahedron: Asymmetry* **2008**, *19*, 2579-2588.

Objectives

The present study constitutes a direct continuation of the investigation carried out in our research group for the synthesis and bioreduction of substituted α-halogenated ketones. With a general purpose to develop new redox processes catalyzed by alcohol dehydrogenases, α,α-dihalosubstituted acetophenone derivatives were proposed as substrates in bioreduction processes. Thus, the project was focused on the following objectives:

- Chemical synthesis of a series of prochiral α,α-dihalogenated substituted acetophenone derivatives and their corresponding racemic alcohols.

- Study of the bioreduction processes using Prelog and anti-Prelog ADHs to access both alcohol antipodes from previously synthesized ketones.

- Investigation of diastereo- and enantioselectivity of screened ADHs in the bioreduction of racemic ketones such as α-bromo-α-chloroacetophenone and α-chloro-α-fluoroacetophenone.

- Investigation of several factors on the diastereoselectivity of selected ADHs using α-bromo-α-chloroacetophenone as model substrate.

Results and discussion

Utility of enzymes in organic synthesis is based on their ability to generate defined stereogenic center(s) in the key intermediate that is(are) maintained during the course of the synthesis. In our research group different methodologies have been successfully applied to gain access to synthetically useful enantiopure intermediates such as hydroxy or amino esters, secondary alcohols and chiral amines.

The work included in this Chapter was focused on the application of alcohol dehydrogenases over α,α-dihalogenated acetophenone derivatives, in order to gain access to enantiopure alcohols *via* environmentally benign methodology. It was then envisaged that in the case of α,α-dihalogenated substrates, due to their different synthetic possibilities from α-halogenated ketones, the scope of further transformations would make worth to explore this family of compounds.

Therefore, a series of ketones with different substituents and localization in the aryl ring were synthesized using 2.05 equiv. of *N*-chloro- (NCS) or 3 equiv. of *N*-bromosuccinamide (NBS) as halogenating agent in the presence of *p*-toluenesulfonic acid (1 equiv.), with high to very high yields as shown in Table 1.1. A facile reduction of ketones with sodium borohydride gave access to the racemic alcohols in high yields (80-90%).

Table 1.1. Chemical synthesis of ketones **2a-j**.

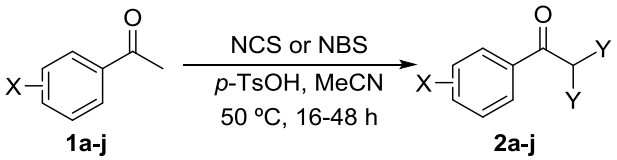

entry	substrate	X	Y	t (h)	**2a-j** (%)[a]
1	**1a**	H	Cl	16	77
2	**1b**	2-Me	Cl	48	82
3	**1c**	2-Cl	Cl	48	77
4	**1d**	3-OMe	Cl	16	75
5	**1e**	3-NO_2	Cl	16	80
6	**1f**	3-Cl	Cl	16	78
7	**1g**	4-NO_2	Cl	16	78
8	**1h**	4-Cl	Cl	16	90
9	**1i**	3,4-diCl	Cl	16	83
10	**1j**	H	Br	16	81

[a] Isolated yields after flash chromatography.

It was reasoned that the nature of both halogen substituents at the vicinity to the carbonyl group would modify substantially the size and electronic character of the aryl

ketone, which in turn might pose a challenge for alcohol dehydrogenases to accommodate such voluminous molecule in their center active pockets. Different ADHs that follow anti-Prelog rule in regards to the absolute configuration in produced alcohols were tried as *Lactobacillus brevis* ADH (LBADH), *Lactobacillus kefir* ADH (LKADH) and PR2. Prelog-enzymes included in this study capable of accepting bulky-bulky ketones were *Sphingobium yanoikuyae* ADH (SyADH) and *Ralstonia* sp. ADH (RasADH), as well as *Rhodococcus ruber* ADH (ADH-A) overexpressed in *E. coli*.

It was encouraging to observe that ADH-A readily accepted most of the substrates screened, apart from *ortho*-methyl and α,α-dibromoacetophenone, and also showed excellent *ee* values. Similar results were obtained for RasADH which gave access to (*R*)-enantiomers (due to the change in Cahn-Ingold-Prelog rule priority), with the exception for *meta*-substituents that apparently affected its stereospecificity. It was more difficult to identify stereocomplementary anti-Prelog ADHs, LBADH providing in most cases the desired (*S*)-alcohols with excellent *ee*. The most demanding ketones for LBADH and LKADH were substrates with *ortho*-substituents regardless their electron-donating or withdrawing character. Figure 1.2 shows the best results obtained for substrates **2a-j**.

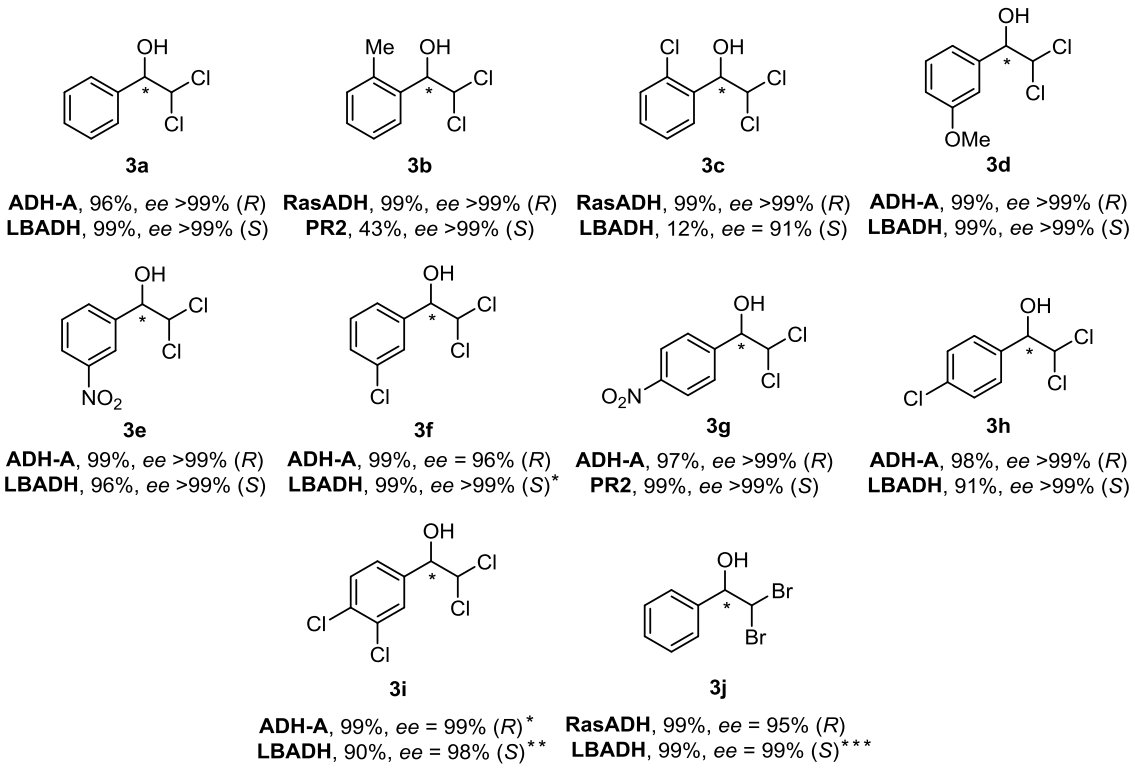

Figure 1.2. Summary of the best results obtained for bioreductions with Prelog and anti-Prelog ADHs (3 U) to synthesize complementary enantiomers of β,β-dihalogenated alcohols **3a-j** (t= 24 h). * 2% v/v DMSO was added in the reaction medium. ** 2% v/v DMSO was added, 48 h of reaction and 4.5 U of enzyme added. *** 2% DMSO was added and 4.5 U of enzyme added.

Encouraged by the excellent *ee* and conversions obtained, two halogenated racemic ketones such as α-bromo-α-chloro- (**2k**) and α-chloro-α-fluoroacetophenone (**2l**) were included into the essay (Table 1.2). Due to the high acidity of the α-proton, it was envisaged a possible dynamic kinetic resolution for these substrates. Moderate diastereomeric excess (59%, entry 1) was observed with ADH-A to afford the (1*R*,2*R*)-diastereomer of **3k** while modest *de* (26%, entry 4) when LBADH to achieve (1*S*,2*R*)-**3k**, though excellent *ee* values (>99%) were obtained in both cases. To our disappointment, **2l** was transformed into alcohol **3l** with hardly any diastereopreference by ADH-A, RasADH and LBADH (entries 5-8).

Table 1.2. Bioreduction of substrates **2k-l** after 24 h at pH 7.5, 30 ºC and 150 rpm.

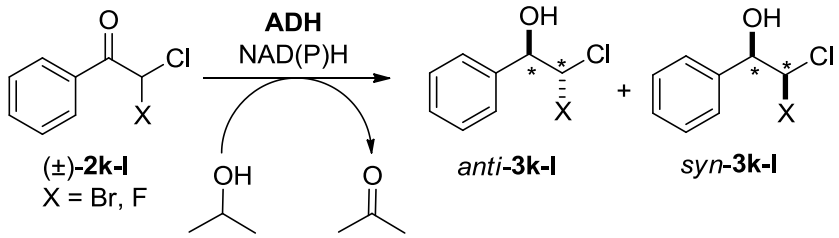

entry	ketone	X	ADH	*c* (%)[a]	*ee* (%)[b]	*de* (%)[b]
1	**2k**	Br	*E. coli*/A	99	>99 (1*R*,2*R*)	59
2	**2k**	Br	*E. coli*/Ras	95	97 (1*R*,2*RS*)	1
3	**2k**	Br	*E. coli*/Sy	94	79 (1*R*,2*S*)	77
4	**2k**	Br	LB	65	>99 (1*S*,2*R*)	26
5	**2l**	F	*E. coli*/A	99	98 (1*R*,2*RS*)	5
6	**2l**	F	*E. coli*/Ras	99	97 (1*R*,2*RS*)	<1
7	**2l**	F	*E. coli*/Sy	98	59 (1*R*,2*RS*)	45
8	**2l**	F	LB	99	>99 (1*S*,2*RS*)	1

[a] Conversion values measured by GC. [b] Enantiomeric and diastereomeric excess measured by chiral HPLC (note the switch in the CIP priority).

Attempts were performed to improve the diastereoselectivity of these processes by change of the temperature, increase of pH or use of additives such as organic bases, ionic liquids or biphasic reaction media. However, small improvement was observed for ADH-A (up to 63% *de*) and LBADH (up to 33% *de*), and further manipulation of temperature or pH encountered enzyme or substrate stability issues. In order to establish the absolute configuration of the major diastereoisomer of 2-bromo-2-chloro-1-phenylethanol, this alcohol was derivatized into the 4-nitrobenzoate ester and crystallized. The crystal structure indicated that *syn*-configuration was preferentially formed by ADH-A as opposed to LBADH and chemical reduction with $NaBH_4$ (to form the racemic derivative), which yielded mainly the *anti*-diastereoisomer.

Conclusions

In summary, work included in this Chapter focused on the application of alcohol dehydrogenases over α,α-dihalogenated acetophenone derivatives in order to develop an environmentally benign methodology to gain access to the corresponding enantiopure alcohols that are useful intermediates in chemical synthesis.

Therefore, a series of α-halo ketones with different pattern substitution in the aromatic ring was synthesized with high to very good yields, using *N*-chlorosuccinimide or *N*-bromosuccinimide as halogenating agents.

A facile reduction of these ketones with sodium borohydride gave access to the racemic alcohols for the development of analytical measurements.

It was observed that ADH-A readily converted most of the substrates with high yields and excellent selectivities, apart from *ortho*-methyl and α,α-dibromoacetophenone. For these sterically demanding substrates, RasADH was successfully employed.

In the case of anti-Prelog ADHs, LBADH and PR2ADH provided in most cases the desired (*S*)-alcohols with excellent *ee*. The most demanding ketones for LBADH and LKADH were substrates with *ortho*-substituents.

In addition, two racemic ketones such as α-bromo-α-chloro- and α-chloro-α-fluoroacetophenone were included into the essay to examine the enantioselectivity of the screened ADHs in dynamic processes.

Moderate diastereomeric excess (up to 63%) was observed for ADH-A, and modest (up to 33%), when LBADH was used for the bioreduction of α-bromo-α-chloroacetophenone, although excellent *ee* values were obtained in both cases.

On the contrary, no enzyme displayed significant diastereopreference towards α-chloro-α-fluoroacetophenone.

Conclusiones

En resumen, el trabajo incluido en este Capítulo describe la aplicación de alcohol deshidrogenasas sobre derivados α,α-dihalogenados de acetofenona, con el fin de desarrollar una metodología medioambientalmente benigna y eficiente para obtener los correspondiente alcoholes enantiopuros, intermedios de un gran interés en química sintética.

Así, se ha sintetizado con buenos rendimientos una familia de cetonas halogenadas aromáticas con diferentes patrones de sustitución en el anillo aromático, utilizando como agentes halogenantes tanto la *N*-cloro- como la *N*-bromosuccinimida. La reducción química con borohidruro de sodio de las cetonas sintetizadas, permitió acceder a los correspondientes alcoholes racémicos, facilitando el desarrollo de métodos analíticos para el seguimiento y análisis temporal de las reacciones enzimáticas.

Se ha observado que la ADH-A reacciona con la mayoría de los sustratos con conversiones altas y selectividades excelentes, excepto con el derivado metilado en la posición *orto* y la α,α-dibromoacetofenona. Con sustratos más impedidos estéricamente se ha empleado con éxito la RasADH. En el caso de los enzimas anti-Prelog, la LBADH y la PR2ADH han sido capaces de reaccionar con la mayoría de los sustratos estudiados dando lugar a los alcoholes de configuración *S* con excelentes excesos enantioméricos, a excepción de los compuestos sustituidos en posición *orto*, más impedidos estéricamente.

Además, dos cetonas racémicas, la α-bromo-α-cloroacetofenona y la α-cloro-α-fluoroacetofenona se sintetizaron y utilizaron como sustratos de partida en procesos dinámicos de biorreducción, para lo cual se emplearon distintas ADHs. Así, con la primera de ellas se obtuvieron excesos diastereoméricos moderados (≤63%) al emplear la ADH-A, mientras que fueron bajos (≤33%) con la LBADH. Sin embargo, los excesos enantioméricos fueron >99% en ambos casos. En el caso de la α-cloro-α-fluoroacetofenona, ningún enzima pudo conducir a la formación del alcohol con excesos diastereoméricos destacados.

Experimental part

1.6.1. General information

Chemicals were purchased from Aldrich, Fluka or Alfa Aesar and used as received. Solvents for chemical reactions were of high purity grade and were dried over sodium or calcium hydride and stored under nitrogen.

Thin-layer chromatography (TLC) was conducted with Merck Silica Gel 60 F254 precoated plates commercialized by Merck and visualized with UV and potassium permanganate stain (1% $KMnO_4$, 5% K_2CO_3, and 5% NaOH).

Flash chromatography was performed using silica gel 60 (230-400 mesh).

Gas chromatography (GC) analyses were performed on a Hewlett Packard 6890 Series II chromatograph using HP-1 achiral column (30 m × 0.32 mm × 0.25 μm) and chiral columns CP-Chiralsil-DEX-CB (25 m × 0.25 mm × 0.25 μm) and Rt-β-dexe (30 m × 0.25 mm × 0.25 μm).

HPLC analyses were performed with Hewlett Packard 1100 LC liquid chromatograph. Detection was performed at 210 and 215 nm. As mobile phase mixtures of hexane and 2-propanol were selected.

IR spectra were recorded on a Perkin-Elmer 1720-X infrared Fourier transform spectrophotometer on NaCl pellets. Bands are described in their maximum ν and expressed in cm^{-1}.

Melting points were obtained on a Gallenkamp apparatus in open tubes and are reported uncorrected.

ESI^+ mode was used to record mass spectra (MS) in a Finigan MAT 95 apparatus coupled to an HP1100 chromatograph and ESI-TOF for HRMS in a Bruker MicroTofQ spectrometer. Values are shown in mass atomic units (uma).

^1H-, ^{13}C-NMR, and DEPT were obtained using a Bruker DPX-300 (^1H, 300.13 MHz and ^{13}C, 75.5 MHz) and Bruker AV-300 (^1H, 300.13 MHz and ^{13}C, 75.5 MHz) spectrometers for routine experiments. The chemical shifts (δ) are given in ppm and the coupling constants (J) in Hertz (Hz).

Optical rotations were measured using a Perkin-Elmer 241 polarimeter and are quoted in units of 10^{-1} deg cm^2 g^{-1}.

1.6.2. General synthetic procedures

1.6.2.1. Synthesis of α,α-dichlorosubstituted acetophenones 2a-h

To a solution of the corresponding acetophenone **1a-h** (3.7 mmol) and *p*-TsOH (708.8 mg, 3.7 mmol) in acetonitrile (10 mL), NCS was added (1 g, 7.6 mmol). The reaction mixture was heated at 50 ºC and stirred till disappearance of the starting material (16-48 h). After completion, the solvent was evaporated under reduced pressure and the crude was purified using flash chromatography (50-80% CH_2Cl_2/hexane), yielding the corresponding prochiral ketones (75-90%).

1.6.2.2. Synthesis of 2,2-dichloro-1-(3,4-dichlorophenyl)ethanone (2i)

To a solution of α-chloroacetophenone **1i** (280 mg, 1.25 mmol) and *p*-TsOH (238 mg, 1.25 mmol) in acetonitrile (4 mL), NCS was added (184 mg, 1.37 mmol). The reaction mixture was heated at 50 ºC and stirred till disappearance of the starting material (16 h). After completion of the reaction, the solvent was evaporated under reduced pressure and the crude was purified using flash chromatography (20% CH_2Cl_2/hexane), yielding product **2i** as a white solid (0.27 g, 83%).

1.6.2.3. Synthesis of 2,2-dibromo-1-phenylethanone (2j)

To a solution of acetophenone (**1a**, 250 mg, 2.08 mmol) and *p*-TsOH (400 mg, 2.08 mmol) in acetonitrile (10 mL), NBS was added (1.11 g, 6.24 mmol). The reaction mixture was heated at 50 ºC and stirred till disappearance of the starting material (16 h). After completion of the reaction, the solvent was evaporated under reduced pressure and the crude was purified using flash chromatography (33% CH_2Cl_2/hexane), yielding product **2j** as a white solid (0.47 g, 81%).

1.6.2.4. Synthesis of racemic 2-bromo-2-chloro-1-phenylethanone (2k)

To a solution of α-chloroacetophenone **1k** (500 mg, 3.2 mmol) and *p*-TsOH (615 mg, 3.2 mmol) in acetonitrile (14 mL), NBS was added (863 mg, 4.85 mmol). The reaction mixture was heated at 50 ºC and stirred till disappearance of the starting material (16 h). After completion of the reaction, the solvent was evaporated under reduced pressure and the crude was purified using flash chromatography (20% CH_2Cl_2/hexane), yielding product **2k** as a white solid (0.64 g, 85%).

1.6.2.5. Synthesis of racemic 2-chloro-2-fluoro-1-phenylethanone (2l)

To a solution of ethyl chlorofluoroacetate (0.5 mL, 4.35 mmol) in dry toluene (5 mL) at -78 ºC under nitrogen atmosphere, 1.1 equiv. of phenyl magnesium bromide (1.6 mL of a 3 M solution in Et_2O) was added dropwise and the reaction was stirred for one hour. Following that time, the reaction mixture was warmed up to 0 ºC and then left for 10 min prior to quenching with ammonium chloride (saturated solution). The crude was extracted with Et_2O (3 × 10 mL), dried over anhydrous Na_2SO_4 and slowly evaporated under reduced pressure in an ice bath to prevent the loss of the volatile product. The crude mixture was purified using flash chromatography (100% pentane to 70% pentane/CH_2Cl_2), yielding product **2l** as a white crystal solid (0.42 g, 56% yield).

1.6.2.6. General procedure for synthesis of racemic alcohols 3a-l

To a solution of the corresponding ketone **2a-l** (0.2 mmol) in methanol (1 mL) at 0 ºC, $NaBH_4$ was added (4.6 mg, 0.1 mmol) and the temperature maintained at 0 °C. The reaction mixture was stirred till disappearance of the starting material at room temperature (16 h). After completion of the reaction, few drops of diluted HCl (1 N) were added to neutralize the excess of $NaBH_4$ followed by evaporation of the solvent under reduced pressure. Water was added (10 mL) and then was extracted with CH_2Cl_2 (3 x 5 mL), and the combined organic fractions were dried over anhydrous Na_2SO_4, filtered and evaporated under reduced pressure. The reaction crude was purified using flash chromatography (50-80% CH_2Cl_2/hexanes), yielding alcohols **3a-l** with high to excellent yields (70-95%).

1.6.2.7. Derivatization of enantiopure alcohol 3k with 4-nitrobenzoyl chloride

In a Schlenck tube, enantiopure alcohol **3k** (30 mg, 0.13 mmol) was dissolved in 2 mL of dry dichloromethane under nitrogen atmosphere. Then, Et_3N (19.6 μL, 0.14 mmol) was added followed by 4-nitrobenzoyl chloride (26 mg, 0.14 mmol). The reaction mixture was stirred at room temperature for 16 h. After this time, the solvent was removed under reduced pressure and the reaction crude purified by flash chromatography (30% EtOAc/hexanes), yielding a pale yellow oil that crashed out into white crystals upon addition of a minimum amount of Et_2O and then hexane, leaving the sample overnight till the appearance of the crystals.

1.6.3. General enzymatic procedures

1.6.3.1. Reduction of 2a-l with ADH from *Rhodococcus ruber* overexpressed in *E. coli*

To a 15 mg portion of overexpressed *E. coli*/ADH-A (lyophilized cells) in an Eppendorf vial (1.5 mL), Tris-HCl or Tris-H_2SO_4 buffer (510 μL, 50 mM, pH 7.5), NADH (60 μL of a 10 mM solution, final concentration: 1 mM), 2-propanol (30 μL, 5% v/v), and the corresponding ketone **2a-l** (25 mM) were added. The reaction tubes were shaken horizontally at 30 ºC for 24 h and 150 rpm. After that time, the reaction products were extracted with EtOAc (2 × 0.5 mL). The organic layers were separated by centrifugation (1.5 min, 13000 rpm) and dried over anhydrous Na_2SO_4. Conversion and *ee* values were determined by GC or HPLC analysis.

1.6.3.2. Reduction of 2a-l with ADH from *Sphingobium yanoikuyae* overexpressed in *E. coli*

To a 15 mg portion of overexpressed *E. coli*/SyADH (lyophilized cells) in an Eppendorf vial (1.5 mL), Tris-HCl or Tris-H_2SO_4 buffer (510 μL, 50 mM, pH 7.5), NADPH (60 μL of a 10 mM solution, final concentration: 1 mM), 2-propanol (30 μL, 5% v/v), and the corresponding ketone **2a-l** (25 mM) were added. The reaction tubes were shaken horizontally at 30 ºC for 24 h and 150 rpm. After that time, the reaction products were extracted with EtOAc (2 × 0.5 mL). The organic layers were separated by centrifugation (1.5 min, 13000 rpm) and dried over anhydrous Na_2SO_4. Conversion and *ee* values were determined by GC or HPLC analysis.

1.6.3.3. Reduction of 2a-l with ADH from *Ralstonia* sp. overexpressed in *E. coli*

To a 15 mg portion of overexpressed *E. coli*/RasADH (lyophilized cells) in an Eppendorf vial (1.5 mL), Tris-HCl or Tris-H_2SO_4 buffer (510 μL, 50 mM, pH 7.5), NADPH (60 μL of a 10 mM solution, final concentration: 1 mM), glucose (30 μL of a 1 M solution, final concentration: 50 mM), glucose dehydrogenase (10 μL, 3 U) and the corresponding ketone **2a-l** (25 mM). The reaction tubes were shaken horizontally at 30 ºC for 24 h and 150 rpm. After that time, the reaction products were extracted with EtOAc (2 × 0.5 mL). The organic layers were separated by centrifugation (1.5 min,

13000 rpm) and dried over anhydrous Na_2SO_4. Conversion and *ee* values were determined by GC or HPLC analysis.

1.6.3.4. Reduction of 2a-l with ADH from *Lactobacillus brevis* (LBADH)

In an Eppendorf vial (1.5 mL), LBADH (10 μL, 3 U) was added into 450 μL of Tris-HCl or Tris-H_2SO_4 buffer (50 mM, pH 7.5), followed by NADPH (60 μL of a 10 mM solution, final concentration: 1 mM), $MgCl_2$ (60 μL of a 10 mM solution, final concentration: 1 mM), 2-propanol (30 μL, 5% v/v) and the corresponding ketone **2a-l** (25 mM). The reaction tubes were shaken horizontally at 30 ºC for 24 h and 150 rpm. After that time, the reaction products were extracted with EtOAc (2 × 0.5 mL). The organic layers were separated by centrifugation (1.5 min, 13000 rpm) and dried over anhydrous Na_2SO_4. Conversion and *ee* values were determined by GC or HPLC analysis.

1.6.3.5. Reduction of 2a-j with ADH from *Lactobacillus kefir* (LKADH)

In an Eppendorf vial (1.5 mL), LKADH (7 mg, 3 U) was added into 510 μL of Tris-HCl or Tris-H_2SO_4 buffer (50 mM, pH 7.5), followed by NADPH (60 μL of a 10 mM solution, final concentration: 1 mM), glucose (30 μL of a 1 M solution, final concentration: 50 mM), glucose dehydrogenase (10 μL, 3 U) and the corresponding ketone **2a-j** (25 mM). The reaction tubes were shaken horizontally at 30 ºC for 24 h and 150 rpm. After that time, the reaction products were extracted with EtOAc (2× 0.5 mL). The organic layers were separated by centrifugation (1.5 min, 13000 rpm) and dried over anhydrous Na_2SO_4. Conversion and *ee* values were determined by GC or HPLC analysis.

1.6.3.6. Reduction of 2a-j with PR2ADH

In an Eppendorf vial (1.5 mL), PR2ADH (23 mg, 3 U) was added into 510 μL of Tris-HCl or Tris-H_2SO_4 buffer (50 mM, pH 7.5), followed by NADH (60 μL of a 10 mM solution, final concentration: 1 mM), 2-propanol (30 μL, 5% v/v) and the corresponding ketone **2a-j** (25 mM). The reaction tubes were shaken horizontally at 30 ºC for 24 h and 150 rpm. After that time, the reaction products were extracted with EtOAc (2 × 0.5 mL). The organic layers were separated by centrifugation (1.5 min, 13000 rpm) and dried over anhydrous Na_2SO_4. Conversion and *ee* values were determined by GC or HPLC analysis.

1.6.3.7. Effect of the base on the racemization rate of ketone 2k

In an Eppendorf tube, the biocatalyst was resuspended in 570 μL of Tris-H_2SO_4 buffer (pH 7.5, 50 mM, 1 mM NADH for *E. coli*/ADH-A, or NADPH for LBADH or *E. coli*/RasADH). Then the corresponding base was added (1 equiv.) followed by the addition of 2-propanol (30 μL, 5% v/v) for *E. coli*/ADH-A or LBADH, or glucose (30 μmol, 50 mM) and glucose dehydrogenase (10 μL, 3 U) for *E. coli*/RasADH, and ketone **2k** (14.9 μmol, 25 mM). The reaction mixture was left shaking at 30 ºC for 24 h. After that time, the reaction products were extracted with EtOAc (2 x 0.5 mL). The organic layers were separated by centrifugation (1.5 min, 13000 rpm) and dried over anhydrous Na_2SO_4. Conversion and *ee* values were determined by GC and HPLC analysis, respectively.

1.6.3.8. Effect of non-conventional media on the racemization rate of ketone 2k

To a solution of Tris-H_2SO_4 buffer (50 mM, pH 7.5, 1 mM NADH) containing 20 mg of the enzymatic lyophilized preparation of *E. coli*/ADH-A with the substrate **2k** (3.5 mg, 25 mM) in an Eppendorf tube, different quantities of hexanes or ionic liquid (Ammoeng 102, tetraalkylammonium sulphate, Merck KGaA), were added to have a final concentration of 20, 30, 40 or 50% v/v (final volume: 600 μL). After 24 h of incubation at 30 ºC and 250 rpm, the reaction was stopped by extraction with EtOAc (2 x 0.5 mL). The organic layers were separated by centrifugation (1.5 min, 13000 rpm), dried over anhydrous Na_2SO_4 and aliquots were analyzed on GC and HPLC to determine conversions and *ee*.

Publication

ChemPubSoc Europe

DOI: 10.1002/cctc.201300834

Expanding the Scope of Alcohol Dehydrogenases towards Bulkier Substrates: Stereo- and Enantiopreference for α,α-Dihalogenated Ketones

Kinga Kędziora,[a] Fabricio R. Bisogno,[a, b] Iván Lavandera,[a] Vicente Gotor-Fernández,[a] Jose Montejo-Bernardo,[c] Santiago García-Granda,[c] Wolfgang Kroutil,[d] and Vicente Gotor*[a]

Alcohol dehydrogenases (ADHs) were identified as suitable enzymes for the reduction of the corresponding α,α-dihalogenated ketones, obtaining optically pure β,β-dichloro- or β,β-dibromohydrins with excellent conversions and enantiomeric excess. Among the different biocatalysts tested, ADHs from *Rhodococcus ruber* (ADH-A), *Ralstonia* sp. (RasADH), *Lactobacillus brevis* (LBADH), and PR2ADH proved to be the most efficient ones in terms of activity and stereoselectivity. In a further study, two racemic α-substituted ketones, namely α-bromo-α-chloro- and α-chloro-α-fluoroacetophenone were investigated to obtain one of the four possible diastereoisomers through a dynamic kinetic process. In the case of the brominated derivative, only the (1*R*)-enantiomer was obtained by using ADH-A, although with moderate diastereomeric excess (>99% *ee*, 63% *de*), whereas the fluorinated ketone exhibited a lower stereoselectivity (up to 45% *de*).

Introduction

β,β-Dihalogenated alcohols, also called *gem*-dihalo alcohols or β,β-dihalohydrins,[1] are a family of interesting compounds because of their versatility in organic synthesis,[2] and because of their role as precursors of biologically active derivatives such as antineoplastic drugs like mitotane.[3] Thus, owing to the highly activated nature of these compounds, they can be used as synthetic intermediates of interesting molecules such as alkenes,[4] terminal alkynes,[5] epoxides,[6] and α-methoxy alkyl acetic acid derivatives.[7] Additionally, owing to their reactivity in aqueous medium, they have been described as chemical analogues of α-hydroxy aldehydes, opening the scope towards other types of substrates, for example, α-hydroxy acids (Scheme 1).[8]

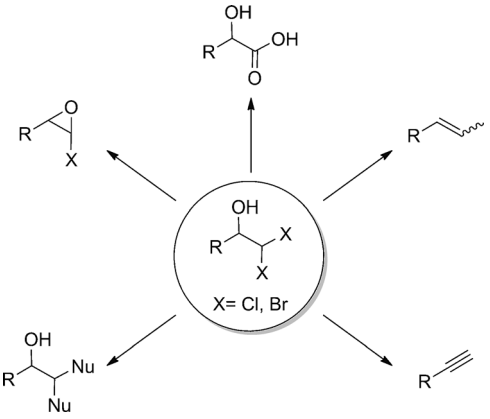

Scheme 1. Synthetic applicability of the *gem*-dihalo alcohol core.

The preparation of the racemic derivatives can be achieved by means of different synthetic approaches such as the Hunsdiecker reaction,[9] the decarboxylative heterodifunctionalisation of α,β-unsaturated carboxylic acids[10] or the reduction of the corresponding ketone precursors.[11] Unfortunately, these methods usually afford a mixture of products because of the formation, among others, of dehydrated, hydrolysed or over-reduced compounds. It is even more difficult to find in the literature an appropriate methodology to stereoselectively achieve these chiral precursors. Unfortunately, the selectivities obtained in these processes by reduction of the ketones using chiral oxaborolidines[12] or borane complexes were moderate (<83%),[13] and, alternatively, dichlorocarbene C–H insertion re-

[a] *K. Kędziora, Dr. F. R. Bisogno, Dr. I. Lavandera, Dr. V. Gotor-Fernández, Prof. V. Gotor*
Department of Organic and Inorganic Chemistry
Instituto Universitario de Biotecnología de Asturias, University of Oviedo
Avenida Julián Clavería s/n, 33006 Oviedo (Spain)
E-mail: vgs@uniovi.es

[b] *Dr. F. R. Bisogno*
INFIQC-CONICET, Dpto. de Química Orgánica
Facultad de Ciencias Químicas
Universidad Nacional de Córdoba
Ciudad Universitaria, CP 5000, Córdoba (Argentina)

[c] *Dr. J. Montejo-Bernardo, Prof. S. García-Granda*
Departamento de Química Física y Analítica
Universidad de Oviedo
Avenida Julián Clavería s/n, Oviedo 33006 (Spain)

[d] *Prof. W. Kroutil*
Department of Chemistry, Organic and Bioorganic Chemistry
University of Graz
Heinrichstrasse 28, 8010 Graz (Austria)

Supporting information for this article is available on the WWW under http://dx.doi.org/10.1002/cctc.201300834.

actions[14] led to incomplete conversions (< 90%) starting from an expensive enantiopure alcohol precursor.

Interestingly, the use of biocatalytic methods under mild reaction conditions has allowed the selective synthesis of difluorohydrins,[15] However, for the chlorinated or brominated counterparts, and although the formation of by-products was minimised, the enantioselectivities or yields obtained in these processes were still not high enough. For instance, (*R*)-2,2-dibromo-1-(4′-benzyloxy-3′-hydroxymethylphenyl)ethanol was obtained in 82% yield and 92% *ee* by using *Rhodotorula rubra* whole cells in the presence of a surfactant.[16] The lipase-catalysed resolution of 2,2-dichloro-1-phenylethanol (**3a**) was achieved with Amano *Pseudomonas cepacia* lipase (PSL), but 44% conversion of the final product was reached after 142 h.[17] On the other hand, the bioreduction of the α,α-dihalo ketone precursor **2a** has been tested with whole cells from *Geotrichum candidum* APG4[18] and baker's yeast,[19] but stereoselectivities remained modest (< 55% *ee*). Based on the high selectivities displayed by alcohol dehydrogenases (ADHs),[20] and as α-monohalogenated ketones are excellent substrates for these enzymes,[19,21] the bioreduction of a series of bulkier α,α-dihalogenated acetophenones is presented herein. Several partially purified/overexpressed ADHs were tested to gain access to the enantiopure β,β-dihalohydrins. Moreover, the reduction of two racemic derivatives was also tried to study the formation of two contiguous stereocentres in a dynamic kinetic resolution (DKR) process catalysed by an ADH through racemisation in basic conditions.

Results and Discussion

Preparation of α,α-dihaloacetophenones and the corresponding alcohols

The synthesis of α,α-dichloroacetophenones **2a–h** was performed in good to very high yields starting from commercially available acetophenones **1a–h**, bearing different substitution pattern in the aromatic ring, by reaction with a 2-fold molar excess of *N*-chlorosuccinimide (NCS) in the presence of *para*-toluenesulfonic acid (*p*-TsOH) using acetonitrile as a solvent at 50 °C (Table 1).

A lower reactivity for the *ortho*-substituted derivatives **2b–c** was observed, thus longer reaction times were required in these cases (entries 2 and 3), probably owing to steric hindrance. In addition, to achieve the synthesis of 2,2-dichloro-1-(3,4-dichlorophenyl)ethanone (**2i**), the corresponding α-chloroacetophenone derivative **1i** was used as starting material utilising 1.1 equivalents of NCS, obtaining **2i** in 83% yield. Starting from **1a** with a 3-fold molar excess of *N*-bromosuccinimide (NBS), 2,2-dibromoacetophenone **2j** was achieved in 81% isolated yield. Racemic dihalohydrins **3a–j** were obtained in good to very high yields (70–96%) by reduction of the corresponding ketones with $NaBH_4$ in MeOH at room temperature (see the Supporting Information).

Table 1. Preparation of α,α-dichloroacetophenones **2a–h**.

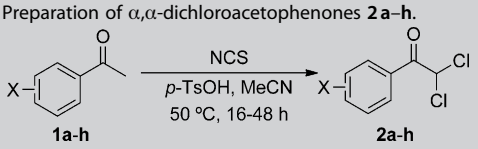

1a-h **2a-h**

Entry	X	*t* [h]	**2a–h** [%][a]
1	H	16	77 (**a**)
2	2-Me	48	82 (**b**)
3	2-Cl	48	77 (**c**)
4	3-OMe	16	75 (**d**)
5	3-NO_2	16	80 (**e**)
6	3-Cl	16	78 (**f**)
7	4-NO_2	16	78 (**g**)
8	4-Cl	16	90 (**h**)

[a] Isolated yields of prochiral ketones **2a–h** after flash chromatography. In brackets appears the identification of the corresponding α,α-dihalogenated acetophenone, **2a–h** obtained from **1a–h**. For more details see the Experimental Section.

Bioreduction of prochiral α,α-dihaloketones 2a–j

Once synthesised, the asymmetric bioreduction of α,α-dihaloketones **2a–j** was studied by using commercially available and overexpressed ADHs. Owing to our previous experience with similar α-halogenated substrates,[15a,21c,f] six enzymes were used in this study, including also those accepting bulky–bulky ketones as substrates: ADH-A from *Rhodococcus ruber*,[22] RasADH from *Ralstonia* sp.[23] and SyADH from *Sphingobium yanoikuyae*,[24] which are Prelog enzymes;[25] and on the other hand LBADH from *Lactobacillus brevis*,[26] LKADH from *Lactobacillus kefir*,[27] and PR2ADH that are anti-Prelog ADHs (see the Experimental Section for more details). All these biocatalysts accept aromatic ketones bearing a small substituent at alpha position such as methyl or chloromethyl. Besides, RasADH and SyADH can also reduce bulkier substrates.[23,24] Except for RasADH and LKADH, for which glucose and glucose dehydrogenase (GDH) were used to recycle a catalytic amount of the nicotinamide cofactor, 2-propanol was employed as the hydrogen donor (5% v/v). This is owing to the fact that RasADH and LKADH work better under these conditions, as previously described.[23c,28] For clarity, the best results for the synthesis of both **3a–j** enantiomers are collected in Table 2, and in the Supporting Information more detailed information about the screening process can be found.

Satisfyingly, from the twenty possible enantiopure alcohols, fifteen were obtained in enantiomerically pure form, finding ADH-A, LBADH and PR2ADH as the most versatile biocatalysts for the stereoselective reduction of α,α-dihaloacetophenones, which was achieved in eighteen cases with at least 90% conversion. Initially, α,α-dichloroacetophenone (**2a**) was studied yielding selectively either enantiomer of alcohol **3a** in conversions over 95% by using a Prelog enzyme (ADH-A, entry 1) or anti-Prelog reductases (PR2ADH and LBADH, entries 2 and 3). Then, the influence of electron-donating (Me or OMe) or electron-withdrawing substituents (Cl or NO_2), at different positions in the aromatic ring was studied for α,α-dichloroacetophenone

Table 2. Asymmetric bioreduction of ketones **2a–j**.

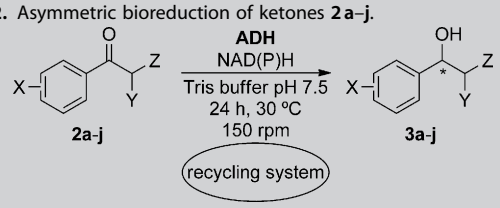

Entry	X	Y	Z	ADH	Conv. [%][a]	*ee* [%][b]
1 (**a**)	H	Cl	Cl	A	96	>99 (*R*)
2 (**a**)	H	Cl	Cl	PR2	99	>99 (*S*)
3 (**a**)	H	Cl	Cl	LB	99	>99 (*S*)
4 (**b**)	2-Me	Cl	Cl	*E. coli*/Ras	99	>99 (*R*)
5 (**b**)	2-Me	Cl	Cl	PR2	43	>99 (*S*)
6 (**c**)	2-Cl	Cl	Cl	*E. coli*/Ras	99	>99 (*R*)
7 (**c**)	2-Cl	Cl	Cl	LB	12	91 (*S*)
8 (**d**)	3-OMe	Cl	Cl	*E. coli*/A	99	>99 (*R*)
9 (**d**)	3-OMe	Cl	Cl	PR2	99	>99 (*S*)
10 (**d**)	3-OMe	Cl	Cl	LB	99	>99 (*S*)
11 (**e**)	3-NO_2	Cl	Cl	A	99	>99 (*R*)
12 (**e**)	3-NO_2	Cl	Cl	LB	96	>99 (*S*)
13 (**f**)	3-Cl	Cl	Cl	A	99	96 (*R*)
14 (**f**)	3-Cl	Cl	Cl	LB[c]	99	>99 (*S*)
15 (**g**)	4-NO_2	Cl	Cl	A	97	>99 (*R*)
16 (**g**)	4-NO_2	Cl	Cl	PR2	99	>99 (*S*)
17 (**h**)	4-Cl	Cl	Cl	A	98	>99 (*R*)
18 (**h**)	4-Cl	Cl	Cl	LB	91	>99 (*S*)
19 (**i**)	3,4-Cl_2	Cl	Cl	*E. coli*/A[c]	99	99 (*R*)
20 (**i**)	3,4-Cl_2	Cl	Cl	LB[c,d]	90	98 (*S*)
21 (**j**)	H	Br	Br	*E. coli*/Ras	99	95 (*R*)
22 (**j**)	H	Br	Br	LB[c,e]	99	99 (*S*)

[a] Conversion values calculated by GC. [b] Enantiomeric excess of alcohols calculated by using chiral GC or HPLC indicating their absolute configuration in brackets [note the switch in the Cahn–Ingold–Prelog (CIP) priority]. [c] DMSO (2% v/v) was added. [d] 48 h and 4.5 U of enzyme employed. [e] 4.5 U of enzyme employed.

derivatives **2b–i**. Clear trends were observed as follows: 1) ADHs led to good levels of activity and stereoselectivity to those substrates with the presence of substituents in the *meta* or *para* position (entries 8–20), whereas for *ortho*-substituted acetophenones **2b,c** (entries 4–7), only the Prelog enzyme RasADH (entries 4 and 6) allowed the isolation of the corresponding (*R*)-alcohols in quantitative yield and enantiopure form. This is especially relevant because the bioreduction of *ortho*-substituted acetophenones remains usually hampered. In a recent contribution, RasADH exhibited good activity for similar ketones;[23b] 2) bulky–bulky ADH from *Ralstonia* sp. was identified as the best enzyme for highly hindered substrates;[23] 3) ADH-A demonstrated also high versatility acting as a very selective enzyme,[22] only leading to low conversion in the case of the 2-methyl derivative **2b** (see also the Supporting Information). Thus, a correct choice between RasADH or ADH-A allowed the synthesis of the (*R*)-alcohols with excellent stereoselectivities and conversions; (iv) the poorest results were generally attained with LKADH, which seemed to be not suitable for dihalohydrins synthesis.

Finally, the bioreduction of a bulkier ketone possessing two bromine atoms at α-position instead of chlorines, α,α-dibromoacetophenone (**2j**), was also analysed, finding complete stereoselectivities for anti-Prelog enzymes PR2ADH and LBADH (entry 22 and see also the Supporting Information), whereas RasADH was found as the best Prelog enzyme (entry 21), ADH-A leading to low conversions and high enantiomeric excess, and SyADH produced (*R*)-**3j** with almost complete conversion but moderate *ee* (see the Supporting Information).

Preparation of racemic α,α-dihaloacetophenones

Owing to the high stereoselectivities obtained for ketones **2a–j**, and to broaden the applicability of the already tested alcohol dehydrogenases, the bioreduction of two halogenated racemic ketones was envisaged, thus 2-bromo-2-chloro-1-phenylethanone (**2k**) and 2-chloro-2-fluoro-1-phenylethanone (**2l**) were prepared by following standard procedures. For **2k**, α-chloroacetophenone was reacted with NBS in the presence of *p*-TsOH in MeCN at 50 °C for 16 h, yielding the ketone in 85% isolated yield. On the other hand, fluoro ketone **2l** was obtained by following the procedure described by Yamazaki et al., starting from ethyl chlorofluoroacetate (56% yield).[29]

Bioreduction of racemic α,α-dihaloketones 2k–l

Owing to the acidity of the α-proton, it was expected that racemisation of the substrates would occur in situ (Scheme 2), making a DKR process feasible obtaining, in the ideal case, one

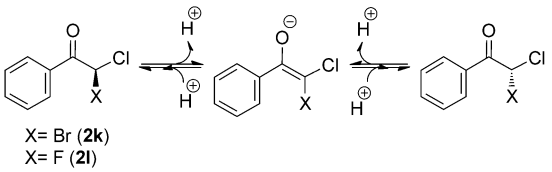

Scheme 2. Interconversion of both **2k** or **2l** enantiomers through an enolate intermediate.

of the four possible diastereoisomer products.[28,30] These enantioenriched alcohols would be of high interest because in a further step they could be selectively modified to obtain more complex and valuable structures as a result of the different reactivity of both halide atoms.

Therefore, we firstly performed a screening with substrate **2k** (Table 3). In a first set of experiments, it was observed that ADH-A, RasADH[23a] and LBADH[26] were the best biocatalysts in terms of activity and selectivity (entries 1–3). Although still far away from a perfect diastereoselectivity, it is remarkable that these enzymes could distinguish between these two halide atoms, because previous results with structurally similar ketones did not show high induction levels.[23b] As ADH-A was the enzyme displaying better diastereoselectivity favouring the formation of the *syn* diastereomer (59%, entry 1), we tried to optimise the process by changing several reaction parameters such as pH or temperature, thus differentially modifying the rate of the enzymatic and the racemisation reactions leading to improved diastereomeric excess (*de*) values. In this regard, low temperatures had a negative influence in the activity of

Table 3. Bioreduction of racemic ketone **2k** ($t = 24$ h).

Entry	ADH	T [°C]	pH	**3k** [%][a]	*ee* [%][b]	*de* [%][b]
1	*E. coli*/ADH-A	30	7.5	99	>99	59 (1*R*,2*R*)
2	*E. coli*/RasADH	30	7.5	95	>99	1 (1*R*,2*RS*)
3	LBADH	30	7.5	65	>99	26 (1*S*,2*R*)
4	*E. coli*/ADH-A	4	7.5	18	>99	58 (1*R*,2*R*)
5	*E. coli*/ADH-A	40	7.5	86	>99	62 (1*R*,2*R*)
6	*E. coli*/ADH-A	30	8.5	98	>99	63 (1*R*,2*R*)
7	LBADH	30	8.5	70	>99	33 (1*S*,2*R*)

[a] Conversion values measured by GC. [b] Enantiomeric and diastereomeric excess measured by chiral HPLC (note the switch in the CIP priority).

the biocatalyst (entry 4), but a higher temperature or pH did not influence the *de* observed (entries 5–7). Higher pH values afforded the decomposition of both substrate and product forming, among other, benzoic acid.

With the aim of gaining a deeper insight in this DKR with ADH-A, we followed the reaction time course to analyse the rate of the racemisation step together with the *de*. In the case of an inefficient racemisation rate, we would detect a decrease of the diastereomeric excess of the alcohol product within the reaction progress (Figure 1). As can be seen, even at low conversions, the *de* values remained almost unaltered during the whole process, showing that the racemisation rate was fast enough for the DKR process.

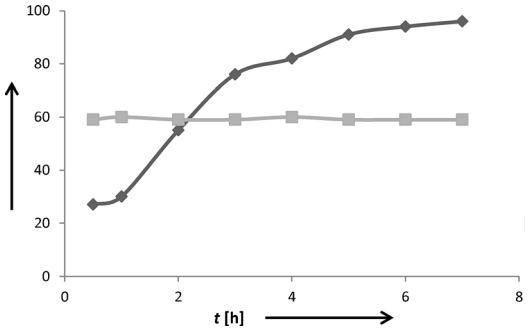

Figure 1. Conversion (◆) and *de* values (■) in the *E. coli*/ADH-A-catalysed bioreduction of ketone **2k** into **3k** at 30 °C and pH 7.5. In all cases, *ee* values were higher than 99%.

Owing to the fact that strong basic conditions decomposed both **2k** and **3k**, several bases in equimolar amounts were added into the reaction medium to study their effect in the DKR process as previously described by us.[30a] Thus, DBU (final pH ≈ 9.0), piperidine (final pH ≈ 9.0), pyridine (final pH ≈ 7.5) and triethylamine (final pH ≈ 8.8) were employed, but no remarkable improvement in the *de* was detected (see the Supporting Information for more details).

Finally, the effect of a non-miscible organic solvent such as *n*-hexane, or a miscible ionic liquid, Ammoeng 102, which already proved to be compatible with ADH-A,[31] was also measured (Figure 2). The use of an external additive could influence both ADH selectivity and reaction rates favouring, in the best scenario, the DKR outcome.[30a] From the results attained, it can be summarised that both biphasic and monophasic media did not have an influence in the enantio- and diastereoselectivity of the process, suggesting that a better biocatalyst to achieve this goal might be constructed by active-site architecture modification rather than medium engineering.

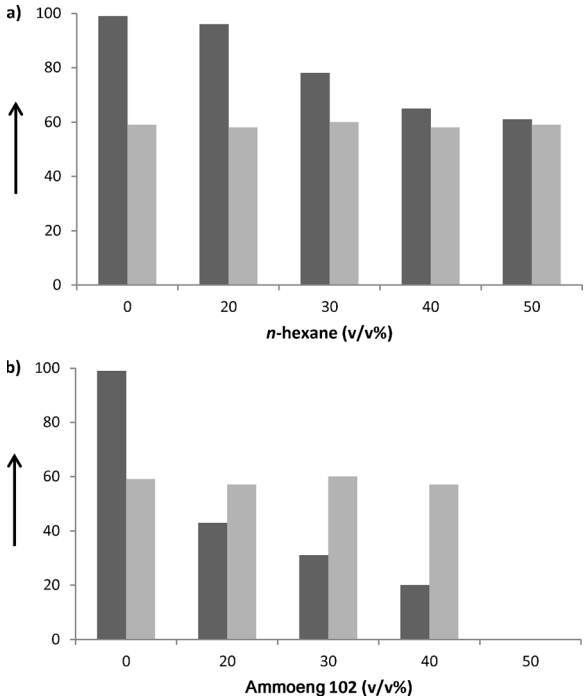

Figure 2. Conversion (■) and *de* values (■) after 24 h in the *E. coli*/ADH-A-catalysed bioreduction of ketone **2k** into **3k** at 30 °C and pH 7.5 with different proportions of: a) *n*-hexane; and b) Ammoeng 102, as cosolvents. In all cases, the *ee* values were higher than 97%.

Crystallisation of acylated alcohol 4

Different attempts were made to obtain suitable crystals for X-ray diffraction analysis to confirm the relative and absolute configuration of the stereogenic centres of **3k**. The most successful approach was achieved, converting the optically active alcohol obtained from the ADH-A-catalysed bioreduction of **2k** into ester **4**, after reaction with 4-nitrobenzoyl chloride in the presence of triethylamine in dry dichloromethane, and subsequent crystallisation using a mixture of diethyl ether and *n*-hexane. As can be seen in Figure 3, both stereogenic centres presented the (*R*)-configuration, and data for the C–OH bond are in agreement with the known stereopreference exhibited by ADH-A as a Prelog enzyme, which determined the absolute configuration at position 2 bearing both halogens.[32]

From the data shown in Table 3, it is remarkable that ADH-A produced the (1*R*,2*R*)-**3k** diastereoisomer with moderate diastereomeric excess (63% *de*), which stands for a *syn* configuration, whereas LBADH slightly preferred the formation of the (1*S*,2*R*)-**3k** diastereoisomer (33% *de*), which accounts for an *anti* configuration. On the other hand, it is noteworthy that the reduction of racemic ketone **2k** with sodium borohydride

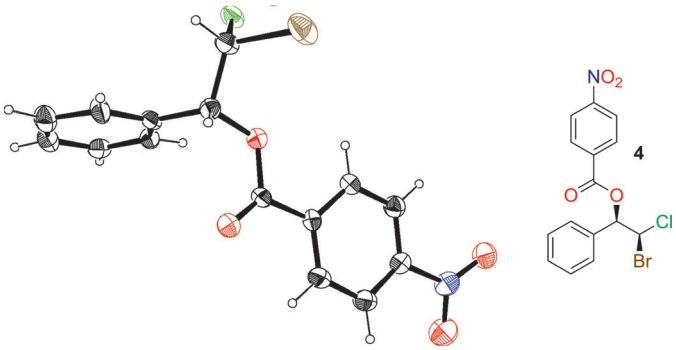

Figure 3. X-Ray structure of ester (*R*,*R*)-**4** synthesised through ADH-A-catalysed bioreduction of racemic ketone **2k**.

led to the formation of the racemic mixtures at a proportion 3:1 (50% *de*) favouring the *anti* diastereoisomer. The opposite diastereopreference displayed by ADH-A compared to $NaBH_4$ or LBADH-catalysed reductions is a very interesting feature, and will be the object of further studies.

Next, the DKR of 2-chloro-2-fluoro-1-phenylethanone (**2l**) was also tried under the best conditions found for ketone **2k**, but as shown in Table 4, although excellent conversions and enantioselectivities were observed, low *de* values were achieved. *Sphingobium yanoikuyae* ADH overexpressed in *E. coli* afforded the highest value of *de* (45%), although with low *ee* (59%, entry 4), whereas the other biocatalysts studied gave access to the enantiopure alcohol **3l** but with vanished diastereoselectivity (entries 1–3). The effect exerted by the fluorine in the diastereomeric excess values was remarkable, probably as a result of a better recognition of the bulky Br atom in substrate **2k** as that of fluorine in ketone **2l**.

Table 4. Bioreduction of racemic ketone **2l** at pH 7.5 and 30 °C ($t = 24$ h).

Entry	ADH	**3l** [%][a]	*ee* [%][b]	*de* [%][b]
1	*E. coli*/ADH-A	99	98	5 (1*R*,2*RS*)
2	*E. coli*/RasADH	99	97	< 1 (1*R*,2*RS*)
3	LBADH	99	> 99	1 (1*S*,2*RS*)
4	*E. coli*/SyADH	98	59	45 (1*R*,2*RS*)

[a] Conversion values measured by GC. [b] Enantiomeric and diastereomeric excess measured by chiral HPLC (note the switch in the CIP priority).

Conclusions

The successful preparation of α,α-dihaloacetophenones as well as an ADH selection guideline for their stereoselective reduction was provided. Enantioenriched dihalohydrins are precursors in the chemical synthesis of a wide number of valuable compounds, but their selective synthesis by traditional chemical methods is hampered by low asymmetric induction or formation of by-products. Thus, different ADHs under mild reaction conditions in aqueous medium were considered as suitable catalysts yielding both enantiomers depending on the choice of the enzyme. A series of dihalohydrins bearing different substitutions in the phenyl ring were obtained with enantiomeric excess values over 95% for both (*R*)- and (*S*)-enantiomers by the correct selection of the ADH for the bioreduction process. In addition, eighteen out of twenty of these alcohol enantiomers were achieved with over 90% conversion, finding lower conversions for the *ortho*-substituted substrates.

Moreover, the asymmetric bioreduction of two racemic ketones, namely α-bromo-α-chloroacetophenone and α-chloro-α-fluoroacetophenone, was also studied. The use of an organic base or cosolvent, and the modification of the temperature or the pH did not have a significant effect on the stereoselectivity of the DKR process. For the first substrate, the corresponding enantiopure alcohol was obtained in excellent conversions, albeit with moderate diastereomeric excess. By using X-ray diffraction, the absolute configuration of the major diastereoisomer obtained could be assigned. For the second racemic ketone, the ADHs could not differentiate between both halogen atoms. Overall, the bioreduction of α,α-dihaloacetophenones was studied by using different ADHs, giving access to valuable enantiopure β,β-dihalohydrins selecting the proper biocatalyst. This study enables the future application of these enzyme-catalysed processes in the syntheses of more complex chiral compounds.

Experimental Section

Overexpressed ADHs from *Rhodococcus ruber* (*E. coli*/ADH-A), from *Ralstonia* species (*E. coli*/RasADH) and *Sphingobium yanoikuyae* (*E. coli*/SyADH) were used as lyophilised cells.[23c,24,33] Glucose dehydrogenase (GDH 002, 30 U mg^{-1}), ADH-A (20 U mg^{-1}), PR2ADH (0.13 U mg^{-1}), and LBADH from *Lactobacillus brevis* (3.7 U μL^{-1}) were purchased from Codexis. LKADH from *Lactobacillus kefir* (0.42 U mg^{-1}) was obtained from Fluka. For the bioreduction processes, Tris–H_2SO_4 buffer was employed in all cases with α-brominated ketones to avoid undesired S_N2 reactions.

Syntheses

Prochiral ketones **2a–h** (general procedure): To a solution of the corresponding acetophenone **1a–h** (3.7 mmol) and *p*-TsOH (708.8 mg, 3.7 mmol) in acetonitrile (10 mL), NCS was added (1 g, 7.6 mmol). The reaction mixture was heated at 50 °C and stirred till disappearance of the starting material (16–48 h). After completion, the solvent was evaporated under reduced pressure and the crude was purified using flash chromatography (50–80% CH_2Cl_2/hexane) yielding the corresponding prochiral ketones (see Table 1).[34]

2,2-Dichloro-1-(3,4-dichlorophenyl)ethanone (**2i**): To a solution of α-chloroacetophenone **1i** (280 mg, 1.25 mmol) and *p*-TsOH (238 mg, 1.25 mmol) in acetonitrile (4 mL), NCS was added (184 mg, 1.37 mmol). The reaction mixture was heated at 50 °C and stirred till disappearance of the starting material (16 h). After completion of the reaction, the solvent was evaporated under reduced pressure and the crude was purified using flash chromatography (20% CH_2Cl_2/hexane) yielding product **2i** as a white solid (0.27 g, 83%).

2,2-Dibromo-1-phenylethanone (**2j**): To a solution of acetophenone (**1a**, 250 mg, 2.08 mmol) and *p*-TsOH (400 mg, 2.08 mmol) in acetonitrile (10 mL), NBS was added (1.11 g, 6.24 mmol). The reaction

mixture was heated at 50 °C and stirred till disappearance of the starting material (16 h). After completion of the reaction, the solvent was evaporated under reduced pressure and the crude was purified using flash chromatography (33% CH_2Cl_2/hexane) yielding product **2j** as a white solid (467 mg, 81%).

Racemic 2-bromo-2-chloro-1-phenylethanone (**2k**): To a solution of α-chloroacetophenone **1k** (500 mg, 3.2 mmol) and *p*-TsOH (615 mg, 3.2 mmol) in acetonitrile (14 mL), NBS was added (863 mg, 4.85 mmol). The reaction mixture was heated at 50 °C and stirred till disappearance of the starting material (16 h). After completion of the reaction, the solvent was evaporated under reduced pressure and the crude was purified using flash chromatography (20% CH_2Cl_2/hexane) yielding **2k** as a white solid (0.64 g, 85%).

Racemic 2-chloro-2-fluoro-1-phenylethanone (**2l**): To a solution of ethyl chlorofluoroacetate (4.35 mmol, 0.5 mL) in dry toluene (5 mL) at −78 °C under nitrogen atmosphere, 1.1 equiv. of phenyl magnesium bromide (1.6 mL of a 3 M solution in Et_2O) was added dropwise and the reaction was stirred for one hour. Following that time, the reaction mixture was warmed up to 0 °C and then left for 10 min prior to the quenching with ammonium chloride (saturated solution). The crude was extracted with Et_2O (3×10 mL), dried over anhydrous Na_2SO_4 and was slowly evaporated under reduced pressure in an ice bath to prevent the loss of the volatile product. The crude mixture was purified using flash chromatography (100% pentane to 70% pentane/CH_2Cl_2) yielding **2l** as a white crystal solid (0.42 g, 56% yield).[29]

Bioreductions

Ketones **2a**–**l** with *E. coli*/ADH-A: To a 15 mg portion of overexpressed *E. coli*/ADH-A (lyophilised cells) in an Eppendorf vial (1.5 mL), Tris–HCl or Tris–H_2SO_4 buffer (510 μL, 50 mM, pH 7.5), NADH (60 μL of a 10 mM solution, final concentration: 1 mM), 2-propanol (30 μL, 5% v/v), and the corresponding ketone (**2a**–**l**, 25 mM) were added. The reaction tubes were shaken horizontally at 30 °C for 24 h and 150 rpm. After that time, the reaction products were extracted with EtOAc (2×0.5 mL). The organic layers were separated by centrifugation (1.5 min, 13000 rpm) and dried over anhydrous Na_2SO_4. Conversion and *ee* values were determined by GC or HPLC analysis.

Scale-up (**2a** with *E. coli*/ADH-A): In an Erlenmeyer flask (10 mL), *E. coli*/ADH-A (100 mg) was suspended in Tris–HCl buffer (3.6 mL, 50 mM, pH 7.5, 1 mM NADH) and preincubated for 30 min at 30 °C. Then, ketone **2a** (50 mg, 0.26 mmol) and 2-propanol (0.4 mL, 10% v/v) were added to the mixture. The reaction was shaken at 30 °C and 250 rpm for 48 h. After incubation, the enzymatic reaction was stopped by extraction with EtOAc (3×5 mL). The organic layers were combined and dried over Na_2SO_4. The solvent was concentrated under vacuum, furnishing the enantiopure alcohol (*R*)-**3a** (isolated yield: 65%).

Ketones **2a**–**l** with LBADH: In an Eppendorf vial (1.5 mL), LBADH (10 μL, 3 U) was added to a 450 μL volume of Tris–HCl or Tris–H_2SO_4 buffer (50 mM, pH 7.5), followed by NADPH (60 μL of a 10 mM solution, final concentration: 1 mM), $MgCl_2$ (60 μL of a 10 mM solution, final concentration: 1 mM), 2-propanol (30 μL, 5% v/v) and the corresponding ketone (**2a**–**l**, 25 mM). The reaction tubes were shaken horizontally at 30 °C for 24 h and 150 rpm. After that time, the reaction products were extracted with EtOAc (2× 0.5 mL). The organic layers were separated by centrifugation (1.5 min, 13000 rpm) and dried over anhydrous Na_2SO_4. Conversion and *ee* values were determined by GC or HPLC analysis.

Ketones **2a**–**l** with LKADH: In an Eppendorf vial (1.5 mL), LKADH (7 mg, 3 U) were added to a 510 μL volume of Tris–HCl or Tris–H_2SO_4 buffer (50 mM, pH 7.5), NADPH (60 μL of a 10 mM solution, final concentration: 1 mM), glucose (30 μmol of a 1 M solution, 50 mM), glucose dehydrogenase (10 μL, 3 U) and the corresponding ketone (**2a**–**l**, 25 mM). The reaction tubes were shaken horizontally at 30 °C for 24 h and 150 rpm. After that time, the reaction products were extracted with EtOAc (2×0.5 mL). The organic layers were separated by centrifugation (1.5 min, 13000 rpm) and dried over anhydrous Na_2SO_4. Conversion and *ee* values were determined by GC or HPLC analysis.

Ketones **2a**–**l** with PR2 ADH: In an Eppendorf vial (1.5 mL), PR2ADH (23 mg, 3 U), a 510 μL volume of Tris–HCl or Tris–H_2SO_4 buffer (50 mM, pH 7.5) were added, NADH (60 μL of a 10 mM solution, final concentration: 1 mM), 2-propanol (30 μL, 5% v/v) and the corresponding ketone (**2a**–**l**, 25 mM). The reaction tubes were shaken horizontally at 30 °C for 24 h and 150 rpm. After that time, the reaction products were extracted with EtOAc (2×0.5 mL). The organic layers were separated by centrifugation (1.5 min, 13000 rpm) and dried over anhydrous Na_2SO_4. Conversion and *ee* values were determined by GC or HPLC analysis.

Ketones **2a**–**l** with *E. coli*/RasADH: To a 15 mg portion of overexpressed *E. coli*/RasADH (lyophilised cells) in an Eppendorf vial (1.5 mL), Tris–HCl or Tris–H_2SO_4 buffer (510 μL, 50 mM, pH 7.5) were added, NADPH (60 μL of a 10 mM solution, final concentration: 1 mM), glucose (30 μmol of a 1 M solution, 50 mM), glucose dehydrogenase (10 μL, 3 U) and the corresponding ketone (**2a**–**l**, 25 mM). The reaction tubes were shaken horizontally at 30 °C for 24 h and 150 rpm. After that time, the reaction products were extracted with EtOAc (2×0.5 mL). The organic layers were separated by centrifugation (1.5 min, 13000 rpm) and dried over anhydrous Na_2SO_4. Conversion and *ee* values were determined by GC or HPLC analysis.

Ketones **2a**–**l** with *E. coli*/SyADH: To a 15 mg portion of overexpressed *E. coli*/SyADH (lyophilised cells) in an Eppendorf vial (1.5 mL), Tris-HCl or Tris-H_2SO_4 buffer (510 μL, 50 mM, pH 7.5) were added, NADPH (60 μL of a 10 mM solution, final concentration: 1 mM), 2-propanol (30 μL, 5% v/v) and the corresponding ketone (**2a**–**l**, 25 mM). The reaction tubes were shaken horizontally at 30 °C for 24 h and 150 rpm. After that time, the reaction products were extracted with EtOAc (2×0.5 mL). The organic layers were separated by centrifugation (1.5 min, 13000 rpm) and dried over anhydrous Na_2SO_4. Conversion and *ee* values were determined by GC or HPLC analysis.

Acknowledgements

This project is supported by the BIOTRAINS Marie Curie Initial Training Network, financed by the European Union through the 7th Framework People Programme (grant agreement number 238531). Financial support from the Spanish Ministerio de Ciencia e Innovación (MICINN-12-CTQ2011-24237), Ministerio de Economía y Competitividad (MAT2010-15094, Factoría de Cristalización—Consolider Ingenio 2010), ERDF and the Principado de Asturias (SV-PA-13-ECOEMP-42 and SV-PA-13-ECOEMP-43) is also gratefully acknowledged. F.R.B. acknowledges INFIQC-CONICET and Universidad Nacional de Córdoba. I.L. acknowledges MICINN for his research contract under the Ramón y Cajal Program.

Keywords: enantioselectivity · enzyme catalysis · halogens · ketones · reduction

[1] These compounds are also described elsewhere as α,α-dihalogenated alcohols or α,α-dihalohydrins but we consider this naming inappropriate for this family of compounds.
[2] a) K. Shibatomi, A. Narayama, Y. Soga, T. Muto, S. Iwasa, *Org. Lett.* **2011**, *13*, 2944 – 2947; b) J. M. Concellón, P. L. Bernad, J. A. Pérez-Andrés, *Angew. Chem. Int. Ed.* **1999**, *38*, 2384 – 2386; *Angew. Chem.* **1999**, *111*, 2528 – 2530.
[3] S. Hahner, M. Fassnacht, *Curr. Opin. Invest. Drugs* **2005**, *6*, 386 – 394.
[4] H. Kakiya, H. Shinokubo, K. Oshima, *Tetrahedron* **2001**, *57*, 10063 – 10069.
[5] Z. Wang, J. Yin, S. Campagna, J. A. Pesti, J. M. Fortunak, *J. Org. Chem.* **1999**, *64*, 6918 – 6920.
[6] R. N. McDonald, R. C. Cousins, *J. Org. Chem.* **1980**, *45*, 2976 – 2984.
[7] a) C. Lee, J. Kim, H. Lee, S. Lee, Y. Kho, *J. Nat. Prod.* **2001**, *64*, 659 – 660; b) R. Ulrich, D. Martin, *J. Med. Chem.* **1992**, *35*, 2238 – 2243.
[8] B. Singh, P. Gupta, A. Chaubey, R. Parshad, S. Sharma, S. C. Taneja, *Tetrahedron: Asymmetry* **2008**, *19*, 2579 – 2588.
[9] a) D. Naskar, S. Roy, *Tetrahedron* **2000**, *56*, 1369 – 1377; b) S. Chowdhury, S. Roy, *Tetrahedron Lett.* **1996**, *37*, 2623 – 2624.
[10] S. Khamarui, D. Sarkar, P. Pandit, D. K. Maiti, *Chem. Commun.* **2011**, *47*, 12667 – 12669.
[11] B. L. Jensen, J. Jewett-Bronson, S. B. Hadley, L. G. French, *Synthesis* **1982**, 732 – 735.
[12] M. Nakagawa, T. Kawate, T. Kakikawa, H. Yamada, T. Matsui, T. Hino, *Tetrahedron* **1993**, *49*, 1739 – 1748.
[13] P. V. Ramachandran, B. Gong, A. V. Teodorović, *J. Fluorine Chem.* **2007**, *128*, 844 – 850.
[14] H. Arasaki, M. Iwata, D. Nishimura, A. Itoh, Y. Masaki, *Synlett* **2004**, 546 – 548.
[15] See, for instance: a) W. Borzęcka, I. Lavandera, V. Gotor, *J. Org. Chem.* **2013**, *78*, 7312 – 7317; b) K. Nakamura, R. Yamanaka, *Tetrahedron: Asymmetry* **2002**, *13*, 2529 – 2533.
[16] A. Goswami, R. L. Bezbaruah, J. Goswami, N. Borthakur, D. Dey, A. K. Hazarika, *Tetrahedron: Asymmetry* **2000**, *11*, 3701 – 3709.
[17] K. Lundell, T. Raijola, L. T. Kanerva, *Enzyme Microb. Technol.* **1998**, *22*, 86 – 93.
[18] T. Matsuda, T. Harada, N. Nakajima, T. Itoh, K. Nakamura, *J. Org. Chem.* **2000**, *65*, 157 – 163.
[19] B. Barkakaty, Y. Takaguchi, S. Tsuboi, *Tetrahedron* **2007**, *63*, 970 – 976.
[20] Recent bibliography: a) F. Hollmann, K. Bühler, B. Bühler, in *Enzyme Catalysis in Organic Synthesis* (Eds.: K. Drauz, H. Gröger, O. May), Wiley-VCH, Weinheim, **2012**, pp. 1325 – 1438; b) F. Hollmann, I. W. C. E. Arends, D. Holtmann, *Green Chem.* **2011**, *13*, 2285 – 2313; c) E. García-Urdiales, I. Alfonso, V. Gotor, *Chem. Rev.* **2011**, *111*, PR110 – PR180; d) M. M. Musa, R. S. Phillips, *Catal. Sci. Technol.* **2011**, *1*, 1311 – 1323.
[21] Selected recent examples: a) G.-C. Xu, H.-L. Yu, X.-Y. Zhang, J.-H. Xu, *ACS Catal.* **2012**, *2*, 2566 – 2571; b) J. Mangas-Sánchez, E. Busto, V. Gotor-Fernández, F. Malpartida, V. Gotor, *J. Org. Chem.* **2011**, *76*, 2115 – 2121; c) F. R. Bisogno, A. Cuetos, A. A. Orden, M. Kurina-Sanz, I. Lavandera, V. Gotor, *Adv. Synth. Catal.* **2010**, *352*, 1657 – 1661; d) J. H. Schrittwieser, I. Lavandera, B. Seisser, B. Mautner, W. Kroutil, *Eur. J. Org. Chem.* **2009**, 2293 – 2298; e) E. Alanvert, C. Doherty, T. S. Moody, N. Nesbit, A. S. Rowan, S. J. C. Taylor, F. Vaughan, T. Vaughan, J. Wiffen, I. Wilson, *Tetrahedron: Asymmetry* **2009**, *20*, 2462 – 2466; f) F. R. Bisogno, I. Lavandera, W. Kroutil, V. Gotor, *J. Org. Chem.* **2009**, *74*, 1730 – 1732.
[22] a) E. Hamnevik, C. Blikstad, S. Norrehed, M. Widersten, *J. Mol. Catal. B*, DOI: 10.1016/j.molcatb.2013.10.023; b) M. Karabec, A. Łyskowski, K. C. Tauber, G. Steinkellner, W. Kroutil, G. Grogan, K. Gruber, *Chem. Commun.* **2010**, *46*, 6314 – 6316.
[23] a) J. Kulig, A. Frese, W. Kroutil, M. Pohl, D. Rother, *Biotechnol. Bioeng.* **2013**, *110*, 1838 – 1848; b) J. Kulig, R. C. Simon, C. A. Rose, S. M. Husain, M. Häckh, S. Lüdeke, K. Zeitler, W. Kroutil, M. Pohl, D. Röther, *Catal. Sci. Technol.* **2012**, *2*, 1580 – 1589; c) I. Lavandera, A. Kern, B. Ferreira-Silva, A. Glieder, S. de Wildeman, W. Kroutil, *J. Org. Chem.* **2008**, *73*, 6003 – 6005.
[24] I. Lavandera, A. Kern, V. Resch, B. Ferreira-Silva, A. Glieder, W. M. F. Fabian, S. de Wildeman, W. Kroutil, *Org. Lett.* **2008**, *10*, 2155 – 2158.
[25] This article specifies the stereopreference of some ADHs, see: V. Prelog, *Pure Appl. Chem.* **1964**, *9*, 119 – 130.
[26] a) S. Leuchs, L. Greiner, *Chem. Biochem. Eng. Q.* **2011**, *25*, 267 – 281; b) M. Wolberg, W. Hummel, C. Wandrey, M. Müller, *Angew. Chem. Int. Ed.* **2000**, *39*, 4306 – 4308; *Angew. Chem.* **2000**, *112*, 4476 – 4478.
[27] W. Hummel, *Appl. Microbiol. Biotechnol.* **1990**, *34*, 15 – 19.
[28] A. Cuetos, A. Rioz-Martínez, F. R. Bisogno, B. Grischek, I. Lavandera, G. de Gonzalo, W. Kroutil, V. Gotor, *Adv. Synth. Catal.* **2012**, *354*, 1743 – 1749.
[29] T. Yamazaki, T. Terajima, T. Kawasaki-Takasuka, *Tetrahedron* **2008**, *64*, 2419 – 2424.
[30] For other recent dynamic protocols involving ADHs, see: a) J. Mangas-Sánchez, E. Busto, V. Gotor, V. Gotor-Fernández, *Org. Lett.* **2013**, *15*, 3872 – 3875; b) F. Xu, J. Y. L. Chung, J. C. Moore, Z. Liu, N. Yoshikawa, R. S. Hoerrner, J. Lee, M. Royzen, E. Cleator, A. G. Gibson, R. Dunn, K. M. Maloney, M. Alam, A. Goodyear, J. Lynch, N. Yasuda, P. N. Devine, *Org. Lett.* **2013**, *15*, 1342 – 1345; c) D. Kalaitzakis, I. Smonou, *Eur. J. Org. Chem.* **2012**, 43 – 46; d) G. A. Applegate, R. W. Cheloha, D. L. Nelson, D. B. Berkowitz, *Chem. Commun.* **2011**, *47*, 2420 – 2422.
[31] a) G. de Gonzalo, I. Lavandera, K. Faber, W. Kroutil, *Org. Lett.* **2007**, *9*, 2163 – 2166; b) G. de Gonzalo, I. Lavandera, K. Durchschein, D. Wurm, K. Faber, W. Kroutil, *Tetrahedron: Asymmetry* **2007**, *18*, 2541 – 2546.
[32] Crystallographic data: $C_{15}H_{11}BrClNO_4$, $M = 384.61$, monoclinic, $a = 12.2449(7)$ Å, $b = 10.0624(8)$ Å, $c = 13.1537(7)$ Å, $\beta = 90.428(5)^\circ$, $V = 1620.7(2)$ Å^3, $T = 293(2)$ K, space group $P2_1$, $Z = 4$. CCDC 963560 contains the crystallographic data for the structure of ester (*R*,*R*)-**4**. These data can be obtained free of charge from the Cambridge Crystallographic Data Centre through www.ccdc.cam.ac.uk/data_request/cif.
[33] K. Edegger, C. C. Gruber, T. M. Poessl, S. R. Wallner, I. Lavandera, K. Faber, F. Niehaus, J. Eck, R. Oehrlein, A. Hafner, W. Kroutil, *Chem. Commun.* **2006**, 2402 – 2404.
[34] Adapted from: J. C. Lee, Y. H. Bae, S. K. Chang, *Bull. Korean Chem. Soc.* **2003**, *24*, 407 – 408.

Received: September 30, 2013
Published online on February 12, 2014

CHAPTER II

Crystal structure of alcohol dehydrogenase from *Sphingobium yanoikuyae*

Introduction

2.1.1. X-ray crystallography of macromolecules

X-ray diffraction crystallography occupies a solid position among the modern techniques for structural determination of macromolecules, which comprise nucleic acids, viruses, ribosomes and in particular proteins. Thus, this methodology has been used in 88.5% out of 90.852 cases of protein structures currently deposited in Protein Data Bank.[105] Other methods involve solution and solid state NMR, electron microscopy, neutron diffraction and electron crystallography. Knowledge of enzyme structure involved in any biological or chemical study is of paramount importance, regardless whether is basic science or applied biotechnology, as it allows:

a) elucidation of enzymatic mechanisms and structure–function relationships,
b) studies of protein complexes, as well as structural comparison between native and mutated proteins,
c) structure-based drug design,
d) and establishment of protein taxonomy.[106]

Since launching structural genome programs that have provided an insight into the genomic profile of diverse families of organisms, it has become apparent that proteins with the same fold and quaternary structure show no sequence identity. Moreover, these proteins can perform the same, similar or different functions, which implies that knowledge of the structure alone is not sufficient in deciphering the biochemical function of the protein. It also became evident that proteins are made of smaller domains that are being reused to perform different functions.[107] Rapid advances in structural biology have been attributed to the improvement in molecular biology techniques, which are used during the protein production. Recombinant technologies for gene cloning and protein expression have also been critical to achieve this goal.[108]

2.1.1.1. Gene cloning

Among the molecular biology techniques routinely used in the production of recombinant DNA, gradient PCR (polymerase chain reaction) and ligation independent

[105] http://www.rcsb.org/pdb/home/home.do, state of 3 March 2014.
[106] E. F. Garman, *Science* **2014**, *343*, 1102-1108.
[107] A. Joachimiak, *Curr. Opin. Struct. Biol*. **2009**, *19*, 573-584.
[108] A. Yonath, *Curr. Opin. Struct. Biol*. **2011**, *21*, 622-626.

cloning (LIC vectors) are highly efficient and time-saving approaches employed in this study.

Since 1983 when PCR was invented, gene engineering has undergone rapid development. The method aims the amplification of DNA material in repeated cycles of the enzymatic reaction using a thermostable polymerase. Each cycle of the process consists of three steps: DNA template denaturation, primers annealing and DNA extension.[109] The crucial step of the PCR technique is the annealing of primers to both ends of the denaturized DNA strands. In case of the failure of the initial experiment, the annealing temperature is being modified in the first place. Therefore, gradient PCR allows performing simultaneous PCR reactions in one block for rapid screening towards the optimum annealing temperature. It strongly depends on the melting temperature (T_m) of the primers, which in turn depends on the length and base composition, guanine and cytosine having greater impact on T_m.

Another technique that has significantly improved the robustness of the cloning process is the ligation independent cloning, which avoids the usage of restriction enzymes but takes advantage of electrostatic forces between complementary base pairs (Figure 2.1). This method uses T4 DNA polymerase that also catalyzes the reverse reaction of nucleotides cleavage, and thus acts as a 3'-5'-exonuclease.[109]

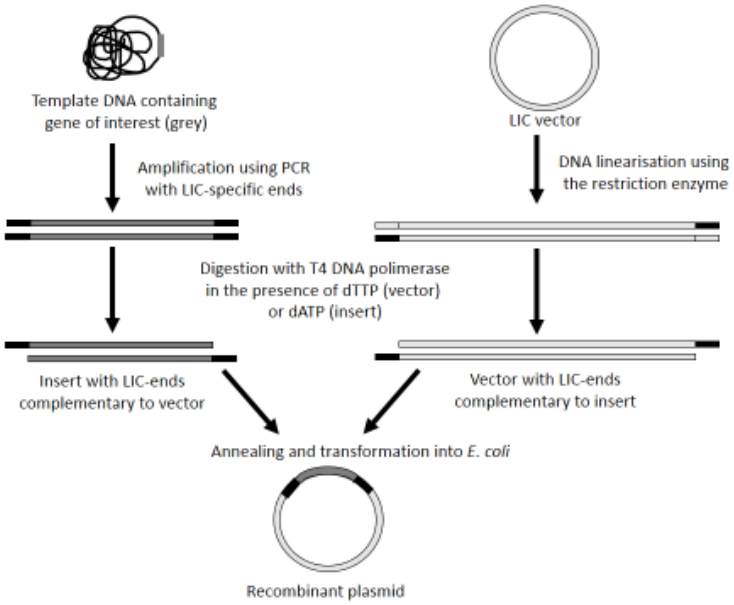

Figure 2.1. Ligation independent cloning (LIC-PCR). Adapted from reference 109.

[109] G. Grogan, *Practical Biotransformations: A Beginner´s Guide*, Wiley-Blackwell, Chichester, **2009**.

The idea behind this technique relies on the formation of 10-15 single base overhangs on the especially designed vector plasmid, and complementary sticky ends set on the insert that match to each other. These single strand overhangs are generated by T4 DNA polymerase, which in the presence of only one type of deoxynucleotide triphosphate in the reaction mixture, for example deoxythymidine triphosphates (dTTPs), switches to exonuclease activity and cleaves off nucleotides until the first complementary base, in this case adenine. The annealing of the insert and the vector is performed in the absence of ligase by simple mixing of DNA fragments. This process is very efficient because only the desired products can be formed.

2.1.1.2. Protein expression and purification

Efficient production of the recombinant protein depends on many factors, among which selection of the right host system and a DNA vector determine the correctly folded protein. The most commonly used expression systems for protein production are bacteria *E. coli*, yeast *Saccharomyces cerevisiae* or *Pichia pastoris*, and insect cells Sf9. The choice of the host organism depends on the type of protein to be overexpressed, *i.e.* eukaryotic proteins often require post-translational modifications like glycosylation, which prokaryotic machinery cannot provide. Therefore, eukaryotic systems of yeast or insect cells are exploited to overexpress multi-domain proteins, since in the case of the *E. coli* system, it produces them in a form of insoluble inclusion bodies. In terms of DNA vector systems, plasmids, viruses (like baculovirus), artificial chromosomes or bacteriophages (like lambda that infects *E. coli*) have been used.[110]

In the most general view, protein expression is a three-step process: (i) transcription of the cell DNA to messenger RNA (mRNA); (ii) translation of mRNA into an amino acid sequence at the ribosome, and (iii) folding of the amino acid sequence into a protein, as shown in Figure 2.2.[111] Regulation of the protein synthesis takes place usually at the beginning of the level of transcription. In order to induce the protein production, the gene encoding this protein has to be expressed. It is achieved by introducing beside the gene sequence in the plasmid vector an additional promoter

[110] D. L. Nelson, M. M. Cox, *Lehninger Principles of Biochemistry*, 3rd Ed., Chapter 29, W. H. Freeman and Company, New York, **2001**.
[111] D. L. Nelson, M. M. Cox, *Lehninger Principles of Biochemistry*, 3rd Ed., Chapter 28, W. H. Freeman and Company, New York, **2001**.

sequence, like *lac* operon, that controls the production of the given protein upon inducement. To trigger protein expression, an allolactose analog, *i.e.* isopropyl β-D-1-thiogalactopyranoside (IPTG), is added to the growing cells. Since IPTG binds to the *lac* suppressor[112] which forms part of the *lac* operon regulatory system, transcription of genetic information is activated.

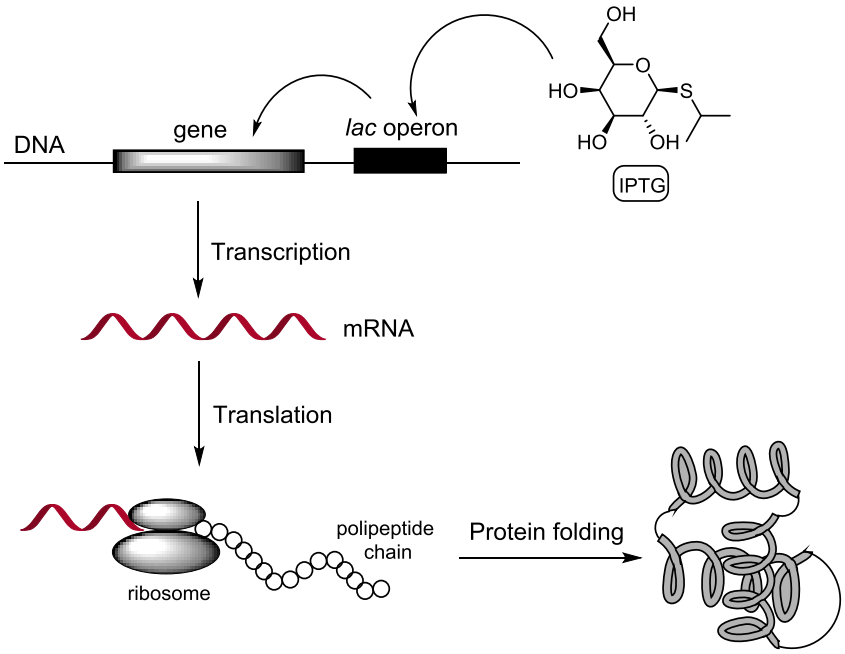

Figure 2.2. Simplified steps leading from gene to protein expression: (i) Transcription involves production of messenger RNA (mRNA) from DNA template using RNA polymerase. The important feature of the mRNA sequence is its complementary character to the template DNA sequence and it is built of adenine, cytosine, guanine, and uracil (replacing thymine) nucleotides; (ii) translation is the process where the cell forms a polypeptide chain using the mRNA sequence as a template. A ribosome translates the mRNA in three-nucleotide segments which code a different amino acid; (iii) protein folding is the process where a polypeptide chain folds into a functional protein. Due to the aqueous environment inside the cell, the amino acid chain folds in order to hide the hydrophobic amino acids from the cell content, and exposes those with hydrophilic character.

[112] Regulatory protein that inhibits the expression of β-galactosidase in the absence of lactose (lac).

Purity of a protein is a critical condition to obtain high quality crystals. For this purpose, at least two different separation methods are applied in order to ensure a minimum of 95% homogeneity of the target protein. To facilitate the purification process, recombinant proteins are usually expressed as either fused proteins or tagged with a short sequence of additional residues (*e.g.*, histidine-tagged). These changes should not interfere with the natural enzyme folding, but add a new physical property that is used in the course of the purification. As a result, proteins can be separated from their impurities using chromatography techniques which take advantage of their specific properties, as shown in Table 2.1.

Table 2.1. Separation principles in chromatography protein purification.[113]

Property	Technique
Size	Gel filtration (GF)/ Size exclusion chromatography (SEC)
Hydrophobicity	Hydrophobic interaction chromatography (HIC) Reversed phase chromatography (RPC)
Charge	Ion exchange chromatography (IEX)
Ligand specificity	Affinity chromatography (AC)
Isoelectric point	Chromatofocusing (CF)

2.1.1.2.1. Immobilized metal affinity chromatography (IMAC)

Affinity chromatography takes advantage of the so-called affinity tags expressed together with the protein of interest. Among several known protein tags, the most commonly incorporated are short peptide sequences (5-10 amino acids), like the histidine tag comprising six histidine amino acids (His-tag), the Strep-tag II,[114] a sequence of 8 amino acids which binds to Strep-Tactin, an engineered streptavidin protein, or fused protein tags like GST (glutathione-S-transferase) and MBP (maltose binding protein).[113] The purification is simplified by the high affinity of the tagged protein to the modified agarose matrix that contains covalently bound ligands, such as metal ions (when using His-tag), proteins like streptavidin (in the case of Strep-tag), specific substrates such as glutathione (in the case of GST) or amylose agarose (for MBP). First, the sample is loaded on the column under conditions that favor the binding

[113] http://www.gelifesciences.com/handbooks, from *Gel filtration. Principles and methods*, GE Healthcare.
[114] T. G. M. Schmidt, A. Skerra, *Nat. Protoc.* **2007**, *2*, 1528-1535.

to the ligand, while the unbound material is washed away. Next, the bound target protein is recovered by changing conditions to those favoring elution. This is performed specifically, using a competitive ligand (imidazole for His-tag affinity or D-desthiobiotin for Strep-Tag II), or non-specifically, by changing the pH and/or the ionic strength. Alternatively, the target protein can be eluted by cleaving off the affinity tag.

In immobilized metal affinity chromatography, the interaction of certain superficial protein residues such as cysteine, histidine, and to a lesser extent tryptophan with transition metal cations that form chelates such as Ni^{2+}, Co^{2+}, Zn^{2+}, or Cu^{2+}, is used. Among the mentioned cations, cobalt displaces the highest selectivity towards a poly-His sequence, but the lowest loading capacity on the column. On the contrary, copper possess high loading capacity with low selectivity. Therefore, the compromise involves the usage of nickel or zinc in metal affinity chromatography as they are characterized by intermediate selectivity and loading capacity.

2.1.1.2.2. Size exclusion chromatography (SEC)

Molecules such proteins are separated according to differences in their size as they pass through a gel filtration medium packed in the column (Figure 2.3). In contrast to affinity chromatography, molecules do not bind to the stationary phase, so buffer composition does not directly affect the resolution. Therefore, this is a method of choice for biomolecules that may be sensitive to pH changes, concentration of metal ions or cofactors and harsh environmental conditions, as the separation processes can be performed in the presence of essential ions or cofactors, detergents, urea and guanidine hydrochloride, at high or low ionic strength, 37 °C or at low temperatures according to the requirements of the experiment.

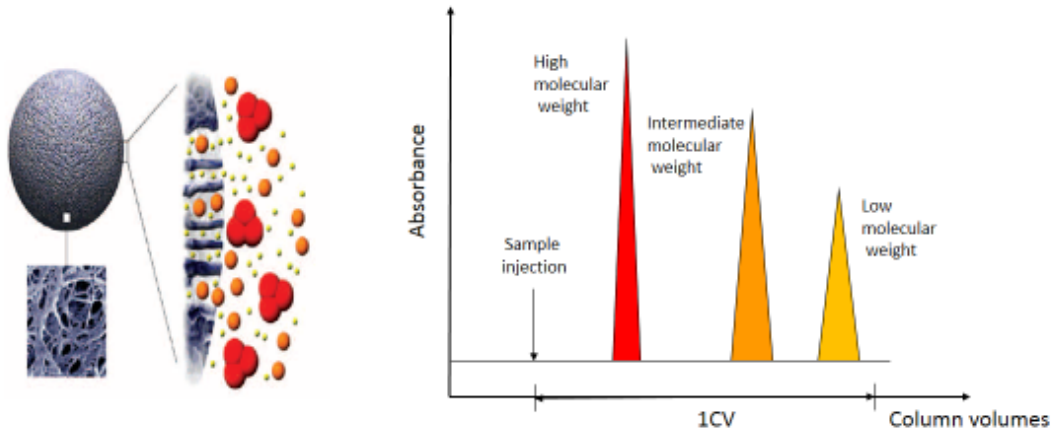

Figure 2.3. Order of elution from the Superdex™ column based on the size of the proteins in the mixture: the largest molecule (red) is eluted first while the smallest molecule (yellow) is the most delayed. Adapted from reference 113.

One of the most commonly used gel filtration column packing is Superdex™, composed of highly cross linked porous agarose particles with dextran chains covalently bonded. The resulting material combines high physical and chemical stability due to the agarose matrix, and excellent gel filtration properties mainly determined by the dextran chains.

2.1.2. X-ray crystallography of proteins

In possession of single and reasonable sized crystals, X-ray diffraction on synchrotron bean allows the collection of the necessary data to build an atomic model of the protein. X-ray diffraction analyses yield electron density maps that reflect the exact position for each atom of a given molecule. In order to calculate these electron densities from the diffraction map, three pieces of data are needed: (i) reflection coordinates in three dimensions (known as the Miller indices h,k,l); (ii) reflection intensity I (hkl); and (iii) reflection phase angles α (hkl). The two first values are directly determined during

the experiment, but the last one accounts for the so-called phase problem and has to be determined indirectly.[115]

It was found that synchrotron radiation provides unprecedented experimental tools for the determination of the crystallographic phases, since properties such as high beam brightness, collimation and wavelength tunability enable accurate structural determination. As a result, resonant diffraction methods capable of direct phase determination were pioneered. They were based on the discovery of the critical connection between the desired phases and discrete points in continuous wavelength spectra of the synchrotron radiation. This phasing method utilizes selected wavelengths that cover the absorption edge of specific atoms serving as anomalous scatters.

In addition, X-ray crystallography of macromolecules has benefited from developments in genetic manipulations that occurred at the same time. Multi/single-wavelength anomalous dispersion (MAD/SAD) involves the benign introduction of selenium instead of sulfur into proteins, as a vehicle for direct protein structure determination and has replaced soaking with heavy atom methods (multiple isomorphous replacement). Importantly, over 90% of the currently available atomic-level *de novo* structures were determined by MAD/SAD. Among them, nearly 70% used selenomethionine.[108] However, the usage of these direct methods with the naturally or artificially introduced presence of heavy metals (Hg, Pt, Au, Ag, Cu or Fe), requires longer exposition times to X-ray, which in turn results in the decay of the diffraction signal. One of the consequences of crystal exposure to different doses of intense X-ray radiation from synchrotron is the formation of free radicals that determines the lifetime of a given crystal even at 100 K. Since high beam brightness causes instant damages to the biological crystals, the experiment requires cryo temperatures.[116]

Apart from *de novo* methods of crystal structure determination, an indirect approach has been developed and is known as molecular replacement. This method is based on the structural homology between already solved protein structures and the unknown protein. In case when such model is not available, isomorphic methods or extraction of anomalous signals are techniques of choice to afford the final structure.

[115] P. Atkins, J. de Paula, *Physical Chemistry*, 8th Ed., Chapter 20, Oxford University Press, New York, **2006**.
[116] J. A. K. Howard, M. R. Probert, *Science* **2014**, *343*, 1098-1102.

2.1.3. Crystal formation phenomena

Crystallization of a molecule from its solution represents a reversible equilibrium phenomenon driven by the thermodynamic principle of minimization of the system free energy. Crystallization of a macromolecule categorically entails the creation of a supersaturated state. When more molecules are added into solution, there is no sufficient solvent to maintain full hydration of the molecules. Under these conditions, the system is no longer at equilibrium (Figure 2.4).

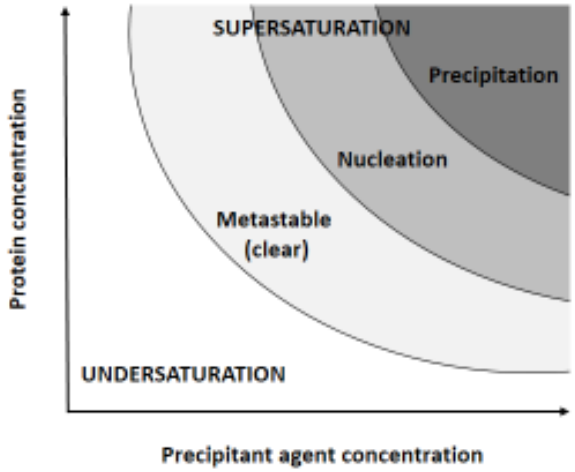

Figure 2.4. Crystallization phase diagram: the solubility curve divides the concentration space into two main areas that correspond to the undersaturated and supersaturated states of a protein solution. Within the supersaturation zone can be distinguished: (i) the precipitation zone where the excess of protein molecules immediately separates from the solution to form amorphous aggregates; (ii) the nucleation zone where the excess of protein molecules aggregates in the crystalline form, so microcrystal clusters tend to appear near the precipitation zone; and (iii) a metastable zone where the protein in supersaturated state may not nucleate for a long period of time unless a seed crystal is introduced.[117]

The equilibrium is re-established by formation of a solid state such as crystals, to compensate the excess of the solute in the saturated solvent. Formation of crystals is known to lower the free energy of proteins by 3-6 kcal/mol relative to the dissolved

[117] D. Chirgadze, *Protein Crystallisation in Action*, Cambridge University, **2001**. http://www.xray.bioc.cam.ac.uk/xray_resources/whitepapers/xtal-in-action/xtal-in-action-html.html.

state in the solution.[118] However, proteins can also precipitate in the form of amorphous aggregates that are kinetically favored over crystal nuclei. It is noteworthy that formation of crystal does not directly imply subsequent growth of macroscopic crystals. Nucleus must first exceed the critical size, defined by the ratio between the surface area to its volume. This critical nuclei corresponds to the activation energy. By analogy to conventional chemical reactions, an energy barrier must be overcome to create a stable nucleus of a crystal. The higher the energy barrier, the slower the rate of nucleation is. Molecules crystallize from metastable supersaturated solutions as long as the non-equilibrium forces prevail.[117]

Although crystals formed by macromolecules and inorganic or small organic compounds share the same mechanistic pathways of growth, thermodynamic and kinetic regulation of the crystallization of macromolecules is affected by the following factors: (i) the complexity and high mobility at the surface and as a whole for large molecules; (ii) the electrostatic nature of macromolecules; (iii) relatively low chemical and physical stability of proteins (unfolding, hydration requirements, mechanical and temperature sensitivity); and (iv) extremely high level of supersaturation required for nucleation to occur.[117] Specific characteristics of macromolecular crystals are also a high content of solvent surrounding the molecules (up to 90%) and the fact that crystalline order deteriorates if the crystals are allowed to dehydrate. Such high sensitivity to dehydration implies that the intermolecular interactions supporting the crystalline lattice are weak.[106]

2.1.4. Selected crystallization techniques

2.1.4.1. High throughput screenings

Crystallization of a protein is a challenge. Once problems with the protein expression in an adequate system are overcome, the purification protocol must yield more than 95% pure protein. Then, adequate crystallization conditions have to be found. In the last years, despite the considerable progress in understanding the crystallization events, crystals have still been obtained in a trial and error manner with the aid of high throughput screening. These miniaturized multifactorial screens combined with automation systems allow exposing a protein to a number of different crystallization parameters, such as pH, buffer type, salts, organic solvents or polymers (polyethylene

[118] A. McPherson, *Methods* **2004**, *34*, 254-256.

glycols, PEGs). Commercially available scare matrix screenings are designed to obtain maximum information on the protein while using a minimal amount of the sample by systematic analysis. Examples of screening strategies behind the commercial products are shown in Table 2.2.

Table 2.2. Basic concepts behind typical screening kits.

INDEX[119] (by Hampton Research)	**PACT**[120] (by QIAGEN)	**CSSI&II**[121] (by Molecular Dimensions Ltd.)
Traditional salts *vs* pH Neutralized organic acids High [salt] with low [polymer] High [polymer] with low [salt] Low ionic strength *vs* pH PEG & Salt *vs* pH PEG & Salt	Systematic analysis of the effect of pH and anions and cations PEG/ion combinations for systematic analysis of cations and anions at defined pHs	At pH of choice analysis of: Low [salt] *vs* increasing [PEG] High [salt] High [aliphatic diols]

Following crystals growth, scale-up experiments are performed around the best conditions by subtle tuning of crucial parameters like pH, salt and organic precipitant concentrations.

2.1.4.2. Hanging drop vapor diffusion technique

The most common approach to grow crystals is the hanging or sitting drop vapor diffusion technique as shown in Figure 2.5. This method involves water evaporation and

[119] https://hamptonresearch.com/product_detail.aspx?cid=1&sid=24&pid=5.
[120] http://www.qiagen.com/products/protein/crystallization/compositiontables/pdf/1057791_ps_xtal_pact-suite_update_160609_lowres.pdf.
[121] A. M. Brzozowski, J. Walton, *J. Appl. Cryst.* **2001**, *34*, 97-101.

diffusion between a diluted protein solution and a mother liquor (precipitant) to reach the supersaturation state necessary for protein crystallization.[117] Generally, protein solution is mixed with the precipitant at a ratio 1:1 on the glass slide and sealed over the well containing the precipitant at the desired concentration in the excessive volume. Difference in the precipitant concentration between the mother liquor and the drop causes the evaporation of water from the drop until the precipitant concentration remains equal in both solutions. In thermodynamic terms, the protein concentration in the drop changes from undersaturation to supersaturation state, and once crystals appear the protein concentration decreases. Crystal will grow then until the system reaches the equilibrium.

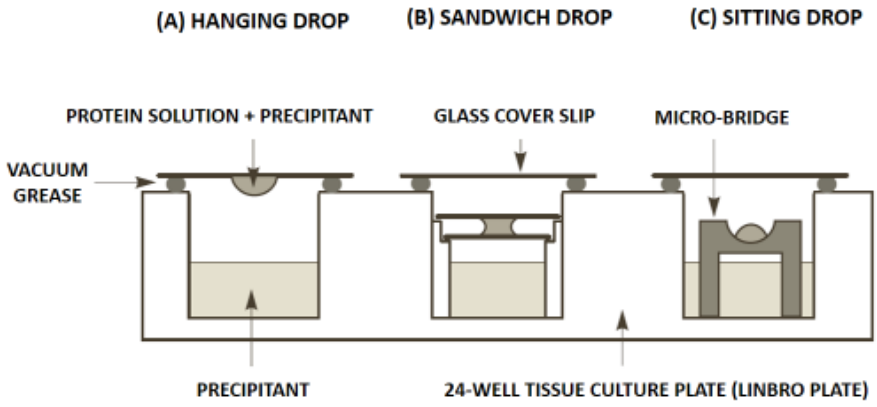

Figure 2.5. Crystallization settings in vapor diffusion techniques. Adapted from reference 117.

2.1.5. Alcohol dehydrogenase from *Sphingobium yanoikuyae* (SyADH)

Bacteria of genus *Sphingomonas* have been found in soils contaminated with polycyclic aromatic hydrocarbons (PAHs), such as anthracene and benzopyrene, as they are able to degrade a wide range of xenobiotics also including chlorinated and sulfonated aromatics.[122] Alcohol dehydrogenase from strain *Sphingobium yanoikuyae* DSM 6900 was first identified by Kroutil's group during routine screening for a non-selective biooxidant of secondary alcohols.[34a] Biochemical analysis revealed that the enzyme belonged to the family of short chain dehydrogenases as it was 262 amino acids long. Moreover, it showed NADPH preference. In terms of stereo-discrimination of

[122] (a) M. Cunliffe, A. Kawasaki, E. Fellows, M. A. Kertesz, *FEMS Microbiol. Ecol.* **2006**, *58*, 364-372; (b) M. Ochou, M. Saito, Y. Kurusu, *Biosci. Biotechnol. Biochem*. **2008**, *72*, 1130-1133.

prochiral substrates, it was non-selective toward substrates with one small group, like aliphatic secondary alcohols including 2-hexanol or 2-octanol.[34a] However, once the ketone contained in its structure an aryl group and the other substituent next to the carbonyl group was at least 3 carbon long, this is, a 'bulky-bulky' ketone, it was readily accepted affording high conversions and increasing *ee* towards *S*-alcohols, as shown in Figure 2.6.[123] Additionally, recent studies involving a series of α-alkyl-β-keto esters have found high preference for α-methylated β-keto methyl, ethyl and benzyl esters while low enantiodiscrimination when testing esters substituted with larger groups at α-position (Figure 2.6).[58]

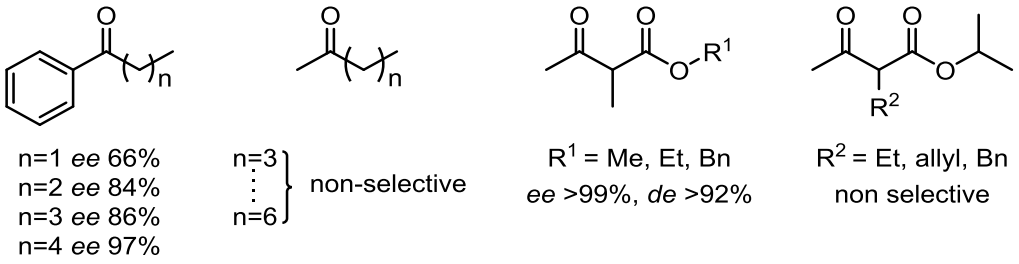

Figure 2.6. Examples of substrates investigated with SyADH.

In the present work, *Sphingobium yanoikuyae* was included in the screening of known 'bulky-bulky' alcohol dehydrogenases to accept α,α-dihalogenated aryl ketones, as shown in Chapter I. Interestingly, results obtained for this enzyme gave the most diverse response with respect to stereospecificities and conversions *vs* substrate structure, as presented in Figure 2.7. It could be clearly seen that nitro substituents in *meta* or *para* position (substrates **2e** and **2g**) hugely affected SyADH performance, yielding (*R*)-alcohols with low yields (<50%) and even worse *ee* (<35%). In contrast, the most favorable substrate among all tested compounds was ketone **2d** bearing a methoxy substituent at *meta* position of the aryl group, which was transformed with both excellent conversion and *ee* values (>99%). For substrates bearing chlorine (**2c, 2f** and **2h**), less electronegative than the nitro group, very good conversion rates (>75%) and moderate *ee* were observed, with the exception for 2',2'-dichloro-(3,4-dichlorophenyl)ethanone (**2i**) that yielded the (*R*)-alcohol with very low *ee* (<20%).

[123] I. Lavandera, G. Oberdorfer, J. Gross, S. de Wildeman, W. Kroutil, *Eur. J. Org. Chem.* **2008**, 2539-2545.

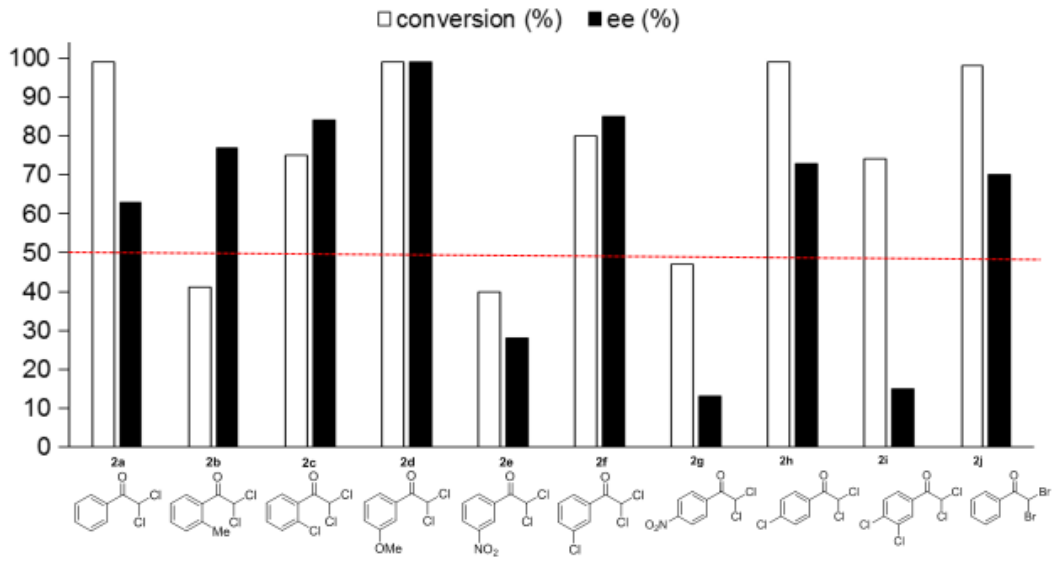

Figure 2.7. Effect of substrate structure on SyADH-catalyzed bioreduction reactions of α,α-dihalogenated aryl ketones. In all cases the alcohol preferred presented *R*-configuration (Prelog selectivity).

Finally, for unsubstituted substrates such as dichloro- and dibromoacetophenone (**2a** and **2j**), conversion values obtained with this enzyme were excellent, but enantiomeric excess reached a moderate level (63 and 70%, respectively). Interestingly, trials with racemic α-bromo-α-chloro- and α-chloro-α-fluoroacetophenone gave the highest diastereomeric excess values (77 and 45% *de*, respectively) in comparison to other ADHs, although with moderate enantioselectivity (79 and 59%, respectively). All these data encouraged us to further investigate the molecular basis for SyADH substrate recognition.

Objectives

Since crystal structure of alcohol dehydrogenase from *Sphingobium yanoikuyae* was not known at the time of this study, it was set as a goal to crystallize and resolve the structure of this enzyme. This ADH is a highly versatile biocatalyst capable of accepting voluminous substrates, therefore it would be of interest to elucidate the structural features which makes possible for this ADH the acceptance of these type of ketones/alcohols. With this purpose, a short term placement at the York Structural Biology Laboratory at the University of York was performed under the supervision of Prof. Gideon Grogan. To achieve this, the following objectives were put forward:

- Subcloning of the SyADH gene into a pET-YSBLIC-3C vector.

- Expression of the protein in an *E. coli* system as a soluble fraction.

- Purification of the protein till the highest possible level (>95%).

- Screening for crystallization conditions using high-throughput methods.

- Scale up and optimization of the crystallization conditions to grow single crystals suitable for high resolution X-ray diffraction.

In addition, modeling of a voluminous ketone such as aryl *n*-pentyl ketone into the active site of *Sphingobium yanoikuyae* ADH was also envisaged to get insight into substrate discrimination and stereoselectivity issues.

Results and discussion

Since the crystal structure of SyADH was not available at the time to explain the diverse results obtained in Chapter I (Figure 2.7), we attempted to crystallize the protein and gain structural insights into its substrate discrimination and enantioselectivity. Therefore, during the short term placement at YSBL (University of York), gene encoding His-tagged SyADH was subcloned into the pET-YSBLIC-3C vector, and expressed in the soluble fraction of the BL21 (DE3) strain of *E. coli*. Gel filtration analysis suggested that SyADH was predominantly a dimer in solution. Preceded by metal affinity and size exclusion chromatographies, such purified protein was suitable for crystallization (Figure 2.8).

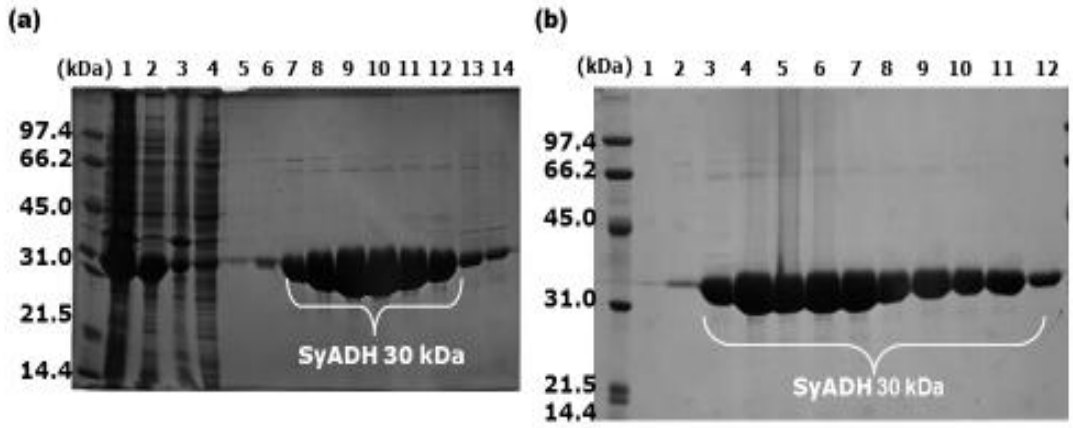

Figure 2.8. SDS-PAGE (4-12%) of purified SyADH: (a) using Ni-NTA column; lane: 1- crude cell extract; 2- soluble fractions; 3- insoluble fractions; 4- flow through; 5-14- elution fractions; (b) using size exclusion gel filtration (S75 column); lanes 1-12- elution fractions.

In addition, the hexahistidine tag from SyADH was cleaved off due to observed interference with the protein stability. Routine screening using sparse matrix 96-well screens in the sitting drop format was performed for the enzyme at different concentrations and in the presence of the NADPH cofactor. After several days, crystals were obtained in a 2-(*N*-morpholino)ethanesulfonic acid (MES) buffer 100 mM at pH 5.5, with sodium acetate (0.3 M) and 15% v/v PEG 4000 as precipitants, though in the form of clustered needles unsuitable for X-ray diffraction. Scale-up experiments in 24 well-plates using the hanging-drop method of crystallization were then performed with the addition of polyalcohols and detergents, aiming to slow down the crystallization process and obtain single crystals. Eventually, crystals were observed in several cases, however they stacked one over another, as shown in Figure 2.9.

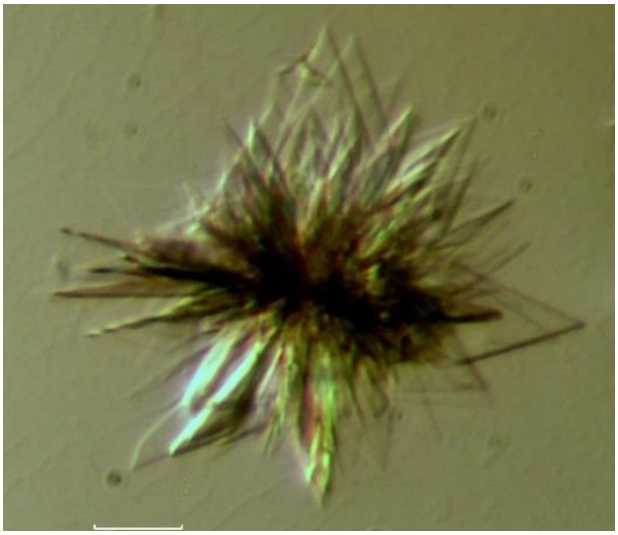

Figure 2.9. The positive hit was obtained in the CSSI screen for the following conditions: MES buffer 100 mM at pH 5.5, with sodium acetate (0.3 M) and 15% v/v PEG 4000 as precipitants.

In a final attempt, seeding beads were used to produce crystal seed stock solutions and suitable crystals were grown as separate plaques as shown in Figure 2.10. SyADH crystals diffracted at 2.5 Å, belonging to the P21 space group.

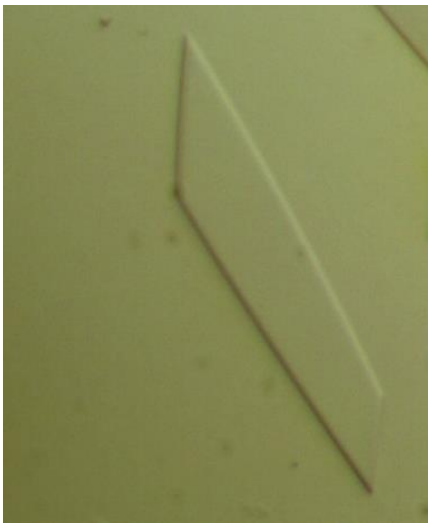

Figure 2.10. The single crystal of SyADH was grown in the following optimized conditions: MES buffer 100 mM pH 5.5; sodium acetate (0.36 M) and 18% v/v PEG 4000, using seeding beads.

The structure was resolved using the BALBES system, which selected a monomer of the NADPH-dependent blue fluorescent protein from *Vibrio vulificus* (3P19; 25% sequence identity with SyADH) as a model. Comparative study revealed that the asymmetric unit contained ten monomers arranged in five dimer pairs. Each monomer that formed a pair exhibited characteristic Rossmann $(\alpha\beta)_8$ fold, as shown in Figure 2.11. This structural motif featured eight helices forming the central bundle and a eighth α8 helix that was closely associated with the neighboring monomer. Mutual interactions between helices α4 and α5, as well as between residues in α8 helix, such as the salt bridge between the side-chain of an aspartic acid (Asp248) and an arginine (Arg234) in each subunit, added to dimer stabilization.

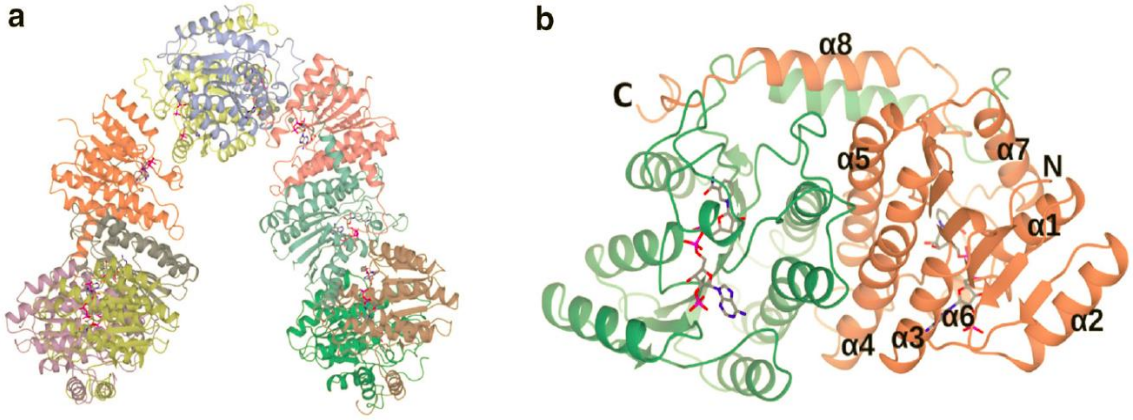

Figure 2.11. Structure of SyADH: (a) The asymmetric unit contains ten monomers that constitute five dimers shown in ribbon format and colored by chain. (b) Each dimer consists of two monomers, colored green and coral, each of which exhibits the Rossmann $(\alpha\beta)_8$ fold, with eight helices (numbered α1–4 and α6–8 for the coral monomer; α5 is obscured), forming the central bundle and the eighth helix α8 that associates closely with the neighboring monomer. The N and C termini of the coral monomer are also indicated. The cofactor NADPH is shown in cylinder format with carbon atoms shown in grey, oxygen in red, nitrogen in blue and phosphorus in magenta.

Crystal structure revealed that the active site of SyADH (Figure 2.12) presented a hydrophobic tunnel situated between two loops formed by a glycine and a valine (Gly195-Val204) and a phenylalanine and a methionine (Phe144-Met150). The nicotinamide ring of NADPH sit at the base of this tunnel, lined by residues that formed the catalytic tetrad: a tyrosine (Tyr153), a serine (Ser140), a methionine (Met150) and a valine (Val14). Other residues distinguished in the tunnel were relatively small and hydrophobic: Ala92, Ala145 and Ala194, which would suggest, at least superficially, an overall big active site volume for SyADH. The active site-tunnel was also constituted with some bulky amino acids such as tryptophan (Trp191) and phenylalanine (Phe148), both representing nonpolar aromatic amino acids.

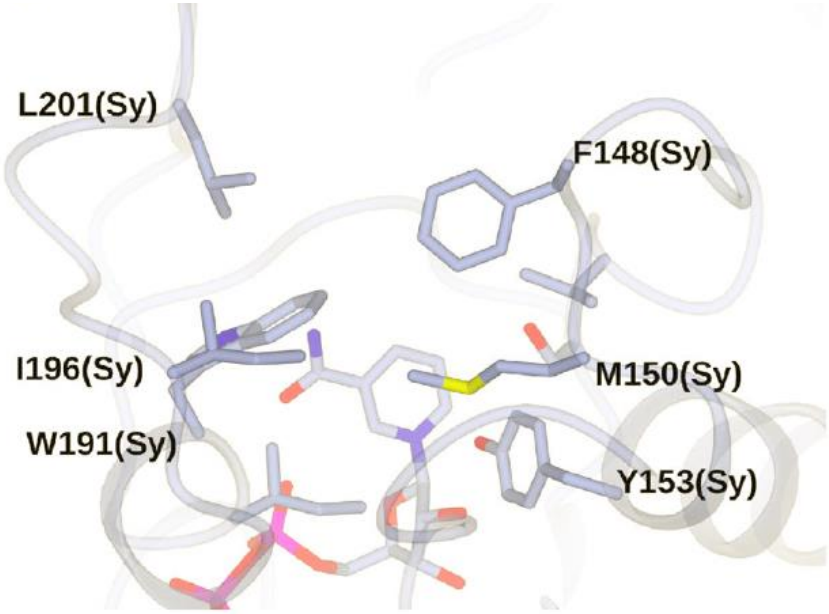

Figure 2.12. Side chain components of the hydrophobic tunnel that shapes the active site of SyADH and placement of NADPH cofactor.

The 2'-ribose phosphate group of NADPH was constrained in SyADH by the presence of an arginine (Arg36), which is a polar and basic residue, a negatively charged aspartate (Asp37) that pointed away from the phosphate binding site, and a serine (Ser13) that directly interacted with the phosphate group by hydrogen bond formation. The C4 atom of the nicotinamide ring, from which a hydride will be delivered to the carbonyl substrate, was 4.3 Å away from the phenolic hydroxyl group of the key tyrosine (Tyr153), which was the proton donor.

Moreover, having the structure of the enzyme resolved, it was possible to model the structure of *n*-pentyl phenyl ketone into SyADH active site. The known Prelog stereospecificity of SyADH with this substrate implied, that *Re*-face from the prochiral ketone had to be preferentially presented to the C4-nicotinamide atom that delivers the hydride, and also that the oxygen atom from the carbonyl group must be situated within a short H-bonding distance from the relevant conserved serine (Ser140) and tyrosine (Tyr153) proton donors that were involved in the catalysis.

Therefore, in the resulting enzyme-substrate model, the phenyl ring was bound by the proximal region of the hydrophobic tunnel nearer from the surface of the enzyme and the alkyl chain was bound in a distal region towards the enzyme interior (Figure

2.13). The *Re*-face of the carbonyl group in the substrate was situated opposite to the nicotinamide ring of NADPH, with the C=O oxygen positioned between the side chains of putative proton donors Tyr153 and Ser140. As a consequence, the phenyl ring was accommodated in the proximal region of the tunnel, bounded by hydrophobic residues valine (Val141), alanine (Ala184), leucine (Leu201) and phenylalanine (Phe148). Pendant *n*-pentyl group entered into the distal region of the tunnel and was bounded by further hydrophobic residues tryptophan (Trp191), isoleucine (Ile190), alanine (Ala92) and methionine (Met150).

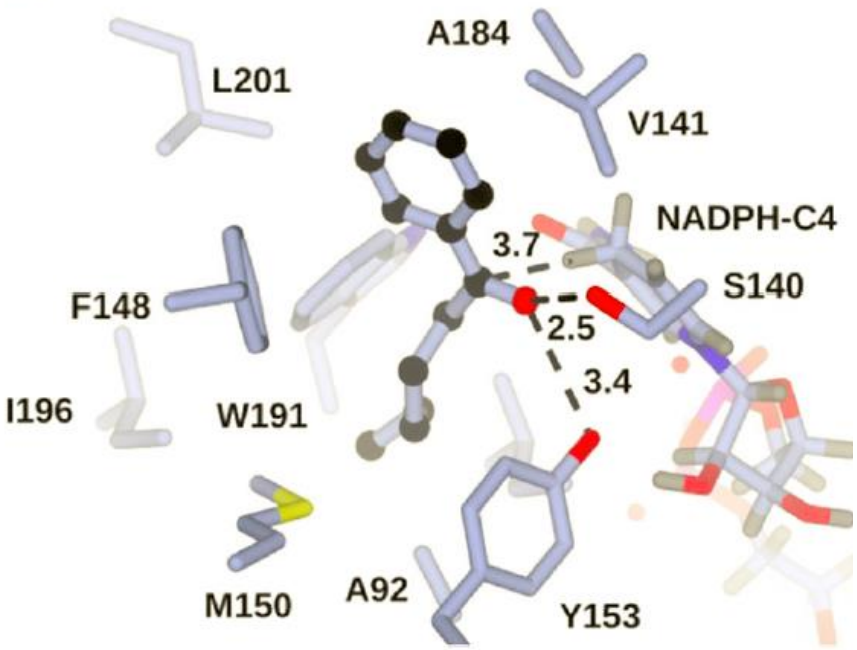

Figure 2.13. *n*-Pentyl phenyl ketone modelled into the active site of SyADH.

The model suggested that SyADH was well suited to accommodate this substrate, but also implied non- or low selectivity towards smaller prochiral ketones such as acetophenone. Due to the large capacity of the hydrophobic tunnel of SyADH, the space available for these substrates would allow the accommodation in such a way that either the *Si*- or *Re*-face of the carbonyl group could be presented at C4 position of the cofactor nicotinamide ring. Interestingly, the model suggested that NADPH provided its pro-*S* hydride to attack the *Re*-face of the carbonyl moiety of *n*-pentyl phenyl ketone, proceeding through an 'E4 pathway' (Figure I.8).

Conclusions

The crystal structure of alcohol dehydrogenase from *Sphingobium yanoikuyae* in a complex with its nicotinamide cofactor (NADPH) bound has been successfully resolved by means of a molecular displacement method. In addition, modelling of its active site with a ketone substrate gave insight into the substrate discrimination and stereoselectivity.

To achieve this, gene encoding SyADH was subcloned into the pET-YSBLIC-3C vector, expressed into the soluble fraction of *E. coli* strain and purified in two steps using metal affinity and size exclusion chromatographies, yielding a highly homogenous solution of the protein. In addition, the hexahistidine tag of SyADH was cleaved off due to observed interference with the protein stability.

Routine screening using sparse matrix 96-well plates in the sitting drop format was performed, allowing the identification of adequate crystallization conditions in MES buffer 100 mM at pH 5.5, with sodium acetate (0.3 M) and 15% v/v PEG 4000, although in the form of clustered needles unsuitable for X-ray diffraction. Scale-up experiments in 24-well plates using the hanging-drop crystallization method were then performed to optimize the growth of single crystals suitable for X-ray diffraction.

SyADH crystals diffracted at 2.5 Å, belonging to the P21 space group. The structure was resolved using the BALBES system. This study revealed that the asymmetric unit contained ten monomers arranged in five dimer pairs. Each monomer exhibited characteristic Rossmann $(\alpha\beta)_8$ fold.

The active site of SyADH presented a hydrophobic tunnel situated between two hydrophobic loops. The nicotinamide ring of NADPH sited at the base of this tunnel, lined by residues that formed the catalytic tetrad: Tyr153, Ser140, Met150 and Val14. Other small hydrophobic residues shaped the tunnel suggesting a big active site volume. The 2'-ribose phosphate group of NADPH was constrained by the presence of Arg36, Asp37, which pointed away from the phosphate binding site, and Ser13, which directly interacted with the phosphate group by hydrogen bond formation. The C4 atom of the nicotinamide ring, from which the hydride is delivered to the carbonyl group of the substrate, was 4.3 Å away from the phenolic hydroxyl moiety of Tyr153, responsible of the proton donation.

The structure of a 'bulky-bulky' ketone, namely *n*-pentyl phenyl ketone, was modelled into the active site. While the phenyl ring was accommodated in the proximal

region of the tunnel, the pendant alkyl chain entered into the distal region of the tunnel. This model suggested that SyADH is well suited to accommodate this substrate, but also implied non- or low selectivity towards smaller prochiral ketones. Furthermore, due to the large capacity of the hydrophobic tunnel, the substrate was accommodated in such a way that preferentially the *Re* face of the carbonyl group was presented to the NADPH hydride, providing the formation of the (*S*)-alcohol by a 'E4 pathway'.

Conclusiones

En este Capítulo se ha descrito la resolución de la estructura cristalina de la alcohol deshidrogenasa de *Sphingobium yanoikuyae* (SyADH) unida a su cofactor (NADPH). Para este fin se ha empleado la técnica de difracción de Rayos X. Además se ha llevado a cabo un estudio de modelización molecular introduciendo una cetona en el centro activo del enzima para obtener información acerca de su selectividad.

Para realizar este estudio, en un primer paso se clonó el gen que codifica a la SyADH en un vector de tipo pET-YSBLIC-3C, para luego expresarlo en *E. coli* y dar lugar a grandes cantidades de la proteína, que fue purificada posteriormente a través de cromatografías de afinidad y por exclusión de tamaños. Además se observó que la secuencia de seis histidinas, necesarias para realizar la purificación, interfería con la estabilidad de la ADH, con lo que en un posterior paso se eliminó.

Para cristalizar la proteína se realizó un barrido de condiciones de cristalización empleando el método de la gota sedente, pudiéndose identificar las siguientes condiciones de cristalización: reguladora MES 0.1 M pH 5.5, con acetato de sodio (0.3 M) y un 15% v/v de PEG 4000. Sin embargo, los cristales obtenidos no resultaron ser apropiados para realizar su difracción, por lo que hubo que aumentar la escala y reoptimizar las condiciones hasta encontrar cristales adecuados.

Se obtuvieron cristales de la SyADH con una resolución de 2.5 Å, perteneciendo al grupo espacial P21. La estructura fue resuelta con el sistema BALBES. Dicho estudio reveló que la unidad asimétrica contiene diez monómeros en una disposición de cinco pares de dímeros. Además, cada monómero exhibe la estructura característica de tipo Rossmann $(\alpha\beta)_8$.

El centro activo de la SyADH presenta un túnel hidrofóbico situado a su vez entre dos hélices de carácter hidrofóbico. El anillo de nicotinamida del NADPH se encuentra en la base de dicho túnel, rodeado por los residuos que forman la tétrada catalítica: Tyr153, Ser140, Met150 y Val14. Otros residuos hidrofóbicos pequeños que forman el túnel dan lugar a un centro activo de gran volumen. El grupo 2'-fosfato del NADPH se encuentra cerca de la Arg36, la Arg37 y la Ser13, que interacciona directamente con dicho grupo a través de un puente de hidrógeno. El átomo de carbono C4 del anillo de nicotinamida, responsable de la transferencia del hidruro, se encuentra a una distancia de 4.3 Å del grupo hidroxilo fenólico de la Tyr153, encargada de realizar la protonación del intermedio formado en la reducción.

Por otro lado, una cetona voluminosa, la 1-fenilhexan-1-ona, se modelizó dentro del centro activo de la ADH. Mientras que el grupo fenilo se acomoda en una zona próxima al túnel de entrada, la cadena alquílica se coloca en la parte interior de la proteína. Este modelo sugiere que la SyADH es capaz de acomodar correctamente este sustrato, lo que implica que para otros sustratos más pequeños esta enzima pueda tener una menor selectividad. Además este sustrato se acomoda de tal manera que el ataque del hidruro por parte del cofactor NADPH se realizara por la cara *Re* del grupo carbonilo, dando lugar al alcohol de configuración *S* a través de un mecanismo de tipo 'E4'.

Experimental part

2.6.1. General procedures

2.6.1.1. Primers preparation for subcloning

Plasmid pET26b containing *Sy*ADH gene was kindly provided by Prof. Wolfgang Kroutil from the University of Graz (Austria). The gene was successfully amplified using gradient PCR with especially designed primers containing LIC specific ends. The primers were designed at YSBL and their sequences were as follows:

Forward (5'->3') CCAGGGACCAGCAATGACCACCCTGCCGACCGTTCTG (37)

Reverse (5'->3') GAGGAGAAGGCGCGTTATTATTATTTTTCAAACTGCGGATGTGACCATGC (50)

They were synthesized by Eurofins MWG Operon, Ebersberg, Germany and upon arrival were dissolved in autoclaved water (Milli-Q grade water) to yield 1 µg/µL stock solutions stored at -20 °C.

2.6.1.2. Gradient PCR protocol

200 µL of a stock solution from the PCR mixture were prepared by mixing 4 µL of template DNA (125 ng/µL); 4 µL 1/5 primer F (1:4 dilution of stock; 0.2 µg/µL); 4 µL 1/5 primer R (1:4 dilution of stock; 0.2 µg/µL); 20 µL dNTPs (2 mM each in stock; Novagen/Merck); 12 µL $MgSO_4$ (25 mM stock; Novagen/Merck); 20 µL KOD buffer[124] (Novagen/Merck); 4 µL KOD Hot Start DNA Polymerase (1 U[125]/µL; Novagen/Merck) and 132 µL autoclaved Milli-Q water. In a 0.2 mL thin wall PCR tube, 25 µL of the above prepared premix was placed. In addition 200 µL of PCR mixture containing 4 µL of DMSO was prepared and dispensed into the 0.2 mL PCR tubes. Gradient PCR was performed in Thermal Cycler "Mastercycler gradient". In Table 2.3., the PCR program is shown.

[124] Buffer composition: information not disclosed by the manufacturer, available as 10 × concentrated stock solution.

[125] One unit of KOD Hot Start DNA Polymerase is defined as the amount of enzyme that will catalyze the incorporation of 10 nmol of dNTP into acid insoluble form in 30 minutes at 75 °C in a reaction containing 20 mM Tris-HCl (pH 7.5 at 25 °C), 8 mM $MgCl_2$, 7.5 mM DTT, 50 µg/mL BSA, 150 µM each of dATP, dCTP, dGTP, dTTP (a mix of unlabeled and [^{3}H]-dTTP) and 150 µg/mL activated calf thymus DNA.

Table 2.3. PCR program employed.

Step	Temperature (°C)	N° cycles	Duration (min)
Initial denaturation	94	1	2
Denaturation	94	35	0.5
Annealing	Range*	35	0.5
Extension	72	35	0.5
Final extension	72	1	3
Hold	4	1	undetermined

*Annealing temperatures tested (°C): 45.3; 48.2; 50.4; 53.0; 55.8; 58.5; 61.0; and 64.7.

2.6.1.3. Agarose gel electrophoresis protocol

PCR products were analyzed performing agarose gel electrophoresis. To 0.6 g of agarose (Sigma) was added 60 mL of 7 mM TAE[126] buffer pH 8.0 to yield 1% w/v agarose solution and the mixture was heated till agarose was dissolved completely. Prior to pouring the solution over a gel form, 1 µL of SYBR dye[127] (Invitrogen) was added and well mixed. Once the gel solidified, 10 µL of sample and 2 µL of the loading buffer[128] (Gel Loading Dye Blue; New England BioLabs Inc.) were loaded to the wells. To verify the DNA size, 1.5 µL of DNA ladder (1 kb DNA ladder; 500 µg/mL; New England BioLabs Inc.), 1.5 µL of loading buffer[128] and 6 µL of water, were loaded in addition. Electrophoresis was performed in a HB710 model tank (Hybaid Ltd.) for 55 min at 100 V and 400 mA. Bands were visualized using BioImaging System Gene Genius, Syngene (Synoptics group).

2.6.1.4. SyADH-LIC ends gene purification from gel

SyADH gen bands were cut off out the gel and placed in 1.5 mL microtubes to be further extracted with GenElute Gel Extraction Kit (Sigma). Finally DNA was eluted in 50 µL of preheated water (65 ^{o}C) and the concentration was measured using

[126] 7 mM TAE buffer pH 8.0 composition: Tris-base (0.84 g), glacial acetic acid (1.14 mL), EDTA (2 mL 0.5 M).
[127] Recommended usage by the supplier is at a 1:10,000 dilution in 0.5 M TAE buffer pH 7.5 of the stock solution in DMSO.
[128] Buffer composition: 15% Ficoll®-400; 66 mM EDTA, 20 mM Tris-HCl, 0.1% SDS, 0.1% bromophenol blue, pH 8.0 at 25 °C.

Biophotometer (Eppendorf AG). Using the equation bp x 650 = pg/pmol, the DNA concentration was calculated as $455 \cdot 10^3$ pg/pmol (31 ng/µL). The desired 0.2 pmol of SyADH DNA referred to $91 \cdot 10^3$ pg ≈ 91 ng so 3 µL of the purified insert solution was further proceeded.

2.6.1.5. Insert LIC T4 polymerase reaction-protocol

Into a 0.5 mL PCR tube, 3 µL of the purified insert solution (containing 0.2 pmol of DNA) was transferred followed by addition of 2 µL of the T4 DNA polymerase buffer[129] (Novagen), 2 µL of dATP (stock of 25 mM, Novagen), 1 µL of DTT (stock of 100 mM), 0.4 µL T4 polymerase (2.5 U/µL LIC qualified T4 DNA polymerase; Novagen) and 11.6 µL of Milli-Q autoclaved water to have a final volume of 20 µL. The reaction mixture was placed in the PCR machine (model TC312, Techne, UK) and left at 22 ^{o}C for 30 min with further 20 min at 75 ^{o}C (to inactivate the polymerase).

2.6.1.6. LIC Annealing protocol

3 µL of the insert LIC T4 pol reaction product was added to 1 µL of LIC vector (50 ng/µL, previously prepared at YSBL), and incubated for 10 min at r.t. Next, 1 µL of EDTA (25 mM stock) was added, mixed with a pipette tip and left for further 10 min at r.t.

2.6.1.7. Transformation of competent *E. coli*

Into 50 µL of XL-10 gold competent cells (Agilent) were added 5 µL of the annealing reaction product, and the mixture was left on ice for 30 min prior to the heat shock (42 ^{o}C for 45 s). Immediately after the thermal shock, cells were incubated on ice for 2 min. Following that time, 1 mL of LB media was added and cells were allowed to recover at 37 ^{o}C for one hour prior to plating them on agar plates containing kanamycin (30 µg/mL). Plates were incubated overnight at 37 ^{o}C and the resulting colonies were checked for plasmid expression by performing minipreparations of 4 randomly chosen colonies (Sigma GenElute™ plasmid Miniprep kit). Double enzyme digestion with

[129] Buffer composition: information not disclosed by the manufacturer.

NcoI and *NdeI* restriction endonucleases (NEB™) was performed and the products were analyzed by electrophoresis in 1% agarose gel (100 V, 55 min). Miniprep samples containing the gene in this vector were sequenced at the Department of Biology (University of York).

2.6.1.8. Protein expression

Competent BL21 cells (50 µL) were chemically transformed with SyADH plasmid (1 µL) following the previous protocol, and 1 L of LB media with kanamycin (30 µg/mL) was inoculated with 5 mL of the starting culture grown overnight. When cell density reached an OD of 0.6 at 600 nm, the protein expression was induced with 1 mM IPTG, and then incubated at 18 ^{o}C overnight. Cells were harvested by centrifugation at 5000 rpm for 30 min at 4 ^{o}C and resuspended in 50 mL of 50 mM Tris/HCl buffer pH 7.5 containing 300 mM NaCl. The cell membrane was disrupted by sonication performed three times for 45 s at 12-14 amplitude microns, and cell debris was separated from the supernatant by centrifugation at 15000 rpm for 30 min. Prior to loading on the nickel column, the protein solution was filtered off on a 0.8 µm filter.

2.6.1.9. Protein purification and His-tag cleavage

Fast protein liquid chromatography on ÄCTA$_{FPLC}$ system was applied to perform protein purification. First, 5 mL of His-Trap™ Chelating HP Nickel column was loaded with the protein solution using a peristaltic pump, and later connected to the ÄCTA system for elution with an imidazole gradient (30-500 mM) in 50 mM Tris/HCl buffer pH 7.5 and 300 mM NaCl. Collected protein fractions (10 µL) were tested on 12% SDS-PAGE gel (120 V, 45 min) to determine the purity. Following that, protein fractions containing the protein were pooled together and concentrated on the centrifuge filters to a final volume of 5 mL to be loaded on a S75 Superdex™ column. Protein fractions were pooled with the addition of 120 mM imidazole to maintain protein stable. A portion of the purified SyADH was set aside to remove the hexahistidine tag. For this, the protein was diluted to 1mg/mL and incubated with 3C protease at a ratio of 1:10 for 16 hours. To separate the protein from its cleaved tag and the His-tagged protease, a second Ni-affinity purification was carried out. This way, cleaved SyADH could be

eluted in buffer free of imidazole whereas histidines and 3C protease would be retained on the column until application of a 0-500 mM imidazole gradient.

2.6.1.10. Sodium dodecyl sulfate polyacrylamide gel electrophoresis (SDS PAGE)

For the sample preparation, 5 µL of the protein solution was mixed with 5 µL SDS-PAGE sample buffer and denaturated at 95 ^{o}C for 5 min prior to loading on solidified acrylamide gel (12% w/v). The gel was placed in a vertical tank filled with running buffer (25 mM Tris, 192 mM glycine, 0.1% w/v SDS), and voltage (200 V) was applied for 50 min. Following that time, the gel was removed from the apparatus and placed into the staining solution, heated in the microwave for 3 min, rinsed with water and left overnight into the distaining solution. Finally, the gel was visualized using SnGene BioImaging System Gen Genius and printed (Sony, UP-D895).

Staining solution (1 L): 250 mL of 2-propanol, 100 mL of glacial acetic acid, 650 mL of deionized water and 2 g of Coomassie brilliant blue R. Filtered before used.

Distaining solution (5 L): 250 mL of 2-propanol, 350 mL of glacial acetic acid and 4.4 L of deionized water.

Running buffer (100 mM stock, 2 L): 115.2 g of glycine (electrophoresis grade), 24 g of Tris base, made up to 2 L with deionized water.

Resolving Gel buffer (0.5 L): 1.5 M Tris pH 8.8 (92.4 g Tris in 480 mL deionized water with pH adjusted to 8.8 with HCl) with 0.4% w/v SDS (20 mL of 10% w/v SDS).

Stacking Gel buffer (0.5 L): 0.5 M Tris pH 6.8 (30.3 g Tris in 480 mL deionized water with pH adjusted to 6.8 with HCl) with 0.4% w/v SDS (20 mL of 10% w/v SDS).

SDS-PAGE sample buffer (10 mL): 4.8 mL of deionized water, 1.2 mL of 0.5 M Tris/HCl pH 6.8, 1 mL of glycerol, 2 mL of a 10% w/v SDS solution, 0.5 mL of a 0.1% w/v bromophenyl blue solution and 0.5 mL of mercaptoethanol.

Low molecular weight standards solution: 25 µL of the low molecular weight standards mix (Biorad) added to 375 µL of SDS-PAGE sample buffer and stored as 10 µL aliquots at -20 ^{o}C. Standards: phosphorylase b (97.4 kDa); bovine serum albumin

(66.2 kDa), ovalbumin (45 kDa), carbonic anhydrase (31 kDa), soybean trypsin inhibitor (21.5 kDa) and lysozyme (14.4 kDa).

Stacking gel: 3.2 mL of deionized water, 1.3 mL of stacking gel buffer, 0.5 mL of acrylamide stock [National diagnostics, Protogel stock solution: 30% w/v acrylamide and 0.8% w/v bis-acrylamide (37.5:1)], 25 µL of a 10% w/v ammonium persulfate (APS) solution and 8 µL of *N,N,N',N'*-tetramethylethylenediamine (TEMED).

Resolving gel (12% polyacrylamide): 3.2 mL of deionized water, 2.5 mL of resolving gel buffer, 4.2 mL of an acrylamide stock [National diagnostics, Protogel stock solution: 30% w/v acrylamide, 0.8% w/v bis-acrylamide (37.5:1)], 50 µL of 10% w/v APS and 8 µL of TEMED.

2.6.1.11. Crystallization of SyADH

For SyADH, three crystallization screens in 96-well plates were set up using the sitting-drop vapor diffusion method: INDEX, PACT and the Clear Strategy Screen (CSS) from Molecular Dimensions Ltd. Protein (10 and 20 mg/mL) was co-crystallized with its NADPH cofactor (10 mM) using 300 nL drops (150 nL protein plus 150 nL precipitant solution). The positive hit was obtained in CSSI screen for the following conditions: 0.1 M MES buffer (2-(*N*-morpholino)ethanesulfonic acid) at pH 5.5, with 0.3 M sodium acetate and 15% (v/v) PEG 4000 as precipitants. The positive hit were scaled up in 24 well Linbro dishes using the hanging-drop vapor diffusion method, with crystallization drops containing 1 µL of protein solution (20 mg/mL) and 1 µL of precipitant reservoir. Since initial crystals were produced in the form of clustered needles unsuitable for X-ray diffraction, the crystal growth for SyADH was optimized to the following conditions: 0.1 M MES buffer pH 5.5; 0.36 M sodium acetate and 18% PEG 4000, using seeding beads. Obtained crystals were flash cooled in the crystallization conditions with addition of 20% ethylene glycol for cryoprotection and 10 mM NADPH.

2.6.1.12. Data collection and processing

Complete dataset for the SyADH complex with NADPH was collected on beamline I04 at the Diamond Light Source, Didcot, Oxfordshire, UK. Data were processed and integrated using XDS[130] and scaled using SCALA[131] as part of the Xia2 processing system. The structure of SyADH was solved using the program BALBES,[132] which selected a monomer of the PDB code structure 3P19 as a model. The solution contained five dimers in the asymmetric unit. All structures were built and refined using iterative cycles of Coot[133] and REFMAC[134] employing local NCS restraints. For NADPH complex of SyADH, the omit maps, after building and refinement of the proteins, revealed residual density at the active sites, which could in each case be successfully modelled and refined as NADPH. The final structures of SyADH-NADPH exhibited R_{cryst} and R_{free} values of 23.4/25.1 respectively. The structures were validated using PROCHECK[135] Coordinates and structure factors for SyADH–NADPH have been deposited in the Protein Data Bank with the accession code 4bmv.

[130] W. Kabsch, *Acta Crystallogr. Sect. D* **2010**, *66*, 125-132.
[131] P. Evans, *Acta Crystallogr. Sect. D* **2006**, *62*, 72-82.
[132] F. Long, A. A. Vagin, P. Young, G. N. Murshudov, *Acta Crystallogr. Sect. D* **2008**, *64*, 125-132.
[133] P. Emsley, K. Cowtan, *Acta Crystallogr. Sect. D* **2004**, *60*, 2126-2132.
[134] G. N. Murshudov, A. A. Vagin, E. J. Dodson, *Acta Crystallogr. Sect. D* **1997**, *53*, 240-255.
[135] R. A. Laskowski, M. W. Macarthur, D. S. Moss, J. M. Thornton, *J. Appl. Crystallogr.* **1993**, *26*, 283-291.

Publication

Top Catal (2014) 57:356–365
DOI 10.1007/s11244-013-0191-2

ORIGINAL PAPER

Structures of Alcohol Dehydrogenases from *Ralstonia* and *Sphingobium* spp. Reveal the Molecular Basis for Their Recognition of 'Bulky–Bulky' Ketones

Henry Man · Kinga Kędziora · Justyna Kulig · Annika Frank · Iván Lavandera · Vicente Gotor-Fernández · Dörte Rother · Sam Hart · Johan P. Turkenburg · Gideon Grogan

Published online: 13 November 2013

Abstract Alcohol dehydrogenases (ADHs) are applied in industrial synthetic chemistry for the production of optically active secondary alcohols. However, the substrate spectrum of many ADHs is narrow, and few, for example, are suitable for the reduction of prochiral ketones in which the carbonyl group is bounded by two bulky and/or hydrophobic groups; so-called 'bulky–bulky' ketones. Recently two ADHs, RasADH from *Ralstonia* sp. DSM 6428, and SyADH from *Sphingobium yanoikuyae* DSM 6900, have been described, which are distinguished by their ability to accept bulky–bulky ketones as substrates. In order to examine the molecular basis of the recognition of these substrates the structures of the native and NADPH complex of RasADH, and the NADPH complex of SyADH have been determined and refined to resolutions of 1.5, 2.9 and 2.5 Å, respectively. The structures reveal hydrophobic active site tunnels near the surface of the enzymes that are well-suited to the recognition of large hydrophobic substrates, as determined by modelling of the bulky–bulky substrate *n*-pentyl phenyl ketone. The structures also reveal the bases for NADPH specificity and (*S*)-stereoselectivity in each of the biocatalysts for *n*-pentyl phenyl ketone and related substrates.

H. Man · A. Frank · S. Hart · J. P. Turkenburg · G. Grogan (✉)
Department of Chemistry, University of York, Heslington, York YO10 5DD, UK
e-mail: gideon.grogan@york.ac.uk

K. Kędziora · I. Lavandera · V. Gotor-Fernández
Facultad de Química, Química Orgánica e Inorgánica, Universidad de Oviedo, Julian Clavería 8, C.P. 33006 Oviedo, Asturias, Spain

J. Kulig · D. Rother
Institute of Bio- and Geosciences, IBG-1: Biotechnology, Forschungszentrum Jülich GmbH, 52425 Jülich, Germany

Keywords Alcohol dehydrogenase · Ketoreductase · NADPH · Oxidoreductase · Enzyme structure

1 Introduction

Alcohol dehydrogenases (ADHs) have been employed for many years in both academic and industrial groups for the asymmetric reduction of prochiral carbonyl groups to optically active secondary alcohols [8, 25]. The natural diversity of ADHs has ensured that enzymes encompassing a broad range of catalytic characteristics have been made available for applications. Hence there are ADHs that offer (*R*)-[31] or (*S*)-[13] selectivity, thermostability [9, 22] and an impressive tolerance to organic solvents that allows the enzymes to be used in the presence of high substrate concentration [13] or even neat substrate itself [11]. One such niche application of ADHs is served by a subgroup of these enzymes that transforms prochiral ketones that feature large hydrophobic groups on either side of the carbonyl group; 'bulky–bulky' ketones.

As part of a culture collection screening programme, Kroutil and co-workers [18] described the cloning, expression and application of an ADH from *Ralstonia* sp. DSM 6428, which was able to accept these bulky–bulky ketones as substrates. The *Ralstonia* ADH (RasADH from hereon) enzyme was applied to the reduction of *n*-butyl phenyl ketone and *n*-pentyl phenyl ketone **1** with (*S*)-enantioselectivity and with enantiomeric excesses (e.e.s) of up to >99 % (Fig. 1) [18]. The excellent enantioselectivity was also extended to bulky-small ketones such as acetophenone. RasADH has subsequently been characterised in some detail by one of our groups [16]. The enzyme was reported to be of the short chain dehydrogenase (SDR) family, with a subunit

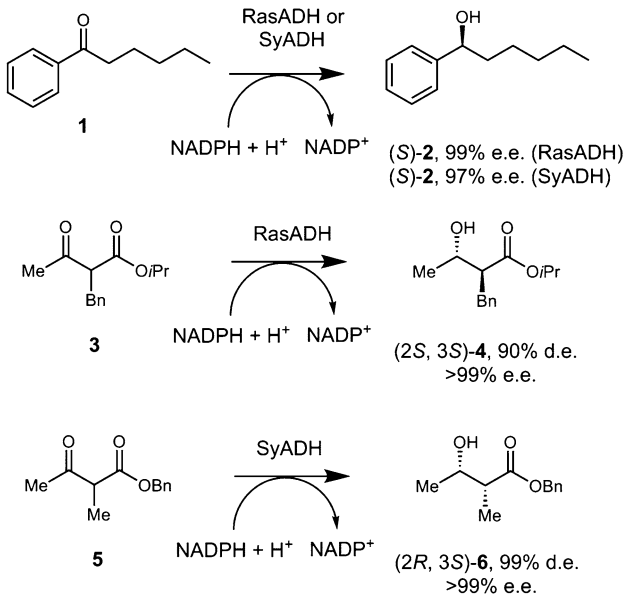

Fig. 1 Representative asymmetric reductions of bulky–bulky ketones catalysed by alcohol dehydrogenases from *Ralstonia* sp. DSM 6428 (RasADH) and *Sphingobium yanoikuyae* DSM 6900 (SyADH)

molecular weight of 26.7 kDa (249 amino acids) and it was suggested that three subunits of the enzyme associated to form a trimer in solution. RasADH exhibited a broad pH optimum for the reductive transformation of benzaldehyde and had a half-life of 80 h at 25 °C. The stability of the enzyme could be augmented by the addition of calcium ions. RasADH was subsequently also applied to the reduction of α-hydroxy ketones [15] and in the dynamic kinetic resolution (DKR) of α-alkyl-β-keto esters such as **3** (Fig. 1) to give (2*S*, 3*S*)-products of type **4** [3].

Further screening of microbial culture collections for the reduction of bulky–bulky ketones revealed a strain of *Sphingobium yanoikuyae* DSM 6900 that was also able to reduce *n*-pentyl phenyl ketone **1** to the (*S*)-alcohol **2** in up to 97 % e.e. [19]. This short chain dehydrogenase, named SyADH, was isolated and the relevant gene cloned and expressed, and subsequently used for the non-selective oxidation of some small prochiral alcohols [20]. Like RasADH, SyADH has also recently been employed in the DKR of α-alkyl-β-keto esters such as **5** [3], in this case to give (2*R*, 3*S*)-diol products **6** with excellent d.e.s and e.e.s

Ralstonia ADH and SyADH therefore present distinctly useful biocatalysts as they catalyse the transformation of sterically challenging substrates and with, in some cases, complementary stereo- and diastereo-selectivities to established ADHs. In the case of each of these enzymes, knowledge of their three-dimensional structure would not only provide information for the first time on the determinants of bulk-bulky ketone recognition in such ADHs, but also serve to inform the engineering of other ADHs for transformation of those substrates, or for the expanded substrate specificity of RasADH and SyADH themselves. In this report, we present the X-ray crystal structures of the *apo*- and NADPH-complex of RasADH at 1.5 and 2.9 Å resolution respectively, and also the structure of the NADPH complex of SyADH at 2.5 Å resolution. These structures reveal the hydrophobic characteristics of the active site(s) that allow accommodation of large hydrophobic substrates, and also shed light on the determinants of cofactor specificity in these 'bulky–bulky' ADH enzymes.

2 Results and Discussion

2.1 Structure of RasADH

Ralstonia ADH was expressed from a strain of *E. coli* BL21 (DE3) that had been transformed with the gene encoding RasADH ligated into the pET-YSBLIC-3C vector [1]. After purification using nickel affinity and gel filtration chromatography, the pure protein was initially concentrated to 8 mg mL^{-1}. During this process problems with precipitation were encountered, but these were successfully addressed through the inclusion of Ca^{2+} ions, 500 mM sodium chloride and glycerol in the cell resuspension and protein purification buffers (see "Sect. 6"). Gel filtration studies on the protein derived in this way were suggestive of a tetramer of RasADH monomers in solution, rather than the trimer suggested by earlier studies [16].

Crystals of RasADH were obtained in two forms, each of which was soaked with 10 mM NADPH before testing diffraction quality. It was found that the first form diffracted to a resolution of 1.5 Å with a $C2_1$ space group. Data collection and refinement statistics can be found in Table 1. The structure of RasADH was solved by molecular replacement using a monomer of a 'probable dehydrogenase protein' from *Rhizobium etli* CFN42 (55 % sequence identity with RasADH; PDB code 4FGS) as a model. In the structure solution there were four monomers A-D in the asymmetric unit, which made up a tetramer (Fig. 2a), a quaternary association common to some other short-chain ADHs such as the carbonyl reductase from *Candida parapsilosis* (PDB code 3CTM, [40]) and levodione reductase from *Corynebacterium aquaticum* (1IY8, [33]).

Each monomer of RasADH (Fig. 2b) was made up of a classical Rossman fold with a central β-sheet composed of seven β-strands: β1 (residues 8–13); β2 (33–37); β3 (54–58); β4 (83–87); β5 (131–135); β6 (174–180) and β7 (239–242). The β-sheet was surrounded by six alpha helices: α1 (residues 17–30); α2 (40–50); α3 (64–77); α 4

Table 1 Data collection and refinement statistics for RasADH (*apo*- and in complex with NADPH) and SyADH in complex with NADPH

	RasADH (*apo*)	RasADH (NADPH complex)	SyADH (NADPH complex)
Beamline	Diamond I02	Diamond I04	Diamond I02
Wavelength (Å)	0.97950	0.97950	0.97949
Resolution (Å)	60.86–1.52 (1.57–1.52)	74.54–2.89 (2.93–2.89)	139.0–2.5 (2.56–2.50)
Space group	$C2_1$	$C2_1$	$P2_1$
Unit cell (Å)	a = 136.5; b = 52.5; c = 151.5; α = γ = 90.0; β = 116.6	a = 192.3; b = 135.6; c = 93.6; α = γ = 90.0; β = 100.1	a = 144.9; b = 86.8; c = 155.6; α = γ = 90.0; β = 106.4
No. of molecules in the asymmetric unit	4	6	10
Unique reflections	149646 (45160)	52465 (3880)	133601 (10900)
Completeness (%)	97.7 (96.8)	99.2 (98.8)	99.7 (99.8)
R_{merge} (%)	0.03 (0.25)	0.18 (0.73)	0.14 (0.54)
$R_{p.i.m.}$	0.03 (0.23)	0.16 (0.64)	0.12 (0.46)
Multiplicity	3.3 (3.5)	4.2 (4.2)	4.2 (4.3)
$<I/\sigma(I)>$	15.6 (4.9)	7.4 (2.0)	8.2 (3.0)
$CC_{1/2}$	1.00 (0.95)	0.98 (0.74)	0.99 (0.82)
Overall *B* factor from Wilson plot (Å^2)	24	41	43
R_{cryst}/R_{free} (%)	15.8/18.8	26.8/29.3	23.4/25.1
No. protein atoms	6,942	11,081	18,948
No. water molecules	846	37	290
r.m.s.d 1–2 bonds (Å)	0.02	0.01	0.01
r.m.s.d 1–3 angles (°)	1.69	1.60	1.60
Avge main chain B (Å^2)	20	35	35
Avge side chain B (Å^2)	23	36	37
Avge water B (Å^2)	33	14	20
Avge ligand B (Å^2)	–	32	30

Numbers in brackets refer to data for highest resolution shells

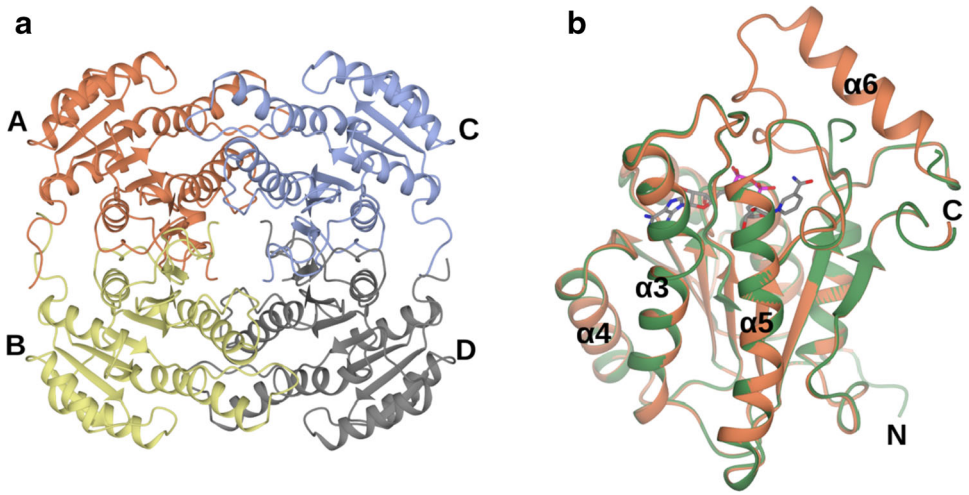

Fig. 2 Structure of RasADH. **a** The asymmetric unit of the *apo*-enzyme contained four monomers A–D that constituted one tetramer, which is shown in *ribbon format* and *coloured by chain*. **b** Monomer of RasADH apoenzyme (*green ribbon*) superimposed with monomer of RasADH *holo*-enzyme (*coral ribbon*) in complex with NADPH. The r.m.s.d for the two structures over 201 C-alphas was 0.42 Å. The monomer(s) display the typical Rossman fold, with a central β-sheet surrounded by six helices, four of which, α3, α4, α5 and α6. Helix α6, which was absent in the *apo*-enzyme structure, appears to act as a lid to the active site, closing over the NADPH molecule when cofactor is bound. The N and C termini of the *apo*-enzyme monomer are also indicated. The cofactor NADPH is shown in cylinder format with carbon atoms shown in *grey*

(101–126); α5 (148–168) and α7 (217–228). A further helix, the sixth in sequence order α6 (195–208, as revealed by the NADPH complex structure—vide infra), was largely missing from the density in the *apo* structure of RasADH. This helix was part of a sequence of residues in the region of Thr185 to Phe205 that in each subunit could not be modelled (although residues Glu200 to Lys204 were present in subunit 'C'). A possible role for this helix is discussed below. Notwithstanding helix α6, the overall fold of the RasADH monomer (Fig. 2b) is well-conserved amongst SDR structures; a superimposition of the 'A'-chain of RasADH with that of a monomer of 4FGS gave an r.m.sd. of 0.71 Å over 240 Cα atoms. The RasADH monomer is most similar to 4FGS and a putative oxidoreductase protein from *Sinorhizobium meliloti* 1021, (PDB code 4ESO; with 41 % sequence identity to RasADH), as determined by analysis using the DALI server [10], with r.m.s.d values for the latter structure 1.4 Å. over 250 residues. In this first, higher resolution, structure of RasADH no residual density in the omit map corresponding to the NADP(H) cofactor could be observed in the putative active site of the enzyme.

A monomer of RasADH (for example, subunit 'A') closely associates with its neighbours 'C' and 'B', and to a lesser extent, 'D', to form the tetramer. Subunit 'A' makes a contact surface area of 1,540 $Å^2$ with subunit 'C', as calculated using PISA [14], with interactions dominated by the reciprocal association of helices α7, including stacking interactions between Phe226 residues of each subunit, and strands β7, which are largely governed by hydrophobic side-chain interactions. 'A' also closely interacts with subunit 'B', with a calculated shared interface of 1,670 $Å^2$. This pair of monomers interacts most closely through reciprocal interactions between helices α4 and α5, including the indole nitrogen of Trp164 of 'A' with the carboxylate side chain of 'B' Asp148 and a salt bridge between the side-chains of 'A' Asp105 and 'B' Arg 113.

The other crystal form of RasADH diffracted more poorly, to a resolution of 2.9 Å, and in the same $C2_1$ space group as the *apo*-enzyme. Using the monomer of the *apo*-structure as a model, the structure solution in this instance yielded six monomers in the asymmetric unit, representing one full tetramer and one half-tetramer. In this case, each monomer featured extensive density in the omit map in the active site that was representative of the cofactor NADPH at full occupancy. In addition, density for the helix α6 in the region of Thr185 to Phe205 was now largely complete, and could be modelled, save for one or two residues in the region of Val191. Chain 'F' was complete, however. The loop density in the NADPH complex confirmed that the loop appears to act as lid for the active site, closing over the cofactor in the *holo*-form of the enzyme (Fig. 2b).

2.2 Structure of SyADH

SyADH was also subcloned into the pET-YSBLIC-3C vector, and was again expressed well in the soluble fraction of the BL21 (DE3) strain of *E. coli*. In this case however, gel filtration analysis suggested that SyADH was predominantly a dimer in solution. Crystallisation of SyADH followed cleavage of the hexahistidine tag as described in the "Sect. 6". Crystals were of the $P2_1$ space group. The structure was solved using the programme BALBES [21], which selected a monomer of the NADPH-dependent blue fluorescent protein from *Vibrio vulificus* (3P19; 25 % sequence identity with SyADH) as a model. The solution featured five dimer pairs in the asymmetric unit (Fig. 3a).

The monomer of SyADH (Subunit 'A' will serve as the model for the description below), again features the characteristic Rossman-type fold, again featuring a central

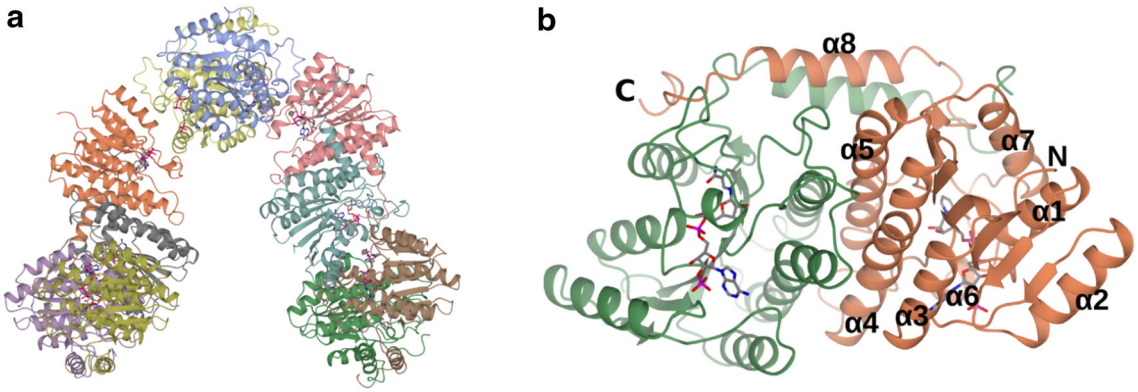

Fig. 3 Structure of SyADH. **a** The asymmetric unit contains ten monomers that constitute five dimers shown in *ribbon format* and *coloured by chain*. **b** Each dimer consists of two monomers, coloured *green and coral*, each of which exhibits the Rossman $(\alpha\beta)_8$ fold, with eight helices (numbered α1–4 and α6–8 for the coral monomer; α5 is obscured) forming the central bundle and a ninth helix α9 that associates closely with the neighbouring monomer. The N and C termini of the coral monomer are also indicated. The cofactor NADPH is shown in cylinder format with carbon atoms shown in *grey*

β-sheet of seven strands: β1 (residues 6–11); β 2 (31–34); β 3 (56–58); β 4 (82–88); β 5 (134–138); β 6 (177–181) and β 7 (224–225). In SyADH, the sheet is surrounded by seven α-helices: α 1 (residues 15–27); α2 (38–52) α3 (66–78); α4 (102–130); α5 (151–171) α6 (190–194) and α7 (207–220). A last helix, α8, stretching from residues 234–238, is at the C-terminus of the protein and participates in pronounced monomer–monomer ('A'/'B') interactions, helping to form the dimer (Fig. 3b). Electron density allowed the modelling of residues Thr3 or Leu 4 through Tyr258 in all subunits, with only residue Asn199 not modeled in subunits 'I' and 'J', owing to poor electron density. The monomer of SyADH was most similar to monomers of clavulanic acid dehydrogenase from *Streptomyces clavuligerus* (PDB code 2JAH; 26 % sequence identity with SyADH; r.m.s.d 2.2 Å over 245 Cα atoms) [23] and sepiapterin reductase from *Chlorobium tepidum* (PDB code 2BD0; 25 % sequence identity with SyADH; r.m.s.d 2.4 Å over 240 Cα atoms) [34] The overall structural fold of the monomer of SyADH was very similar to that of 2JAH, save for a loop region Phe218-Leu223 between α7 and β7 in SyADH which was longer in 2JAH (Ala227–Val236). Monomer 'A' was calculated to form an interface of 3,700 $Å^2$ with its dimer partner, subunit 'B', as calculated using PISA [14]. The dimer is stabilised by reciprocal interactions between residues in helices α8, including a salt bridge between the side-chain of residues Asp248 and Arg234 in each subunit, but also reciprocal interactions between α4 and α5, which are structurally homologous with helices α4 and α5 in RasADH, described above.

3 The Substrate Binding Sites

The active site of RasADH is a hydrophobic tunnel that is formed at the top of the central β-sheet of the Rossman fold as seen in Figs. 2b, 4a, and is partially covered by helix α6 in the NADPH-complex structure. The nicotinamide ring of NADPH sits at the base of this tunnel, lined by residues Tyr150 (the likely proton donor to a nascent alcohol in the reductive ADH-catalysed reaction [6]), Ser137, Phe205, Leu144, Leu142, Leu201, Val138, Ile91, His147 and Gln191. The strict specificity for the phosphorylated cofactor NADPH is governed by interactions of adjacent arginine residues Arg38 and Arg39 and Asn15, with Arg38 also participating in π-stacking interactions with the adenine ring. The interactions with the phosphate explain the preference of RasADH for NADPH over the non-phosphorylated cofactor NADH.

The active site tunnel in SyADH (Fig. 4b) is situated between two loops formed by Gly195-Val204 and Phe144-Met150, the former in place of helix α6 in RasADH. The nicotinamide ring again occupies the base of the tunnel, the lining of which shares significant homology with RasADH, with probable proton donor Tyr153 (Ras-ADH-Tyr150), Ser140 (Ser137), Met150 (His147),and Val141 (Val138), conserved in respect of steric bulk, but with three larger hydrophobic residues from RasADH replaced by alanine: Ala92 (equivalent to RasADH Ile91) and Ala145 (Leu142) and Ala194 (Gln191), suggestive, at least superficially, of a greater active site volume in SyADH overall. Additional steric bulk is provided in the active site by Trp191 (Ile188) and Phe148 (Leu144). The 2′-ribose phosphate group of NADPH is less constrained in SyADH than in RasADH; Arg36 mirrors the location and function of RasADH-Arg38, but RasADH-Arg39 is not present and is replaced by an aspartate (Asp37) that points away from the phosphate binding site. Ser13 replaces RasADH Gln15 in the other direct interaction with phosphate. The side-chain of an additional arginine, Arg40, which is not present in RasADH is close to the phosphate in SyADH, but, with both terminal N-atoms of the side chain at 3.6 and 3.8 Å from the phosphate oxygen, too far away to suggest a major role in phosphate binding.

The nicotinamide rings of the NADPH cofactors in each case are presented to the active site cavity. The C4 atom of the nicotinamide ring, from which hydride will be delivered to the substrate carbonyl, is in each case 4.2 Å (RasADH) or 4.3 Å (SyADH) from the phenolic hydroxyl of the tyrosine proton donor. In SyADH, the region extending from the space between the nicotinamide C4 and the phenolic hydroxyl of Tyr153, and out into the hydrophobic cavity, contained electron density although no obvious ligands that featured in the crystallization conditions could be modelled.

4 Modelling Bulky–Bulky Ketones in the Active Sites

Ralstonia ADH and SyADH are distinctive in their ability to reduce ketones in which the prochiral carbonyl group is bounded on either side by hydrophobic groups, such as *n*-pentyl phenyl ketone **1**, which is transformed by each enzyme into the (*S*)-alcohol with excellent enantiomeric excess, thus exhibiting a Prelog selectivity [29]. With the structures of the enzymes in hand, it was now possible to model the structure of **1** into their active sites, in the knowledge that, given the known (*S*)-stereospecificity of the enzymes with this substrate, only the *re*-face of the prochiral ketone would be presented to the C4-nicotinamide atom that delivers hydride, and also that the carbonyl group must be situated within H-bonding distance of the relevant conserved serines (Ser137 in RasADH and S140 in SyADH) and tyrosine proton donors (Tyr150 in RasADH and Tyr153 in SyADH) that are involved in catalysis [6]. **1** was modelled into the active sites of

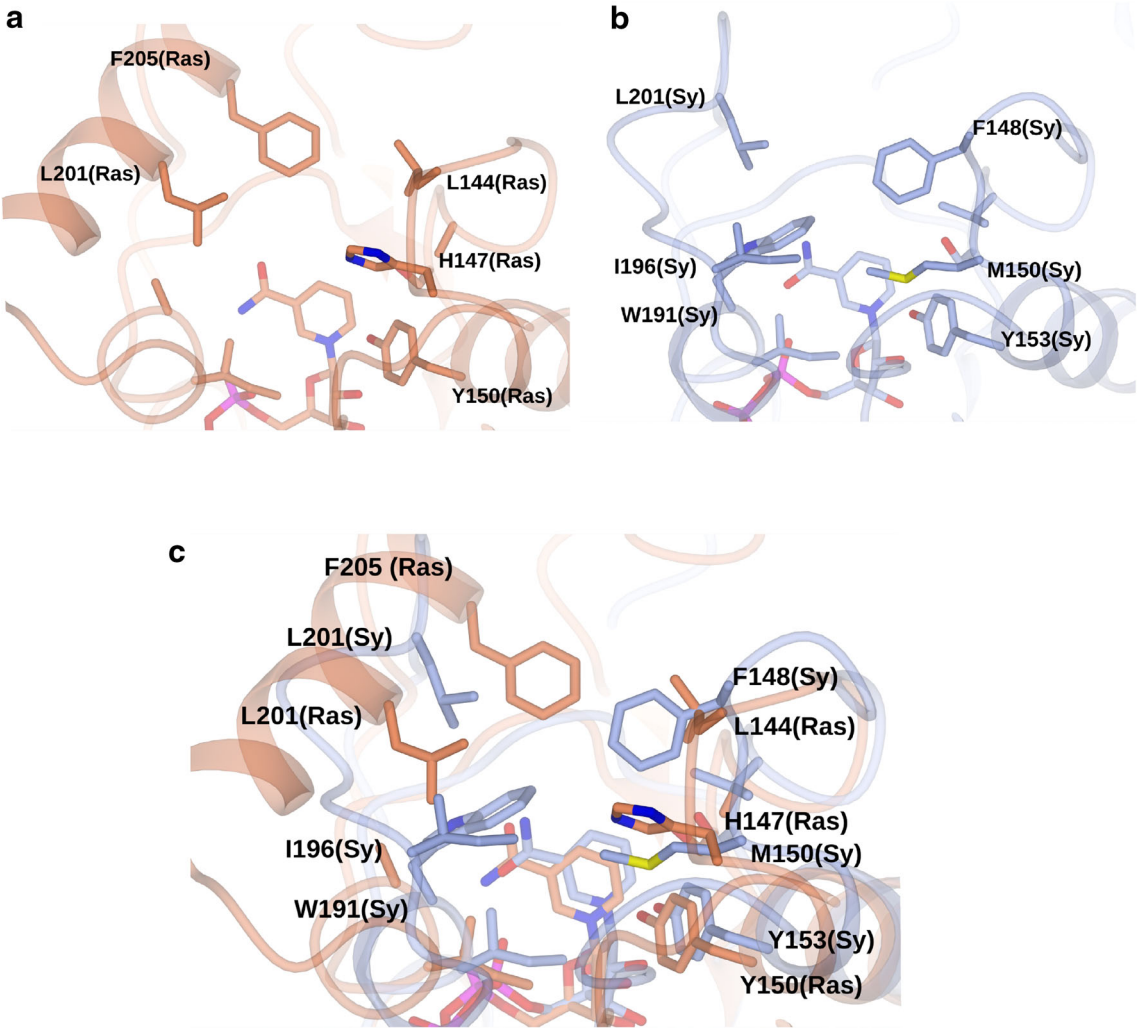

Fig. 4 Active sites of **a** RasADH and **b** SyADH illustrating side-chain components of the hydrophobic tunnel in both active sites. RasADH is shown in ribbon format in *coral* with side chains projecting from the backbone and the nicotinamide ring of NADPH (*centre*) shown (*carbon atoms in coral*). SyADH is shown in light blue ribbons with NADPH and side chains (*carbon atoms in light blue*). **c** Superimposed active sites of RasADH (*coral*) a nd SyADH (*light blue*)

RasADH and SyADH using the programme AUTODOCK-VINA [35] applying a procedure described in the "Sect. 6". A comparison of these models is shown in Fig. 5.

In the model of SyADH with substrate **1**, the hydrophobic tunnel can be described in terms of a proximal region nearer the surface of the enzyme, in which the phenyl ring is bound, and a distal region towards the enzyme interior, which binds the alkyl chain. The *re*-face of the carbonyl in **1** is situated against the nicotinamide ring of NADPH, with the C=O oxygen positioned between the side chains of putative proton donor Tyr153 and Ser140 (Fig. 5a). As a consequence, the phenyl ring is accommodated in the proximal region of the tunnel, bounded by hydrophobic residues Val141, Ala184, Leu201 and Phe148. The pendant *n*-pentyl group penetrates the distal region of the tunnel and is bounded by further hydrophobic residues Trp191, Ile190, Ala92 and Met150. In RasADH, the requisite interactions of the carbonyl group with the C4 of NADPH and the side chains of Tyr150 and Ser137 are still observed, but the phenyl ring of the substrate is pressed further into the active site in relation to the SyADH model complex, as a result of steric repulsion by residue Phe205, which is part of the 'lid' helix α6 (Fig. 5b). In the distal region of the hydrophobic tunnel, penetration of the *n*-pentyl chain is prevented by Gln191 and is displaced into the region of the active site occupied by Ile188, which would not be permitted in SyADH because of the presence of bulky Trp191 (seen behind the substrate in Fig. 5a). The alkyl chain now makes favourable hydrophobic interactions in this position with Phe205 and Ile188 (seen behind the substrate in Fig. 5b). The models suggest that although each accepts **1**, SyADH is better suited to accommodate the

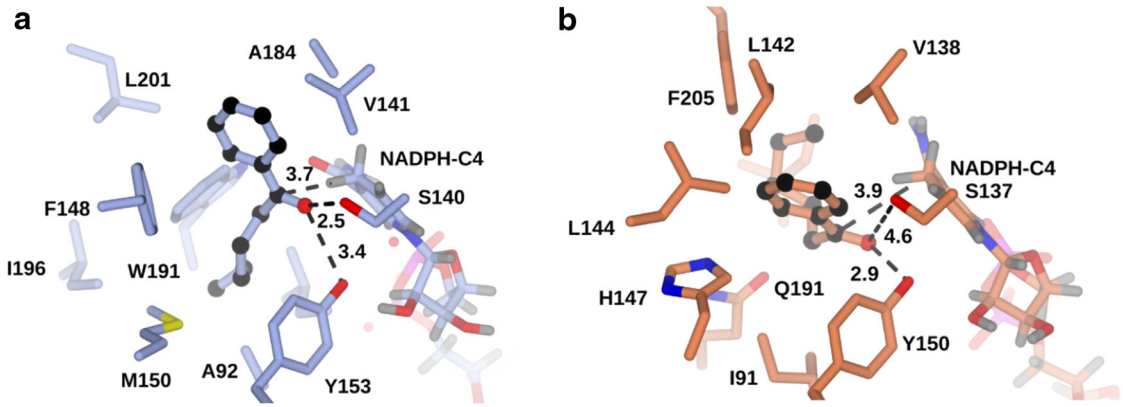

Fig. 5 Ketone **1** modelled into the active site of **a** SyADH and **b** RasADH using the programme AUTODOCK VINA [35]. In **a**, the carbon atoms of the side chains of SyADH are shown in *light blue* in cylinder format; **1** is shown in ball-and-stick format with the carbon atoms in *black*. In **b**, the carbon atoms of the side chains of RasADH are shown in *coral* in cylinder format; **1** is again shown in ball-and-stick format with the carbon atoms in *black*. Distances are given in Angstroms

substrate. The models are useful in revealing the hydrophobic characteristics of the active sites that permit binding of hydrophobic substrates but also the distinctive substrate ranges of SyADH and RasADH. The model suggest that while the flexible alkyl chain of **1** can be accommodated in the distal region of hydrophobic tunnel through contortion in RasADH, less flexible substituents, such as aromatics, would not be accommodated. This is supported by substrate specificity studies [16], which show that compounds such as benzoin are poor substrates for RasADH. For SyADH, however, the larger distal portion of the hydrophobic tunnel may allow for the accommodation of such bulky groups. The large capacity of the hydrophobic tunnel of SyADH also suggests a basis for its non-selectivity towards smaller prochiral ketones such as acetophenone [20] with space available for these substrates to be accommodated in such a way that presents the *si*- or the *re*- face of the carbonyl group to the NADPH hydride at C4 of the cofactor nicotinamide ring.

Interestingly, from Fig. 5 the models suggest that, in both cases, NADPH provides its pro-*S* hydride to attack the *re*-face of the carbonyl moiety of *n*-pentyl phenyl ketone, suggesting that the reaction proceeds by the 'E4 pathway' [2]. Whilst the confirmation of pro-*S* hydride transfer in RasADH and SyADH awaits analysis using experiments with C4-deuterated cofactors, the structural observation is in agreement with the observed stereospecificity of hydride delivery by other short chain ADHs with Prelog selectivity [27, 28]. Other ADHs of Prelog selectivity such as yeast [YADH, 38], horse liver [HLADH, 7], *Rhodococcus erythropolis* [39], or *Thermoanaerobacter ethanolicus* [26] ADHs, supply the NADPH pro-*R* hydride, thus following the E3 pathway [2], but in these cases the enzymes are of the zinc-dependent Medium Chain Reductase (MDR) family, in which the opposite face of the nicotinamide ring (of NADH in these cases) is presented to the active site, through rotation around the bond between the nicotinamide ring and the ribose, relative to the conformation observed in the SDR, and as seen in PDB structures 2HCY (YADH, [30]) and 1LDE (HLADH).

5 Conclusion

The structures of RasADH and SyADH have revealed the structural basis for the recognition of bulky–bulky ketones in a hydrophobic tunnel near the surface of the enzymes. The structures of enzymes with potential use in biocatalytic applications can be valuable in identifying active site determinants of substrate specificity and enantioselectivity that may inform rational engineering, or randomised mutagenesis at targeted residues, for improved or altered specificity.

6 Experimental Section

6.1 Gene Cloning, Expression and Protein Purification

The genes encoding RasADH and SyADH were obtained from the laboratory of Professor Wolfgang Kroutil, University of Graz, Austria. Each gene was sub-cloned into the pET-YSBLIC-3C vector in York. This vector equips each expressed gene product with an N-terminal hexa-histidine tag. RasADH was amplified by PCR from the template plasmid using the following primers: 5′- CCAGGGACCA GCAATGTATCGTCTGCTGAATAAAACCGCAGTTAT TACCG -3′ (Forward) and 5′- GAGGAGAAGGCGCGTT ATTAAACCTGGGTCAGACCACCATCAACAAACAG -3′ (Reverse). SyADH was amplified using primers 5′- CC

AGGGACCAGCAATGACCACCCTGCCGACCGTTCT G -3′ (Forward) and 5′- GAGGAGAAGGCGCGTTA TTATTATTTTTCAAACTGCGGATGTGACCATGC -3′ (Reverse). Following agarose gel analysis of the PCR products, the relevant bands were eluted from the gels using a PCR Cleanup kit® (Qiagen). The genes were then sub-cloned into the pET-YSBL-LIC-3C vector using previously published techniques [1]. The resultant plasmids were then used to transform *E. coli* XL1-Blue cells (Novagen), yielding colonies which in turn gave plasmids using standard miniprep procedures that were sequenced to confirm the identity and sequence of the genes.

The recombinant vector(s) containing the RasADH and SyADH genes were used to transform *E. coli* BL21 (DE3) cells using 30 μg mL^{-1} kanamycin as antibiotic marker on Luria–Bertani (LB) agar. Single colonies from agar plate grown overnight were used to inoculate 5 mL cultures of LB broth, which were then grown overnight at 37 °C with shaking at 180 rpm. The starter cultures served as inocula for a 1 L cultures of LB broth in which cells were grown until the optical density (OD_{600}) had reached a value of 0.8. Expression of either RasADH or SyADH were then induced by the addition of 1 mM isopropyl β-D-1-thiogalactopyranoside (IPTG). The cultures were then incubated at 18 °C in an orbital shaker at 180 rpm for approximately 18 h. The cells were harvested by centrifugation for 15 min at 4,225 g in a Sorvall GS3 rotor in a Sorvall RC5B Plus centrifuge. At this point, considerations specific to each protein applied and purification strategies diverged.

For RasADH, cell pellets were resuspended in 20 mL of 50 mM Tris–HCl buffer pH 7.5 containing 500 mM NaCl, 20 mM imidazole, 1 mM $CaCl_2$ and 10 % glycerol (v/v) (buffer 'A') per 1 L of cell culture. The cell suspensions were then sonicated for 10 × 45 s bursts at 4 °C with 30 s intervals. The soluble and insoluble fractions were separated by centrifugation for 30 min at 26,892 g in a Sorvall SS34 rotor. The crude cell lysate from 1L cell culture was loaded onto a 5 mL HisTrap FF crude column (GE Healthcare), which was then washed with buffer 'A') and then the protein eluted with a linear gradient of 20–300 mM imidazole over 20 column volumes at a flow rate of 2.5 mL min^{-1}. Fractions containing RasADH were combined and concentrated using a 10 kDa cut-off Centricon® filter membrane. The concentrated RasADH was then loaded onto a pre-equilibrated S75 Superdex™ 16/60 gel filtration column, which was then eluted with 120 mL of buffer 'A' without imidazole, using a flow rate of 1 mL min^{-1}. Fractions containing pure RasADH, as determined by SDS-PAGE analysis were combined and stored at 4 °C. For SyADH, an equivalent procedure was employed using, in place of buffer 'A', a 50 mM Tris–HCl buffer containing 300 mM NaCl and 20 mM imidazole only (buffer 'B'). All subsequent procedures were equivalent to the strategy employed for RasADH, with purification performed using Ni–NTA chromatography followed by gel filtration. In the case of SyADH, prior to crystallisation, the histidine tag was cleaved using C3 protease using a procedure described previously [1].

6.2 Protein Crystallisation

Crystallization conditions for both enzymes were determined using commercially available screens in the sitting-drop format in 96-well plates using 300 nL drops (150 nL protein plus 150 nL precipitant solution). Positive hits were scaled up in 24 well Linbro dishes using the hanging-drop method of crystallisation, with crystallisation drops containing 1 μL of protein solution and 1 μL of precipitant reservoir. For the apo-RasADH, the best crystals were obtained in 0.1 M Bis–tris propane pH 7.0 containing 20 % (w/v) PEG 3350 and 0.02 M sodium–potassium phosphate. The protein concentration was 24 mg mL^{-1}. For the RasADH NADPH complex, the best crystals were obtained in 0.1 M Bis–tris propane pH 8.0, containing 16 % (w/v) PEG 3350, 0.2 M potassium isothiocyanate and 5 % (w/v) ethylene glycol. The protein concentration in each case was 24 mg mL^{-1}. In each case, the crystals were picked and transferred to a solution of the mother liquor containing 20 % (v/v) ethylene glycol as cryoprotectant and 10 mM NADPH, and left for 5 min. The crystals were then flash cooled in liquid nitrogen prior to diffraction analysis.

For the SyADH-NADPH complex, the best initial crystals were obtained in conditions containing 0.1 M MES buffer pH 5.5 with 0.3 M sodium acetate and 15 % (w/v) PEG 4 K, with a protein concentration of 20 mg mL^{-1}. As with RasADH, crystals were picked and transferred to a solution of the mother liquor containing 20 % (v/v) ethylene glycol as cryoprotectant and 10 mM NADPH, and left for 5 min. The crystals were then flash-cooled in liquid nitrogen prior to diffraction analysis.

Crystals were tested for diffraction using a Rigaku Micromax-007HF fitted with Osmic multilayer optics and a Marresearch MAR345 imaging plate detector. Those crystals that diffracted to greater than 3 Å resolution were retained for full dataset collection at the synchrotron.

6.3 Data Collection, Structure Solution, Model Building and Refinement of RasADH and SyADH

Complete datasets for the *apo*-RasADH and its NADH complex, and the SyADH complex with NADPH were collected on beamlines I04, I02 and I04 respectively, at the Diamond Light Source, Didcot, Oxfordshire, UK. Data were processed and integrated using XDS [12] and scaled using SCALA [5] as part of the Xia2 processing system [37]. Data collection statistics are given in Table 1. The

structure of the *apo*-RasADH was solved using MOLREP [36], using a monomer of structure PDB code 4FGS as a search model. The solution contained four molecules in the asymmetric unit, representing one tetramer. The structure of the RasADH NADPH complex was then solved using the monomer of the *apo*-RasADH. The structure of SyADH was solved using the programme BALBES [21], which selected a monomer of the PDB code structure 3P19 as a model. The solution contained five dimers in the asymmetric unit. All structures were built and refined using iterative cycles of Coot [4] and REFMAC [24] employing local NCS restraints. For NADPH complexes of both RasADH and SyADH, the omit maps, after building and refinement of the proteins, revealed residual density at the active sites, which could in each case be successfuly modelled and refined as NADPH. The final structures of *apo*-RasADH, Ras-ADH (NADPH) and SyADH (NADPH) exhibited R_{cryst} and R_{free} values of 15.8/18.8 %, 26.8/29.3 % and 23.4/25.1 respectively. The structures were validated using PROCHECK [17]. Refinement statistics are presented in Table 1. The Ramachandran plot for *apo*-RasADH showed 97.8 % of residues to be situated in the most favoured regions, 1.6 % in additional allowed and 0.5 % outlier residues. For the Ras-ADH-NADPH complex, the corresponding values were 95.3, 4.6 and 0.1 % respectively. For the SyADH–NADPH complex, the corresponding values were 99.0 and 1 % with no residues in outlier regions. Coordinates and structure factors for *apo*–RasADH Ras–NADPH and SyADH–NADPH have been deposited in the Protein Data Bank with the accession codes 4bmn, 4bms and 4bmv respectively.

6.4 Docking

Automated docking was performed using AUTODOCK VINA 1.1.2 [2]. Structures for RasADH, SyADH were prepared using AUTODOCK utility scripts. Coordinates for substrate **1** were prepared using PRODRG [32]. A monomer model was used for RasADH and a dimer model was used for SyADH with the appropriate pdbqt files prepared in AUTODOCK Tools. The active site of RasADH and SyADH was contained in a grid of 20 × 30 × 20 and 24 × 18 × 14 respectively with 0.375 Å spacing, centred around the catalytic centre which was generated using AutoGrid in the AUTODOCK Tools interface. The number of runs for genetic algorithm was set to 10 and the rest of the docking parameters were set to default parameters. The dockings were performed by VINA, therefore the posed dockings were below 2 Å rmsd. The results generated by VINA were visualised in AUTODOCK Tools 1.5.6 where the ligand conformations were assessed upon lowest VINA energy, but also the following criteria: The known mechanisms of short-chain ADHs [6] and experimentally-determined enantioselectivity of both RasAH and SyADH for ketone **1** dictated that only poses in which the carbonyl of **1** was observed to make appropriate interactions with the phenolic hydroxyl of the catalytic tyrosine residue (Tyr150 or Tyr153 for RasADH or SyADH respectively); the conserved active site serine [6] (Ser137 or Ser140 for RasADH or SyADH respectively) and which presented the (*re*)-face of the carbonyl to the nicotinamide ring of NADPH (resulting in the (*S*)-alcohol product), were considered.

Acknowledgments This research was supported by a Marie Curie Network for Initial Training fellowships to K.K., J.K. and A.F. in the project BIOTRAINS (FP7-PEOPLE-ITN-2008-238531). We would also like to thank Prof. Wolfgang Kroutil of the University of Graz for genes encoding both RasADH and SyADH.

References

1. Atkin KE, Reiss R, Turner NJ, Brzozowski AM, Grogan G (2008) Cloning, expression, purification, crystallization and preliminary X-ray diffraction analysis of variants of monoamine oxidase from *Aspergillus niger*. Acta Crystallogr Sect F 64:182–185
2. Bradshaw CW, Fu H, Shen GJ, Wong CH (1992) A *Pseudomonas* sp. alcohol dehydrogenase with broad substrate specificity and unusual stereospecificity for organic synthesis. J Org Chem 57:1526–1532
3. Cuetos A, Rioz-Martínez A, Bisogno FR, Grischek B, Lavandera I, de Gonzalo G, Kroutil W, Gotor V (2012) Access to enantiopure α-alkyl-β-hydroxy esters through dynamic kinetic resolutions employing purified/overexpressed alcohol dehydrogenases. Adv Synth Catal 354:1743–1749
4. Emsley P, Cowtan K (2004) Coot: model-building tools for molecular graphics. Acta Crystallogr Sect D 60:2126–2132
5. Evans P (2006) Scaling and assessment of data quality. Acta Crystallogr Sect D 62:72–82
6. Filling C, Berndt KD, Benach J, Knapp S, Prozorovski T, Nordling E, Ladenstein R, Jörnvall H, Oppermann U (2002) Critical residues for structure and catalysis in short-chain dehydrogenases/reductases. J Biol Chem 277:25677–25684
7. Groman EV, Schultz RM, Engel LL, Orr JC (1976) Horse liver alcohol dehydrogenase and *Pseudomonas testosteroni* 3(17)β-hydroxysteroid dehydrogenase transfer epimeric hydrogens from NADH to 17β-hydroxy-5α-androstan-3-one. An exception to one of the Alworth–Bentley rules. Eur J Biochem 63:427–429
8. Hollman F, Arends IWCE, Holtmann D (2011) Enzymatic reductions for the chemist. Green Chem 13:2285–2313
9. Höllrigl V, Hollmann F, Kleeb A, Buehler K, Schmid A (2008) TADH, the thermostable alcohol dehydrogenase from *Thermus* sp. ATN1: a versatile new biocatalyst for organic synthesis. Appl Microbiol Biotechnol 81:263–273
10. Holm L, Sander C (1996) Mapping the protein Universe. Science 273:560–595
11. Jakoblinnert A, Mladenov R, Paul A, Sibilla F, Schwaneberg U, Ansorge-Schumacher MB, de Maria PD (2011) Asymmetric reduction of ketones with recombinant *E. coli* whole cells in neat substrates. Chem Commun 47:12230–12232
12. Kabsch W (2010) XDS. Acta Crystallogr Sect D 66:125–132
13. Karabec M, Lyskowski A, Tauber KC, Steinkellner G, Kroutil W, Grogan G, Gruber K (2010) Structural insights into substrate specificity and solvent tolerance in alcohol dehydrogenase ADH-'A' from *Rhodococcus ruber* DSM 44541. Chem Commun 46:6314–6316

14. Krissinel E, Henrick K (2007) Inference of macromolecular assemblies from crystalline state. J Mol Biol 372:774–797
15. Kulig J, Simon RC, Rose CA, Husain SM, Hackh M, Ludeke S, Zeitler K, Kroutil W, Pohl M, Rother D (2012) Stereoselective synthesis of bulky 1,2-diols with alcohol dehydrogenases. Catal Sci Technol 2:1580–1589
16. Kulig J, Frese A, Kroutil W, Pohl M, Rother D (2013) Biochemical characterization of an alcohol dehydrogenase from *Ralstonia* sp. Biotechnol Bioeng 110:1838–1848
17. Laskowski RA, Macarthur MW, Moss DS, Thornton JM (1993) PROCHECK: a program to check the stereochemical quality of protein structures. J Appl Crystallogr 26:283–291
18. Lavandera I, Kern A, Ferreira-Silva B, Glieder A, de Wildeman S, Kroutil W (2008) Stereoselective bioreduction of bulky–bulky ketones by a novel ADH from *Ralstonia* sp. J Org Chem 73:6003–6005
19. Lavandera I, Oberdorfer G, Gross J, de Wildeman S, Kroutil W (2008) Stereocomplementary asymmetric reduction of bulky–bulky ketones by biocatalytic hydrogen transfer. Eur J Org Chem 2008:2539–2543
20. Lavandera I, Kern A, Resch V, Ferreira-Silva B, Glieder A, Fabian WMF, de Wildeman S, Kroutil W (2008) One-way biohydrogen transfer for oxidation of sec-alcohols. Org Lett 10: 2155–2158
21. Long F, Vagin AA, Young P, Murshudov GN (2008) BALBES: a molecular replacement pipeline. Acta Crystallogr Sect D 64:125–132
22. Machielsen R, Uria AR, Kengen SWM, van der Oost J (2006) Production and characterization of a thermostable alcohol dehydrogenase that belongs to the aldo-keto reductase superfamily. Appl Environ Microbiol 72:233–238
23. MacKenzie AK, Kershaw NJ, Hernandez H, Robinson CV, Schofield CJ, Andersson I (2007) Clavulanic acid dehydrogenase: structural and biochemical analysis of the final step in the biosynthesis of the β-lactamase inhibitor clavulanic acid. Biochemistry 46:1523–1533
24. Murshudov GN, Vagin AA, Dodson EJ (1997) Refinement of macromolecular structures by the maximum-likelihood method. Acta Crystallogr Sect D 53:240–255
25. Musa MM, Phillips RS (2011) Recent advances in alcohol dehydrogenase-catalysed asymmetric production of hydrophobic alcohols. Catal Sci Technol 1:1311–1323
26. Musa MM, Ziegelmann-Fjeld KI, Vieille C, Zeikus JG, Phillips RS (2010) In: Whittall J, Sutton P (eds) Practical methods for biocatalysis and biotransformations. Wiley, Chichester, pp 284–287
27. Pennacchio A, Giordano A, Esposito L, Langella E, Rossi M, Raia CA (2010) Insight into the stereospecificity of short-chain *Thermus thermophilus* alcohol dehydrogenase showing pro-*S* hydride transfer and prelog enantioselectivity. Protein Pept Lett 17:437–443
28. Pennacchio A, Giordano A, Pucci B, Rossi M, Raia CA (2010) Biochemical characterization of a recombinant short-chain NAD(H)-dependent dehydrogenase/reductase from *Sulfolobus acidocaldarius*. Extremophiles 14:193–204
29. Prelog V (1964) Specification of the stereospecificity of some oxido-reductases by diamond lattice sections. Pure Appl Chem 9:119–130
30. Ramaswamy S, Scholze M, Plapp BV (1997) Binding of formamides to liver alcohol dehydrogenases. Biochemistry 36: 3522–3527
31. Schlieben NH, Niefind K, Müller J, Riebel B, Hummel W, Schomburg D (2005) Atomic resolution structures of R-specific alcohol dehydrogenase from *Lactobacillus brevis* provide the structural bases of its substrate and cosubstrate specificity. J Mol Biol 349:801–813
32. Schüttelkopf AW, van Aalten DMF (2004) PRODRG: a tool for high-throughput crystallography of protein-ligand complexes. Acta Crystallogr Sect D 60:1355–1363
33. Sogabe S, Yoshizumi A, Fukami TA, Shiratori Y, Shimizu S, Takagi H, Nakamori S, Wada M (2003) The crystal structure and stereospecificity of levodione reductase from *Corynebacterium aquaticum* M-13. J Biol Chem 278:19387–19395
34. Supangat S, Seo KH, Choi YK, Park YS, Son D, Han C-D, Lee KH (2006) Structure of *Chlorobium tepidum* sepiapterin reductase complex reveals the novel substrate binding mode for stereospecific production of L-threo-tetrahydrobiopterin. J Biol Chem 281:2249–2256
35. Trott O, Olson AJ (2010) AutoDock Vina: improving the speed and accuracy of docking with a new scoring function, efficient optimization and multithreading. J Comp Chem 31:455–461
36. Vagin A, Teplyakov A (1997) MOLREP: an automated program for molecular replacement. Appl Crystallogr 30:1022–1025
37. Winter G (2010) *xia2*: an expert system for macromolecular crystallography data reduction. J Appl Cryst 3:186–190
38. You K-S (1984) Stereospecificity for nicotinamide nucleotides in enzymic and chemical hydride transfer reactions. Crit Rev Biochem 17:313–451
39. Zelinski T, Kula M-R (1994) A kinetic study and application of a novel carbonyl reductase isolated from *Rhodococcus erythropolis*. Bioorg Med Chem 2:421–428
40. Zhang R, Zhu G, Zhang W, Cao S, Ou X, Li X, Bartlam M, Xu Y, Zhang XC, Rao Z (2008) Crystal structure of a carbonyl reductase from *Candida parapsilosis* with anti-Prelog stereospecificity. Protein Sci 17:412–1423

CHAPTER III

Laccase/TEMPO-mediated system for oxidation of 2,2-dihalo-1-phenylethanol derivatives

Introduction

3.1.1. Laccase/TEMPO system for the oxidation of secondary alcohols

As mentioned in the Introduction, laccases are copper-based enzymes able to achieve the oxidation of phenols and aromatic amines. However, when dealing with other substrates, these oxidases are not able to perform this reaction, therefore needing the use of another molecule called mediator (Scheme I.10). These laccase-mediator systems have been successfully applied for the oxidation of primary alcohol moieties in non-phenolic compounds, such as aliphatic, allylic and benzylic alcohols, sugars like glycosides and soluble starch.[36,60] Probably the most commonly used laccase mediator is 2,2,6,6-tetramethylpiperidinoxyl radical (TEMPO, Figure I.18). The usage of this system for the oxidation of secondary alcohols has been less frequently reported and usually these studies were performed in the context of selective oxidations of primary alcohols over secondary ones, or of benzylic alcohols over aliphatic ones (Scheme 3.1).[72,76]

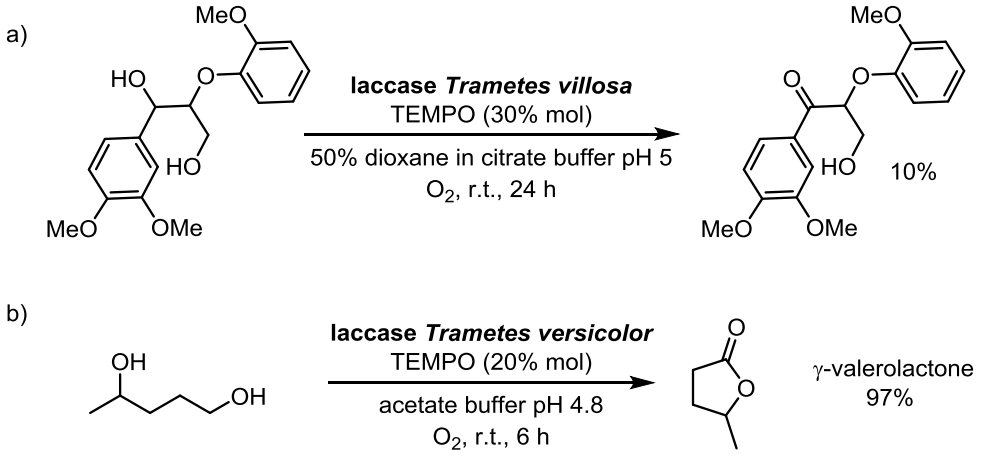

Scheme 3.1. a) The oxidation of adlerol to adlerone using the laccase/TEMPO redox pair is an example of chemoselectivity where a secondary benzylic moiety has been preferentially oxidized versus a primary aliphatic alcohol moiety.[72,136] b) Regioselective oxidation of 1,4-pentanediol to γ-valerolactone using the laccase/TEMPO system.[76]

On the other hand, our research group has recently reported an example of exploiting the TEMPO preference towards primary alcohols in detriment of secondary alcohols (Scheme 3.1b).[76] While the oxidation of long aliphatic primary alcohols has

[136] A. M. Barreca, M. Fabbrini, C. Galli, P. Gentili, S. Ljunggren, *J. Mol. Catal. B: Enzym*. **2003**, *26*, 105-110.

resulted in rather poor conversions,[137] for diols such as 1,4-pentanediol the reaction outcome can be shifted thanks to the spontaneous cyclization of the hydroxy aldehyde intermediate to form an hemiacetal which was subsequently oxidized into the lactone.

Among the different secondary alcohols tested as substrates for the laccase/TEMPO pair, (poly)cyclic alcohols and benzylic secondary alcohols can be found (Figure 3.1). For instance, in the study performed by Fabbrini *et al*.,[137a] the tested substrates included 1-(4-methoxyphenyl)ethanol (**3.1**), 1-(4-methoxyphenyl)-1-propanol (**3.2**) and cyclohexanol (**3.3**), which were oxidized to the corresponding ketones with 85%, 95% and 35% conversion, respectively, clearly showing the preference towards benzylic substrates. Reactions were performed using the laccase from *Trametes villosa* and TEMPO (33% mol) in citrate buffer 100 mM pH 4.5.

In a very recent report carried out by Kroutil and co-workers,[74d] laccases from *Trametes versicolor* or *Agaricus bisporus* coupled to several TEMPO derivatives as mediators were screened for the oxidation of isosorbide (**3.5**), its isomer isomannide and 1-indanol (**3.6**, Figure 3.1). Reactions were initially performed in acetate or phosphate buffers 50 mM pH 4.5, however the yields significantly improved for diol **3.5** when the oxidations were achieved at pH 6 at 5-10 mM buffer concentrations. Interestingly, very low conversions to the diketone were observed in citrate or bis-Tris buffers. Additionally, at optimum reaction conditions the mediator loading could be reduced from 30% to 4% mol. Among the mediators screened, TEMPO coupled to the laccase from *Trametes versicolor* was found to be the best one in the oxidation of diol **3.5** and alcohol **3.6**.

[137] (a) M. Fabbrini, C. Galli, P. Gentili, D. Macchitella, *Tetrahedron Lett*. **2001**, *42*, 7551-7553; (b) I. Matijosite, Ph D Thesis, Technical University of Delft, **2008**.

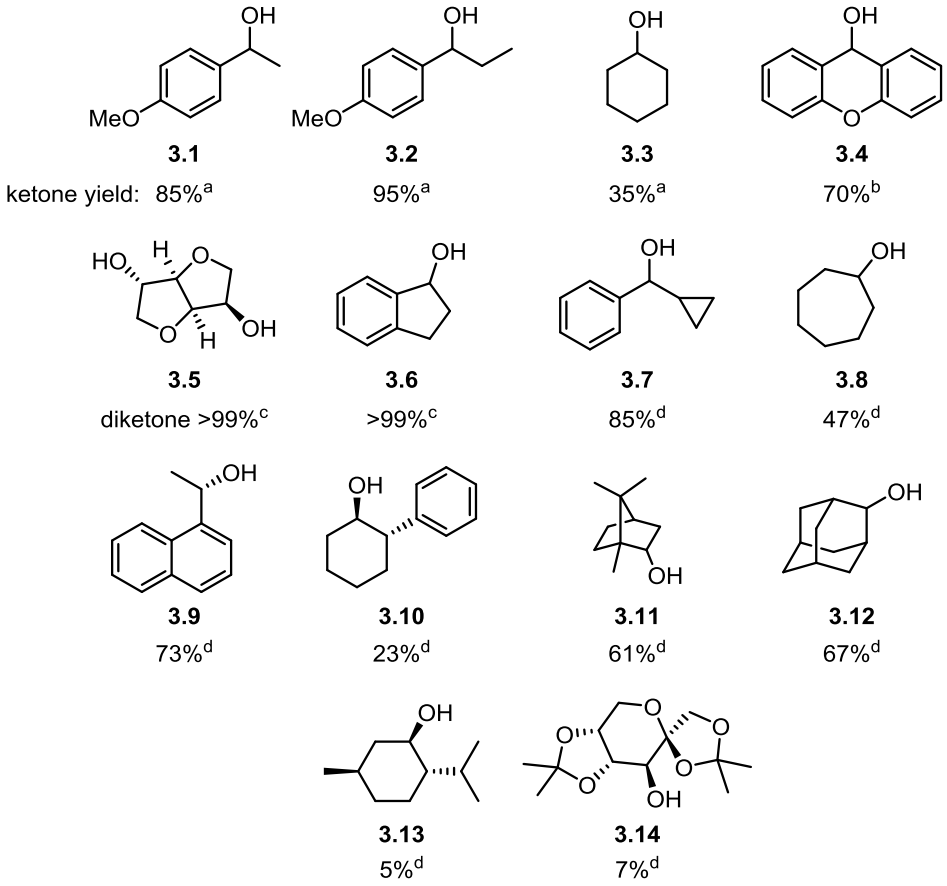

Figure 3.1. Chemical structure of secondary alcohols **3.1**-**3.14** tested as substrates for the laccase/TEMPO oxidation system, affording the corresponding ketones. Based on the following references: (a) Fabbrini *et al.* (2001);[137a] (b) d'Acunzo *et al.*[72] (c) Gross *et al.* (2014);[74d] and (d) Zhu *et al.* (2014).[75]

Additionally, several secondary alcohols were oxidized in the study of Zhu *et al.*[75] including (poly)cyclic structures of natural derivatives like borneol (**3.11**), menthol (**3.13**), and fructopyranose (**3.14**), as shown in Figure 3.1. They appeared to be difficult substrates for the laccase/TEMPO mediated system in acetate buffer 200 mM pH 4.5 and usually gave poor to moderate conversions to the corresponding ketones. However, employment of other *N*-oxyl stable radical compounds such as AZADO (Figure I.19) considerably improved the conversions for all secondary alcohols tested, although further addition of the organic cosolvent benzotrifluoride ($PhCF_3$, 16% v/v) was required, allowing in some cases the synthesis of the desired ketones in high yields (80-90% over 12 hours).

In the last few years, a considerable number of TEMPO structurally-related derivatives, including those with higher redox potential, have been synthesized and screened with laccases and metal-catalysts.[71,74] However, the redox potential seems irrelevant in the results obtained due to the ionic mechanism underpinning the oxidation process when stable nitroxyl radicals are involved. Steric hindrances posed by the methyl substituents flanking the nitroxyl radical in TEMPO and less available secondary hydroxyl groups in alcohol molecules, account for the rate-limiting step of the substrate-mediator intermediate formation and subsequent product release.

3.1.2. Effect of organic cosolvents in laccase-TEMPO systems

In many cases the tested secondary alcohols are molecules of low solubility in the aqueous solvent, which also contributes to low conversions achieved in laccase-mediator oxidation systems. A usual strategy to improve the substrate availability is the addition of an organic cosolvent.

D'Acunzo *et al.*[138] studied the effect of several miscible cosolvents: ethylene glycol, acetonitrile, isopropanol and 1,4-dioxane, in the oxidation of 4-methoxybenzyl alcohol using laccase from *Poliporus pinsitus* and mediators such as TEMPO, ABTS, NHPI, and VLA, representative for different oxidation mechanisms.[139] Increasing concentrations of water-miscible cosolvents in citrate buffer pH 5 had a negative effect on the initial enzymatic activity, while further incubation of the laccase in 50% v/v of the organic solvent over 24 h affected the enzyme stability, apart from ethylene glycol that did not influence the enzyme performance. Additionally, for all cosolvents tested, except for ethylene glycol, lower conversions to 4-methoxybenzaldehyde were observed when reactions were carried out in 50% v/v of organic media regardless the mediator used. Similar results were obtained by Baratto *et al.*,[140] who investigated the effect of miscible cosolvents like acetone, DMSO, 1,4-dioxane, acetonitrile, tetrahydrofuran and DMF in the oxidation of the natural glycoside thiocolchicoside with the laccase from *Trametes pubescens* and TEMPO. Since experiments were performed over 6 days, the

[138] F. d'Acunzo, A. M. Barreca, C. Galli, *J. Mol. Catal. B: Enzym*. **2004**, *31*, 25-30.
[139] ABTS acts *via* electron transfer, TEMPO *via* ionic mechanism, HPI and VLA *via* hydrogen atom abstraction. For detailed mechanisms and mediator structures, see the Introduction.
[140] L. Baratto, A. Candido, M. Marzorati, F. Sagui, S. Riva, B. Danieli, *J. Mol. Catal. B: Enzym*. **2006**, *39*, 3-8.

addition of cosolvents at 20% v/v affected negatively the reaction outcome, except for 1,4-dioxane which proved to be more convenient.

On the other hand, the employment of biphasic systems has the advantage of separating the hydrophilic enzyme from the hydrophobic substrate, which is solubilized in the organic reservoir phase. Despite the slowdown in the mass transfer between both phases, the enzymatic activity can be fully retained allowing a good reaction progress though at expenses of longer time intervals. For instance, a biphasic system consisting of 50% v/v of toluene and acetate buffer pH 4.5 was applied by Arends *et al.*[74b] in the oxidation of 1-phenylethanol by laccase from *Trametes villosa* coupled to different TEMPO derivatives under atmospheric pressure of oxygen supplied into the vessel. Unfortunately, the conversion was not improved with any of the mediators tested and in the case of TEMPO, only 28% of acetophenone was obtained after 24 h in comparison to the 67% yielded in plain buffer after 5.5 h.

In a recent work, Zue *et al.*[75] tested several water immiscible organic cosolvents to improve the conversion in the oxidation of model compound **3.14** (Figure 3.1) using the laccase from *Trametes versicolor* and the nitroxyl mediator AZADO in acetate buffer pH 4.5, obtaining 63% of conversion after 12 h. Different cosolvents were tested at 16% v/v concentration, and the addition of, *e.g.* cyclohexane, hexane, benzene, toluene, fluorobenzene, or hexafluorobenzene did not affect the reaction conversion (around 61-77%). While for ethyl acetate a considerable decrease in the conversion was found, the presence of benzotrifluoride resulted in a rise of the ketone production up to 87%. Nevertheless, further optimization of the amount of this organic cosolvent (10-30% v/v) did not improve the product yield. Noteworthy, the mediator loading could be reduced from 20% to 5% mol in the optimized reaction conditions.

3.1.3. Biocatalytic oxidation of halohydrins

Biooxidation of chiral primary and secondary alcohols using ADHs remains as a less developed research area in comparison to bioreductions, due to the limitation posed by the high stereospecificity of these enzymes, allowing a maximum of 50% conversion into the corresponding aldehydes or ketones.[141] In this regard, the search for non-

[141] (a) W. Kroutil, H. Mang, K. Edegger, K. Faber, *Adv. Synth. Catal*. **2004**, *346*, 125-142; (b) D. Romano, R. Villa, F. Molinari, *ChemCatChem* **2012**, *4*, 739-749.

selective ADHs like the one from *Sphingobium yanoikyuae* has gained new significance when designing efficient enzymatic oxidations.[34a]

Moreover, some substrates such as alcohols substituted at β-position with electron-withdrawing groups (EWG), *e.g.* halohydrins, are challenging compounds since their conversions into the corresponding α-substituted ketones is hardly feasible under alcohol dehydrogenase (ADH)-catalyzed hydrogen transfer conditions. While the high redox potential of the pair ketone/alcohol is considered as a merit that favors the bioreduction processes, it is a serious drawback when considering biooxidations into the carbonylic compounds.

In a study performed by Kroutil and co-workers[34a] even though ADHs reduced smoothly α-chloro ketones into the corresponding 1-chloro-2-alcohols, the oxidation of halohydrins, like 1-chloro-2-octanol and 2-chloro-1-phenylethanol, was not observed in a screening of a library of more than 60 commercial ADHs with acetone as hydrogen acceptor. Nevertheless, the oxidation of halohydrins is not obstructed, and they can be oxidized *via* HT pathway when providing a coupled hydrogen acceptor which possesses a suitable redox potential. In this way, 2-chloro-1-phenylethanol was oxidized using *Lactobacillus brevis* alcohol dehydrogenase (LBADH) as biocatalyst and chloroacetone as hydrogen acceptor, as shown in Scheme 3.2.[95] Following an optimization of the hydrogen acceptor and donor (from 1:2 to 4:1), it was possible to observe enzymatic conversions in the range of 3-12% after 24 h.

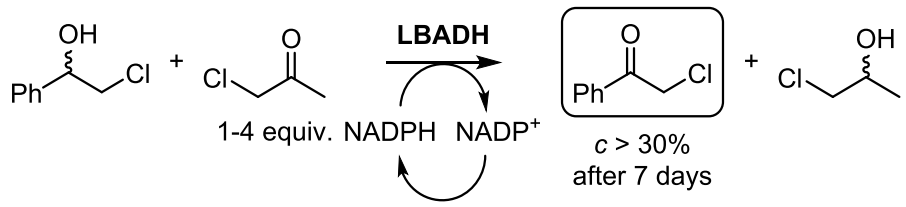

Scheme 3.2. Biooxidation of a halohydrin with LBADH was feasible due to adequate coupling of an activated co-substrate, also possessing a high redox potential that favored its bioreduction as driving force for cofactor regeneration.

Longer reaction times (7 days) and addition of fresh biocatalyst and cofactor every day led to higher conversions (>30%). Nevertheless, biooxidation of halohydrins

using alcohol oxidoreductases has shown low efficiency in terms of larger scale applications.

3.1.4. Deracemization processes applied to the synthesis of halohydrins

Dynamic kinetic resolution (DKR) of racemic secondary alcohols allows accessing to enantiomerically pure alcohols in quantitative yields. A typical DKR approach combines the stereoselective lipase-catalyzed acylation of a secondary alcohol and a transition-metal assisted racemization, as shown in Scheme 3.3.[142] Although lipases allow kinetic resolution of esters and alcohols in organic solvents, their efficiency is limited to 50% of maximum theoretical yield. Therefore, transition metal catalysts like ruthenium, iridium and rhodium complexes have been studied as racemization agents in terms of their compatibility with the enzymatic reaction conditions.

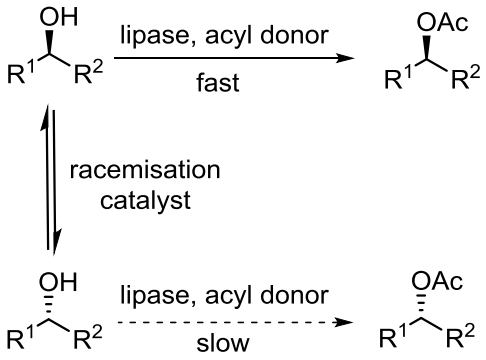

Scheme 3.3. DKR process combining the use of a lipase-catalyzed kinetic resolution of a secondary alcohol, with *in situ* racemization of the slow-reacting enantiomer mediated by a transition metal complex in hydrogen transfer conditions.

For the specific case of halohydrins, Träff *et al.* reported the combined use of a ruthenium catalyst for the racemization of aromatic chlorohydrins with *Pseudomonas*

[142] (a) O. Pámies, J.-E. Bäckvall, *J. Org. Chem.* **2002**, *67*, 9006-9010; (b) J. H. Choi, Y. K. Choi, Y. H. Kim, E. S. Park, E. J. Kim, M.-J. Kim, J. Park, *J. Org. Chem.* **2004**, *69*, 1972-1977; (c) T. Jerphagnon, A. J. A. Gayet, F. Berthiol, V. Ritleng, N. Mršić, A. Meetsma, M. Pfeffer, A. J. Minnaard, B. L. Feringa, J. G. de Vries, *Chem. Eur. J.* **2009**, *15*, 12780-12790.

cepacia lipase (PSL-C) for their enzymatic resolution through acetylation reaction, yielding the corresponding chlorohydrin acetates in high yields and *ee* (Scheme 3.4a).[143]

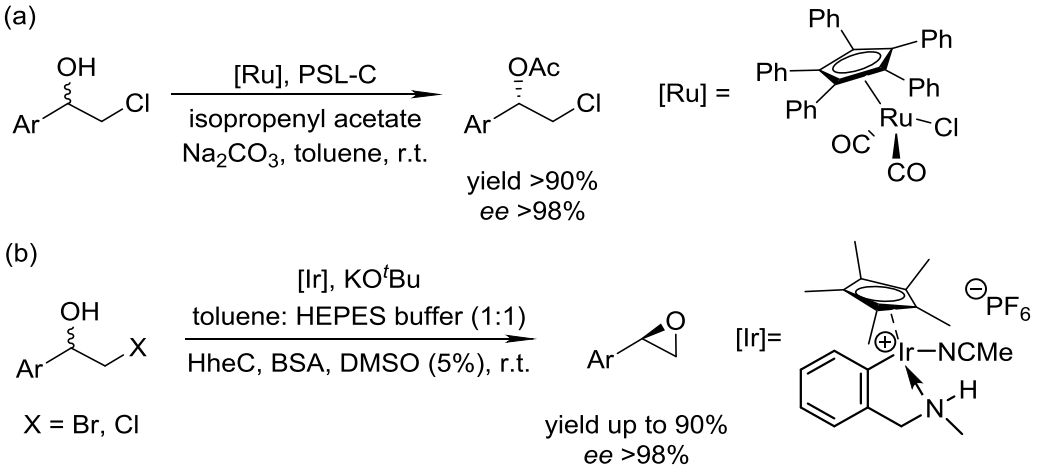

Scheme 3.4. DKR of aromatic halohydrins using: a) a ruthenium catalyst combined with a lipase yielding enantioenriched acetates; and b) an iridium catalyst combined with a halohydrin dehalogenase yielding enantioenriched epoxides.

In other study, the direct chemoenzymatic DKR of racemic β-haloalcohols was developed to provide the corresponding enantioenriched epoxides (Scheme 3.4b). Racemization was achieved using an iridium catalyst while the stereoselective biocatalyst was in this case a halohydrin dehalogenase (HheC) in a biphasic system.[144]

A more recent work from Kroutil's group has combined the non-selective iridium-catalyzed oxidation of racemic halohydrins with the concomitant stereoselective reduction using an alcohol dehydrogenase, namely ADH-A (from *Rhodococcus ruber*), to deracemize them through the α-chloro ketone intermediate in a biphasic reaction media.[145] Oxidation proceeded *via* hydrogen transfer (HT) pathway where 2-chloro-6,6-dimethylcyclohexanone served as hydrogen acceptor as its reduction was thermodynamically highly favored. For the NADH-dependent alcohol dehydrogenase bioreduction, the cofactor was regenerated using a coupled-enzyme approach with formate dehydrogenase, as shown in Scheme 3.5.

[143] A. Träff, K. Bogár, M. Warner, J.-E. Bäckvall, *Org. Lett*. **2008**, *10*, 4807-4810.
[144] R. M. Haak, F. Berthiol, T. Jerphagnon, A. J. A. Gayet, C. Tarabiono, C. P. Postema, V. Ritleng, M. Pfeffer, D. B. Janssen, A. J. Minnaard, B. L. Feringa, J. G. de Vries, *J. Am. Chem. Soc*. **2008**, *130*, 13508-13509.
[145] F. G. Mutti, A. Orthaber, J. H. Schrittwieser, J. G. de Vries, R. Pietschnig, W. Kroutil, *Chem. Commun*. **2010**, *46*, 8046-8048.

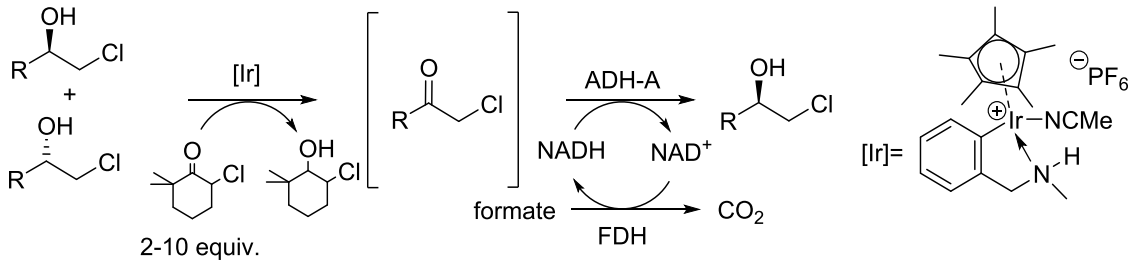

Scheme 3.5. Enzymatic deracemization of halohydrins using an iridium complex and an alcohol dehydrogenase.

However, the yield achieved in the optimized conditions did not reach 40% since the usage of a non-selective oxidant led to undesired loss of the final enantioenriched halohydrin.

Objectives

Since biooxidation of β,β-dihalogenated alcohols using ADHs is not feasible due to disfavored thermodynamics, another chemoenzymatic system, *e.g.* a laccase coupled with a mediator such as TEMPO, was proposed for the oxidation of these secondary alcohols *via* environmentally benign protocol. The following objectives were set for the study:

- Optimize the reaction conditions for a model substrate (2,2-dichloro-1-phenylethanol) in terms of type of aeration, reaction temperature, buffer type and pH, TEMPO equivalents, and substrate concentration.

- Examine the effect of the increasing concentration of miscible and immiscible organic solvents in the reaction efficiency.

- Compare the kinetics of the reaction progress in a biphasic system and in sole buffer to unravel the effect of the cosolvent.

- Study the feasibility of the optimized system for a series of β,β-dihalogenated substrates with different substituents in the aryl ring, as well as a halohydrin and 1-phenylethanol.

- Couple the laccase/TEMPO system with an ADH to deracemize a secondary alcohol in a one-pot reaction.

- Compare our system with other chemical oxidative methods applied to the model substrate.

- Calculate and compare the environmental impact factor for the laccase/TEMPO process regarding other chemical approaches.

Results and discussion

The laccase/mediator oxidation system has attracted much interest as environmentally benign methodology for the oxidation of a wide range of primary and secondary alcohols, as well as ethers. Among all known mediators, TEMPO and its derivatives have been one of the most efficient oxidants coupled to laccases, despite the differences in the requirements for the optimal performance shown by each component. While most of the fungal laccases prefer acidic pHs and physiological temperatures,[146] TEMPO is more stable at low temperatures and its regeneration works better at basic pHs (8-10).[147] The compromise pH (4.5-5) of the aqueous media makes necessary to apply substoichiometric amounts of TEMPO, usually between 15-30% mol, instead of 1-5% mol used in the original Anelli's oxidation protocol[78b] in a biphasic system (dichloromethane: water) at basic pH.

[146] (a) P. Torres-Salas, D. M. Mate, I. Ghazi, F. J. Plue, A. O. Ballesteros, M. Alcalde, *ChemBioChem* **2013**, *14*, 934-937; (b) U. N. Dwivedi, P. Singh, V. P. Pandey, A. Kumar, *J. Mol. Catal. B: Enzym*. **2011**, *68*, 117-128.
[147] A. E. J. Nooy, A. C. Besemer, H. van Bekkum, *Carbohydr. Res*. **1995**, *269*, 89-98.

In the present study, a series of β,β-dihaloaryl secondary alcohols were used as substrates with the laccase/TEMPO oxidation system to afford the corresponding ketones, as shown in Scheme 3.6.

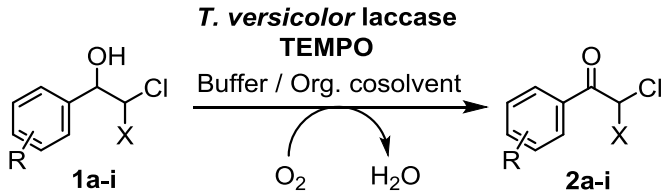

a, R= H, X= Cl; **b**, R= *o*-Cl, X= Cl; **c**, R= *m*-Cl, X= Cl
d, R= *p*-Cl, X= Cl; **e**, R= *m*-OMe, X= Cl; **f**, R= *m*-NO_2, X= Cl
g, R= H, X= Br; **h**, R= H, X= F; **i**, R= H, X= H

Scheme 3.6. General methodology to synthesize α,α-dihalogenated acetophenone derivatives **2a-h** and 2-chloroacetophenone (**2i**) through oxidative reactions with the laccase/TEMPO system.

These substrates are hardly soluble in water and decompose easily at pH above 9,[148] which makes the laccase preference for acidic conditions a highly advantageous trait. Additionally, the high Gibbs free energy difference of the halohydrin/halo ketone redox pair, blocked the oxidation of these alcohols *via* the HT mechanism presented by ADHs.[95] For the above reasons, the TEMPO-mediated oxidation through an ionic mechanism and its regeneration by the laccase at acidic conditions (pH 4-5.5), made this system as a very attractive option to access the corresponding α-halogenated ketones in an environmentally benign way.

Initial experiments over substrate **1a** with laccase from *Trametes versicolor* combined with TEMPO in solely acetate buffer pH 4.5 purged with oxygen, allowed obtaining dihalogenated ketone as the exclusive product although at not satisfactory yields. Several factors were investigated, like pH, temperature, TEMPO equivalents, aeration, substrate concentration and addition of cosolvents to address the problem of the low substrate solubility in aqueous media. The most pronounced effects on the reaction outcome were found in the aeration mode with oxygen and the addition of an organic cosolvent. Even though many reports stated sufficient level of aeration of the reaction vessel in an open-to-air system, it was found that stable oxygen purge increased

[148] E. B. Ayres, C. R. Hauser, *J. Am. Chem. Soc.* **1943**, *65*, 1095-1096.

conversions over 24 h. In terms of the cosolvents used, our results were consistent with other reports showing that water miscible solvents at higher concentrations negatively affect the enzyme performance despite the positive effect on the substrate solubility. Therefore, up to 20% v/v of acetonitrile increased the observed conversion into the ketone, however further rise in the organic content had a negative impact on the system performance, as shown in Figure 3.2.

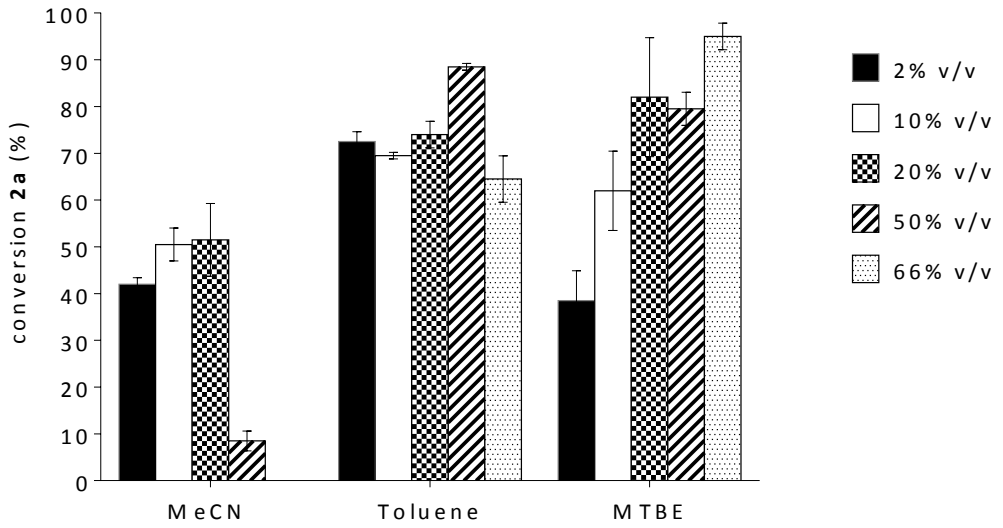

Figure 3.2. Effect of the organic cosolvent concentration using the *T. versicolor* laccase/TEMPO (20% mol) system to oxidize alcohol **1a** (50 mM), bubbling oxygen in NaOAc buffer 50 mM pH 4.5 at 20 °C (toluene and MTBE) or 30 °C (MeCN) after 24 h.

These observations led to the employment of a biphasic system, whose advantages include spatial separation of the hydrophilic enzyme and mediator from the hydrophobic substrate solubilized in the organic reservoir. Despite the expected slowdown in mass transfer between both phases, the reaction progressed to its completeness after 24 hours when MTBE was employed up to 66% v/v. It is noteworthy that MTBE evaporated during the course of the reaction, meaning that after the first 2-3 h the reaction underwent basically in aqueous media. Nevertheless, a kinetic study performed for the biphasic system showed that 50% of conversion was reached within the first 3 h and after 8 h there was 80% of the product formed. Since much attention in

the literature has been given to the topic about enzyme and TEMPO stability in organic media, the kinetic study was also performed in plain buffer to explain the role of the organic solvent. It was observed that during the first 8 h only 12% of ketone **2a** was formed, while after 24 h a 40% overall yield was reached, clearly indicating that the organic cosolvent helped to overcome solubility problems as the system remained active up to 24 h when the reaction course was followed (Figure 3.3).

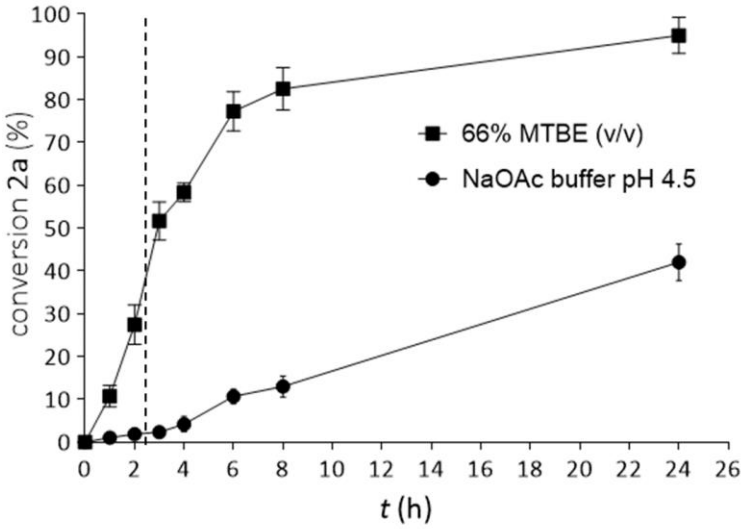

Figure 3.3. Reaction course of the *T. versicolor* laccase/TEMPO (20% mol) system to oxidize alcohol **1a** (50 mM) into **2a** bubbling oxygen in NaOAc buffer 50 mM pH 4.5 at 20 °C in the presence of MTBE (66% v/v). For comparison, the reaction progress in plain buffer was also studied. After 2-3 h, it was observed the disappearance of the organic solvent.

In agreement with other available reports, a minimum 15% mol of TEMPO was required in the reaction media to obtain quantitative conversions to dihalogenated ketones. Working at 5% and 10% mol of TEMPO at optimized reaction conditions, conversions were not complete. Furthermore, reactions were scalable at 100 mg and this system was efficient with substrate concentrations up to 200 mM. The scope of the secondary alcohols successfully transformed into the corresponding ketones comprised dihalogenated alcohols with substituents at different positions at the aryl ring (yields ranging from 75 to 95%), with the exception of an *ortho*-substituted compound that

hardly gave any conversion. Additionally, halohydrin **1i** (62%) and 1-phenylethanol (**1j**, 78%) were readily oxidized.

For the model dihalogenated aryl alcohol **1a**, halohydrin **1i** and 1-phenylethanol (**1j**), the difference of the Gibbs free energy for their oxidation processes were calculated to reflect the feasibility of our oxidation system. From these results, there was no correlation between this energy, and therefore with the redox potential, compared to the results obtained with the laccase/TEMPO pair. This fact supports the ionic mechanism postulated for nitroxyl mediators such as TEMPO. Additionally, reports on the TEMPO preference for primary alcohols *vs* secondary ones encouraged us to study whether the laccase/TEMPO system could selectively oxidize a mixture of two *sec*-alcohols. Unfortunately, no discrimination between alcohol pairs 2,2-dichloro-1-phenylethanol and 2-chloro-1-phenylethanol or 2,2-dichloro-1-phenylethanol and 1-phenylethanol was observed, as shown in Scheme 3.7.

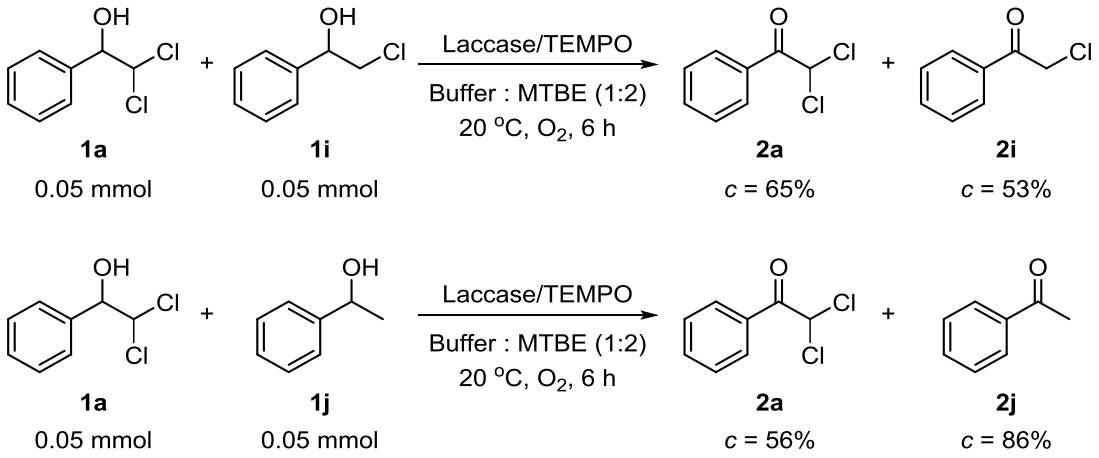

Scheme 3.7. Oxidation of *sec*-alcohols **1a** and **1i** or **1j** mediated by the laccase/TEMPO system.

Finally, the laccase/TEMPO oxidation was applied in a one-pot transformation together with ADH-A to deracemize **1a** into (*R*)-**1a** (40 mg, >97% conv., 97% *ee*). Eventually, other TEMPO recycling systems were tried to oxidized **1a**, such as NaOCl (9 equiv.), NaOCl (1 equiv.)/KBr (0.2 equiv.), $NaOCl_2$ (1.5 equiv.)/NaOCl (0.2 equiv.), CuCl (0.2 equiv.), $CuBr_2$ (0.2 equiv.), or iodine (1.5 equiv.), but reactions gave by-

products or were inefficient. Dess-Martin reagent worked as expected in organic media (dichloromethane),[149] but not in water (Figure 3.4).

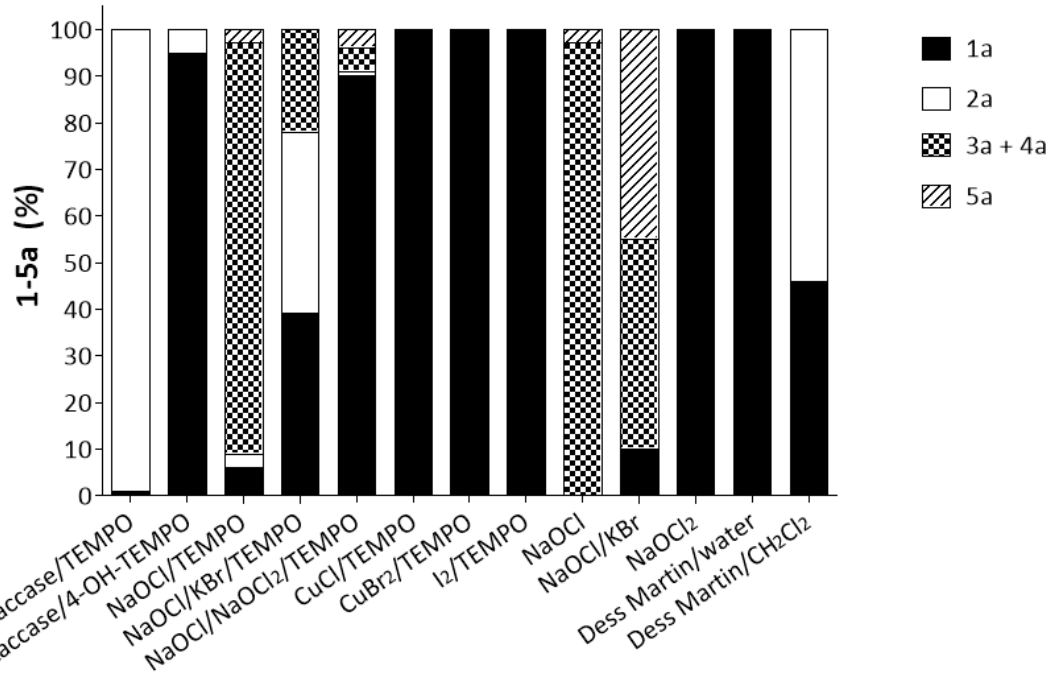

Figure 3.4. Oxidation of alcohol **1a** into ketone **2a** employing different reaction conditions. Observed side products: benzaldehyde (**3a**); benzoic acid (**4a**); mandelic acid (**5a**).

The results obtained allowed assessing the environmental impact by simple E-factor calculations using the free software EATOS, Environmental Assessment Tool for Organic Syntheses. The basis of the program relies on a correct stoichiometry of the reaction and inclusion of all auxiliary reagents used throughout the process, for instance during work-up and product isolation. The interpretation of E-factor is always relative and must be put in the right context with other methods. Apart from rising awareness of the environmental impact, it allows to identify weak points of a designed process and amount of waste generated. Definitively, the high conversion rate and the catalytic amounts of reagents used, lowered the impact on the environment of this process, making it very convenient for further development.

[149] V. Pace, A. C. Cabrera, M. Fernández, J. V. Sinisterra, A. R. Alcántara, *Synthesis* **2010**, 3545-3555.

Conclusions

To sum up, the oxidation of a series of β,β-dihalogenated-α-aryl alcohols has been achieved using the laccase/TEMPO redox pair in a biphasic system composed by acetate buffer 50 mM pH 4.5 and MTBE, thus overcoming the instability of these substrates at basic pHs and their poor solubility in aqueous media.

Extensive optimization of the reaction conditions was carried out and several factors such as buffer pH, temperature, TEMPO equivalents, aeration mode, substrate concentration and addition of organic cosolvents were investigated. The most pronounced effects on the reaction outcome were related to the aeration with oxygen and the addition of a water-immiscible cosolvent. The presence of water-miscible organic solvents such as acetonitrile affected relatively the enzyme performance at concentrations above 20% v/v despite the positive effect on the substrate solubility. In contrary, the employment of a biphasic reaction media with MTBE (66% v/v), allowed the oxidation to the corresponding ketone at high conversions (>95%).

A comparative study of the reaction kinetics over 24 h showed that 80% of the product was formed after 8 h in the biphasic system, while in plain buffer only 12% of the ketone was formed within this time frame. However, an overall yield of 40% was reached after 24 h in solely aqueous system, clearly indicating that the role of MTBE was more related with an improvement of the substrate availability rather than with the system stability.

Reactions were scaled-up and the system was efficient for model substrate **1a** until concentrations up to 200 mM using 20% mol of TEMPO. This study was expanded towards a series of β,β-dihalogenated alcohols with different substituents at the aryl ring, as well as for halohydrin **1i** and 1-phenylethanol (**1j**), proving its robustness with the exception for an *ortho*-substituted substrate.

No correlation was found between theoretically calculated differences in Gibbs free energy for the oxidation of **1a**, **1i** and **1j**, and the results obtained with the laccase/TEMPO pair, supporting the ionic mechanism postulated for nitroxyl mediators like TEMPO.

Finally, the laccase/TEMPO oxidation was combined in a one-pot sequential protocol with ADH-A from *R. ruber* to deracemize **1a** into the (*R*)-enantiomer with excellent conversion and *ee*.

Other typical TEMPO recycling systems were examined such as NaOCl, NaOCl/KBr, $NaOCl_2$/NaOCl, CuCl, $CuBr_2$, or iodine, but those reactions afforded either by-products or were less efficient than the laccase counterpart. The results obtained allowed assessing a simple environmental impact measurement by calculation of the E-factor using the EATOS tool, also showing a great benefit when employing the chemoenzymatic method.

Conclusiones

En este Capítulo se ha realizado la oxidación de una serie de alcoholes α-arilo-β,β-dihalogenados, empleando el sistema lacasa/TEMPO en un medio bifásico compuesto por una disolución reguladora de acetato 50 mM a pH 4.5 y *tert*-butil metil éter (TBME) como cosolvente orgánico, evitando así la descomposición de estos compuestos en medio básico y aumentando su solubilidad en el medio de reacción.

Se llevó a cabo la optimización de las condiciones de reacción variando diferentes parámetros tales como el pH de la disolución reguladora, la temperatura, los equivalentes de TEMPO, el modo de aireación, la concentración del sustrato y la adición de cosolventes orgánicos. Así se observaron los mayores cambios relacionados con el modo de aireación empleando oxígeno y usando un disolvente inmiscible con el agua. La presencia de disolventes miscibles tales como el acetonitrilo, demostró ser beneficiosa hasta un 20% v/v, pero cantidades mayores inhibieron la actividad enzimática. Por el contrario, se pudo utilizar TBME en un medio bifásico hasta un 66% v/v, permitiendo obtener una conversión mayor del 95% tras 24 horas de reacción.

Un estudio comparativo de las cinéticas de reacción durante las primeras 24 horas, mostró que en el sistema bifásico se obtenía una conversión a la cetona de un 80% tras 8 horas, mientras que solo un 12% en la disolución reguladora. Sin embargo, tras 24 horas se pudo llegar a una conversión del 40%, lo que parece indicar que el TBME juega un papel más relacionado con la solubilidad del sustrato, que con la mejora de la estabilidad del sistema.

Las reacciones se pudieron escalar fácilmente con el sustrato modelo **1a**, pudiéndose llegar a concentraciones de hasta 200 mM utilizando un 20% mol de TEMPO. Se realizó la oxidación sobre otros alcoholes β,β-dihalogenados con diferentes patrones de sustitución en el grupo arilo como la halohidrina **1i** y el 1-feniletanol (**1j**), obteniéndose buenas conversiones en todos los casos a excepción de un derivado sustituido en posición *orto*.

No se observó una correlación entre las energías de Gibbs teóricas calculadas para los procesos de oxidación de **1a**, **1i** y **1j**, con las conversiones en el proceso de oxidación obtenidas con este sistema, demostrándose el mecanismo de tipo iónico postulado para las oxidaciones catalizadas por TEMPO.

Este sistema se acopló en un proceso secuencial *one-pot* con la alcohol deshidrogenasa ADH-A de *R. ruber* para desracemizar **1a**, obteniéndose el enantiómero *R* del alcohol con conversiones y excesos enantioméricos altos.

Se estudiaron otros sistemas de oxidación acoplados con el TEMPO tales como el NaOCl, el NaOCl/KBr, el $NaOCl_2$/NaOCl, el CuCl, el $CuBr_2$, o el yodo, pero dichas reacciones dieron lugar a conversiones muy bajas o a la formación de subproductos. Así, estos resultados permitieron realizar un cálculo del impacto medioambiental de estas estrategias midiendo el factor E utilizando el software EATOS, obteniéndose los mejores resultados con el sistema de oxidación quimioenzimático.

Experimental part

3.6.1. Enzymatic protocols

3.6.1.1. Optimization of the conditions for the laccase/TEMPO-mediated oxidation of 1a in the monophasic aqueous/organic solvent system

3.6.1.1.1. Effect of oxygen supply (open air)

To a test tube containing 1.8 mL of acetate buffer (50 mM, pH 4.5) saturated with O_2 for an hour prior to the experiment, were added **1a** (19.1 mg, 0.1 mmol) dissolved in 200 µL of acetonitrile (final concentration: 10% v/v), TEMPO (3.1 mg, 0.02 mmol) and laccase from *Trametes versicolor* (2.3 mg, 31.3 U). The solution was vigorously shaken to dissolve all reactants. The resulting solution was left to open air and stirred at 30 ºC for 24 h. Then, the reaction was stopped by addition of EtOAc (2 x 2 mL). The organic layers were combined, dried over Na_2SO_4 and an aliquot was filtered before spiking to GC for conversion of **2a** (33±1.4%).

3.6.1.1.2. Effect of the temperature

To a microwave tube containing 1.8 mL of acetate buffer (50 mM, pH 4.5), were added **1a** (19.1 mg, 0.1 mmol) dissolved in 200 µL of acetonitrile (final concentration: 10% v/v), TEMPO (3.1 mg, 0.02 mmol) and laccase from *Trametes versicolor* (2.3 mg, 31.3 U). The tube was sealed and the reaction mixture vigorously shaken prior to the attachment of a balloon filled with oxygen (1 atm). Pressure was equilibrated placing an additional needle outlet into the rubber lid and the oxygen flow was set to gently purge the reaction mixture. The reaction mixture was left stirring at 20, 30 or 40 ºC for 24 h and the balloon was refilled with oxygen during the first 8 h of the reaction (0.4±0.1 mL/s). Then, the reaction was stopped by addition of EtOAc (2 x 2 mL). Organic layers were combined, dried over Na_2SO_4 and an aliquot was filtered before spiking to GC for conversion of **2a**: 20 ºC (56%), 30 ºC (53%), and 40 ºC (8%).

3.6.1.1.3. Effect of the TEMPO equivalents

To a microwave tube containing 1.8 mL of acetate buffer (50 mM, pH 4.5), were added **1a** (19.1 mg, 0.1 mmol) dissolved in 200 µL of acetonitrile (final concentration: 10% v/v), TEMPO (3.1-6.3 mg, 0.02-0.04 mmol) and laccase from *Trametes versicolor* (2.3 mg, 31.3 U). The tube was sealed and the mixture vigorously shaken prior to the attachment of a balloon filled with oxygen (1 atm). Pressure was equilibrated placing an additional needle outlet in the rubber lid and the oxygen flow was set to gently purge

the reaction mixture. The reaction mixture was left stirring at 30 ºC for 24 h and the balloon was refilled with oxygen during the first 8 h of reaction (0.4±0.1 mL/s). Then, the reaction was stopped by addition of EtOAc (2 x 2 mL). Organic layers were combined, dried over Na_2SO_4 and an aliquot was filtered before spiking to GC for conversion of **2a**: 20% mol (53±4.2%), 30% mol (40±9.9%), and 40% mol (63±5.7%).

3.6.1.1.4. Effect of the NaOAc buffer pH

To a microwave tube containing 1.8 mL of acetate buffer (50 mM, pH 3.5-6.0), were added **1a** (19.1 mg, 0.1 mmol) dissolved in 200 µL of acetonitrile (final concentration: 10% v/v), TEMPO (3.1 mg, 0.02 mmol) and laccase from *Trametes versicolor* (2.3 mg, 31.3 U). The tube was sealed and the mixture vigorously shaken prior to the attachment of a balloon filled with oxygen (1 atm). Pressure was equilibrated placing an additional needle outlet in the rubber lid and the oxygen flow was set to gently purge the reaction mixture. The reaction mixture was left stirring at 30 ºC for 24 h and the balloon was refilled with oxygen during the first 8 h of reaction (0.4±0.1 mL/s). Then, the reaction was stopped by addition of EtOAc (2 x 2 mL). Organic layers were combined, dried over Na_2SO_4 and an aliquot was filtered before spiking to GC for conversion of **2a**: pH 3.5 (13%), pH 4.0 (26%), pH 4.5 (53%), pH 5.5 (37%), and pH 6.0 (23%).

3.6.1.1.5. Effect of the buffer type

To a microwave tube containing 1.8 mL of acetate or citrate buffer (50 mM, pH 4.5), were added **1a** (19.1 mg, 0.1 mmol) dissolved in 200 µL of acetonitrile (final concentration: 10% v/v), TEMPO (3.1 mg, 0.02 mmol) and laccase from *Trametes versicolor* (2.3 mg, 31.3 U). The tube was sealed and the reaction mixture vigorously shaken prior to the attachment of a balloon filled with oxygen (1 atm). Pressure was equilibrated placing an additional needle outlet in the rubber lid and the oxygen flow was set to gently purge the reaction mixture. The reaction mixture was left stirring at 30 ºC for 24 h and the balloon was refilled with oxygen during the first 8 h of reaction (0.4±0.1 mL/s). Then, the reaction was stopped by addition of EtOAc (2 x 2 mL). Organic layers were combined, dried over Na_2SO_4 and an aliquot was filtered before spiking to GC for conversion of **2a**: NaOAc buffer (53±4.2%) and citrate buffer (35±2.8%).

3.6.1.1.6. Effect of the organic solvent (Figure 3.5)

To a microwave tube containing **1a** (19.1 mg, 0.1 mmol) dissolved in 40 µL of DMSO or 200 µL of acetonitrile, CH_2Cl_2, toluene or MTBE (final concentration: 2% for DMSO; 10% v/v for the others), 1.96 mL for DMSO and 1.80 mL of acetate buffer (50 mM, pH 4.5) for the other solvents were added followed by TEMPO (3.1 mg, 0.02 mmol) and laccase from *Trametes versicolor* (2.3 mg, 31.3 U). The tube was sealed and the reaction mixture vigorously shaken prior to the attachment of a balloon filled with oxygen (1 atm). Pressure was equilibrated placing an additional needle outlet in the rubber lid and the oxygen flow was set to gently purge the reaction mixture. The reaction mixture was left stirring at 20 ºC for 24 h and the balloon was refilled with oxygen during the first 8 h of reaction (0.4±0.1 mL/s). Then, the reaction was stopped by addition of EtOAc (2 x 2 mL). Organic layers were combined, dried over Na_2SO_4 and an aliquot was filtered before spiking to GC for conversion of **2a**: DMSO (43±8.5%), MeCN (56±4.9%), CH_2Cl_2 (49±4.9%), toluene (70±0.7%), and MTBE (62±8.5%). In the reaction with MTBE, the evaporation of the organic solvent was noticed. As a control experiment, the same reaction was achieved only in NaOAc buffer pH 4.5 50 mM (2 mL), obtaining a conversion of 47±2.1%.

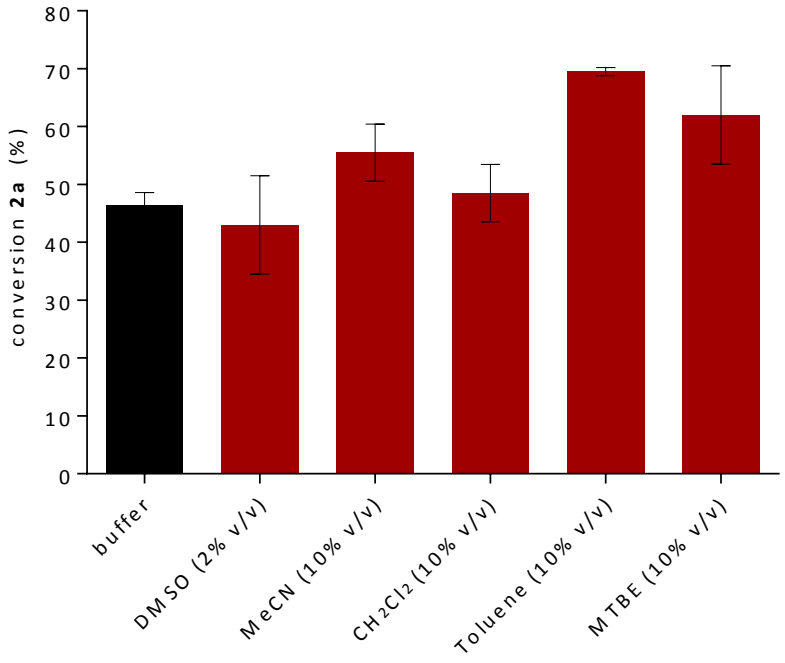

Figure 3.5. Effect of the organic solvent in the laccase/TEMPO-catalyzed oxidation of **1a**.

3.6.1.1.7. Effect of the organic solvent concentration (Figure 3.2)

To a microwave tube containing **1a** (19.1 mg, 0.1 mmol) dissolved in 40-1330 µL of MeCN, toluene or MTBE (final concentration: 2-66% v/v, respectively), were added 1.96-0.66 mL of acetate buffer (50 mM, pH 4.5), TEMPO (3.1 mg, 0.02 mmol) and laccase from *Trametes versicolor* (2.3 mg, 31.3 U). The tube was sealed and the mixture vigorously shaken prior to the attachment of a balloon filled with oxygen (1 atm). Pressure was equilibrated placing an additional needle outlet in the rubber lid and the oxygen flow was set to gently purge the reaction mixture. The reaction mixture was left stirring at 20 ºC for 24 h and the balloon was refilled with oxygen during the first 8 h of reaction (0.4±0.1 mL/s). Then, the reaction was stopped by addition of EtOAc (2 x 2 mL). Organic layers were combined, dried over Na_2SO_4 and an aliquot was filtered before spiking to GC for conversion of **2a** (Table 3.1). In the reaction with MTBE, the evaporation of the organic solvent was noticed.

Table 3.1. Effect of the organic solvent concentration in the laccase/TEMPO-catalyzed oxidation of **1a**.

organic solvent content	**2a (%)**[a]		
(% v/v)	**MeCN**	**toluene**	**MTBE**
2	42±7.1	73±2.1	39±6.4
10	56±4.9	70±0.7	62±8.5
20	52±7.8	74±2.8	82±12.7
50	9±2.1	89±0.7	80±3.5
66	n.d.	65±4.9	95±2.8

[a] Conversion values measured by GC. n.d. not determined.

3.6.1.2. Oxidation of 1a in a biphasic aqueous/MTBE system

3.6.1.2.1. Use of a lower amount of TEMPO equivalents

Laccase from *Trametes versicolor* (4.6 mg, 62.6 U) was dissolved in 2 mL of acetate buffer (50 mM, pH 4.5) in a microwave tube, followed by addition of 4 mL of MTBE (final concentration: 66% v/v), alcohol **1a** (38.2 mg, 0.2 mmol) and TEMPO (1.55-6.2 mg, 0.01-0.04 mmol). The tube was sealed and the mixture vigorously shaken prior to the attachment of a balloon filled with oxygen (1 atm). Pressure was equilibrated placing an additional needle outlet in the rubber lid and the oxygen flow was set to gently purge the reaction mixture. The reaction mixture was left stirring at 20 ºC for 24 h and the balloon was refilled with oxygen during the first 8 h of reaction (0.4±0.1 mL/s). Then, the reaction was stopped by addition of EtOAc (2 x 4 mL). Organic layers were combined, dried over Na_2SO_4 and an aliquot was filtered before spiking to GC for conversion of **2a**: 5% mol (51±4.2%), 10% mol (85±7.8%), and 20% mol (95±4.2%).

3.6.1.2.2. Time course study of the laccase/TEMPO-mediated oxidation of 1a in a biphasic aqueous/MTBE system or in plain buffer (Figure 3.3)

Laccase from *Trametes versicolor* (2.3 mg, 31.3 U) was dissolved in 1 mL of acetate buffer (50 mM, pH 4.5) in a microwave tube, followed by addition of 2 mL of MTBE (final concentration: 66% v/v), alcohol **1a** (28.5 mg, 0.15 mmol), and TEMPO (4.6 mg, 0.03 mmol). The tube was sealed and the reaction mixture vigorously shaken prior to the attachment of a balloon filled with oxygen (1 atm). Pressure was equilibrated placing an additional needle outlet in the rubber lid and the oxygen flow was set to gently purge the reaction mixture. The reaction mixture was left stirring at 20^{o}C and the balloon was refilled with oxygen during the reaction course (0.4±0.1 mL/s). Then, the reaction was stopped at different times (see Table 3.2) by addition of EtOAc (2 x 3 mL). Organic layers were combined, dried over Na_2SO_4 and a filtered aliquot was spiked to GC instrument to measure conversion of **2a**. In the oxidations with a reaction time higher than 2-3 h, the evaporation of the organic solvent was noticed.

For a comparative study, into 3 mL of NaOAc buffer pH 4.5 (50 mM) were added: substrate **1a** (50 mM, 28.5 mg, 0.15 mmol), TEMPO (4.6 mg, 20% mol, 0.03 mmol) and laccase from *Trametes versicolor* (2.3 mg, 31.3 U). The reaction was left at

20 ºC with oxygen bubbling (1 atm, 0.4±0.1 mL/s) for the first 8 h of reaction. Then, the reaction was stopped at certain time by adding EtOAc (2 x 3 mL) and worked-up in an analogous way as for the biphasic system.

Table 3.2. Oxidation of **1a** at different reaction times using the laccase/TEMPO system in a biphasic medium aqueous/MTBE system or just in plain buffer.

***t* (h)**	**2a (%)**[a,b]	**2a (%)**[a,c]
1	10.7±2.5	1.1±0.2
2	27.5±4.6	1.9±0.2
3	51.7±4.5	2.4±0.2
4	58.4±2.2	4.2±1.9
6	77.3±4.6	10.7±1.7
8	82.5±4.9	13±2.5
24	95±4.2	42±4.2

[a] Conversion values measured by GC.

[b] In a buffer/MTBE biphasic system.

[c] In solely buffer.

3.6.1.2.3. Effect of the substrate concentration

Laccase from *Trametes versicolor* (2.3 mg, 31.3 U) was dissolved in 1 mL of acetate buffer (50 mM, pH 4.5) in a microwave tube, followed by addition of 1 mL of MTBE (final concentration: 50% v/v), alcohol **1a** (9.5-76.4 mg, 0.05-0.4 mmol) and 20% mol of TEMPO (1.5-12.4 mg, 0.01-0.08 mmol). The tube was sealed and the mixture was vigorously shaken prior to the attachment of a balloon filled with oxygen (1 atm). Pressure was equilibrated placing an additional needle outlet in the rubber lid and the oxygen flow was set to gently purge the reaction mixture. The reaction mixture was left stirring at 20 ºC for 24 h and the balloon was refilled with oxygen during the first 8 h of reaction (0.4±0.1 mL/s). Then, the reaction was stopped by addition of EtOAc (2 x 4 mL). Organic layers were combined, dried over Na_2SO_4 and a filtered aliquot was spiked to GC instrument to measure conversion of **2a**: 25 mM (65±1.4), 100

mM (93±6.8), and 200 mM (93±2.1). After 2-3 h, the evaporation of the organic solvent was noticed.

3.6.1.3. General method for the oxidation of alcohols 1a-j using laccase and TEMPO in a biphasic aqueous/organic solvent system

Laccase from *Trametes versicolor* (2.3 mg, 31.3 U) was dissolved in 1 mL of acetate buffer (50 mM, pH 4.5) in a microwave tube, followed by addition of 2 mL of MTBE (final concentration: 66% v/v), the corresponding alcohol **1a-j** (0.1 mmol) and TEMPO (3.1 mg, 0.02 mmol). The tube was sealed and the mixture was vigorously shaken prior to the attachment of a balloon filled with oxygen (1 atm). Pressure was equilibrated placing an additional needle outlet in the rubber lid and the oxygen flow was set to gently purge the reaction mixture. The reaction mixture (Figure 3.6) was left stirring at 20 ºC for 24 h and the balloon was refilled with oxygen for the first 8 h of reaction (0.4±0.1 mL/s). Then, the reaction was stopped by addition of EtOAc (2 x 2 mL). Organic layers were combined, dried over Na_2SO_4 and a filtered aliquot was spiked to GC instrument to measure conversions of alcohols **2a-j** (see Table 1 in the article). After 2-3 h, the evaporation of the organic solvent was noticed.

Figure 3.6. Reaction set-up without thermostatic control.

3.6.1.4. Scale-up of the laccase/TEMPO-mediated synthesis of dihalogenated ketones 2a,c,d in a biphasic system

To 5.2 mL of acetate buffer (50 mM, pH 4.5) in a 25 mL round bottom flask 12 mg of laccase from *Trametes versicolor* (163 U) and 100 mg of the corresponding alcohols **1a**, **1c**, or **1d** were added. Later, 10.4 mL of MTBE were transferred to the reaction vessel and 16 mg of TEMPO (20% mol) added to the reaction mixture. The flask was sealed with a rubber and the mixture vigorously shaken prior to the attachment of a balloon filled with oxygen (1 atm). Pressure was equilibrated placing an additional needle outlet in the rubber lid and the oxygen flow was set to gently purge the reaction mixture. The reaction was stirred at 20 °C for 24 h and the balloon was refilled with oxygen for the first 8 h of experiment (0.4±0.1 mL/s). The flask was closed with a stopper and the pressure equilibrated by a needle outlet. The reaction was ended by addition of EtOAc (3 x 5 mL). The organic fractions were combined and dried over Na_2SO_4. A small aliquot was used for GC analysis (>95% conversion). After filtration and solvent removal under reduced pressure, the crude was loaded on a silica column. Flash chromatography was performed using 10 % dichloromethane/hexanes as mobile phase and pure ketones **2a** (76% isolated yield), **2c** (81% isolated yield), and **2d** (80% isolated yield).

3.6.1.5. Selectivity in the laccase/TEMPO system to oxidize simultaneously two *sec*-alcohols

Laccase from *Trametes versicolor* (2.3 mg, 31.3 U) was dissolved in 1 mL of acetate buffer (50 mM, pH 4.5) in a microwave tube, followed by addition of 2 mL of MTBE (final concentration: 66% v/v), substrate **1a** (9.5 mg, 0.05 mmol), substrate **1i** or **1j** (0.05 mmol), and TEMPO (3.1 mg, 0.02 mmol). The tube was sealed and the reaction mixture vigorously shaken prior to the attachment of a balloon filled with oxygen (1 atm). Pressure was equilibrated placing an additional needle outlet in the rubber lid and the oxygen flow was set to gently purge the reaction mixture. The reaction mixture was left stirring at 20 ºC for 6 h and the balloon was refilled with oxygen during the reaction course (0.4±0.1 mL/s). After that time, the reactions were stopped by addition of EtOAc (2 x 2 mL). Organic layers were combined, dried over Na_2SO_4 and a filtered aliquot was spiked to GC instrument to measure conversions of **2a** and **2i** or **2j** (Scheme 3.7). After 2-3 h, the evaporation of the organic solvent was noticed.

3.6.1.6. One-pot two-step sequential reaction with the laccase/TEMPO system and *E. coli*/ADH-A for the deracemization of racemic alcohol 1a (Scheme 3.8)

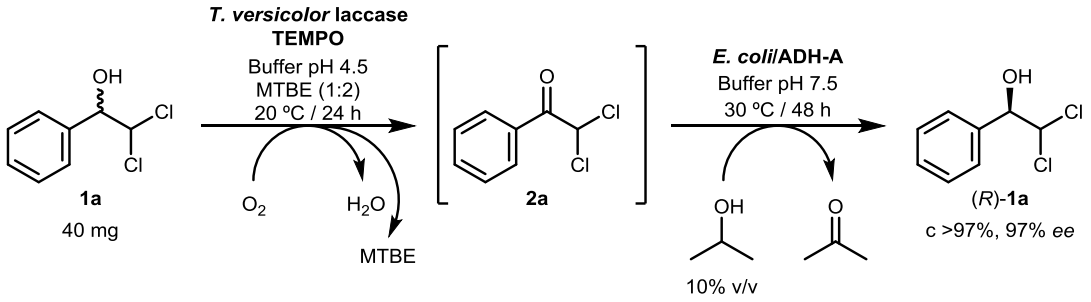

Scheme 3.8. One-pot two-step protocol to deracemize alcohol **1a** *via* oxidation with the laccase/TEMPO system plus reduction with an alcohol dehydrogenase and 2-propanol.

To 2 mL of acetate buffer (50 mM, pH 4.5) in a microwave tube, laccase from *Trametes versicolor* (4.6 mg, 62.6 U) and 40 mg of alcohol **1a** (0.2 mmol) were added. Later, 4 mL of MTBE (final concentration: 66% v/v) were transferred to the reaction vessel and 6.2 mg of TEMPO were added to the reaction mixture (0.04 mmol). The tube was sealed and the reaction mixture vigorously shaken prior to the attachment of a balloon filled with oxygen (1 atm). The flask was closed with a stopper and the pressure was equilibrated by a needle outlet. The reaction was stirred at 20 °C for 24 h and the balloon was refilled with oxygen during the first 8 h of the experiment (0.4±0.1 mL/s). Then, an aliquot of 50 µL was taken for routine conversion analysis by GC (97%) and the pH was readjusted to 7.5 with 2 mL of Tris base solution in water (300 mM) and a few drops of HCl (2 M). Subsequently, 10% v/v of isopropanol (440 µL), 100 mg of lyophilized *E. coli*/ADH-A cells as well as NAD^+ (final concentration: 1 mM), were added to the reaction mixture and left at 30°C for 48 h shaking at 250 rpm. After that time, the reaction mixture was centrifuged at 5000 rpm for 5 min and the supernatant was collected. The pellet was washed with EtOAc (3 x 5 mL) and the reaction products present in the supernatant were also extracted with EtOAc (4 x 5 mL) and added to the previous organic fraction. Na_2SO_4 was added, filtered and an aliquot of the organic extract was spiked to GC analysis to assess conversion (94.5%) and *ee* (97%). After solvent removal under reduced pressure, the crude was loaded on a silica column. Flash chromatography was performed using 40% dichloromethane/hexanes as mobile phase

and enantiopure alcohol (*R*)-**1a** was obtained as a white solid (isolated yield: 20 mg, 53%, *ee* 97%).

3.6.2. Other chemical systems used to oxidize alcohol 1a (Figure 3.4)

Table 3.3. Other chemical methods employed to oxidize alcohol **1a**.

system	areas (%)[a]			
	1a	**2a**	**3a+4a**	**5a**
Laccase *T. versicolor*/4-OH-TEMPO	95	5	<3	<3
NaOCl/TEMPO	6	3	88	3
NaOCl/KBr/TEMPO	39	39	22	<3
$NaOCl_2$/NaOCl/TEMPO	90	<3	5	4
CuCl/TEMPO	>97	<3	<3	<3
$CuBr_2$/TEMPO	>97	<3	<3	<3
I_2/TEMPO	>97	<3	<3	<3
NaOCl	<3	<3	97	3
NaOCl/KBr	10	<3	45	45
$NaOCl_2$	>97	<3	<3	<3
Dess-Martin periodinane/H_2O	>97	<3	<3	<3
Dess-Martin periodinane/CH_2Cl_2	46	54	<3	<3

[a] Measured by NMR.

3.6.2.1. Laccase from *Trametes versicolor*/4-OH-TEMPO

To a microwave tube containing 1.8 mL of acetate buffer (50 mM, pH 4.5), were added **1a** (19.1 mg, 0.1 mmol) dissolved in 200 µL of acetonitrile (final concentration: 10% v/v), 4-OH-TEMPO (3.4 mg, 0.02 mmol) and laccase from *Trametes versicolor* (2.3 mg, 31.3 U). The tube was sealed and the mixture vigorously shaken prior to the attachment of a balloon that was filled with oxygen (1 atm). Pressure was equilibrated placing an additional needle outlet in the rubber lid and the oxygen flow was set to

gently purge the reaction mixture. The reaction mixture was left stirring at 30 ºC for 24 h and the balloon was refilled with oxygen during the first 8 h of reaction (0.4±0.1 mL/s). Then, the reaction was stopped by addition of EtOAc (2 x 2 mL). Organic layers were combined, dried over Na_2SO_4 and an aliquot was filtered before spiking to GC for conversion (see Table 3.3).

3.6.2.2. NaOCl/TEMPO system

This procedure was adapted from Anelli *et al.*[78b] In a round bottom flask, **1a** (40 mg, 0.2 mmol) was resuspended in water (5 mL), followed by addition of TEMPO (6.2 mg, 0.04 mmol) and 9 equiv. of NaOCl (1.16 mL of 10% solution). The reaction mixture was stirred at 0 ºC for 7 h. After that time, the crude was acidified with an aqueous HCl solution (1 M) and extracted with EtOAc (3 x 5 mL). Organic fractions were combined and dried over Na_2SO_4. Later the solvent was evaporated and the crude was dried under high vacuum for ^{1}H-NMR analysis (see Table 3.3).

3.6.2.3. NaOCl/KBr/TEMPO system

This procedure was adapted from Anelli *et al.*[78b] In a round bottom flask, **1a** (40 mg, 0.2 mmol) was dissolved in 0.42 mL of acetonitrile and 3.76 mL of phosphate buffer (50 mM, pH 7.5), followed by addition of TEMPO (6.2 mg, 0.04 mmol), 1 equiv. of NaOCl (0.123 mL of 10% solution), and KBr (4.8 mg, 0.04 mmol). The reaction mixture was stirred at room temperature for 24 h. After that time, the crude was acidified with an aqueous HCl solution (1 M) and extracted with EtOAc (3 x 5 mL). Organic fractions were combined and dried over Na_2SO_4. Later the solvent was evaporated and the crude was dried under high vacuum for ^{1}H-NMR analysis (see Table 3.3).

3.6.2.4. $NaOCl_2$/NaOCl/TEMPO system

This procedure was adapted from Zhao *et al.*[79] In a round bottom flask, **1a** (40 mg, 0.2 mmol) was dissolved in 0.4 mL of acetonitrile and 3.6 mL of phosphate buffer (100 mM, pH 7.5), followed by addition of TEMPO (6.2 mg, 0.04 mmol), 1.5 equiv. of $NaOCl_2$ (34 mg, 0.3 mmol) and NaOCl (25 µL of 10% solution, 0.04 mmol). The reaction mixture was stirred at room temperature for 24 h. After that time, the crude was acidified with an aqueous HCl solution (1 M) and extracted with EtOAc (3 x 5 mL). Organic fractions were combined and dried over Na_2SO_4. Later the solvent was

evaporated and the crude was dried under high vacuum for ^{1}H-NMR analysis (see Table 3.3).

3.6.2.5. CuCl/TEMPO system

This procedure was adapted from Semmelhack *et al*.[80] In a round bottom flask, **1a** (40 mg, 0.2 mmol) was dissolved in 1 mL of acetonitrile and 4 mL of water, followed by addition of TEMPO (6.2 mg, 0.04 mmol) and CuCl (4 mg, 0.04 mmol). The reaction mixture was stirred at room temperature for 24 h. After that time, the crude was acidified with an aqueous HCl solution (1 M) and extracted with EtOAc (3 x 5 mL). Organic fractions were combined and dried over Na_2SO_4. Later the solvent was evaporated and the crude was dried under high vacuum for ^{1}H-NMR analysis (see Table 3.3).

3.6.2.6. $CuBr_2$/TEMPO system

This procedure was adapted from Miyazawa and Endo.[150] In a round bottom flask, **1a** (40 mg, 0.2 mmol) was dissolved in 1 mL of acetonitrile and 4 mL of water, followed by addition of TEMPO (6.2 mg, 0.04 mmol) and $CuBr_2$ (9 mg, 0.04 mmol). The reaction mixture was stirred at room temperature for 24 h. After that time, the crude was acidified with an aqueous HCl solution (1 M) and extracted with EtOAc (3 x 5 mL). Organic fractions were combined and dried over Na_2SO_4. Later the solvent was evaporated and the crude was dried under high vacuum for ^{1}H-NMR analysis (see Table 3.3).

3.6.2.7. I_2/TEMPO system

This procedure was adapted from Miller and Hoerrner.[151] In a round bottom flask, **1a** (19 mg, 0.1 mmol) was resuspended in 2.5 mL of Tris-HCl buffer (50 mM, pH 7.5), followed by addition of TEMPO (3.1 mg, 0.02 mmol) and I_2 (38 mg, 0.15 mmol). The reaction mixture was stirred at 30 ºC for 24 h. After that time, the excess of iodine was quenched with a $Na_2S_2O_3$ solution (10% w/v) and the crude was extracted with EtOAc (3 x 5 mL). Organic fractions were combined and dried over Na_2SO_4. Later the solvent was evaporated and the crude was dried under high vacuum for ^{1}H-NMR analysis (see Table 3.3).

[150] T. Miyazawa, T. Endo, *J. Mol. Catal.* **1985**, *32*, 357-360.
[151] R. A. Miller, R. S. Hoerrner, *Org. Lett.* **2003**, *5*, 285-287.

3.6.2.8. NaOCl

In a round bottom flask, **1a** (40 mg, 0.2 mmol) was resuspended in water (5 mL), followed by addition of 9 equiv. of NaOCl (1.16 mL of 10% solution). The reaction mixture was stirred at 30 ºC for 24 h. After that time, the crude was acidified with an aqueous HCl solution (1 M) and extracted with EtOAc (3 x 5 mL). Organic fractions were combined and dried over Na_2SO_4. Later the solvent was evaporated and the crude was dried under high vacuum for ^{1}H-NMR analysis (see Table 3.3).

3.6.2.9. NaOCl/KBr system

In a round bottom flask, **1a** (40 mg, 0.2 mmol) was resuspended in 5 mL of water, followed by addition of 9 equiv. of NaOCl (1.16 mL of 10% solution) and KBr (4.8 mg, 0.04 mmol). The reaction mixture was stirred at 0 ºC for 7 h. After that time, the crude was acidified with an aqueous HCl solution (1 M) and extracted with EtOAc (3 x 5 mL). Organic fractions were combined and dried over Na_2SO_4. Later the solvent was evaporated and the crude was dried under high vacuum for ^{1}H-NMR analysis (see Table 3.3).

3.6.2.10. $NaOCl_2$

In a round bottom flask, **1a** (40 mg, 0.2 mmol) was resuspended in water (5 mL), followed by addition of 9 equiv. of $NaOCl_2$ (213 mg, 1.88 mmol). The reaction mixture was stirred at 0 ºC for 7 h. After that time, the crude was acidified with an aqueous HCl solution (1 M) and extracted with EtOAc (3 x 5 mL). Organic fractions were combined and dried over Na_2SO_4. Later the solvent was evaporated and the crude was dried under high vacuum for ^{1}H-NMR analysis (see Table 3.3).

3.6.2.11. Dess-Martin periodinane in aqueous media

In a round bottom flask, **1a** (50 mg, 0.26 mmol) was resuspended in 5 mL of H_2O, followed by addition of the Dess-Martin periodinane reagent (133 mg, 0.314 mmol). The reaction mixture was stirred at 30 ºC for 24 h. After that time, the excess of the reagent was quenched with $Na_2S_2O_3$ (10% w/v solution), and then 10 mL of $NaHCO_3$ (saturated solution) was added and finally was extracted with CH_2Cl_2 (3 x 5 mL). Organic phases were combined, dried over Na_2SO_4 and the solvent was evaporated. Finally, the crude was dried under high vacuum prior ^{1}H-NMR analysis (see Table 3.3).

3.6.2.12. Dess-Martin periodinane in CH_2Cl_2

This procedure was adapted from Pace *et al.*[149] In a round bottom flask, **1a** (50 mg, 0.26 mmol) was dissolved in 5 mL of CH_2Cl_2, followed by addition of the Dess-Martin periodinane reagent (133 mg, 0.314 mmol). The reaction mixture was stirred at room temperature for 1.5 h. After that time, 10 mL of Et_2O, 2.5 mL of a 1% w/v solution of $Na_2S_2O_3$ and 10 mL of $NaHCO_3$ (saturated solution) were added and left stirring for 15 min. The organic phase was separated and dried over Na_2SO_4. Later the solvent was evaporated and the crude was dried under high vacuum prior ^{1}H-NMR analysis (see Table 3.3).

3.6.3. *Ab initio* calculations

To emphasize the ability of the laccase/TEMPO system to oxidize secondary alcohol substrates with varying redox strength, we evaluated the relative thermodynamic stability of the halogenated alcohol/ketone pairs **1a**,**i**,**j**/**2a**,**i**,**j** with respect to the acetone/2-propanol pair by computing the Gibbs free energy change in aqueous solution ($\Delta_r G$) for the isodesmic reactions shown in Table 3.4.

Table 3.4. Total number of conformers (N_{conf}) of the alcohol/ketone pairs examined computationally and Boltzmann-averaged free energies (kcal/mol) both in solution ($\Delta_r G$) and in the gas-phase ($\Delta_r G_{gas}$) for the redox equilibrium with respect to 2-propanol/acetone. The corresponding changes in the free energy over the most stable conformers in solution ($\Delta_r G_{min}$) are also indicated.

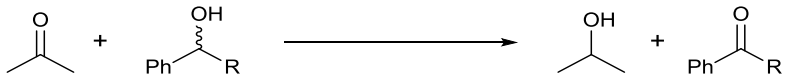

1a,**i**,**j** **2a**,**i**,**j**

alcohol/ketone	R	N_{conf}	$\Delta_r G$	$\Delta_r G_{gas}$	$\Delta_r G_{min}$	Reference
A	$CHCl_2$	9/1	+7.35	+7.61	+6.92	this work
I	CH_2Cl	6/2	+4.86	+4.98	+4.29	95
J	CH_3	2/1	+0.61	+0.20	+0.36	95

The computed values, which could be correlated with the standard reduction potential of the corresponding alcohol/ketone pairs, showed clearly that the

dichlorinated alcohol **1a** was a weaker reducing agent compared to the mono- (**1i**, by 2.5 kcal/mol) or unsubstituted (**1j**, by 6.7 kcal/mol) derivatives. Since **1a** showed a larger conversion value (95%) than those of **1i**,**j** (62-78%), it turned out that the differences in the intrinsic redox strength of **1a**,**i**,**j** did not affect their oxidation, highlighting thus the flexibility of the laccase/TEMPO system. Moreover, the lack of thermodynamic effects due to the alcohol substituents in the experimentally observed conversions, pointed out that these values for substrates **1i** or **1j** could be further improved by tuning the reaction conditions.

We applied the same computational protocol that has been used in our previous work[95] to calculate the Gibbs free energy of reactants and products in aqueous solution. Thus, preliminary conformational search calculations were carried out by means of gas-phase Molecular Dynamics simulations using the generalized AMBER force field (GAFF) and the *Sander* program.[152] The resulting conformers were then optimized at the HF/cc-pVDZ level and characterized by analytical frequency calculations using the *Gaussian03* program.[153] Subsequently, all the structures were reoptimized at the MP2/cc-pVTZ level of theory. MP2 energies were extrapolated to the complete basis set limit (CBS) by means of single-point MP2/cc-pVXZ (X=Q,5) calculations and using the Schwartz extrapolation scheme. Solvation free energies were estimated from single-point COSMO-MP2/cc-pVTZ calculations in the framework of the conductor-like screening model representing continuum solvent effects.[154] All the MP2 and COSMO calculations were performed with the TURBOMOLE program[155] package. Further details of the computational protocol can be found elsewhere.[95]

---

[152] D. A. Case, T. A. Darden, T. E. Cheatham, III, C. L. Simmerling, J. Wang, R. E. Duke, R. Luo, M. Crowley, R. C. Walker, W. Zhang, K. M. Merz, B. Wang, S. Hayik, A. Roitberg, G. Seabra, I. Kolossváry, K. F. Wong, F. Paesani, J. Vanicek, X. Wu, S. R. Brozell, T. Steinbrecher, H. Gohlke, L. Yang, C. Tan, J. Mongan, V. Hornak, G. Cui, D. H. Mathews, M. G. Seetin, C. Sagui, V. Babin, P. A. Kollman, AMBER 10, University of California, San Francisco, **2008**.

[153] Gaussian 03, Revision C.02, M. J. Frisch, G. W. Trucks, H. B. Schlegel, G. E. Scuseria, M. A. Robb, J. R. Cheeseman, J. A. Montgomery, Jr., T. Vreven, K. N. Kudin, J. C. Burant, J. M. Millam, S. S. Iyengar, J. Tomasi, V. Barone, B. Mennucci, M. Cossi, G. Scalmani, N. Rega, G. A. Petersson, H. Nakatsuji, M. Hada, M. Ehara, K. Toyota, R. Fukuda, J. Hasegawa, M. Ishida, T. Nakajima, Y. Honda, O. Kitao, H. Nakai, M. Klene, X. Li, J. E. Knox, H. P. Hratchian, J. B. Cross, V. Bakken, C. Adamo, J. Jaramillo, R. Gomperts, R. E. Stratmann, O. Yazyev, A. J. Austin, R. Cammi, C. Pomelli, J. W. Ochterski, P. Y. Ayala, K. Morokuma, G. A. Voth, P. Salvador, J. J. Dannenberg, V. G. Zakrzewski, S. Dapprich, A. D. Daniels, M. C. Strain, O. Farkas, D. K. Malick, A. D. Rabuck, K. Raghavachari, J. B. Foresman, J. V. Ortiz, Q. Cui, A. G. Baboul, S. Clifford, J. Cioslowski, B. B. Stefanov, G. Liu, A. Liashenko, P. Piskorz, I. Komaromi, R. L. Martin, D. J. Fox, T. Keith, M. A. Al-Laham, C. Y. Peng, A. Nanayakkara, M. Challacombe, P. M. W. Gill, B. Johnson, W. Chen, M. W. Wong, C. Gonzalez, J. A. Pople, Gaussian, Inc., Wallingford CT, **2004**.

[154] A. Klamt, G. Schüürmann, *J. Chem. Soc., Perkin Trans. 2* **1993**, *5*, 799-805.

[155] R. Ahlrichs, M. Bär, M. Häser, H. Horn, C. Kölmel, *Chem. Phys. Lett.* **1989**, *162*, 165-169.

3.6.4. Environmental assessment using EATOS

E-factor calculations (Figure 3.7) were performed using the EATOS (v. 1.1) software tool,[156] while solvent demand was calculated using Microsoft Excel (determining the solvent use of each protocol to obtain 1 g of **2a**). All reactions were treated as proceeding to the corresponding conversion, hence all losses in yield are accounted for as 'unknown by-products'.

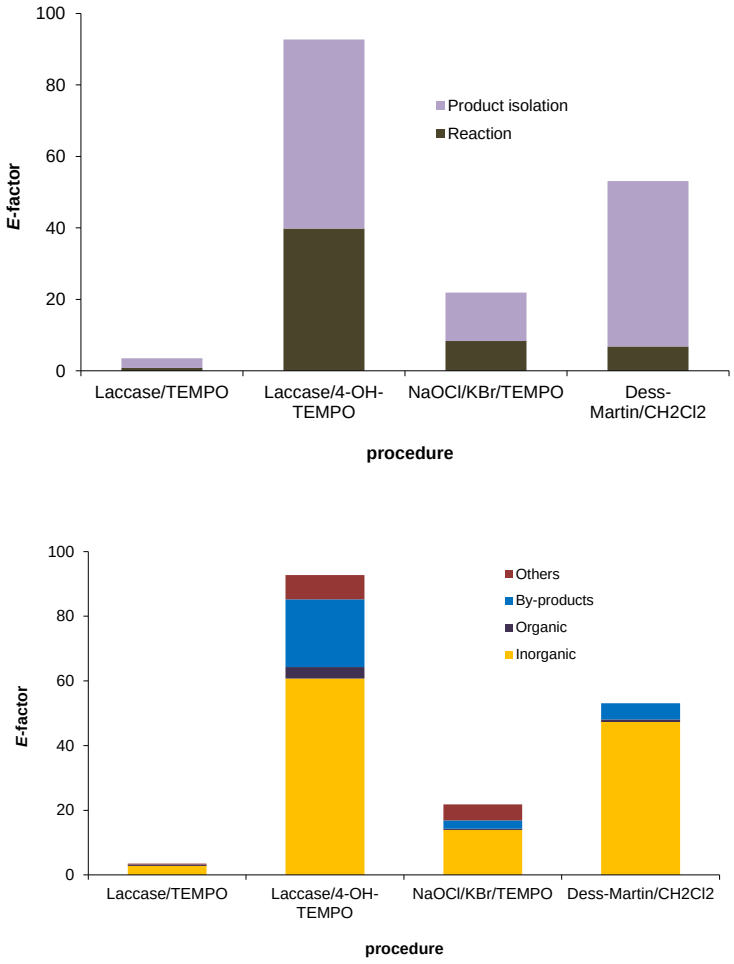

Figure 3.7. Contribution to E-factor (excluding solvents) for each procedure to synthesize ketone **2a**.

[156] (a) M. Eissen, J. O. Metzger, *Chem. Eur. J.* **2002**, *8*, 3580-3585; (b) EATOS: Environmental Assessment Tool for Organic Syntheses, http://www.metzger.chemie.uni-oldenburg.de/eatos/english.htm.

Publication

Green Chemistry

COMMUNICATION

Laccase/TEMPO-mediated system for the thermodynamically disfavored oxidation of 2,2-dihalo-1-phenylethanol derivatives†

Cite this: *Green Chem.*, 2014, **16**, 2448

Received 14th January 2014,
Accepted 19th February 2014

DOI: 10.1039/c4gc00066h

www.rsc.org/greenchem

Kinga Kędziora, Alba Díaz-Rodríguez, Iván Lavandera, Vicente Gotor-Fernández and Vicente Gotor*

An efficient methodology to oxidize β,β-dihalogenated secondary alcohols employing oxygen was achieved in a biphasic medium using the laccase from *Trametes versicolor*/TEMPO pair, providing the corresponding ketones in a clean fashion under very mild conditions. Moreover, a chemoenzymatic protocol has been applied successfully to deracemize 2,2-dichloro-1-phenylethanol combining this oxidation with an alcohol dehydrogenase-catalyzed bioreduction.

Oxidation of alcohols into the corresponding carbonylic compounds is one of the fundamental reactions in organic chemistry. Traditionally these transformations comprised the use of hazardous metal-based reagents in stoichiometric amounts, however catalytic methodologies employing oxygen (or air) as a mild oxidant in aqueous media are being recognized for large scale applications, and therefore they are currently emerging as potent competitors.[1] From an economic and environmental point of view, these strategies are highly appealing since they produce water as the only by-product.

In this context, biological catalysts are gaining more relevance applied to oxidative processes, especially due to the mild conditions and high selectivities displayed in these transformations.[2] Among the different types of enzymes implicated in these reactions, oxidases have appeared as an interesting class since they use molecular oxygen as the electron acceptor.[3] In particular laccases are multicopper biocatalysts present in many fungi, plants and bacteria, and are responsible for the reduction of O_2 into H_2O at the expense of the substrate oxidation.[3a,4] Additionally, they are accessible and cheap compared to other reported metal complexes. Apart from that, laccases work efficiently in water as the natural medium, although they can also accept organic co-solvents,[5] which can be highly desirable when dealing with hydrophobic derivatives. Phenolic compounds are their natural substrates, but laccases have shown to be also effective towards primary alcohols or amines making use of, *e.g.* ABTS, benzotriazole, or syringaldehyde, among others.[6] One of the most employed is (2,2,6,6-tetramethylpiperidin-1-yl)oxy (TEMPO) due to its accessibility and high compatibility with this class of enzyme. Recently, the laccase/TEMPO catalytic system has been reported as a potent alternative to oxidize chemoselectively benzylic and primary alcohols over secondary ones.[7]

Especially challenging is the oxidation of alcohols substituted at the β-position with electron-withdrawing groups (EWG), *e.g.* halohydrins. To date, Dess–Martin periodinane,[8] ruthenium[9] and iridium-based[10] catalysts, Swern,[11] tetrapropylammonium perruthenate (TPAP),[11,12] and Jones' reagent[13] have been reported for the oxidation of this type of substrates. Owing to their high reactivity, α,α-dihalogenated ketones are versatile building blocks for the synthesis of, among others, mandelic acid,[14] oxazines,[15] triazines,[16] α,β-unsaturated ketones,[17] and triazole derivatives.[18] In the course of our investigations on biocatalyzed redox processes, it was observed that the oxidation of halohydrins was hardly feasible under alcohol dehydrogenase (ADH)-catalyzed hydrogen transfer conditions.[19] Following this study and based on our previous experience with the selective oxidation of alcohols using *Trametes versicolor* laccase and TEMPO,[7a] we have explored this catalytic system in the disfavored oxidation of secondary alcohols **1a–i**.

Since the laccase/mediator system is able to oxidize primary and secondary benzylic alcohols,[7b,d,20] we reasoned that laccase/TEMPO could also lead to carbonylic compounds bearing electron-withdrawing groups at the α-position under aerobic conditions. Therefore, several 2,2-dihalogenated 1-phenylethanol derivatives (**1a–h**) and 2-chloro-1-phenylethanol **1i** (Scheme 1) were synthesized, and these compounds were tested as possible substrates.

In a first set of experiments, the influence of the oxygenation was investigated.[21] Thus, the oxidation of 2,2-dichloro-1-phenylethanol (**1a**, 0.1 mmol, 50 mM) as a model substrate

Departamento de Química Orgánica e Inorgánica, Instituto Universitario de Biotecnología de Asturias, Universidad de Oviedo, C/Julián Clavería 8, 33006 Oviedo, Spain. E-mail: vgs@uniovi.es

†Electronic supplementary information (ESI) available: Experimental procedures, *ab initio* and *E*-factor calculations, substrate characterization, and analytical data are described. See DOI: 10.1039/c4gc00066h

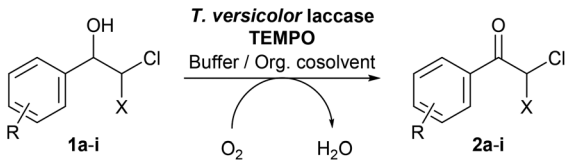

a, R= H, X= Cl; **b**, R= *o*-Cl, X= Cl; **c**, R= *m*-Cl, X= Cl
d, R= *p*-Cl, X= Cl; **e**, R= *m*-OMe, X= Cl; **f**, R= *m*-NO_2, X= Cl
g, R= H, X= Br; **h**, R= H, X= F; **i**, R= H, X= H

Scheme 1 General methodology to synthesize α,α-dihalogenated acetophenone derivatives **2a–h** and 2-chloroacetophenone (**2i**) through oxidation reactions with the laccase/TEMPO system.

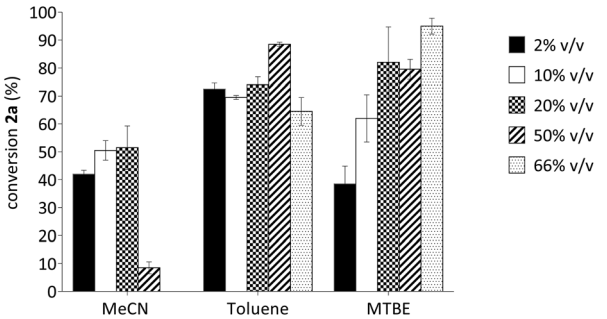

Fig. 1 Effect of the organic co-solvent concentration in the *T. versicolor* laccase/TEMPO (20 mol%) system to oxidize alcohol **1a** (50 mM) into **2a**, bubbling oxygen in a 50 mM NaOAc buffer pH 4.5 at 20 °C (toluene and MTBE) or 30 °C (MeCN) after 24 h.

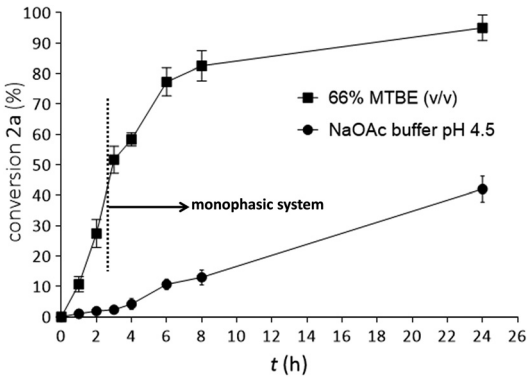

Fig. 2 Reaction course of the *T. versicolor* laccase/TEMPO (20 mol%) system to oxidize alcohol **1a** (50 mM) into **2a**, bubbling oxygen in a 50 mM NaOAc buffer pH 4.5 at 20 °C in the presence of MTBE (66% v/v). After 2–3 h, the disappearance of the organic solvent was observed. For comparison, the reaction in plain buffer was also studied.

was performed in a 50 mM sodium acetate (NaOAc) buffer pH 4.5 at 30 °C and 20 mol% of TEMPO under two different conditions: (a) opening the reaction mixture to ambient air; and (b) bubbling oxygen in the vessel with a balloon. Remarkably, while for the first case a conversion of 33% was attained after 24 h, the second protocol led to 53% of ketone **2a**. The reactions were carried out using 10% v/v of acetonitrile (MeCN) as a result of the low solubility of **1a**. Although the conversions still were not quantitative, we observed that this method was able to afford smoothly the final compound, avoiding the formation of undesired by-products. Therefore, the reaction conditions of bubbling oxygen were chosen for further optimization. Other parameters such as temperature (20–40 °C), TEMPO equivalents (20–40 mol%), or pH (3.5–6.0) were also examined, without finding significant improvements (see ESI†).

Next, we decided to study the effect of the organic co-solvent by adding water miscible and non-miscible co-solvents, giving rise to mono- or biphasic systems. The addition of organic co-solvents can improve the solubility of hydrophobic substrates and the stability of this catalytic method, as observed for similar transformations.[5,22] To minimize mass transfer issues, a gentle magnetic stirring was performed in all cases. Thus, dimethylsulfoxide (DMSO) and MeCN were studied as additives in monophasic mixtures while dichloromethane, toluene and methyl *tert*-butyl ether (MTBE) were added to form biphasic systems (see ESI†). Among them, MeCN, toluene and MTBE afforded the best oxidation conversions (56–70%), so further studies were developed with these organic solvents.

Hence, the effect of the concentration of these organic co-solvents was studied with respect to the NaOAc buffer (2–66% v/v, Fig. 1). Due to the low boiling point of MTBE, the reactions with this solvent were carried out at 20 °C, and therefore, this was also the temperature of choice for the other non-miscible solvent (toluene), while the oxidations with water-miscible MeCN were performed at 30 °C. In this case, it remained clear that percentages higher than 20% v/v inhibited the laccase/TEMPO system while non-miscible solvents could be employed in larger amounts. Especially with MTBE, excellent conversions were achieved after 24 h (95%), showing that the addition of this organic co-solvent displayed a positive influence on the oxidation of **1a**. In addition, following the guidelines of greener alternatives for chlorinated or diethyl ether solvents, MTBE appeared as one of the best options for an immiscible organic co-solvent.[23] We also studied the use of a lower amount of TEMPO equivalents (5–10 mol%), but conversions were incomplete (51–85%).

The continuous oxygen bubbling process evaporated the organic solvent after a short period of time (2–3 h). Overall, it can be considered that this oxidation was accomplished at the end in an aqueous medium. To investigate the possible effect of MTBE in the reaction, we followed the oxidation of **1a** with time (Fig. 2), with and without the presence of MTBE. While a conversion of nearly 50% into **2a** was achieved in the first 3 h for the biphasic system, less than 10% conversion was detected for the solely aqueous system.[24] The positive effect of MTBE seems to be more related to an improvement of the substrate solubility than to the TEMPO stability, as conversions in plain buffer were continuously increasing at comparable rates after 4 h. Similar positive properties have already been described for other water–organic media employing a laccase with a chemical mediator.[22]

Table 1 Oxidation of secondary alcohols **1a–j** using the laccase/TEMPO system[a]

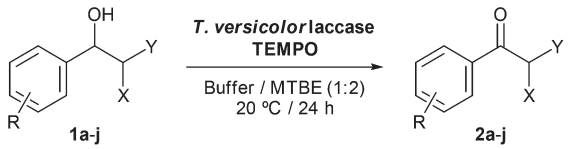

Entry	Alcohol	R	X	Y	**2a–j**[b] (%)
1	**1a**	H	Cl	Cl	95 ± 2.8
2	**1b**	*o*-Cl	Cl	Cl	4 ± 1.4
3	**1c**	*m*-Cl	Cl	Cl	78 ± 3.5
4	**1d**	*p*-Cl	Cl	Cl	91 ± 2.1
5	**1e**	*m*-OMe	Cl	Cl	82 ± 4.2
6	**1f**	*m*-NO_2	Cl	Cl	95 ± 4.2
7	**1g**	H	Cl	Br	89 ± 5.7
8	**1h**	H	Cl	F	75 ± 2.1
9	**1i**	H	Cl	H	62 ± 3.2
10	**1j**	H	H	H	78 ± 3.5

[a] Reaction conditions: alcohol **1a–j** (0.1 mmol), *T. versicolor* laccase (31 U) and TEMPO (20 mol%) in a 50 mM NaOAc buffer pH 4.5 and MTBE (66% v/v) bubbling oxygen at 20 °C for 24 h. [b] Conversion values measured by GC.

Having found appropriate conditions to oxidize alcohol **1a** (Table 1, entry 1), the scope of this transformation was expanded to other dihalogenated derivatives **1b–h**. The system efficiency depended on the position of the phenyl ring substitution, observing high to excellent conversions for *meta*- or *para*-substituted compounds, while a very low formation of ketone **2b** was found for the *ortho*-derived alcohol **1b** (compare entries 2 to 4). On the other side, alcohols with differing electronic properties such as chlorine, methoxy or nitro were oxidized (entries 3–6). Additionally, substrates with other halogen atoms at the α-position such as bromine (entry 7) or fluorine (entry 8) also afforded the halogenated ketones with conversions higher than 75%. It is remarkable that the desired carbonylic compounds were formed as the sole products, without the detection of other derivatives in any case. When using the alcohol **1a**, the substrate concentration could be increased up to 200 mM obtaining a conversion of 93% after 24 h. This is in line with other reports that have demonstrated the performance of laccases at high substrate concentrations.[7b,25] Satisfyingly, some of these oxidative transformations could be easily performed at the 100 mg scale, isolating the corresponding ketones in very high yields (76–81%, see ESI† for more details).

Then, chlorohydrin **1i** was also tested as plausible substrate (entry 9). In this case, we observed a 62% conversion to α-chloro ketone **2i** after 24 h under these oxidative conditions. This result is very important due to the difficulty to achieve this oxidation by other chemical methods, and also because of the versatility of these compounds as intermediates of several high added-value derivatives. Furthermore, when a non-halogenated alcohol such as 1-phenylethanol (**1j**) was used, a similar conversion compared to the dihalogenated counterparts was achieved (78%, entry 10), showing that this methodology can work with different types of secondary alcohols.[26]

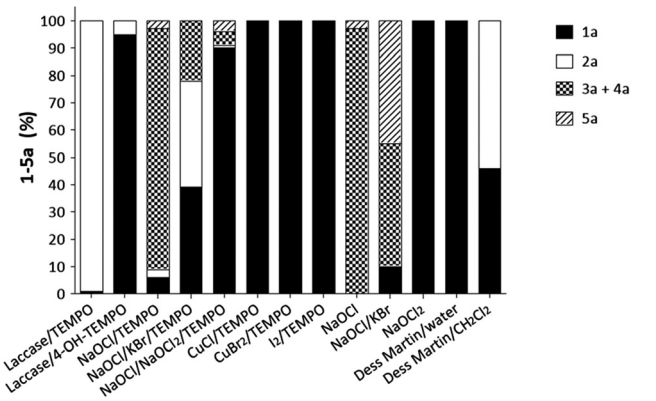

Fig. 3 Oxidation of alcohol **1a** into **2a** employing different reaction conditions. In some cases, benzaldehyde (**3a**), benzoic acid (**4a**), and/or mandelic acid (**5a**) were obtained as by-products.

To emphasize the ability of the laccase/TEMPO system to oxidize secondary alcohols with varying redox strength, we evaluated the relative thermodynamic stability of the halogenated alcohol/ketone pairs **1a**, **i**, **j**/**2a**, **i**, **j** with respect to the acetone/2-propanol pair by computing the Gibbs free energy change in aqueous solution ($\Delta_r G$, see ESI† for more details).[19a] The computed $\Delta_r G$ energies in kcal mol^{-1} were +7.33 (**1a**), +4.86 (**1i**), and +0.61 (**1j**), showing clearly that the dichlorinated alcohol **1a** was a weaker reducing agent compared to the mono- (**1i**, by 2.5 kcal mol^{-1}) or unsubstituted (**1j**, by 6.7 kcal mol^{-1}) derivatives. Since **1a** showed the largest conversion value, it turned out that the differences in the intrinsic redox strength of **1a**, **i**, **j** did not affect their oxidation, which is in agreement with the accepted ionic mechanism of oxidation mediated by TEMPO.[27] These results highlight the flexibility of our laccase/TEMPO system.

To demonstrate the mildness and selectivity of this system to oxidize these substrates, different chemical oxidative methods were assessed for the oxidation of **1a** (Fig. 3). Thus, the laccase was combined with 4-hydroxy-TEMPO (4-OH-TEMPO), but in this case just 5% conversion was achieved after 24 h. Several mixtures of oxidant(s) and TEMPO were tried in aqueous media such as NaOCl (9 equiv.),[28] NaOCl (1 equiv.)/KBr (0.2 equiv.),[28] $NaOCl_2$ (1.5 equiv.)/NaOCl (0.2 equiv.),[29] CuCl (0.2 equiv.),[30] $CuBr_2$ (0.2 equiv.),[31] or iodine (1.5 equiv.),[32] but negligible or very low conversions were attained. Just when using a stoichiometric amount or an excess of NaOCl, a complex mixture of products formed by benzaldehyde (**3a**), benzoic acid (**4a**) and mandelic acid (**5a**) was detected. This observation correlates with previous reports describing the synthesis of mandelic acid from dihalogenated ketones in an aqueous basic medium.[33]

The application of NaOCl or NaOCl/KBr led again to a mixture of compounds **3–5a**, while $NaOCl_2$ or Dess–Martin periodinane in water did not afford any conversion, recovering the starting material. Only the employment of Dess–Martin periodinane in dichloromethane,[8] allowed the synthesis of ketone **2a** at 54% as the sole product at room temperature

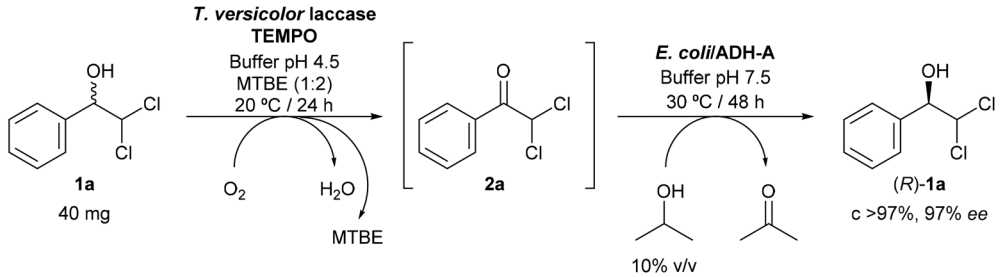

Scheme 2 One-pot two-step protocol to deracemize alcohol **1a** *via* oxidation with the laccase/TEMPO system plus reduction with an alcohol dehydrogenase and 2-propanol.

after 1.5 h. To show the environmental benefits of this system compared to the others, we have performed a simplified environmental impact analysis making use of the *E*-factor concept.[34] Although it provides a rough estimation of the environmental impact, this value assesses the sustainability of a process.[35] Thus, we compared[36] our laccase/TEMPO system with the other three (laccase/4-OH-TEMPO, NaOCl/KBr/TEMPO and Dess–Martin in dichloromethane) which afforded a measurable amount of ketone **2a**, obtaining an *E*-factor of 3.5 for the laccase/TEMPO process (excluding solvents) and values higher than 21 for the others (see ESI† for details). Also, the solvent demand in our method (330 mL g^{-1} product) was much lower in comparison with the other strategies. As a result, these data demonstrate the favorable ecological impact of the laccase/TEMPO pair.

Taken together, we have shown that this methodology, making use of a laccase/TEMPO system in a biphasic medium with oxygen as final electron acceptor, is a practical method to get access to α- or α,α-dihalogenated ketones *via* oxidation of the corresponding (di)halohydrins, which in other reaction conditions cannot be obtained selectively.

Encouraged by these results and as an interesting application of this methodology, we envisaged the deracemization of alcohol **1a** through a one-pot two-step chemoenzymatic procedure. To date, the only example for the deracemization of chlorohydrins has been reported by Kroutil and co-workers,[10a] combining an alcohol dehydrogenase (for the reduction) with an iridium catalyst (for the oxidation) in a one-pot concurrent system. Unfortunately, the *ee* values did not exceed 40% due to undesired interference of both processes. Herein, we propose an alternative strategy starting from the racemic alcohol **1a**. In a first step we achieve the complete oxidation into ketone **2a** with the laccase/TEMPO pair. Subsequently, the addition of a selective ADH leads to enantioenriched alcohol **1a** (Scheme 2).

Hence, this system was successfully applied to deracemize 40 mg of racemic alcohol **2a**. After oxidation mediated by *T. versicolor* laccase and TEMPO under the previously optimized conditions, the buffer pH was adjusted to 7.5 by adding tris(hydroxymethyl)aminomethane (Tris) and a few drops of HCl (thus inactivating the laccase). Then, alcohol dehydrogenase from *Rhodococcus ruber* overexpressed in *Escherichia coli* (*E. coli*/ADH-A)[37] and 2-propanol as hydrogen donor (10% v/v) were successively added. After 48 h at 30 °C, the enantioenriched alcohol (*R*)-**1a** was obtained in total conversion with 97% *ee*. This first example opens the door to sustainable chemoenzymatic deracemization protocols applied to other β-substituted alcohols that under other chemical conditions cannot be obtained easily.

Conclusions

In summary, we have shown here an efficient and green method for the selective oxidation of secondary (di)halohydrins into the corresponding halogenated ketones using the laccase from *Trametes versicolor* and TEMPO pair. Although this process is thermodynamically impeded, the use of this system under aerobic conditions in a biphasic media could provide exclusively the corresponding carbonylic compounds with very high conversions in a clean fashion. This practical method represents a potent alternative to other known oxidative methods, which were not able to oxidize these substrates or afforded undesired by-products. Moreover, coupled with a second enzymatic bioreduction, deracemization of a secondary dihalogenated alcohol in a one-pot two-step protocol was feasible, obtaining the enantioenriched (*R*)-alcohol in a very mild and elegant fashion.

Acknowledgements

Financial support from the Spanish Ministerio de Ciencia e Innovación (MICINN-12-CTQ2011-24237), the Principado de Asturias (SV-PA-13-ECOEMP-42 and SV-PA-13-ECOEMP-43) and the Universidad de Oviedo (UNOV-13-EMERG-01 and UNOV-13-EMERG-07) is gratefully acknowledged. I. L. acknowledges MICINN for his research contract under the Ramón y Cajal Program. We thank Professor Dimas Suárez (University of Oviedo) for *ab initio* calculations and helpful discussions.

Notes and references

1 (*a*) A. Baiker and T. Mallat, *Catal. Sci. Technol.*, 2013, **3**, 267; (*b*) C. Parmeggiani and F. Cardona, *Green Chem.*, 2012, **14**, 547–564; (*c*) I. W. C. E. Arends and R. A. Sheldon, *Modern*

Oxidation Methods, ed. J.-E. Bäckvall, Wiley-VCH, Weinheim, 2nd edn, 2010, pp. 147–185.
2 *Modern Biooxidation: Enzymes, Reactions and Applications*, ed. R. D. Schmid and V. B. Urlacher, Wiley-VCH, Weinheim, 2007.
3 (*a*) *Redox Biocatalysis: Fundamentals and Applications*, ed. D. Gamenara, G. A. Seoane, P. Saenz-Méndez and P. Domínguez de María, John Wiley & Sons, Hoboken, 2013; (*b*) F. Hollmann, K. Bühler and B. Bühler, in *Enzyme Catalysis in Organic Synthesis*, ed. K. Drauz, H. Gröger and O. May, Wiley-VCH, Weinheim, 2012, pp. 1325–1438.
4 (*a*) A. Piscitelli, A. Amore and V. Faraco, *Curr. Org. Chem.*, 2012, **16**, 2508–2524; (*b*) P. Giardina, V. Faraco, C. Pezzella, A. Piscitelli, S. Vanhulle and G. Sannia, *Cell. Mol. Life Sci.*, 2009, **67**, 369–385; (*c*) S. Witayakran and A. J. Ragauskas, *Adv. Synth. Catal.*, 2009, **351**, 1187–1209; (*d*) S. Riva, *Trends Biotechnol.*, 2006, **24**, 219–226; (*e*) S. G. Burton, *Curr. Org. Chem.*, 2003, **7**, 1317–1331; (*f*) H. Claus, *Arch. Microbiol.*, 2003, **179**, 145–150; (*g*) E. I. Solomon, U. M. Sundaram and T. E. Machonkin, *Chem. Rev.*, 1996, **96**, 2563–2605.
5 (*a*) N. A. Mohidem and H. B. Mat, *Bioresour. Technol.*, 2012, **114**, 472–477; (*b*) I. Matijosyte, I. W. C. E. Arends, S. de Vries and R. A. Sheldon, *J. Mol. Catal. B: Enzym.*, 2010, **62**, 142–148; (*c*) S. Ncanana, L. Baratto, L. Roncaglia, S. Riva and S. G. Burton, *Adv. Synth. Catal.*, 2007, **349**, 1507–1513; (*d*) M. Zumárraga, T. Bulter, S. Shleev, J. Polaina, A. Martínez-Arias, F. J. Plou, A. Ballesteros and M. Alcalde, *Chem. Biol.*, 2007, **14**, 1052–1064; (*e*) A. Intra, S. Nicotra, S. Riva and B. Danieli, *Adv. Synth. Catal.*, 2005, **347**, 973–977; (*f*) F. d'Acunzo, A. M. Barreca and C. Galli, *J. Mol. Catal. B: Enzym.*, 2004, **31**, 25–30; (*g*) J. Rodakiewicz-Nowak, S. M. Kasture, B. Dudek and J. Haber, *J. Mol. Catal. B: Enzym.*, 2000, **11**, 1–11.
6 See, for instance: (*a*) P. Könst, S. Kara, S. Kochius, D. Holtmann, I. W. C. E. Arends, R. Ludwig and F. Hollmann, *ChemCatChem*, 2013, **5**, 3027–3032; (*b*) T. Kudanga, G. S. Nyanhongo, G. M. Guebitz and S. Burton, *Enzyme Microb. Technol.*, 2011, **48**, 195–208; (*c*) O. V. Morozova, G. P. Shumakovich, S. V. Shleev and Y. I. Yaropolov, *Appl. Biochem. Microbiol.*, 2007, **43**, 523–535; (*d*) A. Wells, M. Teria and T. Eve, *Biochem. Soc. Trans.*, 2006, **34**, 304–308; (*e*) M. Fabbrini, C. Galli and P. Gentili, *J. Mol. Catal. B: Enzym.*, 2002, **16**, 231–240.
7 (*a*) A. Díaz-Rodríguez, I. Lavandera, S. Kanbak-Aksu, R. A. Sheldon, V. Gotor and V. Gotor-Fernández, *Adv. Synth. Catal.*, 2012, **354**, 3405–3408; (*b*) I. W. C. E. Arends, Y.-X. Li, R. Ausan and R. A. Sheldon, *Tetrahedron*, 2006, **62**, 6659–6665; (*c*) M. Marzorati, B. Danieli, D. Haltrich and S. Riva, *Green Chem.*, 2005, **7**, 310–315; (*d*) M. Fabbrini, C. Galli, P. Gentili and D. Macchitella, *Tetrahedron Lett.*, 2001, **42**, 7551–7553.
8 (*a*) V. Pace and W. Holzer, *Tetrahedron Lett.*, 2012, **53**, 5106–5109; (*b*) V. Pace, A. Cortés Cabrera, M. Fernández, J. V. Sinisterra and A. R. Alcántara, *Synthesis*, 2010, 3545–3555.
9 (*a*) A. Träff, K. Bogár, M. Warner and J.-E. Bäckvall, *Org. Lett.*, 2008, **10**, 4807–4810; (*b*) B. Martín-Matute, M. Edin, K. Bogár, F. B. Kaynak and J.-E. Bäckvall, *J. Am. Chem. Soc.*, 2005, **127**, 8817–8825; (*c*) J. H. Choi, Y. K. Choi, Y. H. Kim, E. S. Park, E. J. Kim, M.-J. Kim and J. Park, *J. Org. Chem.*, 2004, **69**, 1972–1977; (*d*) O. Pàmies and J.-E. Bäckvall, *J. Org. Chem.*, 2002, **67**, 9006–9010.
10 (*a*) F. G. Mutti, A. Orthaber, J. H. Schrittwieser, J. G. de Vries, R. Pietschnig and W. Kroutil, *Chem. Commun.*, 2010, **46**, 8046–8048; (*b*) T. Jerphagnon, A. J. A. Gayet, F. Berthiol, V. Ritleng, N. Mršić, A. Meetsma, M. Pfeffer, A. J. Minnaard, B. L. Feringa and J. G. de Vries, *Chem. – Eur. J.*, 2009, **15**, 12780–12790; (*c*) R. M. Haak, F. Berthiol, T. Jerphagnon, A. J. A. Gayet, C. Tarabiono, C. P. Postema, V. Ritleng, M. Pfeffer, D. B. Janssen, A. J. Minnaard, B. L. Feringa and J. G. de Vries, *J. Am. Chem. Soc.*, 2008, **130**, 13508–13509.
11 T. M. Poessl, B. Kosjek, U. Ellmer, C. C. Gruber, K. Edegger, K. Faber, P. Hildebrandt, U. T. Bornscheuer and W. Kroutil, *Adv. Synth. Catal.*, 2005, **347**, 1827–1834.
12 B. Seisser, I. Lavandera, K. Faber, J. H. Lutje Spelberg and W. Kroutil, *Adv. Synth. Catal.*, 2007, **349**, 1399–1404.
13 F. R. Bisogno, A. Cuetos, A. A. Orden, M. Kurina-Sanz, I. Lavandera and V. Gotor, *Adv. Synth. Catal.*, 2010, **352**, 1657–1661.
14 E. B. Ayres and C. R. Hauser, *J. Am. Chem. Soc.*, 1943, **65**, 1095–1096.
15 (*a*) S. Asghari and A. K. Habibi, *Tetrahedron*, 2012, **68**, 8890–8898; (*b*) R. Zimmer, J. Angermann, U. Hain, F. Hiller and H. U. Reissig, *Synthesis*, 1997, 1467–1474; (*c*) A. Le Rouzic, M. Duclos and H. Patin, *Bull. Soc. Chim. Fr.*, 1991, 952–961.
16 J. Limanto, R. A. Desmond, D. R. Gauthier, Jr., P. N. Devine, R. A. Reamer and R. P. Volante, *Org. Lett.*, 2003, **5**, 2271–2274.
17 (*a*) C. Peppe and R. P. das Chagas, *J. Organomet. Chem.*, 2006, **691**, 5856–5860; (*b*) J. M. Concellón, H. Rodríguez-Solla, C. Concellón and P. Díaz, *Synlett*, 2006, 837–840.
18 (*a*) S. S. van Berkel, S. Brauch, L. Gabriel, M. Henze, S. Stark, D. Vasilev, L. A. Wessjohann, M. Abbas and B. Westermann, *Angew. Chem., Int. Ed.*, 2012, **51**, 5343–5346; (*b*) M. S. Raghavendra and Y. Lam, *Tetrahedron Lett.*, 2004, **45**, 6129–6132; (*c*) K. Sakai, N. Hida and K. Kondo, *Bull. Chem. Soc. Jpn.*, 1986, **59**, 179–183.
19 (*a*) F. R. Bisogno, E. García-Urdiales, H. Valdés, I. Lavandera, W. Kroutil, D. Suárez and V. Gotor, *Chem. – Eur. J.*, 2010, **16**, 11012–11019; (*b*) I. Lavandera, A. Kern, V. Resch, B. Ferreira-Silva, A. Glieder, W. M. F. Fabian, S. de Wildeman and W. Kroutil, *Org. Lett.*, 2008, **10**, 2155–2158.
20 (*a*) A. M. Barreca, M. Fabbrini, C. Galli, P. Gentilli and S. Ljunggren, *J. Mol. Catal. B: Enzym.*, 2003, **26**, 105–110; (*b*) E. Srebotnik and K. E. Hammel, *J. Biotechnol.*, 2000, **81**, 179–188; (*c*) H. Xu, Y.-Z. Lai, D. Slomczynski, J. P. Nakas and S. W. Tanenbaum, *Biotechnol. Lett.*, 1997, **19**, 957–960.
21 The blank experiments using just the laccase or TEMPO (20 mol%), did not afford any conversion.

22 (*a*) G. Cantarella, F. d'Acunzo and C. Galli, *Biotechnol. Bioeng.*, 2003, **82**, 395–398; (*b*) F. d'Acunzo, C. Galli and B. Masci, *Eur. J. Biochem.*, 2002, **269**, 5330–5335; (*c*) J. Rodakiewicz-Nowak, *Top. Catal.*, 2000, **11/12**, 419–434.
23 K. Alfonsi, J. Colberg, P. J. Dunn, T. Fevig, S. Jennings, T. A. Johnson, H. P. Kleine, C. Knight, M. A. Nagy, D. A. Perry and M. Stefaniak, *Green Chem.*, 2008, **10**, 31–36.
24 Another indication that substrate solubilization played an important role in this oxidative reaction was the fact that when alcohol **1a** (a crystal solid) was crushed into very tiny pieces, the conversion in plain NaOAc buffer (50 mM, pH 4.5) increased from less than 10% to 47% after 24 h at 20 °C.
25 I. W. C. E. Ardens, Y. Li and R. A. Sheldon, *Biocatal. Biotransform.*, 2006, **24**, 443–448.
26 Further experiments oxidizing mixtures of dichlorinated alcohol **1a** with monohalogenated derivative **1i** or unsubstituted compound **1j** afforded, as expected, mixtures of the corresponding ketones in similar ratios (see ESI† for more details).
27 (*a*) S. A. Tromp, I. Matijošytė, R. A. Sheldon, I. W. C. E. Arends, G. Mul, M. T. Kreutzer, J. A. Moulijn and S. de Vries, *ChemCatChem*, 2010, **2**, 827–833; (*b*) F. D'Acunzo, P. Baiocco, M. Fabbrini, C. Galli and P. Gentili, *Eur. J. Org. Chem.*, 2002, 4195–4201.
28 P. L. Anelli, S. Banfi, F. Montanari and S. Quici, *J. Org. Chem.*, 1989, **54**, 2970–2972.
29 M. Zhao, J. Li, E. Mano, Z. Song, D. M. Tschaen, E. J. J. Grabowski and P. J. Reider, *J. Org. Chem.*, 1999, **64**, 2564–2566.
30 M. F. Semmelhack, C. R. Schmid, D. A. Cortés and C. S. Chou, *J. Am. Chem. Soc.*, 1984, **106**, 3374–3376.
31 T. Miyazawa and T. Endo, *J. Mol. Catal.*, 1985, **32**, 357–360.
32 R. A. Miller and R. S. Hoerrner, *Org. Lett.*, 2003, **5**, 285–287.
33 J. G. Aston, J. D. Newkirk, J. Dorsky and D. M. Jenkins, *J. Am. Chem. Soc.*, 1942, **64**, 1413–1416.
34 (*a*) R. A. Sheldon, *Chem. Ind.*, 1992, 903–906; (*b*) R. A. Sheldon, *Green Chem.*, 2007, **9**, 1273–1283.
35 A recent example can be found in: J. H. Schrittwieser, F. Coccia, S. Kara, B. Grischek, W. Kroutil, N. d'Alessandro and F. Hollmann, *Green Chem.*, 2013, **15**, 3318–3331.
36 (*a*) M. Eissen and J. O. Metzger, *Chem. – Eur. J.*, 2002, **8**, 3580–3585; (*b*) *EATOS: Environmental Assessment Tool for Organic Syntheses*, http://www.metzger.chemie.uni-oldenburg.de/eatos/english.htm, accessed: 05.02.2014.
37 K. Edegger, C. C. Gruber, T. M. Poessl, S. R. Wallner, I. Lavandera, K. Faber, F. Niehaus, J. Eck, R. Oehrlein, A. Hafner and W. Kroutil, *Chem. Commun.*, 2006, 2402–2404.

REFERENCES

1. R. A. Sheldon, *Green Chem*. **2007**, *9*, 1273-1283.
2. K. Alfonsi, J. Colberg, P. J. Dunn, T. Fevig, S. Jennings, T. A. Johnson, H. P. Kleine, C. Knight, M. A. Nagy, D. A. Perry, M. Stefaniak, *Green Chem*. **2008**, *10*, 31-36.
3. B. M. Trost, *Science* **1991**, *254*, 1471-1477.
4. (a) R. A. Sheldon, *Chem. Commun*. **2008**, 3352-3365; (b) R. A. Sheldon, *Chem. Soc. Rev*. **2012**, *41*, 1437-1451.
5. P. T. Anastas, J. C. Warner, *Green Chemistry: Theory and Practice*, Oxford University Press, Oxford, 1998.
6. R. A. Sheldon, CHEMTECH **1994**, *24*, 38-47.
7. J. Clark, R. Sheldon, C. Raston, M. Poliakoff, W. Leitner, *Green Chem*. **2014**, *16*, 18-23.
8. W. J. W. Watson, *Green Chem*. **2012**, *14*, 251-259.
9. http://www.acs.org/content/acs/en/greenchemistry/industrybusiness/pharmaceutical.html, ACS GCI Pharmaceutical Roundtable Solvent Selection Guide 2011.
10. M. O. Simon, C. J. Li, *Chem. Soc. Rev*. **2012**, *41*, 1415-1427.
11. S. Narayan, J. Muldoon, M. G. Finn, V. V. Fokin, H. C. Kolb, K. B. Sharpless, *Angew. Chem. Int. Ed*. **2005**, *44*, 3275-3279.
12. M. C. Pirrung, K. D. Sarma, *J. Am. Chem. Soc*. **2003**, *126*, 444-445.
13. Activation volume $\Delta V^{\neq}$ is defined as the difference between the volume occupied in the reaction transition state V_{TS} and the occupied by the reactants V_R; $\Delta V^{\neq} = V_{TS} - V_R$. The negative sign of the activation volume indicates that the reaction rate can be increased with the rising pressure in the system.
14. N. Azizi, M. R. Saidi, *Org. Lett*. **2005**, *7*, 3649-3651.
15. P. Pollet, E. A. Davey, E. E. Ureña-Benavides, C. A. Eckert, C. L. Liotta, *Green Chem*. **2014**, *16*, 1034-1055.
16. W. Medina-Ramos, M. A. Mojica, E. D. Cope, R. J. Hart, P. Pollet, C. A. Eckert, C. L. Liotta, *Green Chem.* **2014**, *16*, 2147-2155.
17. ECHA, "REACH Regulation", http://echa.europa.eu/regulations/reach/understanding-reach.
18. ECHA, "Authorisation List," http://echa.europa.eu/web/guest/addressing-chemicals-of-concern/authorisation/recommendation-for-inclusion-in-the-authorisation-list/authorisation-list. The chemicals listed in here are: trichloroethylene, chromium trioxide, acids generated from chromium trioxide

and their oligomers, sodium dichromate, potassium dichromate, ammonium dichromate, potassium chromate, sodium chromate, hexabromocyclododecane, tris(2-chloroethyl)phosphate, 2,4-dinitrotoluene, lead chromate, diarsenic pentaoxide, diarsenic trioxide, lead sulfochromate yellow, lead chromate molybdate sulphate red, bis(2-ethylhexyl) phthalate, benzyl butyl phthalate, diisobutyl phthalate, dibutyl phthalate, 5-*tert*-butyl-2,4,6-trinitro-*m*-xylene, and 4,4'-diaminodiphenylmethane.

19. http://www.cirs-reach.com/REACH/.
20. (a) S. Sánchez, A. L. Demain. *Org. Process Res. Dev.* **2011**, *15*, 224-230; (b) B. M. Nestl, B. A. Nebel, B. Hauer, *Curr. Opin. Chem. Biol.* **2011**, *15*, 187-193.
21. U. T. Bornscheuer, G. W. Huisman, R. J. Kazlauskas, S. Lutz, J. C. Moore, K. Robins, *Nature* **2012**, *485*, 185-194.
22. (a) R. Wohlgemuth, *Curr. Opin. Biotechnol.* **2010**, *21*, 713-724; (b) H.-P. Meyer, *Org. Process Res. Dev*. **2011**, *15*, 180-188.
23. K. Faber, *Biotransformations in Organic Chemistry*. *A textbook*, 5th Ed., Springer, Heidelberg, **2004**.
24. P. A. Santacoloma, G. Sin, K. V. Gernaey, J. M. Woodley, *Org. Process Res. Dev.* **2011**, *15*, 203-212.
25. (a) C. A. Denard, J. F. Hartwig, H. Zhao, *ACS Catal.* **2013**, *3*, 2856-2864; (b) H. Pellissier, *Tetrahedron* **2013**, *69*, 7171-7210.
26. C. E. Paul, I. W. C. E. Arends, F. Hollmann, *ACS Catal.* **2014**, *4*, 788-797.
27. P. F. Mugford, U. G. Wagner, Y. Jiang, K. Faber, R. J. Kazlauskas, *Angew. Chem. Int. Ed.* **2008**, *47*, 8782-8793.
28. (a) G. A. Behrens, A. Hummel, S. K. Padhi, S. Schätzle, U. T. Bornscheuer, *Adv. Synth. Catal.* **2011**, *353*, 2191-2215; (b) M. T. Reetz, *Tetrahedron* **2012**, *68*, 7530-7548.
29. P. Atkins, J. de Paula, *Physical Chemistry*, 8th Ed., Chapter 3, Oxford University Press, New York, **2006**, pp. 95-109.
30. P. Atkins, J. De Paula, *Physical Chemistry*, 8th Ed., Chapter 23, Oxford University Press, New York, **2006**, p. 842.
31. D. Gamenara, G. A. Seoane, P. Saenz-Méndez, P. Domínguez de María, *Redox Biocatalysis: Fundamentals and Applications*, Wiley & Sons, New Jersey, **2013**, pp. 12-18.

32. (a) R. C. Hart, K. E. Stempel, P. D. Boyer, M. J. Cormier, *Biochem. Biophys. Res. Commun.* **1978**, *81*, 980-986; (b) S. Fetzner, R. A. Steiner, *Appl. Microbiol. Biotechnol.* **2010**, *86*, 791-804.
33. (a) F. Hollmann, I. W. C. E. Arends, K. Buehler, *ChemCatChem* **2010**, *2*, 762-782; (b) C. Rodríguez, I. Lavandera, V. Gotor, *Curr. Org. Chem*. **2012**, *16*, 2525-2541; (c) H. Wu, C. Tian, X. Song, C. Liu, D. Yang, Z. Jiang, *Green Chem.* **2013**, *15*, 1773-1789; (d) S. Kara, J. H. Schrittwieser, F. Hollmann, M. B. Ansorge-Schumacher, *Appl. Microbiol. Biotechnol.* **2014**, *98*, 1517-1529.
34. Although some recent approaches have been used to overcome these thermodynamic limitations employing a small excess of the co-substrate. See, for instance: (a) I. Lavandera, A. Kern, V. Resch, B. Ferreira-Silva, A. Glieder, W. M. F. Fabian, S. de Wildeman, W. Kroutil, *Org. Lett.* **2008**, *10*, 2155-2158; (b) S. Kara, D. Spickermann, J. H. Schrittwieser, C. Leggewie, W. J. H. van Berkel, I. W. C. E. Arends, F. Hollmann, *Green Chem.* **2013**, *15*, 330-335.
35. P. Könst, S. Kara, S. Kochius, D. Holtmann, I. W. C. E. Arends, R. Ludwig, F. Hollmann, *ChemCatChem* **2013**, *5*, 3027-3032.
36. A. I. Cañas, S. Camarero, *Biotechnol. Adv*. **2010**, *28*, 694-705.
37. C. W. Bradshaw, H. Fu, G. J. Shen, C. H. Wong, *J. Org. Chem*. **1992**, *57*, 1526-1532.
38. V. Prelog, *Pure Appl. Chem.* **1964**, *9*, 119-130.
39. K. L. Kavanagh, H. Jörnvall, B. Persson, U. Oppermann, *Cell. Mol. Life Sci*. **2008**, *65*, 3895-3906.
40. J. Hedlund, H. Jörnvall, B. Persson, *BMC Bioinformatics* **2010**, *11*, 534-550.
41. H. Jörnvall, J. Hedlund, T. Bergman, U. Oppermann, B. Persson, *Biochem. Biophys. Res. Commun*. **2010**, *396*, 125-130.
42. (a) M. K. Tiwari, R. K. Singh, R. Singh, M. Jeya, H. Zhao, J. K. Lee, *J. Biol. Chem*. **2012**, *287*, 19429-19439; (b) D. S. Auld, T. Bergman, *Cell. Mol. Life Sci*. **2008**, *65*, 3961-3970.
43. M. Karabec, A. Łykowski, K. C. Tauber, G. Steinkellner, W. Kroutil, G. Grogan, K. Gruber, *Chem. Commun.* **2010**, *46*, 6314-6316.
44. W. Stampfer, B. Kosjek, C. Moitzi, W. Kroutil, K. Faber, *Angew. Chem. Int. Ed*. **2002**, *41*, 1014-1017.

45. (a) B. Kosjek, W. Stampfer, M. Pogorevc, W. Goessler, K. Faber, W. Kroutil, *Biotechnol. Bioeng.* **2004**, *86*, 55-62; (b) G. de Gonzalo, I. Lavandera, K. Faber, W. Kroutil, *Org. Lett.* **2007**, *9*, 2163-2166.
46. See, for instance: (a) W. Stampfer, B. Kosjek, K. Faber, W. Kroutil, *J. Org. Chem.* **2003**, *68*, 402-406; (b) M. Kurina-Sanz, F. R. Bisogno, I. Lavandera, A. A. Orden, V. Gotor, *Adv. Synth. Catal.* **2009**, *351*, 1842-1848; (c) J. Mangas-Sánchez, E. Busto, V. Gotor-Fernández, V. Gotor, *Catal. Sci. Technol.* **2012**, *2*, 1590-1595; (d) A. Díaz-Rodríguez, W. Borzęcka, I. Lavandera, V. Gotor, *ACS Catal.* **2014**, *4*, 386-393.
47. Y. Kallberg, U. Oppermann, H. Jörnvall, B. Persson, *Eur. J. Biochem*. **2002**, *269*, 4409-4417.
48. C. Filling, K. D. Berndt, J. Benach, S. Knapp, T. Prozorovski, E. Nordling, R. Ladenstein, H. Jörnvall, U. Oppermann, *J. Biol. Chem*. **2002**, *277*, 25677-25684.
49. A. Lerchner, A. Jarasch, W. Meining, A. Schiefner, A. Skerra, *Biotechnol. Bioeng*. **2013**, *110*, 2803-2814.
50. K. Niefind, J. Müller, B. Riebel, W. Hummel, D. Schomburg, *J. Mol. Biol*. **2003**, *327*, 317-328.
51. S. Leuchs, L. Greiner, *Chem. Biochem. Eng. Q.* **2011**, *25*, 267-281.
52. C. Rodríguez, W. Borzęcka, J. H. Sattler, W. Kroutil, I. Lavandera, V. Gotor, *Org. Biomol. Chem.* **2014**, *12*, 673-681.
53. H. Man, K. Kędziora, J. Kulig, A. Frank, I. Lavandera, V. Gotor-Fernández, D. Rother, S. Hart, J. P. Turkenburg, G. Grogan, *Top. Catal*. **2014**, *57*, 356-365.
54. By definition, the so-called "bulky-bulky" ketones possess both substituents larger than ethyl, azido-, cyano- or halomethyl groups.
55. I. Lavandera, A. Kern, B. Ferreira-Silva, A. Glieder, S. de Wildeman, W. Kroutil, *J. Org. Chem.* **2008**, *73*, 6003-6005.
56. J. Kulig, A. Frese, W. Kroutil, M. Pohl, D. Rother, *Biotechnol. Bioeng*. **2013**, *110*, 1838-1848.
57. J. Kulig, R. C. Simon, C. A. Rose, S. M. Husain, M. Häckh, S. Lüdeke, K. Zeitler, W. Kroutil, M. Pohl, D. Rother, *Catal. Sci. Technol*. **2012**, *2*, 1580-1589.
58. A. Cuetos, A. Rioz-Martínez, F. R. Bisogno, B. Grischek, I. Lavandera, G. de Gonzalo, W. Kroutil, V. Gotor, *Adv. Synth. Catal.* **2012**, *354*, 1743-1749.
59. E. I. Solomon, P. Chen, M. Metz, S. K. Lee, A. E. Palmer, *Angew. Chem. Int. Ed*. **2001**, *40*, 4570-4590.

60. (a) S. Riva, *Trends Biotechnol.* **2006**, *24*, 219-226; (b) S. Witayakran, A. J. Ragauskas, *Adv. Synth. Catal*. **2009**, *351*, 1187-1209; (c) T. Kudanga, G. S. Nyanhongo, G. M. Guebitz, S. Burton, *Enzyme Microb. Technol.* **2011**, *48*, 195-208; (d) D. Gamenara, G. A. Seoane, P. Saenz-Méndez, P. Domínguez de María, *Redox Biocatalysis: Fundamentals and Applications*, Wiley & Sons, New Jersey, **2013**, pp. 317-330; (e) M. Mogharabi, M. A. Faramarzi, *Adv. Synth. Catal.* **2014**, *356*, 897-927.
61. (a) K. Piontek, M. Antorini, T. Choinowski, *J. Biol. Chem*. **2002**, *277*, 37663-37669; (b) T. Bertrand, C. Jolivalt, P. Briozzo, E. Caminade, N. Joly, C. Madzak, C. Mougin, *Biochemistry* **2002**, *41*, 7325-7333.
62. (a) S.-K. Lee, S. DeBeer George, W. E. Antholine, B. Hedman, K. O. Hodgson, E. I. Solomon, *J. Am. Chem. Soc*. **2002**, *124*, 6180-6193; (b) J. Yoon, L. M. Mirica, T. D. P. Stack, E. I. Solomon, *J. Am. Chem. Soc*. **2005**, *127*, 13680-13693; (c) D. E. Heppner, C. H. Kjaergaard, E. I. Solomon, *J. Am. Chem. Soc*. **2013**, *135*, 12212-12215; (d) D. Gamenara, G. A. Seoane, P. Saenz-Méndez, P. Domínguez de María, *Redox Biocatalysis: Fundamentals and Applications*, Wiley & Sons, New Jersey, **2013**, pp.54-56.
63. T. Vogler, A. Studer, *Synthesis* **2008**, 1979-1993.
64. E. Fremy, *Ann. Chim. Phys.* **1845**, *15*, 408.
65. O. Piloty, B. G. Schwerin, *Ber. Dtsch. Chem. Ges*. **1901**, *34*, 1870.
66. O. L. Lebedev, S. N. Kazarnovsky, *Tr. Khim. Khim. Tekhnol.* **1959**, *3*, 649.
67. L. Tebben, A. Studer, *Angew. Chem. Int. Ed*. **2011**, *50*, 5034-5068.
68. P. Giardina, V. Faraco, C. Pezzella, A. Piscitelli, S. Vanhulle, G. Sannia, *Cell. Mol. Life Sci.* **2010**, *67*, 369-385.
69. R. Bourbonnais, M. G. Paice, *FEBS Lett.* **1990**, *267*, 99-102.
70. R. A. Sheldon, I. W. C. E. Arends, *J. Mol. Catal. A: Chem.* **2006**, *251*, 200-214.
71. S. Wertz, A. Studer, *Green Chem*. **2013**, *15*, 3116-3134.
72. F. d'Acunzo, P. Baiocco, M. Fabbrini, C. Galli, P. Gentili, *Eur. J. Org. Chem*. **2002**, 4195-4201.
73. S. A. Tromp, I. Matijošyte, R. A. Sheldon, I. W. C. E. Arends, G. Mul, M. T. Kreutzer, J. A. Moulijn, S. de Vries, *ChemCatChem* **2010**, *2*, 827-833.
74. (a) M. Fabbrini, C. Galli, P. Gentili, *J. Mol. Catal. B: Enzym*. **2002**, *16*, 231-240; (b) I. W. C. E. Arends, Y. X. Li, R. Ausan, R. A. Sheldon, *Tetrahedron* **2006**, *62*, 6659-6665; (c) M. B. Lauber, S. S. Stahl, *ACS Catal.* **2013**, *3*, 2612-2616;

(d) J. Gross, K. Tauber, M. Fuchs, N. G. Schmidt, A. Rajagopalan, K. Faber, W. M. F. Fabian, J. Pfeffer, T. Haas, W. Kroutil, *Green Chem*. **2014**, *16*, 2117-2121.

75. C. Zhu, Z. Zhang, W. Ding, J. Xie, Y. Chen, J. Wu, X. Chen, H. Ying, *Green Chem*. **2014**, *16*, 1131-1138.
76. A. Díaz-Rodríguez, I. Lavandera, S. Kanbak-Aksu, R. A. Sheldon, V. Gotor, V. Gotor-Fernández, *Adv. Synth. Catal.* **2012**, *354*, 3405-3408.
77. (a) F. Minisci, F. Recupero, A. Cecchetto, C. Gambarotti, C. Punta, R. Faletti, R. Paganelli, G. F. Pedulli, *Eur. J. Org. Chem.* **2004**, 109-119; (b) C. Jin, L. Zhang, W. Su, *Synlett* **2011**, 1435-1438.
78. (a) P. L. Anelli, C. Biffi, F. Montanari, S. Quici, *J. Org. Chem.* **1987**, *52*, 2559-2562; (b) P. L. Anelli, S. Banfi, F. Montanari, S. Quici, *J. Org. Chem.* **1989**, *54*, 2970-2972.
79. M. Zhao, J. Li, E. Mano, Z. Song, D. M. Tschaen, E. J. J. Grabowski, P. J. Reider, *J. Org. Chem*. **1999**, *64*, 2564-2566.
80. M. F. Semmelhack, C. R. Schmid, D. A. Cortés, C. S. Chou, *J. Am. Chem. Soc.* **1984**, *106*, 3374-3376.
81. R. N. Patel, *Coord. Chem. Rev*. **2008**, *252*, 659-701.
82. D. Gamenara, G. A. Seoane, P. Saenz-Méndez, P. Domínguez de María, *Redox Biocatalysis: Fundamentals and Applications*, , Wiley & Sons, New Jersey, **2013**, pp. 327-346.
83. B. I. Roman, N. De Kimpe, C. V. Stevens, *Chem. Rev.* **2010**, *110*, 5914-5988.
84. T. Quinto, V. Köhler, T. R. Ward, *Top. Catal.* **2014**, *57*, 321-331.
85. M. Richter, *Nat. Prod. Rep.* **2013**, *30*, 1324-1345.
86. S. Lutz, *Science* **2010**, *329*, 285-287.
87. E. Alanvert, C. Doherty, T. S. Moody, N. Nesbit, A. S. Rowan, S. J. C. Taylor, F. Vaughan, T. Vaughan, J. Wiffen, I. Wilson, *Tetrahedron: Asymmetry* **2009**, *20*, 2462-2466.
88. J. Mangas-Sánchez, E. Busto, V. Gotor-Fernández, F. Malpartida, V. Gotor, *J. Org. Chem*. **2011**, *76*, 2115-2121.
89. D. Tokoshima, K. Hanaya, M. Shoji, T. Sugai, *J. Mol. Catal. B: Enzym*. **2013**, *97*, 95-99.
90. K. Asami, T. Machida, S. Jung, K. Hanaya, M. Shoji, T. Sugai, *J. Mol. Catal. B: Enzym*. **2013**, *97*, 106-109.

91. D. M. Lee, J. C. Lee, N. Jeong, K. I. Lee, *Tetrahedron: Asymmetry* **2007**, *18*, 2662-2667.
92. D. Zhu, C. Mukherjee, L. Hua, *Tetrahedron: Asymmetry* **2005**, *16*, 3275-3278.
93. (a) J. H. Schrittwieser, I. Lavandera, B. Seisser, B. Mautner, J. H. L. Spelberg, W. Kroutil, *Tetrahedron: Asymmetry* **2009**, *20*, 483-488; (b) J. H. Schrittwieser, I. Lavandera, B. Seisser, B. Mautner, W. Kroutil, *Eur. J. Org. Chem.* **2009**, 2293-2298.
94. F. R. Bisogno, A. Cuetos, A. A. Orden, M. Kurina-Sanz, I. Lavandera, V. Gotor, *Adv. Synth. Catal.* **2010**, *352*, 1657-1661.
95. F. R. Bisogno, E. García-Urdiales, H. Valdés, I. Lavandera, W. Kroutil, D. Suárez, V. Gotor, *Chem. Eur. J.* **2010**, *16*, 11012-11019.
96. T. Matsuda, T. Harada, N. Nakajima, T. Itoh, K. Nakamura, *J. Org. Chem*. **2000**, *65*, 157-163.
97. A. Goswami, R. L. Bezbaruah, J. Goswami, N. Borthakur, D. Dey, A. K. Hazarika, *Tetrahedron: Asymmetry* **2000**, *11*, 3701-3709.
98. B. Barkakty, Y. Takaguchi, S. Tsuboi, *Tetrahedron* **2007**, *63*, 970-976.
99. (a) K. Nakamura, R. Yamanaka, *Tetrahedron: Asymmetry* **2002**, *13*, 2529-2533; (b) W. Borzęcka, I. Lavandera, V. Gotor, *J. Org. Chem*. **2013**, *78*, 7312-7317.
100. K. Lundell, T. Raijola, L. T. Kanerva, *Enzyme Microb. Technol*. **1998**, *22*, 86-93.
101. H. Kakiya, H. Shinokubo, K. Oshima, *Tetrahedron* **2001**, *57*, 10063-10069.
102. Z. Wang, J. Yin, S. Campagna, J. A. Pesti, J. M. Fortunak, *J. Org. Chem*. **1999**, *64*, 6918-6920.
103. R. N. McDonald, R. C. Cousins, *J. Org. Chem*. **1980**, *45*, 2976-2984.
104. B. Singh, P. Gupta, A. Chaubey, R. Parshad, S. Sharma, S. C. Taneja, *Tetrahedron: Asymmetry* **2008**, *19*, 2579-2588.
105. http://www.rcsb.org/pdb/home/home.do, state of 3 March 2014.
106. E. F. Garman, *Science* **2014**, *343*, 1102-1108.
107. A. Joachimiak, *Curr. Opin. Struct. Biol*. **2009**, *19*, 573-584.
108. A. Yonath, *Curr. Opin. Struct. Biol*. **2011**, *21*, 622-626.
109. G. Grogan, *Practical Biotransformations: A Beginner´s Guide*, Wiley-Blackwell, Chichester, **2009**.
110. D. L. Nelson, M. M. Cox, *Lehninger Principles of Biochemistry*, 3rd Ed., Chapter 29, W. H. Freeman and Company, New York, **2001**.

111. D. L. Nelson, M. M. Cox, *Lehninger Principles of Biochemistry*, 3rd Ed., Chapter 28, W. H. Freeman and Company, New York, **2001**.
112. Regulatory protein that inhibits the expression of β-galactosidase in the absence of lactose (lac).
113. http://www.gelifesciences.com/handbooks, from *Gel filtration. Principles and methods*, GE Healthcare.
114. T. G. M. Schmidt, A. Skerra, *Nat. Protoc.* **2007**, *2*, 1528-1535.
115. P. Atkins, J. de Paula, *Physical Chemistry*, 8th Ed., Chapter 20, Oxford University Press, New York, **2006**.
116. J. A. K. Howard, M. R. Probert, *Science* **2014**, *343*, 1098-1102.
117. D. Chirgadze, *Protein Crystallisation in Action*, Cambridge University, **2001**. http://www.xray.bioc.cam.ac.uk/xray_resources/whitepapers/xtal-in-action/xtal-in-action-html.html.
118. A. McPherson, *Methods* **2004**, *34*, 254-256.
119. https://hamptonresearch.com/product_detail.aspx?cid=1&sid=24&pid=5.
120. http://www.qiagen.com/products/protein/crystallization/compositiontables/pdf/1057791_ps_xtal_pact-suite_update_160609_lowres.pdf.
121. A. M. Brzozowski, J. Walton, *J. Appl. Cryst.* **2001**, *34*, 97-101.
122. (a) M. Cunliffe, A. Kawasaki, E. Fellows, M. A. Kertesz, *FEMS Microbiol. Ecol.* **2006**, *58*, 364-372; (b) M. Ochou, M. Saito, Y. Kurusu, *Biosci. Biotechnol. Biochem.* **2008**, *72*, 1130-1133.
123. I. Lavandera, G. Oberdorfer, J. Gross, S. de Wildeman, W. Kroutil, *Eur. J. Org. Chem.* **2008**, 2539-2545.
124. Buffer composition: information not disclosed by the manufacturer, available as 10 × concentrated stock solution.
125. One unit of KOD Hot Start DNA Polymerase is defined as the amount of enzyme that will catalyze the incorporation of 10 nmol of dNTP into acid insoluble form in 30 minutes at 75°C in a reaction containing 20 mM Tris-HCl (pH 7.5 at 25°C), 8 mM $MgCl_2$, 7.5 mM DTT, 50 μg/mL BSA, 150 μM each of dATP, dCTP, dGTP, dTTP (a mix of unlabeled and [^{3}H]-dTTP) and 150 μg/mL activated calf thymus DNA.
126. 7 mM TAE buffer pH 8.0 composition: Tris-base (0.84 g), glacial acetic acid (1.14 mL), EDTA (2 mL 0.5 M).

127. Recommended usage by the supplier is at a 1:10,000 dilution in 0.5 M TAE buffer pH 7.5 of the stock solution in DMSO.
128. Buffer composition: 15% Ficoll®-400; 66 mM EDTA, 20 mM Tris-HCl, 0.1% SDS, 0.1% bromophenol blue, pH 8.0 at 25 °C.
129. Buffer composition: information not disclosed by the manufacturer.
130. W. Kabsch, *Acta Crystallogr. Sect. D* **2010**, *66*, 125-132.
131. P. Evans, *Acta Crystallogr. Sect. D* **2006**, *62*, 72-82.
132. F. Long, A. A. Vagin, P. Young, G. N. Murshudov, *Acta Crystallogr. Sect. D* **2008**, *64*, 125-132.
133. P. Emsley, K. Cowtan, *Acta Crystallogr. Sect. D* **2004**, *60*, 2126-2132.
134. G. N. Murshudov, A. A. Vagin, E. J. Dodson, *Acta Crystallogr. Sect. D* **1997**, *53*, 240-255.
135. R. A. Laskowski, M. W. Macarthur, D. S. Moss, J. M. Thornton, *J. Appl. Crystallogr.* **1993**, *26*, 283-291.
136. A. M. Barreca, M. Fabbrini, C. Galli, P. Gentili, S. Ljunggren, *J. Mol. Catal. B: Enzym.* **2003**, *26*, 105-110.
137. (a) M. Fabbrini, C. Galli, P. Gentili, D. Macchitella, *Tetrahedron Lett*. **2001**, *42*, 7551-7553; (b) I. Matijosite, Ph D Thesis, Technical University of Delft, **2008**.
138. F. d'Acunzo, A. M. Barreca, C. Galli, *J. Mol. Catal. B: Enzym.* **2004**, *31*, 25-30.
139. ABTS acts *via* electron transfer, TEMPO *via* ionic mechanism, HPI and VLA *via* hydrogen atom abstraction. For detailed mechanisms and mediator structures, see the Introduction.
140. L. Baratto, A. Candido, M. Marzorati, F. Sagui, S. Riva, B. Danieli, *J. Mol. Catal. B: Enzym*. **2006**, *39*, 3-8.
141. (a) W. Kroutil, H. Mang, K. Edegger, K. Faber, *Adv. Synth. Catal*. **2004**, *346*, 125-142; (b) D. Romano, R. Villa, F. Molinari, *ChemCatChem* **2012**, *4*, 739-749.
142. (a) O. Pámies, J.-E. Bäckvall, *J. Org. Chem.* **2002**, *67*, 9006-9010; (b) J. H. Choi, Y. K. Choi, Y. H. Kim, E. S. Park, E. J. Kim, M.-J. Kim, J. Park, *J. Org. Chem*. **2004**, *69*, 1972-1977; (c) T. Jerphagnon, A. J. A. Gayet, F. Berthiol, V. Ritleng, N. Mršić, A. Meetsma, M. Pfeffer, A. J. Minnaard, B. L. Feringa, J. G. de Vries, *Chem. Eur. J*. **2009**, *15*, 12780-12790.
143. A. Träff, K. Bogár, M. Warner, J.-E. Bäckvall, *Org. Lett*. **2008**, *10*, 4807-4810.

144. R. M. Haak, F. Berthiol, T. Jerphagnon, A. J. A. Gayet, C. Tarabiono, C. P. Postema, V. Ritleng, M. Pfeffer, D. B. Janssen, A. J. Minnaard, B. L. Feringa, J. G. de Vries, *J. Am. Chem. Soc*. **2008**, *130*, 13508-13509.
145. F. G. Mutti, A. Orthaber, J. H. Schrittwieser, J. G. de Vries, R. Pietschnig, W. Kroutil, *Chem. Commun*. **2010**, *46*, 8046-8048.
146. (a) P. Torres-Salas, D. M. Mate, I. Ghazi, F. J. Plue, A. O. Ballesteros, M. Alcalde, *ChemBioChem* **2013**, *14*, 934-937; (b) U. N. Dwivedi, P. Singh, V. P. Pandey, A. Kumar, *J. Mol. Catal. B: Enzym*. **2011**, *68*, 117-128.
147. A. E. J. Nooy, A. C. Besemer, H. van Bekkum, *Carbohydr. Res*. **1995**, *269*, 89-98.
148. E. B. Ayres, C. R. Hauser, *J. Am. Chem. Soc.* **1943**, *65*, 1095-1096.
149. V. Pace, A. C. Cabrera, M. Fernández, J. V. Sinisterra, A. R. Alcántara, *Synthesis* **2010**, 3545-3555.
150. T. Miyazawa, T. Endo, *J. Mol. Catal.* **1985**, *32*, 357-360.
151. R. A. Miller, R. S. Hoerrner, *Org. Lett.* **2003**, *5*, 285-287.
152. D. A. Case, T. A. Darden, T. E. Cheatham, III, C. L. Simmerling, J. Wang, R. E. Duke, R. Luo, M. Crowley, R. C. Walker, W. Zhang, K. M. Merz, B. Wang, S. Hayik, A. Roitberg, G. Seabra, I. Kolossváry, K. F. Wong, F. Paesani, J. Vanicek, X. Wu, S. R. Brozell, T. Steinbrecher, H. Gohlke, L. Yang, C. Tan, J. Mongan, V. Hornak, G. Cui, D. H. Mathews, M. G. Seetin, C. Sagui, V. Babin, P. A. Kollman, AMBER 10, University of California, San Francisco, **2008**.
153. Gaussian 03, Revision C.02, M. J. Frisch, G. W. Trucks, H. B. Schlegel, G. E. Scuseria, M. A. Robb, J. R. Cheeseman, J. A. Montgomery, Jr., T. Vreven, K. N. Kudin, J. C. Burant, J. M. Millam, S. S. Iyengar, J. Tomasi, V. Barone, B. Mennucci, M. Cossi, G. Scalmani, N. Rega, G. A. Petersson, H. Nakatsuji, M. Hada, M. Ehara, K. Toyota, R. Fukuda, J. Hasegawa, M. Ishida, T. Nakajima, Y. Honda, O. Kitao, H. Nakai, M. Klene, X. Li, J. E. Knox, H. P. Hratchian, J. B. Cross, V. Bakken, C. Adamo, J. Jaramillo, R. Gomperts, R. E. Stratmann, O. Yazyev, A. J. Austin, R. Cammi, C. Pomelli, J. W. Ochterski, P. Y. Ayala, K. Morokuma, G. A. Voth, P. Salvador, J. J. Dannenberg, V. G. Zakrzewski, S. Dapprich, A. D. Daniels, M. C. Strain, O. Farkas, D. K. Malick, A. D. Rabuck, K. Raghavachari, J. B. Foresman, J. V. Ortiz, Q. Cui, A. G. Baboul, S. Clifford, J. Cioslowski, B. B. Stefanov, G. Liu, A. Liashenko, P. Piskorz, I. Komaromi, R. L. Martin, D. J. Fox, T. Keith, M. A. Al-Laham, C. Y. Peng, A. Nanayakkara,

M. Challacombe, P. M. W. Gill, B. Johnson, W. Chen, M. W. Wong, C. Gonzalez, J. A. Pople, Gaussian, Inc., Wallingford CT, **2004**.

154. A. Klamt, G. Schüürmann, *J. Chem. Soc., Perkin Trans. 2* **1993**, *5*, 799-805.
155. R. Ahlrichs, M. Bär, M. Häser, H. Horn, C. Kölmel, *Chem. Phys. Lett.* **1989**, *162*, 165-169.
156. (a) M. Eissen, J. O. Metzger, *Chem. Eur. J.* **2002**, *8*, 3580-3585; (b) EATOS: Environmental Assessment Tool for Organic Syntheses, http://www.metzger.chemie.uni-oldenburg.de/eatos/english.htm.